



**Cláudia Marisa
Barreiros Neves**

**(METALO)PORFIRINAS COMO
(FOTO)CATALISADORES HOMOGÉNEOS E
HETEROGÉNEOS NA (FOTO)OXIDAÇÃO DE
XENOBIÓTICOS**

**(METALLO)PORPHYRINS AS HOMOGENEOUS AND
HETEROGENEOUS (PHOTO)CATALYSTS IN THE
(PHOTO)OXIDATION OF XENOBIOTICS**



**Cláudia Marisa
Barreiros Neves**

**(METALO)PORFIRINAS COMO
(FOTO)CATALISADORES HOMOGÉNEOS E
HETEROGÉNEOS NA (FOTO)OXIDAÇÃO DE
XENOBIÓTICOS**

**(METALLO)PORPHYRINS AS HOMOGENEOUS AND
HETEROGENEOUS (PHOTO)CATALYSTS IN THE
(PHOTO)OXIDATION OF XENOBIOTICS**

Tese apresentada à Universidade de Aveiro para cumprimento dos requisitos necessários à obtenção do grau de Doutor em Química Sustentável, realizada sob a orientação científica do Doutor Mário Manuel Quialheiro Simões e da Doutora Maria da Graça de Pinho Morgado Silva Neves, respetivamente Professor Auxiliar e Professora Associada com Agregação do Departamento de Química da Universidade de Aveiro.

Apoio financeiro do POCTI no âmbito do III Quadro Comunitário de Apoio.



Apoio financeiro da FCT e do FSE no âmbito do III Quadro Comunitário de Apoio.



Dedico este trabalho ao meu marido e ao meu filho.

o júri

Presidente

Prof.^a Doutora Susana Isabel Barreto de Miranda Sargento
Professora Catedrática da Universidade de Aveiro

Prof.^a Doutora Luísa Margarida Dias Ribeiro de Sousa Martins
Professora Associada com Agregação da Universidade de Lisboa

Prof. Doutor Joaquim Luís Bernardes Martins de Faria
Professor Associado da Universidade do Porto

Prof.^a Doutora Maria Eduarda Bastos Henriques dos Santos
Professora Auxiliar da Universidade de Aveiro

Doutora Susana Luísa Henriques Rebelo
Investigadora da Universidade do Porto

Prof. Doutor Mário Manuel Quialheiro Simões
Professor Auxiliar da Universidade de Aveiro (Orientador)

agradecimentos

Ao Doutor Mário Simões e à Doutora Graça Neves, orientadores deste trabalho, agradeço a preocupação, a dedicação, o empenho, o tempo disponibilizado, mas sobretudo a orientação que prestaram ao longo deste percurso.

Ao Professor Artur Silva, Diretor do Programa Doutoral em Química Sustentável, o meu sincero reconhecimento pela permanente disponibilidade.

Ao Professor José Cavaleiro pelo importante contributo no período que precedeu este programa doutoral.

À Doutora Susana Rebelo pela realização e pela ajuda na interpretação das análises de SEM e de XPS, fundamentais na caracterização dos catalisadores heterogéneos.

À Doutora Eduarda Santos, pelo apoio e planeamento nos estudos de fotodegradação e por todos os conhecimentos transmitidos. Agradeço também à Doutora Olga Filipe pelo acompanhamento na realização das experiências de fotodegradação e pela ajuda na interpretação dos resultados.

À Doutora Sónia Santos pela realização das análises de HPLC-MS.

Ao Doutor João Tomé por ter proporcionado a colaboração com o grupo da Universidade de Gante.

À Doutora Diana Pinto pela ajuda no uso do equipamento de micro-ondas na imobilização dos catalisadores.

À Doutora Amparo Faustino pela colaboração.

À Doutora Mónica Válega por todo o apoio técnico prestado na utilização dos equipamentos de HPLC, GC e GC-MS e pela amizade.

Ao Dr. Hilário Tavares e às Dr.as Cristina Barros, Manuela Marques, Celeste Azevedo, Rosário Soares, Dulce Helena Teixeira e Teresa Caldeira pelo apoio técnico nas várias valências.

À Carla Santos, à Kelly Castro e a todos os meus colegas de laboratório.

Às minhas companheiras de casa, Rita e Joana pelas conversas e refeições partilhadas no final de dias longos de trabalho.

Aos meus pais e à minha irmã pelo apoio constante.

Ao meu marido por tolerar todos os momentos de mau humor, todos os meus desabafos, mas também todas as conquistas. Por estar sempre ao meu lado, nos bons e maus momentos, por ser um bom marido e ainda melhor pai. Por cuidar do nosso filho nos momentos em que eu tive de me ausentar para ir para o laboratório ou para escrever.

Esta tese foi também escrita no intervalo de mudanças de fraldas, alguns choros (poucos) e canções de embalar, mas sempre com um sentimento de enorme felicidade. Agradeço ao meu “pequeninho” por ter mudado a minha forma de pensar e por mesmo nos dias maus me colocar um sorriso no rosto.

À Fundação para a Ciência e a Tecnologia (FCT) pelo financiamento (PD/BD/52531/2014).

palavras-chave

catálise, síntese, metaloporfirinas, imobilização, manganês(III), oxidação, alcenos, monoterpenos, fotodegradação, metoprolol.

resumo

As reações de oxidação representam um papel crucial na produção de compostos de química fina e na indústria petroquímica, apresentando também um impacto negativo para o ambiente devido à grande quantidade de produtos secundários tóxicos que se podem formar. O uso de catalisadores permite que essas transformações ocorram em condições suaves e seletivas, sem a necessidade do uso de quantidades estequiométricas de oxidantes convencionais, contribuindo para processos de síntese mais sustentáveis. Tem sido dado grande destaque ao desenvolvimento de catalisadores mais robustos e à sua imobilização em suportes sólidos, aliado ao uso de oxidantes e solventes considerados mais inócuos. As metaloporfirinas, devido à sua aptidão para mimetizar o papel das enzimas do citocromo P450, são consideradas eficientes catalisadores em reações de oxidação. As porfirinas são também reconhecidas como fotossensibilizadores, o que as elege como boas candidatas para a fotodegradação de poluentes em contexto de remediação de água. Pelas razões acima referidas, o presente trabalho incidiu na síntese e caracterização de novos complexos de manganês(III) de porfirinas contendo substituintes nas posições *meso* que possibilitam a posterior imobilização em suportes sólidos. Foi estudada a atividade catalítica desses compostos em fase homogénea na oxidação de cicloocteno e de estireno. O catalisador que apresentou melhores resultados catalíticos em fase homogénea foi imobilizado nos suportes sólidos de sílica e resina de Merrifield, o que permite uma fácil separação e reciclagem do catalisador. Os materiais resultantes foram testados sob condições heterogéneas e o catalisador suportado em resina de Merrifield mostrou ser um catalisador muito eficiente, activo em cinco ciclos catalíticos na oxidação do cicloocteno. Foi sintetizado o complexo de manganês(III) de uma porfirina com grupos polietilenoglicol, que apresenta solubilidade em água, que foi testado como catalisador na oxidação dos compostos naturais carvacrol e timol, num meio bifásico água/hexano (1:1), para obter a timoquinona, que é um composto de valor acrescentado. Este sistema catalítico em meio bifásico permitiu a recuperação do catalisador através de uma simples separação de fases e a sua posterior reutilização. O sistema catalítico foi ainda aplicado na oxidação de um óleo de orégão, rico em carvacrol e timol, sendo seletivo para a timoquinona. Nos estudos de oxidação catalítica desenvolvidos no trabalho desta tese usou-se sempre peróxido de hidrogénio ou hidroperóxido de *tert*-butilo como oxidantes, que originam sub-produtos menos tóxicos e, por isso, são considerados mais amigos do ambiente. Num contexto de potencial tratamento de águas residuais, foi testada a possibilidade de a 5,10,15,20-tetraquis(pentafluorofenil)porfirina ser usada como fotocatalisador na fotodegradação de metoprolol em fase homogénea e imobilizada num suporte sólido de sílica, sob radiação solar simulada. Adicionalmente, a fotodegradação de metoprolol foi estudada na presença de luz solar usando a porfirina imobilizada.

keywords

catalysis, synthesis, metalloporphyrins, immobilization, manganese(III), oxidation, alkenes, monoterpenes, photodegradation, metoprolol.

abstract

Oxidation reactions play a crucial role in the production of fine chemicals and in petrochemical industry, also having a negative impact on the environment due to the large amount of toxic by-products that may be obtained. The use of catalysts allows these transformations to proceed under mild and selective conditions, without the need for the use of traditional stoichiometric oxidants, contributing to more sustainable processes. A major highlight has been the development of more robust catalysts and their immobilization on solid supports, coupled with the use of oxidants and solvents which are considered more innocuous. Metalloporphyrins, due to their ability to mimic the role of cytochrome P450 enzymes, are considered as efficient catalysts in oxidation reactions. Porphyrins are also recognized for their photosensitizer character, which makes them good candidates for the photodegradation of pollutants in a context of water remediation. For the reasons mentioned above, the present work focused on the synthesis and characterization of new manganese(III) porphyrin complexes containing substituents at the *meso* positions that allow the subsequent immobilization on solid supports. The catalytic activity of these compounds was studied in the oxidation of cyclooctene and styrene under homogeneous conditions. The catalyst revealing the best catalytic results in homogeneous phase was immobilized on solid supports, silica and Merrifield resin, which allows an easy separation and recycling of the catalyst. The resulting materials were tested under heterogeneous conditions and the Merrifield-supported catalyst showed to be a very efficient catalyst leading to five catalytic cycles in the oxidation of cyclooctene. The manganese(III) complex of a porphyrin with polyethylene glycol groups, presenting water solubility, was tested as catalyst in the oxidation of the natural products carvacrol and thymol, using a water/hexane (1:1) biphasic medium, to obtain thymoquinone, a value-added compound. This biphasic catalytic system allowed the catalyst recovery by simple phase separation and its reuse. The catalytic system was also applied in the oxidation of an oregano essential oil, rich in carvacrol and thymol, being very selective to thymoquinone. In the catalytic oxidation studies developed in the work of this thesis, hydrogen peroxide or *tert*-butyl hydroperoxide were used as oxidants, which originate less toxic by-products and are therefore considered more environmentally friendly. In a wastewater treatment context, the potential of 5,10,15,20-tetrakis(pentafluorophenyl)porphyrin being used as photocatalyst was tested for the degradation of metoprolol in homogeneous conditions and immobilized on a silica support, under simulated solar radiation. The photodegradation of metoprolol was also studied in the presence of sunlight using the immobilized porphyrin.

“Alcança quem não cansa.”
Aquilino Ribeiro

Contents

Abbreviations	xvii
Chapter 1. Introduction.....	3
1.1. Porphyrins and related compounds.....	3
1.2. Metalloporphyrins as catalysts in oxidation reactions	8
1.2.1. Catalytic oxidation as a tool for green and sustainable chemistry	8
1.2.2. Cytochromes P450 - oxidation catalysts present in nature	8
1.2.3. Metalloporphyrins as catalytic biomimetic systems of CYP450	11
1.2.4. Immobilization of porphyrins on solid supports	17
1.2.4.1. Silica.....	18
1.2.4.2. Organic polymers	24
1.3. Porphyrins as photocatalysts in a water remediation context	27
1.3.1. Emerging contaminants in water	27
1.3.2. Natural degradation of PPCPs and other organic contaminants in the aquatic environment.....	28
1.3.3. Advanced oxidation processes for the removal of PPCPs and other organic contaminants from wastewater	29
1.3.3.1. Porphyrins as photosensitizers in the degradation of organic pollutants in water	29
1.4. Objectives of the work.....	33
1.5. References	35
Chapter 2. Synthesis of new second-generation porphyrins bearing potential anchorage units to be used as catalysts in oxidation reactions.....	49
2.1. Synthetic methodologies to obtain 5,10,15,20-tetraarylporphyrins	49
2.2. The new second-generation porphyrins bearing potential anchorage units prepared in this work	54
2.2.1. Synthesis of the free-base porphyrins	57
2.2.2. Synthesis of the manganese(III) complexes	61
2.2.3. Structural characterization.....	63
2.3. Experimental	75
2.3.1. Synthesis of the free-base porphyrins	76
2.3.1.1. Symmetric porphyrins	76
2.3.1.2. Asymmetric porphyrins	78
2.3.2. Manganese(III) porphyrins	82
2.4. References	84
Chapter 3. Catalytic activity evaluation of new second-generation manganese(III) porphyrins in oxidation reactions	89
3.1. Results and discussion	91
3.1.1. Oxidation of cyclooctene under homogeneous catalytic conditions.....	91
3.1.1.1. Mn(TDCPyP)Cl and Mn(mono-DCPyP)Cl catalytic activity evaluation.....	91
3.1.1.2. Comparison between the novel catalysts and analogous Mn(III) porphyrins	93
3.1.1.3. Catalytic activity of Mn(TDCPyP)Cl using a mixture acetonitrile/water.....	97
3.1.2. Synthesis and characterization of the heterogeneous catalysts	100
3.1.2.1. Immobilization of Mn(mono-DCPyP)Cl under classic heating.....	100
3.1.2.2. Immobilization of Mn(mono-DCPyP)Cl and Mn(DC-mono-4PyP)Cl on Merrifield resin under microwave assisted irradiation	102
3.1.2.3. Structural characterization of the immobilized porphyrin materials.....	105
3.1.3. Oxidation of cyclooctene under heterogeneous catalysis	114
3.1.3.1. Silica <i>versus</i> Merrifield Resin and the choice of the oxidant	114
3.1.3.2. Comparison of CAT-MR and CAT-4Py-MR catalytic activity.....	122
3.1.4. Oxidation of styrene	126
3.1.4.1. Oxidation of styrene using Mn(mono-DCPyP)Cl or Mn(TDCPyP)Cl and hydrogen peroxide as oxidant under homogeneous conditions	128
3.1.4.2. Oxidation of styrene catalysed by CAT-MR using TBHP as oxidant	130
3.2. Conclusions	131
3.3. Experimental	133
3.3.1. Reagents and Methods.....	133
3.3.2. Synthesis of the heterogeneous catalysts	134
3.3.3. Oxidation reactions.....	135
3.4. References	138

Chapter 4. Oxidation of monoterpenes and other organic compounds catalysed by a Mn(III) PEG-porphyrin	145
4.1. Results and discussion	147
4.1.2. Synthesis and characterization of MnTPP(PEG) ₄ OAc	147
4.1.2. Catalytic oxidation of monoterpenes	150
4.1.2.1. Catalytic oxidation of carvacrol under homogeneous conditions	151
4.1.2.2. Catalytic oxidation of carvacrol and thymol with MnTPP(PEG) ₄ OAc in a biphasic medium	153
4.1.2.3. Catalytic studies with MnTPP(PEG) ₄ OAc in the oxidation of an oregano essential oil using the biphasic medium.....	155
4.1.2.4. Mechanism of thymoquinone formation.....	158
4.1.3. Catalytic oxidation of other organic compounds	158
4.2. Conclusions	160
4.3. Experimental	160
4.3.1. Reagents and Methods.....	160
4.3.2. Synthesis of MnTPP(PEG) ₄ OAc	162
4.3.3. General procedure for the oxidation reactions.....	162
4.4. References	165
Chapter 5. Photodegradation of metoprolol using a porphyrin as photosensitizer	169
5.1. Results and discussion	171
5.1.1. Preparation of the photocatalysts	171
5.1.2. Evaluation of H ₂ TF ₅ PP as photosensitizer for metoprolol degradation under homogeneous conditions	175
5.1.3. Metoprolol degradation in the presence of H ₂ TF ₅ PP-silica as photosensitizer.....	176
5.1.4. Metoprolol degradation under real sunlight, photosensitized by H ₂ TF ₅ PP-silica.....	181
5.1.5. Comparison of metoprolol photodegradation in wastewater treatment effluent and in buffered aqueous solution	183
5.1.6. Identification of the photodegradation products by HPLC-UV-ESI-MS ⁿ	184
5.2. Conclusions	195
5.3. Experimental	196
5.3.1. Chemicals and solutions	196
5.3.2. Synthesis of H ₂ TF ₅ PP and immobilization on the silica support.....	196
5.3.3. Irradiation apparatus	197
5.3.4. Photodegradation experiments in aqueous solutions	198
5.3.5. Solar irradiation experiments.....	199
5.3.6. Photodegradation experiments in wastewater.....	199
5.3.7. HPLC-UV analysis.....	200
5.3.8. HPLC-UV-ESI-MS ⁿ analysis.....	200
5.4. References	202
Final Remarks.....	207

Abbreviations

a.u.	arbitrary units
AOPs	advanced oxidation processes
ATR	attenuated total reflection
B.E.	binding energy
CAT-4Py-MR	chloro[5,10,15-tris(2,6-dichlorophenyl)-20-(pyridin-4-yl)porphyrinate]manganese(III) immobilized on Merrifield Resin
CAT-MR	chloro[5,10,15-tris(2,6-dichlorophenyl)-20-(3,5-dichloropyridin-4yl)porphyrinate]manganese(III) immobilized on Merrifield Resin
CAT-MR-MW	chloro[5,10,15-tris(2,6-dichlorophenyl)-20-(3,5-dichloropyridin-4yl)porphyrinate]manganese(III) immobilized on Merrifield Resin by microwave-assisted heating
CAT-Si	chloro[5,10,15-tris(2,6-dichlorophenyl)-20-(3,5-dichloropyridin-4yl)porphyrinate]manganese(III) immobilized on 3-bromopropylsilica
CYP450	cytochrome P450
d	doublet
dd	double doublet
DDQ	2,3-dichloro-5,6-dicyanobenzoquinone
DMF	dimethylformamide
DMSO	dimethyl sulfoxide
DOM	dissolved organic matter
EDS	energy dispersive spectroscopy
Eq	molar equivalents
ESI-MS	electrospray ionization mass spectrometry
GC	gas chromatography
GC-FID	gas chromatograph equipped with flame ionization detector

GC-MS	gas chromatograph equipped with a mass spectrometer
H ₂ DC-mono-4PyP	5,10,15-tris(2,6-dichlorophenyl)-20-(pyridin-4-yl)porphyrin
H ₂ mono-DCPyP	5,10,15-tris(2,6-dichlorophenyl)-20-(3,5-dichloropyridin-4-yl)porphyrin
H ₂ TDCPP	5,10,15,20-tetrakis(2,6-dichlorophenyl)porphyrin
H ₂ TDCPyP	5,10,15,20-tetrakis(3,5-dichloropyridin-4-yl)porphyrin
H ₂ TF ₅ PP	5,10,15,20-tetrakis(pentafluorophenyl)porphyrin
H ₂ TPP	5,10,15,20-tetraphenylporphyrin
HPLC	high-performance liquid chromatography
HPLC-UV-ESI-MS ⁿ	high-performance liquid chromatography coupled with ultraviolet detector and electrospray ionization tandem mass spectrometry
HRMS-ESI	high resolution electrospray ionization mass spectrometry
IUPAC	International Union of Pure and Applied Chemistry
<i>J</i>	coupling constant
<i>m</i>	multiplet
<i>m/z</i>	mass-to-charge ratio
MALDI (TOF/TOF)-MS	matrix-assisted laser desorption ionization-time of flight mass spectrometry
MCM-41	mobil catalytic material, number 41
Mn(DC-mono-4PyP)Cl	chloro[5,10,15-tris(2,6-dichlorophenyl)-20-(pyridin-4-yl)porphyrinate]manganese(III)
Mn(mono-DCPyP)Cl	chloro[5,10,15-tris(2,6-dichlorophenyl)-20-(3,5-dichloropyridin-4yl)porphyrinate]manganese(III)
Mn(T-4PyP)Cl	chloro[5,10,15,20-tetra(pyridin-4-yl)porphyrinate]manganese(III)
Mn(TDCPP)Cl]	chloro[5,10,15,20-tetrakis(2,6-dichlorophenyl)porphyrinate]manganese(III)
Mn(TDCPyP)Cl	chloro[5,10,15,20-tetrakis(3,5-dichloropyridin-4-yl)porphyrinate]manganese(III)
MR	Merrifield resin

MS	mass spectrometry
MW	microwave
NMR	nuclear magnetic resonance
PEG	polyethylene glycol
PhIO	iodosylbenzene
PPCPs	pharmaceuticals and personal care products
ppm	part per million
Py	pyridine
s	singlet
S/C	substrate/catalyst
SEM	scanning electron microscopy
t	triplet
TBHP	<i>tert</i> -butyl hydroperoxide
TFA	trifluoroacetic acid
THF	tetrahydrofuran
TLC	thin layer chromatography
TMS	tetramethylsilane
UV-Vis	ultraviolet-visible spectroscopy
WWTPs	wastewater treatment plants
XPS	X-ray photoelectron spectroscopy
δ	chemical shift
ϵ	molar attenuation coefficient
λ	wavelength
λ_{\max}	wavelength of maximum absorbance

CHAPTER 1

Introduction

Chapter 1. Introduction

Porphyrins and metalloporphyrins, besides their presence in nature playing important roles in biological systems, have been the subject of extensive studies in different areas of research. One of the most notable examples is the use of synthetic metalloporphyrin complexes inspired by biology as catalysts in the transformation of diverse compounds, such as the oxidation of abundant and inexpensive alkenes and alkanes to value-added chemicals. Another area that has received great attention, owing to growing environmental concern, is the use of porphyrins and their analogues as photosensitizers in the degradation of organic pollutants.

In this introductory chapter an overview of the main aspects concerning the chemistry and properties of porphyrins and related compounds will be given. The use of metalloporphyrins as oxidative catalysts, inspired by natural biocatalysts, will be highlighted with special emphasis into the development of supported catalysts. Finally, the potential use of porphyrins as photosensitizers for the degradation of chemicals in a water remediation context will be described.

1.1. Porphyrins and related compounds

Porphyrins are purple pigments with a structure consisting in an aromatic macrocycle formed by four pyrrole-type units linked by methinic bridges (**Figure 1.1**).

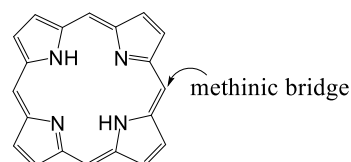


Figure 1.1. Structure of the unsubstituted porphyrin macrocycle.

The nomenclature of porphyrins is usually based on one of two systems: the nomenclature described by Hans Fischer and the nomenclature recommended by IUPAC (**Figure 1.2**).

In the nomenclature proposed by Hans Fischer, the basic ring structure is called porphin; this term however fell into disuse and became porphyrin today. The β -pyrrolic carbons of the macrocycle are numbered from 1 to 8 and the pyrrole carbons next to the nitrogen atoms are called α -positions and remain unnumbered; finally, the four carbons of

the methinic bridges are called *meso*-positions and the Greek letters α , β , γ , δ are attributed (**Figure 1.2** left).¹⁻³ The Fischer nomenclature system is based on trivial names and does not give any structural information. In the case of positional isomers, “type isomers” nomenclatures are employed, using Roman numerals to distinguish them.^{1,2} The Fischer’s system is straightforward for naming simple porphyrins and is still used a few times, however in the case of macrocycles with high complexity, with different substituents on the β - and *meso*-positions, this system becomes disordered. In addition, the need to introduce new trivial names with the emergence of more and more porphyrin molecules made the Fischer’s system unsuitable. It was thus necessary to introduce a more systematic nomenclature to help interdisciplinary communication, considerably diminishing the need for new trivial names. Thus, the IUPAC-IUB Joint Commission on Biochemical Nomenclature introduced some recommendations for the nomenclature of tetrapyrroles.^{4,5} In the case of the nomenclature recommended by IUPAC, all the atoms are numbered, including the nitrogen atoms (**Figure 1.2** right).²⁻⁵ The use of the generic terms *alpha*-, *beta*- and *meso*-positions was discouraged to avoid possible misunderstanding with stereochemical designations.^{4,5}

In the present work the nomenclature of the compounds was generally attributed according with the recommendations of IUPAC. However, for a better understanding, in some cases the designation as β - and *meso*-positions may appear in the text.

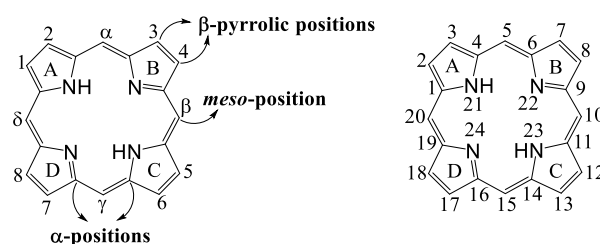


Figure 1.2. Fischer’s numbering system (left) and IUPAC numbering system (right).

Observing the structure of porphyrins, we can check that they have 22 π -electrons, which is in accordance with the Huckel’s rule for aromaticity ($4n + 2$), with $n = 5$; however, only 18 of these electrons are considered responsible for the delocalization pathway, giving ($4n + 2$), with $n = 4$.^{2,3} In other words, only 18 π -electrons contribute to the aromatic character of the macrocycle, and this fact explains the maintenance of aromaticity in chlorins (20 π -electrons), bacteriochlorins and isobacteriochlorins (18

π -electrons). Thus, the porphyrin macrocycle can undergo one or two reductions without losing its aromatic character. Porphyrins can be reduced producing chlorins, in which two hydrogen atoms have been added to the β - β double bond of one of the pyrrolic units (**Figure 1.3**).² Chlorins can suffer an extra reduction, originating a bacteriochlorin if the reduction occurs on opposing pyrrolic rings, or an isobacteriochlorin if the reduction occurs in adjacent pyrrolic rings (**Figure 1.3**).

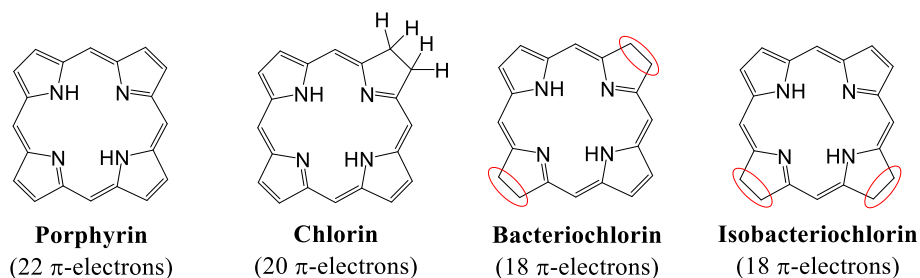


Figure 1.3. Porphyrins' macrocycle and their reduced analogues.

Porphyrins and their related macrocycles, such as chlorins and bacteriochlorins, particularly in their metallated forms, play a crucial role in biological systems.² For example, the iron(II) complex of protoporphyrin IX (**Figure 1.4**) is present as prosthetic group in haem proteins, such as haemoglobin and myoglobin, responsible for oxygen and electron transport and storage. The same group is also present in biocatalysts, such as catalases, peroxidases, lignin peroxidases, or cytochromes P450.^{2,3} The free-base porphyrins are generally present in organisms as precursors of metalloporphyrins and are accumulated and excreted in patients with a physiological disorder called porphyria.³

In chlorophylls, the central metal is magnesium (**Figure 1.4**) and their functions are related with the capture of light photons in near ultra-violet and red regions of the visible spectrum.³

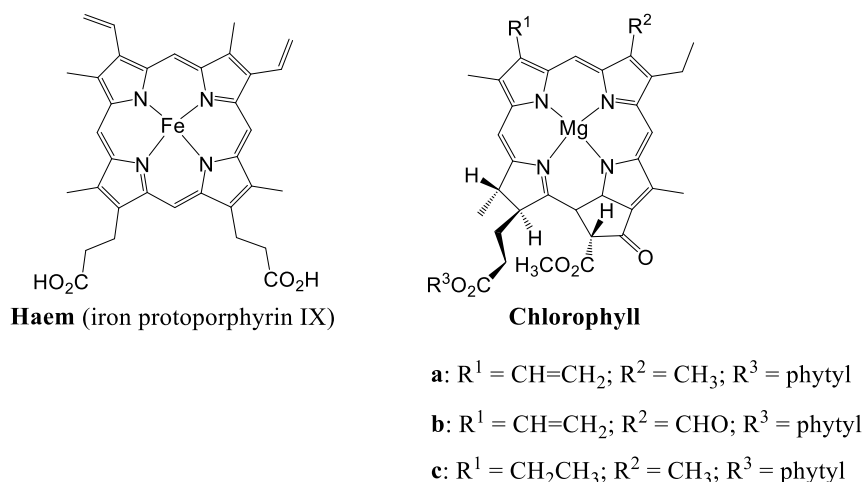


Figure 1.4. Haem and some chlorophylls' structures.

The confirmation of the structure of a porphyrin can require different spectroscopic techniques, but as first approach ^1H NMR and UV-Vis spectroscopies are considered two of the most important tools. The aromaticity of these compounds is easily confirmed by their ^1H NMR spectra. The resonance of the β -pyrrolic and of the *meso* protons appear at low field ($\delta = 8\text{-}9$ ppm and $10\text{-}11$ ppm, respectively) due to the diamagnetic ring current. The *meso* protons are more deshielded, because they are attached to electron-deficient carbons. Contrarily, the inner NH protons appear upfield, usually to the right of TMS (negative δ value between -2 and -3 ppm). This differences between the values of the chemical shifts of the inner protons ($-\text{NH}$) and of the peripheral ones is related to the high effect of magnetic anisotropy resulting from the flow of electronic current around the ring. The ring current deshields protons from the external magnetic field outside the macrocycle and shields the protons inside the macrocycle.^{2,6}

Porphyrins and their analogues have typical absorption spectra, and therefore they can be easily identified by UV-Vis spectrophotometry.^{3,7} In general, the absorption spectra consist of two distinct regions, in the near-ultraviolet and the visible, and the position and intensity of the bands depend on the type of macrocycle.² Typically, porphyrins have an intense absorption band around $390\text{-}425$ nm, depending on whether the porphyrin is β - or *meso*-substituted, which is called the Soret band, and also four weaker bands (I, II, III, IV) between $480\text{-}700$ nm, called the Q bands (**Figure 1.5**).^{2,3,7} The Soret band is related to the delocalization of the 18π -electrons thus being common to all these macrocycles. The number and intensity of the Q bands can give information about the substitution pattern of

the porphyrin and also if we have a metal complex. Metalloporphyrins are more symmetric than the corresponding free-base porphyrins and, for that reason, the Q bands region consists of only two bands, usually called α and β bands.^{2,3,7}

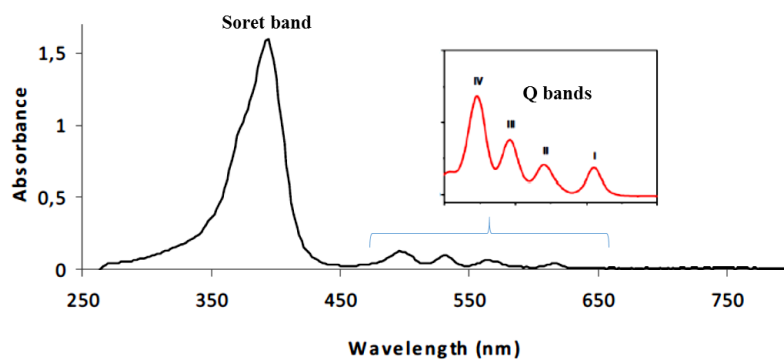


Figure 1.5. Typical UV-Vis absorption spectrum of a free-base porphyrin.⁸

1.2. Metalloporphyrins as catalysts in oxidation reactions

1.2.1. Catalytic oxidation as a tool for green and sustainable chemistry

Oxidation reactions are transformations extensively used in the manufacture of both bulk and fine chemicals, often having a negative impact on the environment. Many oxidations, especially in fine chemicals and pharmaceuticals production, are still carried out using aggressive and ecologically unacceptable stoichiometric amounts of oxidants (e.g. HNO_3 , $\text{K}_2\text{Cr}_2\text{O}_7$, KMnO_4) generating large amounts of wastes.⁹⁻¹² There is a pressing need to replace traditional processes by cleaner catalytic alternatives that allow the use of benign oxidants such as molecular oxygen or hydrogen peroxide.⁹⁻¹² The ideal oxidant would be molecular oxygen, which is inexpensive and abundantly available. However, safety issues, allied to its difficult activation at mild conditions and difficult control of chemo-, regio- and stereoselectivities are limitations to its large-scale application.¹³⁻¹⁵ Besides molecular oxygen, hydrogen peroxide is also considered an ideal oxidant since it still has high active oxygen content (47% based on 100% H_2O_2), releases only water as by-product and is simple to handle.¹⁶ Organic peroxides (e.g. *tert*-butyl hydroperoxide) are also attractive oxygen donor reagents since the by-product can be readily recycled by reaction with hydrogen peroxide and, although an extra step is necessary, afford water as by-product in the overall process.¹⁶ In addition to the oxidant, the choice of the solvent is also an important issue for a greener process. The solvent should be relatively non-toxic and relatively non-hazardous, preferably water or aqueous biphasic systems that allow the separation of the homogeneous catalyst from the reactants and its recycling.¹⁷ The recovery and reuse of the catalyst is also an important aspect to consider in the development of more sustainable oxidation reactions, which can also be achieved by the immobilization of efficient homogeneous catalysts in solid supports.¹⁸

1.2.2. Cytochromes P450 - oxidation catalysts present in nature

It is well-known that cytochrome P450 (CYP450) enzymes (haem-containing monooxygenases) are involved in the oxidative metabolism of a wide variety of xenobiotics (e.g., drugs and pollutants) and endogenous products (e.g., sterols and fat-soluble vitamins) in mammals.¹⁹⁻²² The way for the elimination of xenobiotics is an

enzymatic biotransformation that is usually initiated by oxidation reactions, leading to high rates of clearance, poor bioavailability, and, in some cases, toxic metabolites. The active centre of a CYP450 enzyme contains an iron(III) protoporphyrin-IX species with a cysteine thiolate from a peptide chain as the fifth Fe(III) ligand, and a free sixth coordination site that is used as a binding site for molecular oxygen (**Figure 1.6**). These enzymes are monooxygenases and, therefore, one oxygen atom from molecular oxygen is transferred to the substrate while the other oxygen atom is reduced to a water molecule (Eq. 1). The two electrons needed for this reductive activation of molecular oxygen is usually provided by NADPH *via* a reductase.

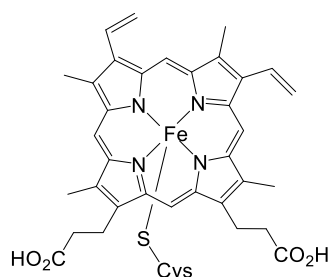
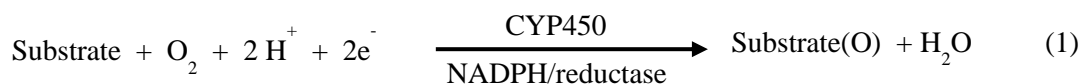
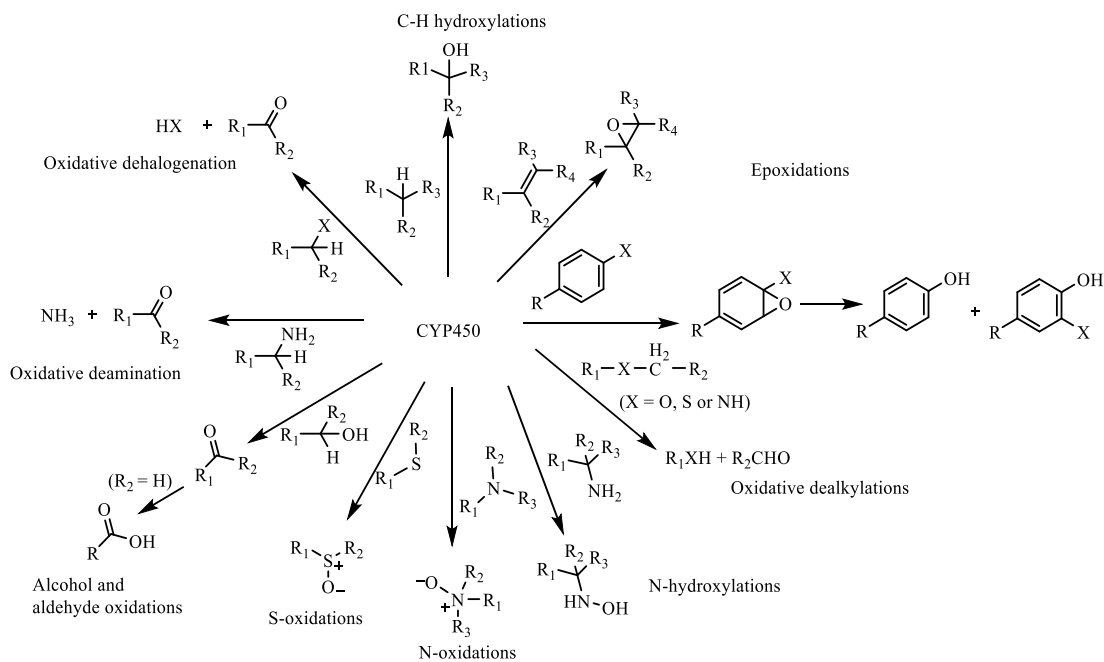


Figure 1.6. Active centre of a CYP450 enzyme.



These CYP450 enzymes catalyse diverse types of oxidation reactions, as illustrated in **Scheme 1.1**.^{23–25} Some examples are the hydroxylation of inert C-H bonds of alkanes; when the C-H bond hydroxylation occurs α to a heteroatom (O in ethers, N in amines or amides or S in thioethers), a hydrolytic cleavage occurs leading to *O*-, *N*- or *S*-dealkylations; hydroxylation of *N*-H bonds of secondary or primary amines; epoxidation of olefins and aromatic epoxidation/hydroxylation; formation of *N*-oxides from tertiary amines, and sulfoxides and sulfones from thioethers.²⁴



Scheme 1.1. The main oxidation reactions catalysed by CYP450 enzymes.^{23–25}

The great diversity of reactions catalysed by CYP450 enzymes appears to be related to the ability of their iron to exist under a great variety of oxidation states with different reactivities. The most generally accepted mechanism for the major events in CYP450 enzymes catalysis reactions is shown in **Scheme 1.2**.^{23,26–35}

The resting form of the enzyme is a six-coordinate low spin ferric state, **1**, with water as the exchangeable distal ligand *trans* to the proximal cysteinate. In the presence of the substrate, the axial water molecule is removed, generating the five coordinate high-spin ferric state, **2**. The conversion of the ferric iron from low to high spin induces a change in the redox potential of the iron centre from -330 to -173 mV after substrate binding.^{23,27} Thus, the modification in the coordination sphere facilitates the reduction of the pentacoordinated ferric centre by an associated reductase with a NADPH-derived electron to generate a ferrous state, **3**. The binding of molecular oxygen to the ferrous haem iron leads to a stable ferric cytochrome P450-dioxygen complex, **4**. A second electron reduction allows the formation of a ferric peroxide adduct **5**, which can be responsible for some reactions catalysed by CYP450 involving a nucleophilic oxidant intermediate such as the oxidative decarboxylation of aldehydes.^{24,27,30,36,37} The peroxo-iron species **5** can be protonated giving the hydroperoxide complex, **6**. This hydroperoxo-iron complex has been considered an active intermediate in epoxidation and hydroxylation reactions.^{38–40} Further protonation of **6** leads to the heterolytic cleavage of the O-O bond with loss of a water

molecule to form a high-valent oxo-iron species **7**, which is believed to be the main active electrophilic oxidant in CYP450. The main probable state for this reactive intermediate is the oxo-iron(IV) π -cation radical, **7** (equivalent to the oxo-iron intermediate of peroxidase enzymes called compound I). This proposal is corroborated by studies using synthetic models, namely iron porphyrins in the presence of oxygen donors.^{41–46} However, some studies demonstrated that the reactive species has also the involvement of a perferryl (**7a**) and an iron(IV)-oxyl (**7b**) states (**Scheme 1.3**).^{27,38,47} Theoretic calculations showed the possibility of compound I behave as a “chameleon” species acquiring multiple states, with different reactivities, depending on the environmental conditions.⁴⁸ The oxo-iron intermediate **7** abstracts a hydrogen atom from the substrate, giving the hydroxo-iron **8** (compound II) and a substrate radical (R \cdot), followed by radical rebound to give the enzyme-product complex, **9**.^{32–35,49} Then, by product release (ROH in a typical hydroxylation) and coordination of water, complex **1** is regenerated.

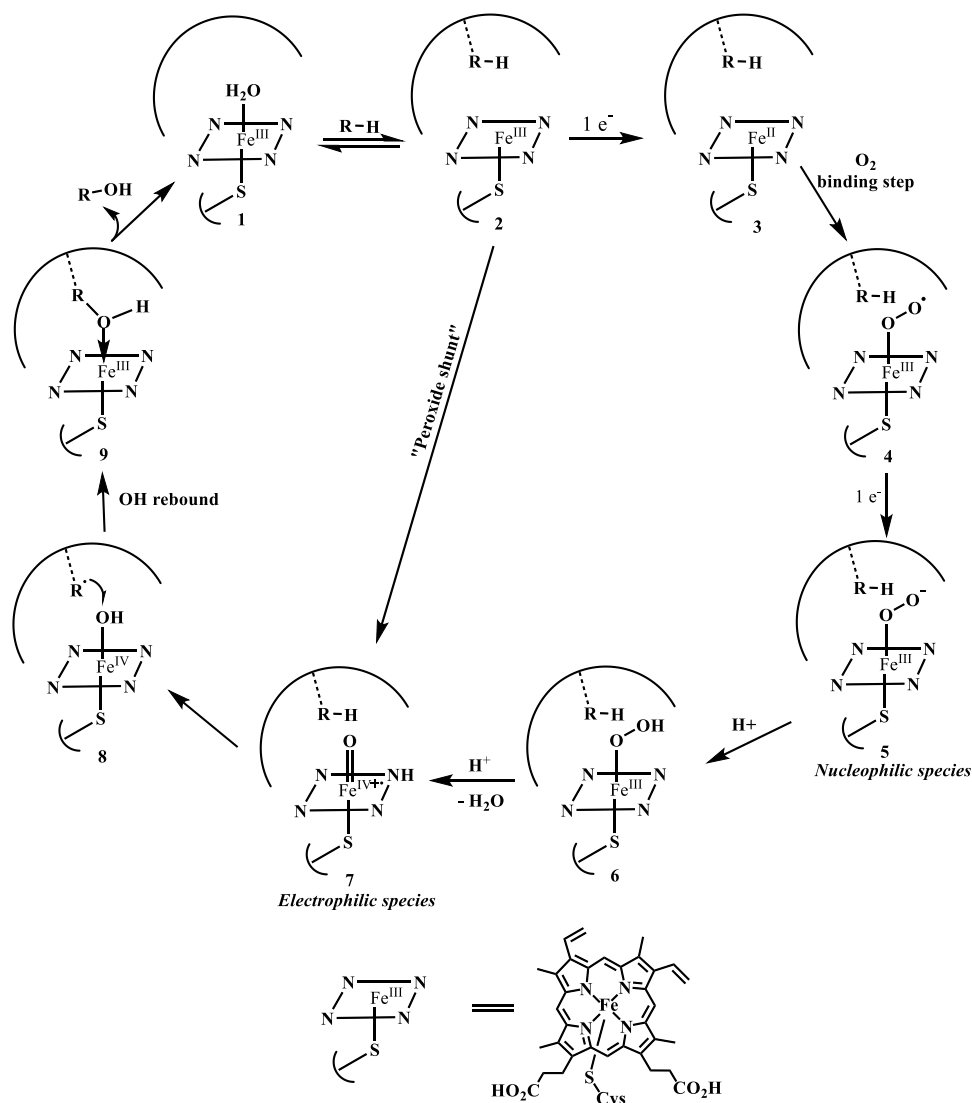
Some oxygen atom donors such as alkyl peroxides, peroxyacids, sodium chlorite, sodium periodate, and iodosylbenzene can replace molecular oxygen and the two electrons needed in the normal cycle and react with intermediate **2** giving directly hydroperoxide complex, **6** or the ferryl-oxo porphyrin π -cation radical intermediate, **7**.²³ This process is usually designated as “short circuit” or “peroxide shunt”.

1.2.3. Metalloporphyrins as catalytic biomimetic systems of CYP450

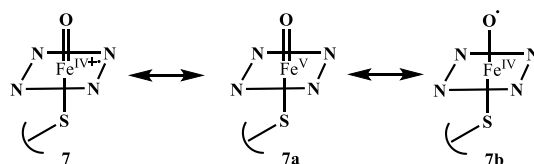
Many advances have been made in the last decades in the characterization of the species involved in the CYP450 catalytic cycle. Yet, the exact nature of the active species responsible for the oxygen insertion step is still a matter of discussion.^{31,38,50} These species have a short lifetime, turning difficult their characterization by classical methods.

The use of metalloporphyrins as oxidation catalysts emerged as an attempt to better understand these CYP450-mediated oxidation processes. In fact, metalloporphyrins, in the presence of active oxygen donors can catalyse a broad range of CYP450-mediated reactions, including epoxidation, aliphatic and aromatic hydroxylation or oxidation of heteroatoms.^{32,41–43,45,51–58} When the substrates belong to a group of *in vivo* xenobiotics, this biomimetic strategy brings the benefit of producing several metabolite candidates, which might be helpful for the identification of those metabolites produced *in vivo*.⁴⁵ Moreover, as the production of metabolites often requires *de novo* synthesis, the access to metabolites

of key biological significance is essential for evaluating their toxicological and pharmacological profile.⁵⁹



Scheme 1.2. Catalytic cycle of cytochrome P450.^{23,26–35}



Scheme 1.3. The three different possible resonance structures for the electrophilic high-valent iron-oxo species in CYP450.^{23,27,30}

The first effective CYP450 model system based on metalloporphyrins for alkene epoxidation and alkane hydroxylation was reported by Groves and co-workers in 1979 by using the iron(III) complex of the 5,10,15,20-tetraphenylporphyrin [Fe(TPP)Cl] as catalyst

and iodosylbenzene (PhIO) as oxygen atom donor.⁶⁰ Therefore, the first-generation of metalloporphyrins as model systems of CYP450 was based on the metal complexes of **H₂TPP** (**Figure 1.7**).^{61–64} During this period, Groves and collaborators isolated and characterized oxo-chromium(V) and oxo-manganese(V) complexes which were able to hydroxylate alkanes and epoxidize olefins.^{61,63} Later, the same group isolated and characterized for the first time a high-valent oxo-iron porphyrin complex with spectral characteristics of an oxo-iron(IV)-porphyrin π -cation radical intermediate identical to peroxidase compound I.⁴⁶

The metalloporphyrins of this first-generation have the drawback of being rapidly destroyed or inactivated, namely by affording catalytically inactive μ -oxo species under the oxidative conditions of the reaction media. Therefore, some progresses have been made in order to develop more robust and efficient biomimetic oxidation catalysts.^{52,65–67} The introduction of electron-withdrawing or bulky substituents at the *meso*-phenyl rings of the macrocycle, as is the case of the 5,10,15,20-tetrakis(2,6-dichlorophenyl)porphyrin (**H₂TDCPP**) or the 5,10,15,20-tetrakis(pentafluorophenyl)porphyrin (**H₂TF₅PP**) (**Figure 1.7**), led to the so-called second-generation of metalloporphyrins known as more resistant towards oxidative degradation.^{65,66} Subsequently, electron-withdrawing substituents were also introduced at the β -pyrrolic positions, thus resulting in the third-generation of metalloporphyrins which, due to an increase on the electrophilicity of their oxo-metal active species, showed to be more efficient, leading to high product yields and selectivities.^{42,67} However, the third-generation of metalloporphyrins not always give rise to more active and stable oxidation catalysts.^{68–72} A possible reason for its lower efficiency may be related with the steric effects due to an excess of electron-withdrawing substituents on the macrocycle.⁷⁰ Studies with third-generation manganese porphyrins also indicated that the presence of chlorine atoms at the β -pyrrolic positions stabilizes Mn(II) being unfavourable to the formation of the active oxo-iron species.^{71,72} Furthermore, the second-generation metalloporphyrins are, in general, more easily prepared and an increase in selectivity to the desired products can be obtained by varying other parameters such as solvent, oxidant, and axial ligands.⁷⁰ For these reasons, the work presented in this thesis is based mainly on the use of second-generation metalloporphyrins as oxidation catalysts.

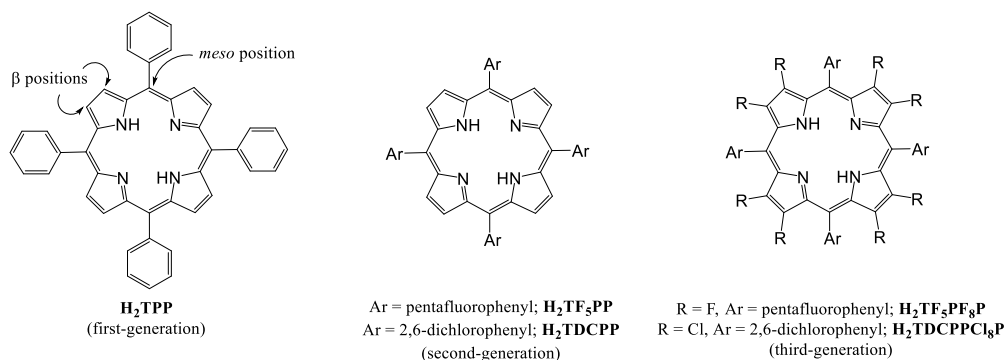


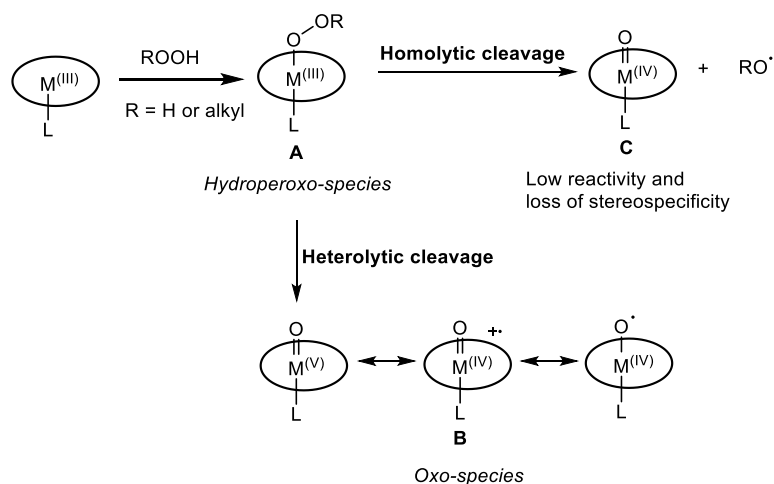
Figure 1.7. The structures of the main representative porphyrin ligands of the first-, second- and third-generation catalysts.

It has been found that not only iron(III) porphyrins are effective catalysts in oxidation reactions, but also chromium(III),^{73,74} ruthenium(III)^{53,75,76} and manganese(III) complexes.^{62,63} Though, iron(III) and manganese(III) porphyrins are considered better oxidation catalysts.^{54,56,77} In addition, manganese(III) porphyrins have been used as analogues of iron(III) porphyrins in models of CYP450 systems due to the enhanced stability of their oxo-manganese species over the corresponding oxo-iron species.⁷⁷

Several oxygen atom donors were used in these biomimetic systems, such as iodosylarenes,^{60,65,71} hypochlorites,⁷⁸ peracids,⁷⁹ alkyl hydroperoxides,⁸⁰ hydrogen peroxide,^{56,81} and molecular oxygen.^{82,83} As previously stated, after molecular oxygen the most appropriate oxidant for a cleaner process is hydrogen peroxide.

Concerning the mechanism of metalloporphyrins' catalysed oxidation reactions, similarly to cytochrome P450, high-valent oxo or hydroperoxo-type intermediates are supposed to be the main active oxidizing species.

In the oxidation of hydrocarbons using H_2O_2 or an alkyl hydroperoxide (ROOH) as oxygen donors two different pathways (**Scheme 1.4**) may occur, depending on the reaction conditions: the heterolytic or the homolytic cleavage of the oxygen-oxygen bond of the hydroperoxo-type intermediate (**A**).^{84–87} The heterolytic cleavage leads to the formation of the active oxo-species (**B**), whereas homolytic cleavage leads to the formation of a M(IV)-oxo complex (**C**), which is less active and gives rise to less stereospecific reactions,⁸⁸ and $\cdot OH$ or $\cdot OR$ radicals.⁸⁷ This last pathway is also responsible for the decomposition of the peroxide.^{86,89} It was also shown that the heterolytic or the homolytic cleavage of the oxygen-oxygen bond of M(III)-O-OR intermediate (**A**) is greatly affected by the reaction conditions.^{84,85,88,90–92}



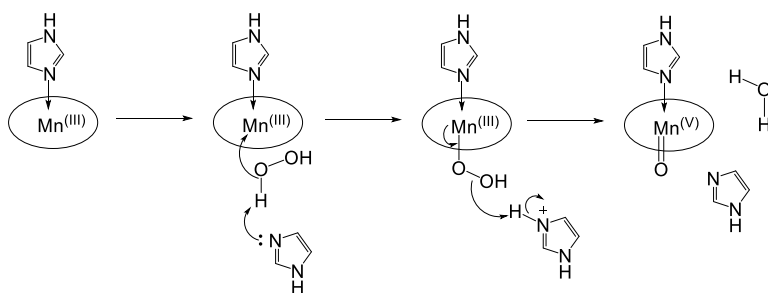
Scheme 1.4. The different courses for the cleavage of the oxygen-oxygen bond of the hydroperoxo-type intermediate (A).

The preferential formation of the hydroperoxo or the oxo species as oxidizing intermediate depends on the reaction conditions, namely the electron-withdrawing characteristics of the porphyrin nucleus, the electronegativity of the central metal, the solvent and the presence of a co-catalyst.^{81,92–95} Nam *et al.*^{93,94} established that in iron porphyrin catalysed oxidation reactions, using an aprotic solvent, the species responsible for oxygen atom transfer, in some cases, is the iron(III)-hydroperoxo intermediate instead the high-valent iron-oxo intermediate. Later, Rebelo *et al.*⁹⁵ have shown that the hydroperoxo active species is favoured in the presence of a protic solvent, iron(III) electron-withdrawing porphyrins in absence of a co-catalyst, while the oxo-species was considered the main active oxidizing entity using an aprotic solvent, manganese as the central atom, porphyrin ligands with lower redox potential and a buffering substance as co-catalyst.

Earlier, Mansuy and co-workers have demonstrated the key role of the addition of imidazole as co-catalyst in Mn(III) porphyrin catalysed oxidation reactions using H₂O₂ as oxidant.^{96,97} Other co-catalysts such as pyridine or imidazole axial bases in the presence of lipophilic carboxylic acids⁹⁸ and tetrabutylammonium hydroxide or other bases such as sodium carbonate or sodium acetate⁹⁹ have improved the Mn(III) porphyrin/H₂O₂ oxidizing system. The main problem when using imidazole as co-catalyst is its possible destruction in the oxidizing medium.⁹⁹ Later, Mansuy and co-workers developed an efficient system based on Mn(III) porphyrins, H₂O₂ and ammonium acetate as co-catalyst for the epoxidation of alkenes and hydroxylation of alkanes.¹⁰⁰

The co-catalyst has a role comparable to that of proximal ligands of haem enzymes, which are essential for the heterolytic process by serving as a strong internal electron donor to destabilize the oxygen-oxygen bond of the iron(III)-hydroperoxo intermediate (“push effect”) and acting as an acid/base to facilitate the heterolytic cleavage (“pull effect”) to obtain the corresponding high-valent iron-oxo species.¹⁰¹ Mansuy and collaborators have evidenced the crucial role of imidazole to act both as proximal ligand and as acid-base catalyst at the distal site to favour the heterolytic cleavage of the peroxydic oxygen-oxygen bond (**Scheme 1.5**).⁹⁷

Thus, systems based on Mn(III) porphyrins of the second-generation using a suitable co-catalyst, such as ammonium acetate and H₂O₂ as oxidant are especially efficient namely for epoxidation of alkenes and hydroxylation of alkanes and electron-rich aromatic rings.



Scheme 1.5. The role of imidazole in olefin epoxidations with H₂O₂ catalysed by manganese porphyrins.⁹⁷

1.2.4. Immobilization of porphyrins on solid supports

Synthetic metalloporphyrins, as already described, have been successfully applied as biomimetic catalysts in several oxidation reactions in homogeneous conditions. However, the low yields usually obtained in the synthesis of porphyrins and the difficulty to recover the catalyst from the reaction medium for future reuse makes them highly costly catalysts, thus limiting their industrial application.¹⁰² As a result, efforts have focused on the search for heterogeneous catalysts through the immobilization of metalloporphyrins on solid supports. There are some advantages when using supported catalysts: easy separation and recycling of the catalyst; possibility of continuous processing; high stability towards heat and pressure. Additionally, the immobilization of metalloporphyrins on solid supports prevents the complex self-oxidation, and also the aggregation or bimolecular self-destruction, recurrent in homogeneous conditions, which leads to catalytic species deactivation and the consequent loss of catalytic activity.^{103–105} However, the immobilization of a homogeneous catalyst usually results in a marked loss of activity. The possibility of leaching of the metalloporphyrin from the support is other aspect that must be considered.

The strategies used to anchor metalloporphyrins to solid supports usually involve interactions between the complex and the support such as adsorption, electrostatic or coordinative binding, covalent bonding, or encapsulation.^{57,106,107} The adsorption method consists on non-specific weak interactions (van der Waals or dipole-dipole attractions) between the metalloporphyrin and the support surface.^{108,109} The electrostatic binding is related to interactions between a positively or negatively charged metalloporphyrin and an oppositely charged support.^{110–116} The easy preparation of the catalytic materials is the main advantage of these two immobilization methods, however they are based on weak interactions between the metalloporphyrin and the support, being more vulnerable to the reaction conditions and the consequent leaching.

Metalloporphyrins may also be anchored to an organic or inorganic support by covalent bonding.^{117–132} This strategy allows a strong interaction between the metalloporphyrin and the support because the immobilization occurs by covalent bonds; therefore, by using this approach the leaching problems can be minimized. However, this strategy may require the chemical modification of the macrocycle or/and the support.

Coordinative binding is also a widely used method to immobilize metalloporphyrins.^{103,133–137} Lewis bases such as pyridine or imidazole, which have high affinities for the axial coordination with the metal centre of the porphyrin, can be covalently linked to the solid support, being the metalloporphyrin posteriorly anchored through the metal. This approach avoids the need for a co-catalyst and often improves catalytic activity and selectivity,¹⁰³ but can be quite sensitive to solvent effects and competitive binding of ligands.

The encapsulation method consists in the physical entrapment of the metalloporphyrin inside the pores or cavities of a polymer or inorganic material, usually by the so-called “ship-in-a-bottle” method, which involves the synthesis of the macrocycle inside the support.^{138–141} The complex obtained at the end of the encapsulation process is expected to be larger than the pores of the support, in order to prevent leaching issues. However, the pore size must be large enough to facilitate the flow of reactants and products in and out the cavities of the support.

A variety of supports have been used to immobilize metalloporphyrins, namely inorganic carriers such as molecular sieves,^{109–115,128,140} silica,^{102,103,120,122,134–136} zeolites,^{116,138,139,141,142} clays,^{143,144} as well as organic polymers.^{117,118,129–132,145,146} Some examples concerning the immobilization of metalloporphyrins on silica and organic polymers, specially Merrifield resins, will be given since they were chosen as solid supports in the present work.

1.2.4.1. Silica

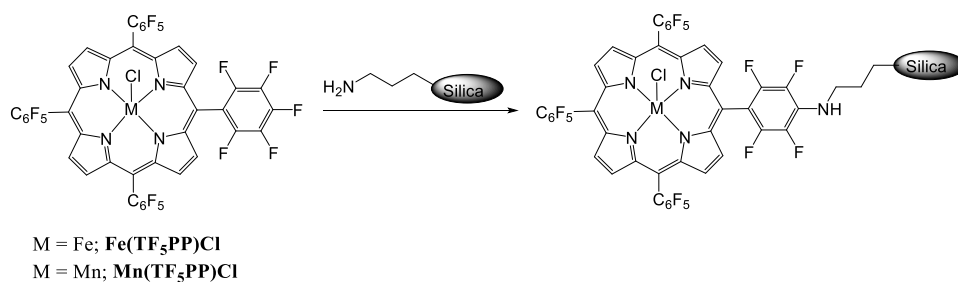
Silica is considered one of the most attractive inorganic supports due to its high thermal and chemical stability, nontoxicity, low cost, and also the large surface area which facilitates the access of the substrate to the active site.¹⁴⁷ Moreover, silica is compatible with water, therefore its use does not represent an obstacle in reactions where water is used as solvent. Silica can also undergo functionalization to become more suitable for the immobilization of a wide range of catalysts.¹⁰²

Battioni *et al.* prepared a supported manganese porphyrin catalyst taking the advantage of a very strong interaction between silica and tetracationic porphyrins.¹⁴⁸ The heterogeneous catalyst was prepared by strong adsorption of manganese(III) complex of the tetracationic 5,10,15,20-tetrakis(4-*N*-methylpyridiniumyl)porphyrin [**Mn(T4MPyP)Cl**]

on silica. The supported catalyst, containing about 10% (w/w) of adsorbed manganese porphyrin, was found to be very efficient for cyclooctene epoxidation using PhIO as oxidant (95% yield, 13 turnovers per min). The authors compared the efficiency of this silica-based catalyst with anionic catalysts supported on alumina or magnesia and higher rates were obtained with the tetracationic catalyst supported on silica. Furthermore, the supported catalyst was stable to oxidative degradation, maintaining its catalytic performance, even when 30 successive additions (1 addition per h) of 1000 equivalents of PhIO (relative to Mn) were added. The silica-based catalyst was also tested for alkane hydroxylation and better results were obtained, when compared with the corresponding soluble manganese porphyrins, with higher alcohol yields and alcohol:ketone ratios.¹⁴⁸

To improve the metalloporphyrin adsorption onto silica gel, some research groups activate silica by creating charged groups or modifying the inorganic support surface with functional groups. The silica modification leads to different kinds of interactions between the metalloporphyrin and the matrix of the support such as covalent, coordinative, and electrostatic interactions. For example, the amino-functionalization of silica allows the covalent interaction with metalloporphyrins which have carboxyl groups leading to the formation of peptide type bonds.

These amino-functionalized silica supports also permit the nucleophilic substitution of good leaving groups, such as chlorine or fluorine atoms, which may be present in the metalloporphyrins. Battioni *et al.* used this strategy to anchor several polyhalogenated metalloporphyrins.¹²⁰ The supported catalysts were obtained through a selective nucleophilic substitution of the *para*-halogen atoms of the porphyrin *meso*-aryl groups by the amino function of the polymer (**Scheme 1.6**). The supported catalysts showed to be active for cyclooctene epoxidation and for cyclohexane and heptane hydroxylation, using PhIO as oxidant. The cyclooctene epoxidation yields varied from 80 to 100% and the best results were obtained using the iron(III) and the manganese(III) complexes of 5,10,15,20-tetrakis(pentafluorophenyl)porphyrin [**Fe(TF₅PP)Cl** and **Mn(TF₅PP)Cl**, respectively] bound to silica.¹²⁰

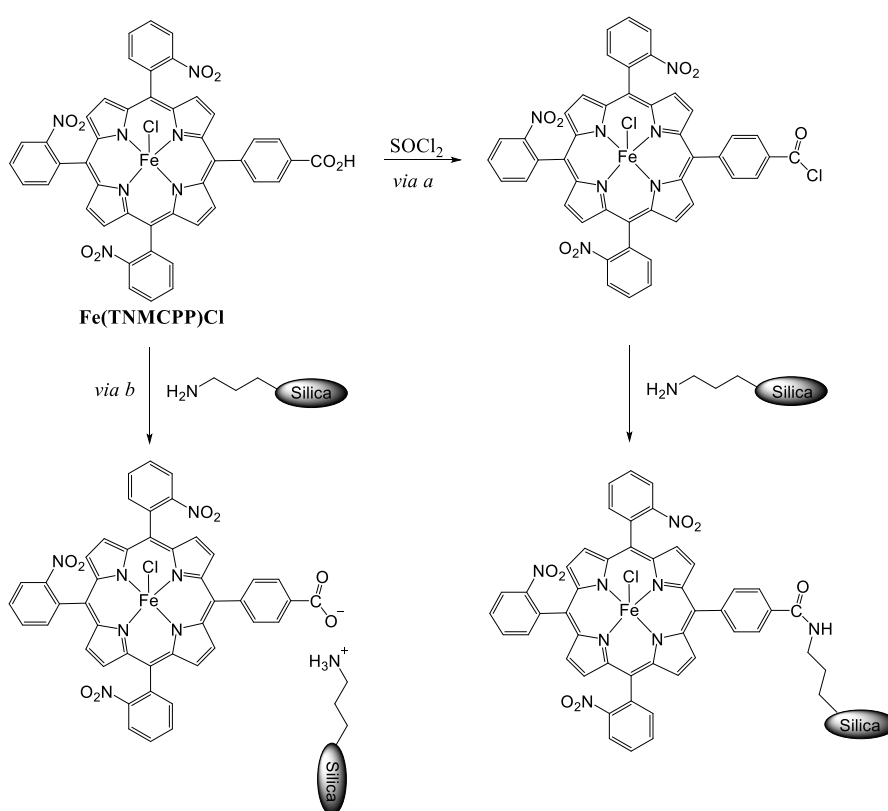


Scheme 1.6. Strategy used by Battioni *et al.* to covalently immobilize polyhalogenated metalloporphyrins onto an amino-functionalized silica support.¹²⁰

Assis and co-workers anchored the manganese and iron complexes of 2,3,7,8,12,13,17,18-octachloro-5-(pentafluorophenyl)-10,15-20-tris(2,6-dichlorophenyl)porphyrin [**Mn(Cl₈PFTDCPP)Cl**] and [**Fe(Cl₈PFTDCPP)Cl**], and the manganese complex of 5-(pentafluorophenyl)-10,15,20-tris(2,6-dichlorophenyl)porphyrin [**Mn(PFTDCPP)Cl**] on aminopropyl-functionalized silica by nucleophilic substitution of the *para*-fluorine atom of the metalloporphyrin aryl substituent with the amino group of the functionalized silica.^{149,150} The obtained materials were tested as catalysts in the oxidation of alkanes and alkenes, using both PhIO and hydrogen peroxide as oxidants. The authors observed that when using PhIO as oxidant, the second-generation manganese porphyrin, **Mn(PFTDCPP)Cl**, was more efficient for the epoxidation of alkenes, while the **Mn(Cl₈PFTDCPP)Cl** presented better results for the hydroxylation of alkanes.¹⁴⁹ The supported **Mn(PFTDCPP)Cl** showed to have the same activity as the homogeneous catalyst and to be stable in the recycling experiments. The supported **Mn(Cl₈PFTDCPP)Cl** and **Fe(Cl₈PFTDCPP)Cl**, however, showed to be less efficient than the corresponding homogeneous catalysts.^{149,150}

The same research group synthesized iron(III) porphyrins containing nitro substituents at the *ortho* positions and -COOH substituents at the *para* positions of the *meso*-phenyl rings of the porphyrin.¹⁵¹ The iron(III) porphyrins were tested as homogeneous catalysts in the oxidation of alkenes and alkanes using PhIO as oxidant and proved to be efficient and selective catalysts for alkene epoxidation and alkane hydroxylation. The iron(III) complex of 5,10,15-tris(2-nitrophenyl)-20-(4-carboxyphenyl)porphyrin [**Fe(TNMCPP)Cl**] was anchored to the aminopropyl-functionalized silica through two different strategies: on one hand, the catalyst was covalently bound to the amino group of the functionalized silica through the -COOH group

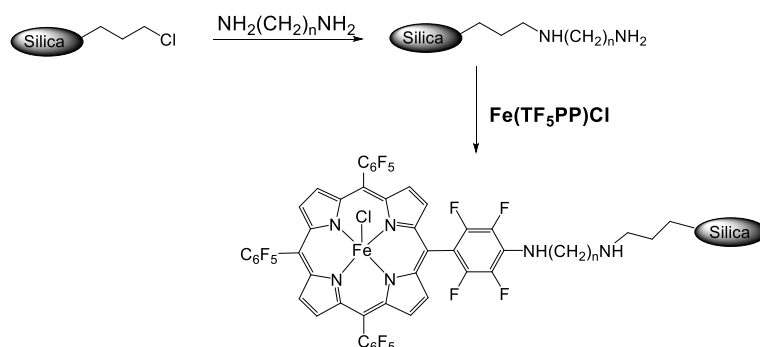
of the metalloporphyrin, after its activation with SOCl_2 (**Scheme 1.7** - *via a*); on the other hand, the iron porphyrin was supported on silica through electrostatic binding (**Scheme 1.7** - *via b*).¹⁵¹ The heterogeneous catalyst resulting from the covalent bonding revealed to be highly efficient for alkene epoxidation; the heterogeneous catalyst resulting from the electrostatic interaction, however, presented low catalytic activity for hydrocarbon oxidation. The authors attributed the low efficiency of this catalyst to the higher polarity of the support and a possible bis-axial coordination among the free amino groups of the silica and the iron centre of the porphyrin, which inhibit the interaction between the non-polar substrates and the catalyst.¹⁵¹



Scheme 1.7. The two different strategies used by Assis and co-workers in the immobilization of $\text{Fe}(\text{TNMCPP})\text{Cl}$ onto an aminopropyl-functionalized silica support. Activation with SOCl_2 and covalent anchorage through the $-\text{COOH}$ group of the metalloporphyrin (*via a*); immobilization through electrostatic binding (*via b*).¹⁵¹

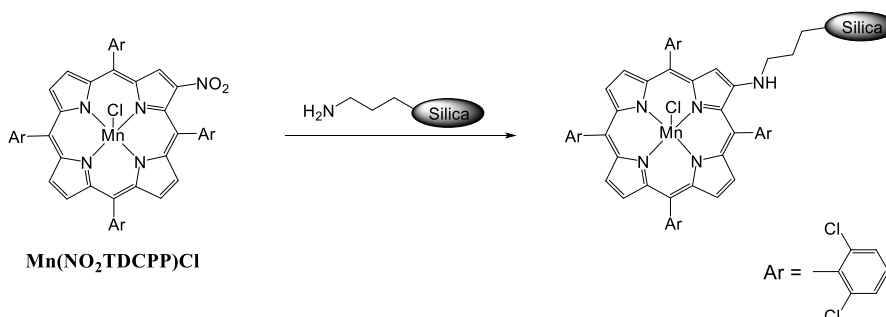
Evans and Lindsay Smith attached covalently the $\text{Fe}(\text{TF}_5\text{PP})\text{Cl}$ on a diamine modified silica obtained by the reaction of chloropropylsilica with α,ω -diamines (**Scheme 1.8**).¹⁵² The diamino-silica catalyst has been further modified by trimethylsilylation, by acetylation and by acid washing and the performance of the resulting materials was

compared. The obtained supported catalysts were used for the oxidation of ethylbenzene by dioxygen. The products obtained were 1-phenyl-ethyl hydroperoxide, 1-phenylethanol and acetophenone, as when **Fe(TF₅PP)Cl** was used as homogeneous catalyst, however the reactions were slower.¹⁵²



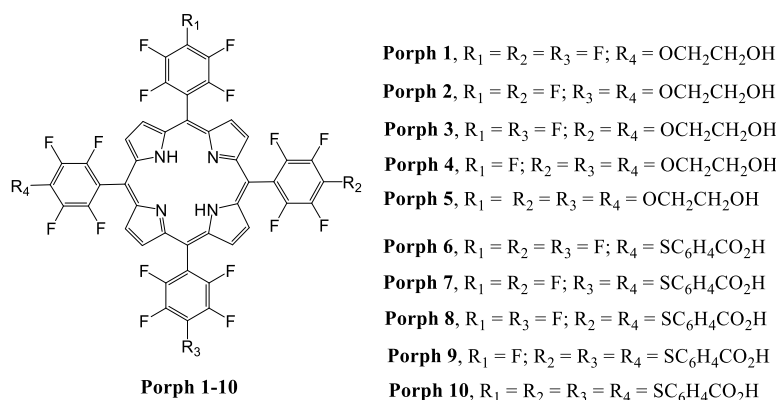
Scheme 1.8. Strategy used by Evans and Lindsay Smith to covalently attach **Fe(TF₅PP)Cl** on a diamine modified silica support.¹⁵²

Rebello *et al.* described the immobilization of the manganese(III) complex of 5,10,15,20-tetrakis(2,6-dichlorophenyl)porphyrin [**Mn(TDCPP)Cl**] on a silica support by a strong covalent bond through the β -position of the macrocycle.¹⁵³ To do that, the chloro 2-nitro-5,10,15,20-tetrakis(2,6-dichlorophenyl)porphyrinatomanganese(III) [**Mn(β NO₂TDCPP)Cl**] was first synthesized and then the immobilization was performed by using an amino-functionalized silica (**Scheme 1.9**). The covalent bonding occurs due to an *ipso* substitution of the nitro group at the β -pyrrolic position of the porphyrin by the amino group of the silica support. The anchored manganese porphyrin showed to be an efficient, selective and reusable catalyst for the oxidation of cyclooctene, using hydrogen peroxide as oxidant.¹⁵³



Scheme 1.9. Strategy used by Rebello *et al.* to immobilize **Mn(TDCPP)Cl** through the β -position on a silica support.¹⁵³

Castro *et al.* prepared, by structural modification of 5,10,15,20-tetrakis (pentafluorophenyl)porphyrin (**H₂TF₅PP**) with ethylene glycol, iron(III) and manganese(III) porphyrins substituted with hydroxyalkyloxy groups at the *para* position of the *meso*-aryl groups, **Porph 1-5** (Scheme 1.10).¹⁵⁴ The metalloporphyrins were immobilized on layered double hydroxide (LDH) and silica (synthesized by the sol-gel process) and the catalytic activity of the obtained materials was evaluated, using PhIO as oxidant. In homogeneous conditions, the metalloporphyrins gave rise to good catalytic conversions for cyclooctene oxidation and, in the case of cyclohexane oxidation, the catalysts were selective for the alcohol instead of the ketone. Using the corresponding supported catalysts, slightly lower yields were obtained; however, these solids were able to retain their catalytic activity for at least three cycles in the case of cyclooctene oxidation.¹⁵⁴



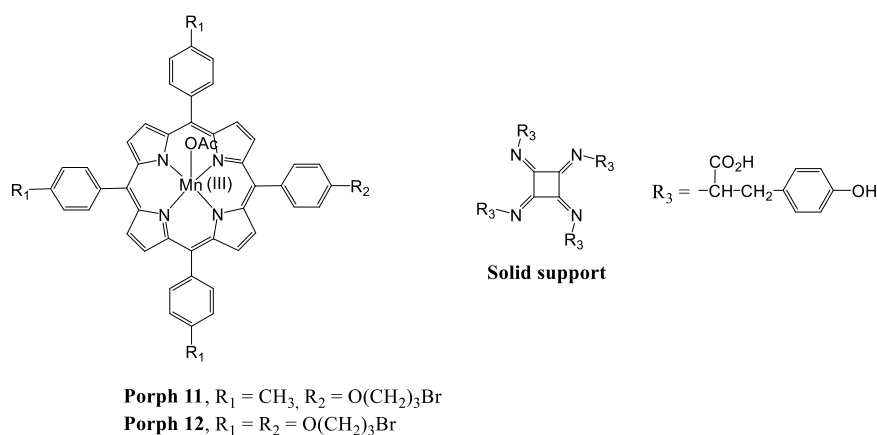
Scheme 1.10. Structure of the porphyrins obtained by reaction of **H₂TF₅PP** with ethylene glycol (**Porph 1-5**) and with 4-mercaptobenzoic acid (**Porph 6-10**).^{154,155}

In a more recent work, using the same synthetic strategy, Castro *et al.* prepared new metalloporphyrins *via* structural modification of **H₂TF₅PP** with 4-mercaptobenzoic acid, **Porph 6-10** (Scheme 1.10).¹⁵⁵ For the tetra-substituted derivatives, the presence of the carboxylic acid groups in the structure of the resulting porphyrin provided insoluble solids after metal insertion, which could potentially serve as heterogeneous catalysts. The presence of the carboxylic groups favours the formation of a structured solid *via* coordination of the carboxylic groups with the metal ions, giving rise to bi- and tri-dimensional structures. The resulting materials provided good to excellent results as catalysts in the oxidation of cyclooctene, cyclohexane and heptane, with high selectivity towards the alcohols in cyclohexane and heptane oxidation. Additionally, when using the tetra-substituted derivatives in the oxidation of cyclooctene under heterogeneous

conditions, it was possible to reuse the catalysts, affording similar results along six cycles.¹⁵⁵

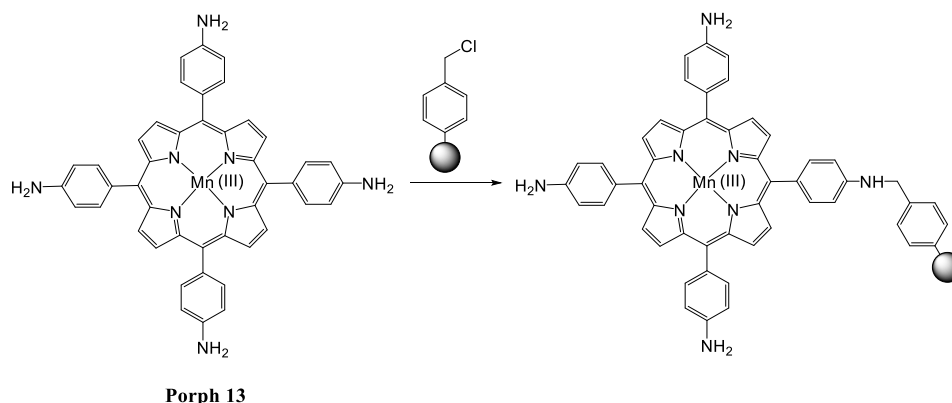
1.2.4.2. Organic polymers

The first use of immobilized metalloporphyrin catalysts for alkene epoxidation was reported in 1983 by Drenth and co-workers.¹¹⁷ The authors used the (*para*-substituted phenylporphyrinato)manganese(III) acetates (**Porph 11** and **Porph 12**) and a polymer of an isocyanide $(R-N=C<)_n$ as the solid support (**Scheme 1.11**). The porphyrins were coupled to the polymer by means of ether linkages with the tyrosine phenyl rings. The anchored catalysts were tested in the epoxidation of cyclohexene using sodium hypochlorite as a single oxygen donor. Using **Porph 11** anchored to the support, higher epoxidation rate was observed. The immobilized catalyst was also approximately 3 times more active than the free catalysts.¹¹⁷



Scheme 1.11. Mn(III) porphyrins and the polymer for the immobilization used by Drenth and co-workers.¹¹⁷

Tangestaninejad and Mirkhani reported the synthesis of a polymer-bound manganese porphyrin using the manganese(III) complex of 5,10,15,20-tetrakis(4-aminophenyl)porphyrin (**Porph 13**) and cross-linked chloromethylated polystyrene, known as Merrifield resin (**Scheme 1.12**).¹²⁹ The obtained solid material was able to efficiently catalyse the epoxidation of various alkenes in the presence of sodium periodate, without evidence of leaching. Furthermore, the oxidation reactions using the heterogeneous catalyst, although slower, were more selective than those occurring in homogeneous conditions.¹²⁹

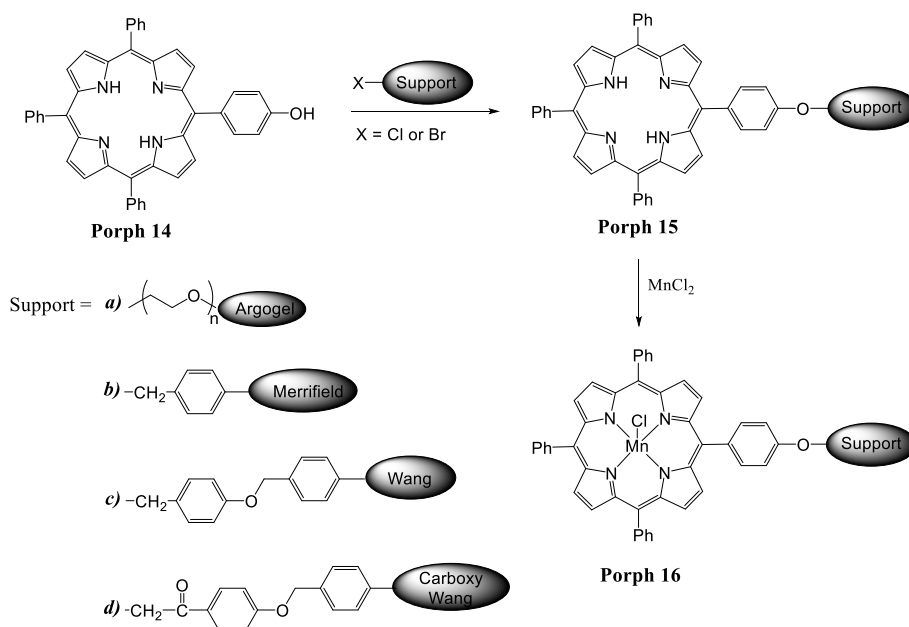


Scheme 1.12. Immobilization of **Porph 13** onto a Merrifield resin support.¹²⁹

Moghadam *et al.* anchored the manganese(III) complex of tetra(4-pyridyl)porphyrin onto a Merrifield resin by one step quaternization reaction.¹⁴⁵ The supported manganese porphyrin was used as catalyst in alkene epoxidation and alkane hydroxylation by sodium periodate. For a wide variety of alkenes, the epoxide yields were comparable to the homogeneous alkene epoxidations using the manganese(III) complex of tetraphenylporphyrin. The supported porphyrin was also efficient in the oxidation of alkanes. The catalyst reuse ability was studied using styrene as model substrate and, after four consecutive uses, the epoxide yield was 92% and no leaching was detected during the experiments.¹⁴⁵ The immobilized manganese porphyrin was also efficient in the oxidation of primary and secondary alcohols using sodium periodate.¹⁴⁶

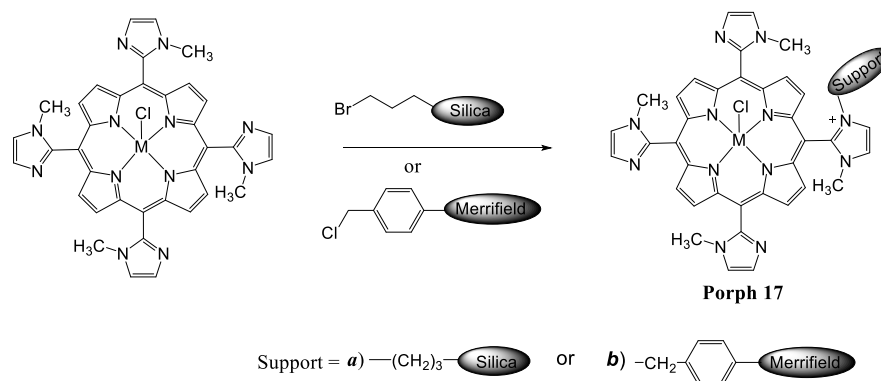
Brulé and Miguel prepared heterogeneous catalysts based on manganese porphyrin catalysts supported on Merrifield and Argogel resins and their catalytic activity was tested for alkene epoxidation.¹³¹ The Argogel-supported porphyrin **Porph 15-a** and the Merrifield-supported analogue **Porph 15-b** were prepared by attachment of 5-(4-hydroxyphenyl)-10,15,20-triphenylporphyrin (**Porph 14**) to the Argogel chloride (a PS-PEG copolymer) and Merrifield resin, respectively, *via* covalent ether linkage (**Scheme 1.13**). The corresponding manganese complexes **Porph 16-a** and **Porph 16-b** were then synthesized using manganese dichloride. The Merrifield-supported catalyst **Porph 16-b** presented a higher level of recyclability than the Argogel-supported catalyst analogue **Porph 16-a** with three reuses and a minimum loss of activity.¹³¹ In other work, following the same approach, two other heterogeneous catalysts **Porph 16-c** and **Porph 16-d** were prepared using bromo-Wang and carboxy bromo-Wang resins as solid supports (**Scheme 1.13**).¹³⁰ The catalytic performance of these new materials was tested for the epoxidation

of three diene substrates (1,5-cyclooctadiene, 7-methyl-1,6-octadiene and limonene) and compared with the Merrifield-supported catalyst **Porph 16-b**. The carboxy-Wang supported catalyst **Porph 16-d** was found to be the most active and robust, when compared to the other two catalysts, with high chemoselectivity and reusability.¹³⁰



Scheme 1.13. Strategy used by Brulé and Miguel to obtain Argogel-, Merrifield-, bromo-Wang- and Carboxy bromo-Wang-supported catalysts.^{130,131}

De Paula *et al.* prepared a catalytic system based on an immobilized imidazolyl manganese porphyrin using Merrifield resin and functionalized silica gel as solid supports (**Scheme 1.14**).¹³² The supported manganese porphyrins **Porph 17-a** and **Porph 17-b** were tested as catalysts for the oxidation of olefins. High reaction rates and high efficiency were observed using the Merrifield resin system **Porph 17-b** and hydrogen peroxide as oxidant in the oxidation of cyclooctene, with good recyclability up to four times, without loss in the catalytic efficiency and selectivity to the corresponding epoxide. In the case of the silica supported **Porph 17-a**, however, the results were not totally satisfactory, even when *tert*-butyl hydroperoxide (TBHP) in decane was used as oxygen donor.¹³²



Scheme 1.14. Strategy used by de Paula *et al.* to immobilize an imidazolyl manganese porphyrin onto solid supports of Merrifield resin and functionalized silica.¹³²

1.3. Porphyrins as photocatalysts in a water remediation context

1.3.1. Emerging contaminants in water

Pharmaceuticals and personal care products (PPCPs) and other xenobiotics are a huge group of chemicals that are used worldwide in very high amounts. Several studies around the world have shown that a large variety of PPCPs and other xenobiotics are detected in sewage effluents, surface and ground waters, and occasionally in drinking waters at trace levels, turning them into real emergent pollutants.^{156–169} Moreover, it was revealed that some xenobiotics may interfere with ecosystems in concentrations as low as a few nanograms per liter.¹⁷⁰ Additionally, these micropollutants are present in aquatic systems as complex mixtures and may act synergistically and cumulatively leading to toxic effects on the ecosystem at environmentally relevant concentrations.^{171–174}

Environmentally concerning groups of organic pollutants include analgesics, antibiotics, antineoplastics, antiepileptics, β -blockers, blood-lipid regulators, antidepressants, anxiolytics, sedatives, contraceptives, perfluorinated compounds, personal care products (e.g. musk compounds, UV filters from sunscreens, alkylphenols), plasticisers and biocides.^{158,175,176} The introduction of these micropollutants into the environment occurs primarily through human excretion.¹⁷⁷ Other pathways include the disposal of unused products,¹⁷⁸ the intensive farming,^{179–181} the application of pharmaceuticals in aquaculture^{182,183} and the effluents from hospitals and drug manufacture.¹⁸⁴ Therefore, the principal source of input of PPCPs in the aquatic

environment is from wastewater treatment plants (WWTPs), which are not prepared to efficiently remove these micropollutants.^{185,186}

1.3.2. Natural degradation of PPCPs and other organic contaminants in the aquatic environment

PPCPs and other organic contaminants present in aquatic environment can be degraded to other compounds through natural processes. For instance, they can undergo biotransformation mediated by animals, plants and microorganisms present in aquatic systems.¹⁸⁷ Among them, microorganisms have a major contribution in the degradation of organic pollutants in aquatic environment, sometimes resulting in mineralization.¹⁸⁸ However, their effectiveness is greatly affected by environmental conditions such as nutrient availability, temperature, oxygen content, pH or salinity.¹⁸⁸ In addition, organic pollutants under solar irradiation can undergo direct degradation or indirectly by reaction with photosensitizers present in water.¹⁸⁷

Direct photodegradation is a process initiated by the direct absorption of photons by a target compound, followed by the excitation of the molecules which are then able to induce a chemical transformation.^{176,188} However, direct degradation is only relevant when the compounds absorb light within the solar spectrum ($\lambda > 290$ nm).¹⁸⁷

In the case of indirect photodegradation, chromophores present in the water absorb light energy, get photosensitized, and produce a series of reactive species such as HO[•], HOO[•], RO[•], ROO[•], ¹O₂, H₂O₂, HO⁻ and O₂^{-•} that cause transformations on the organic pollutants.^{176,188} Dissolved organic matter (DOM), inorganic species such as NO₃⁻, NO₂⁻, and metal complexes are examples of photosensitizers usually present in water. The triplet DOM (³DOM) and CO₃^{-•} obtained by the reaction of bicarbonate with HO[•] are other examples of reactive species usually found.¹⁸⁹ Indirect photolysis is particularly important for the degradation of PPCPs that poorly absorb solar radiation and resist to direct photolysis.

Some factors may affect the efficacy of the PPCPs photodegradation such as temperature, pH, depth below the water surface,¹⁹⁰ cloud coverage, water turbidity, altitude, latitude, and time of day. Most of these transformations do not result in the desired mineralization of the contaminants, but in the formation of other compounds, often unknown or not well-characterised. Furthermore, some of the resulting products are

indicated to be equally or more toxic than the starting compounds. Therefore, it is extremely important to know the transformations to which PPCPs are subject and the products that result from them. In addition, many PPCPs are resistant to biodegradation and are slow or medium photodegradable resulting in their persistence and accumulation in the aquatic environment.¹⁹¹ Therefore, there is an urgent need to find efficient technologies to remove the PPCPs from the wastewater effluents.

1.3.3. Advanced oxidation processes for the removal of PPCPs and other organic contaminants from wastewater

Among the technologies for water treatment, the advanced oxidation processes (AOPs) present great potential for the removal of PPCPs.^{192,193} AOPs consist in the generation of highly reactive oxygen species (ROS) and the reaction of these species with target contaminants.¹⁹⁴ Photocatalysis has been recognized as one of the most promising AOPs for the elimination of organic pollutants from wastewaters. In last years the use of photocatalysts based on TiO₂ has prompted great interest due to its high activity, low cost, high photostability and low toxicity.¹⁹⁵ However, photoactivation of TiO₂ requires radiation with light of wavelength ≤ 387 nm, corresponding to less than 5% of the whole sunlight reaching the surface of Earth.¹⁹⁶ This unable the use of TiO₂ under sunlight conditions, which is an affordable, readily available and sustainable source of radiation compared to UV light systems. Therefore, the search for efficient photocatalysts using such conditions is an important quest.

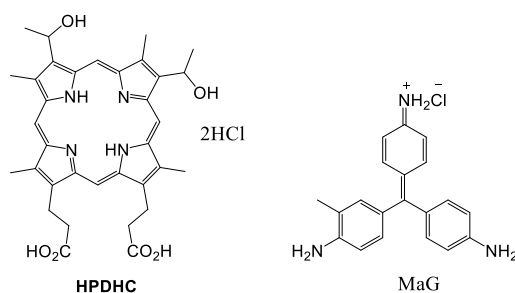
Some porphyrins have high absorption in several wavelengths in the UV-Vis range and high quantum yields for the formation of the triplet states, which makes them potential photosensitizers for the degradation of organic pollutants using sunlight.¹⁹⁷

The work described in the literature, involving the use of porphyrins as photocatalysts in the degradation of some organic pollutants, will be presented next.

1.3.3.1. Porphyrins as photosensitizers in the degradation of organic pollutants in water

The photocatalytic activity of porphyrins has thus far been examined exclusively on target molecules such as textile dyes, pesticides and phenolic compounds. Herath *et al.*¹⁹⁸ used the hematoporphyrin dihydrochloride (**HPDHC**) as a photosensitizer to generate ROS

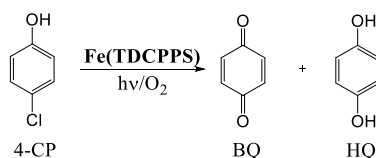
to degrade magenta (MaG), a triphenylmethane carbonium dye frequently used in the textile industry (**Scheme 1.15**). The visible light irradiation of the aqueous solution of MaG at pH 3.0 using **HPDHC** in the presence of O₂ led to a gradual decrease of the optical absorption at 540 nm in the absorption spectra and the pink colour disappeared completely after a 20 h irradiation.¹⁹⁸



Scheme 1.15. The structure of the photosensitizer - hematoporphyrindihydrochloride (**HPDHC**) and the dye - magenta (MaG).¹⁹⁸

Shao *et al.*¹⁹⁹ prepared uniform polyacrylonitrile and polyacrylonitrile copolymer nanofiber materials supporting metalloporphyrins [(**M**)**TPP**; M: Zn(II), Cu(II), Ni(II), Co(II), Fe(III) and Pd(II)] by electrospinning and tested them as photocatalysts for the degradation of various azo-dyes in aqueous solutions under visible light irradiation. In general, the polyacrylonitrile copolymer nanofiber materials were more effective in the immobilization of the metalloporphyrins. The nanofiber material-supported copper-porphyrin and iron-porphyrin complexes were the most active photocatalysts for azo-dye degradation. The photocatalysts were recycled and no significant degradation of the photocatalyst or decreasing of the photocatalytic activities were observed.

Silva *et al.*²⁰⁰ used the iron(III) complex of 5,10,15,20-tetrakis(2,6-dichloro-3-sulfophenyl)porphyrin [**Fe(TDCPPS)**] as photocatalyst in the degradation of 4-chlorophenol (4-CP) in aerated aqueous solution, using monochromatic light from a xenon lamp filtered with a grating monochromator set at 340 nm. The main products identified by HPLC and UV-visible spectroscopy were *p*-benzoquinone (BQ) and *p*-hydroquinone (HQ) (**Scheme 1.16**).



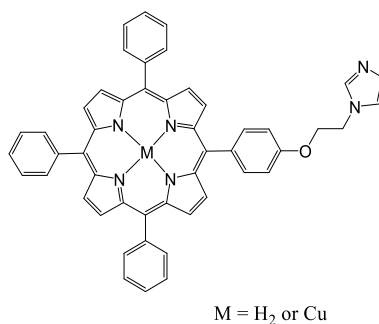
Scheme 1.16. Degradation of 4-chlorophenol using **Fe(TDCPPS)** as photocatalyst.²⁰⁰

The water soluble 5,10,15,20-tetrakis(2,6-dichloro-3-sulfophenyl)porphyrin and its tin and zinc complexes were also applied as photosensitizers in the degradation of 4-CP and 2,6-dimethylphenol, in aqueous solutions.²⁰¹ After 7 h of irradiation, the main products identified by HPLC were BQ and HQ for 4-CP and 2,6-dimethylbenzoquinone in the case of 2,6-dimethylphenol.

Pepe *et al.*²⁰² immobilized porphyrins and phthalocyanines on aminopropyl silica and/or exchange resins to avoid the problem of separation of the homogeneous photosensitizers. The supported materials were tested in the photooxidation of phenol under 900 W/m² visible light, giving 1,4-benzoquinone as product. The 5,10,15,20-tetrakis(4-sulfonatophenyl)porphyrin has shown the best photocatalytic effect.

The photodegradation of 1,5-dihydroxynaphthalene catalysed by 5,10,15,20-tetrakis(4-sulfonatophenyl)porphyrin (**H₂TPPS⁴⁻**) under visible light irradiation in aerated aqueous solution has been studied and the main product has been identified as 5-hydroxy-1,4-naphthoquinone.²⁰³

Yao *et al.*²⁰⁴ synthesized the imidazolyl-linked porphyrin 5-[4-(2-imidazolyl)ethoxy]phenyl-10,15,20-triphenylporphyrin and its copper(II) complex (**Scheme 1.17**) and tested the porphyrin-TiO₂ and copper porphyrin-TiO₂ systems as photocatalysts. The photocatalytic activity was investigated for the photodegradation of 4-nitrophenol (4-NP) in aqueous solution with a small amount of H₂O₂ under visible light irradiation ($\lambda > 400$ nm). In the absence of H₂O₂, the superoxide anion (O₂^{•-}) was mainly formed and was less active for the degradation of 4-NP. Otherwise, by adding an appropriate amount of H₂O₂, the visible-light-driven photocatalytic efficiency of the Cu(II) porphyrin-TiO₂ was enhanced, due to the production of hydroxyl radicals by reaction of H₂O₂ with O₂^{•-} in water, which degraded the 4-NP into smaller molecules.



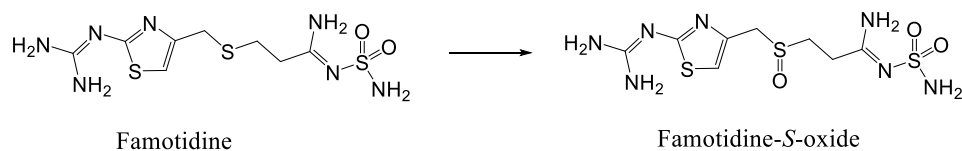
Scheme 1.17. Structure of the 5-[4-(2-imidazolyl)ethoxy]phenyl-10,15,20-triphenylporphyrin and its copper(II) complex.

Héquet *et al.*²⁰⁵ immobilized hemin and an iron sulfophthalocyanine onto a resin and the supported complexes were efficiently used as photocatalysts on the degradation of the herbicide atrazine under a mercury lamp and under simulated solar light. Rebelo *et al.*²⁰⁶ also reported the photodegradation of atrazine and of the herbicide ametryn under visible light in aerated neutral aqueous solutions and 5,10,15,20-tetrakis(2,6-dichloro-3-sulfophenyl)porphyrin or 5,10,15,20-tetrakis(4-sulfophenyl)porphyrin as sensitizers. The degradation reached 30% for atrazine and 63% for ametryn. The final photoproducts were characterized as dealkylated *s*-triazines.²⁰⁶ Granados-Oliveros *et al.*²⁰⁷ investigated the photocatalytic activity of metal-free 5,10,15,20-tetrakis(4-carboxyphenyl)porphyrin and of the porphyrin with different metal centres (Fe(III), Cu(II), Zn(II)), adsorbed on TiO₂ in the photodegradation of atrazine in aqueous solution and under visible light irradiation. However, the photodegradation of atrazine was only possible after adding hydrogen peroxide to the solution, with higher degradation rates using Cu(II) porphyrin as photosensitizer (82% of degradation after 1 h of irradiation).²⁰⁷

Silva *et al.*²⁰⁸ immobilized 5,10,15,20-tetrakis(2-fluorophenyl)porphyrin on the supports MCM-41 mesoporous molecular sieve and NaY zeolite. The obtained materials were used as photocatalysts in the photodegradation of the pesticides, 2,3,5-trimethylphenol and mecoprop using mercury lamps. The best results were obtained using the porphyrin supported on MCM-41 material, with conversions about 50% after 90 min. The 2-hydroxymethyl-hydroquinone and 4-chloro-2-methylphenol were identified as the main degradation products of mecoprop.²⁰⁸ The porphyrin supported on MCM-41 was also highly effective in the photodegradation of pesticides fenamiphos and diuron, when the solutions were irradiated with polychromatic light within the range 300-460nm.¹⁴⁰ The authors also studied the photodegradation of 2,3,5-trimethylphenol using the copper complex of 5,10,15,20-tetrakis(2-fluorophenyl)porphyrin, **H₂TDCPP** and the corresponding copper complex, all immobilized in MCM-41.¹⁴⁰ However, lower levels of photodegradation were obtained in the presence of these materials.

Only few studies concerning the use of porphyrins and chlorins on the photooxidation of pharmaceuticals have been described. Murphy *et al.*²⁰⁹ prepared a 5,10,15,20-tetrakis(4-carboxyphenyl)porphyrin composite (**H₂TCPP**)-TiO₂ and evaluated its photocatalytic activity in the degradation of famotidine, a histamine H₂-receptor antagonist used in the treatment of peptic ulcer disease, under both visible and solar light

irradiation. The photodegradation of famotidine under these conditions did not lead to complete mineralisation, generating a range of products instead, being one major degradation product attributed to famotidine-*S*-oxide (**Scheme 1.18**).



Scheme 1.18. The main product obtained for the photodegradation of famotidine using a $\text{H}_2\text{TCPP-TiO}_2$ composite as photocatalyst.

Kim *et al.*²¹⁰ reported the efficient photodegradation of several pharmaceuticals using a tin complex of 5,10,15,20-tetraphenylporphyrin [$\text{Sn}(\text{OH})_2(\text{TPP})$] immobilized on silica as photosensitizer in distilled water, under visible light irradiation. The authors also showed that the tin porphyrin photosensitizer was more efficient for the degradation of cimetidine and propranolol than the TiO_2 photocatalyst under UV-light in an effluent matrix.²¹⁰

1.4. Objectives of the work

The main objectives of the present work were:

- i) the synthesis and characterization of novel manganese(III) porphyrins with structural functionalities that can enhance its solubility in water or that enables its immobilization onto solid supports such as silica or Merrifield resin;
- ii) the catalytic efficiency evaluation of those porphyrin-based catalysts in oxidation reactions under sustainable and environmentally benign conditions;
- iii) the development of porphyrin-based photosensitizers able to degrade organic pollutants in the presence of light, most importantly with natural sunlight, in an environmental context.

This thesis is divided into 5 chapters. After the present introductory chapter, chapter 2 reports the synthesis and characterization of the novel porphyrins prepared, as well as all the experimental details related to the porphyrins used in this work.

The catalytic studies with the novel manganese(III) porphyrins in the oxidation of cyclooctene under homogeneous conditions are presented in chapter 3. The catalyst showing the best catalytic results in the homogeneous system was immobilized on two

solid supports, silica and Merrifield resin. This chapter also includes the immobilization strategy, the characterization of the obtained solid materials, and the catalytic results for the oxidation of cyclooctene in the presence of the immobilized catalysts.

In chapter 4 the synthesis of the manganese(III) complex of the porphyrin having polyethylene glycol groups is reported. This Mn(III) porphyrin evidences water solubility, and its catalytic activity was evaluated by using a water/hexane (1:1) biphasic medium in the oxidation of carvacrol and thymol, which was then extended to an oregano essential oil with high carvacrol and thymol content.

The potential of the well-known 5,10,15,20-tetrakis(pentafluorophenyl)porphyrin as photocatalyst, in a wastewater treatment context, for the degradation of metoprolol under homogeneous conditions and immobilized on a silica support in the presence of sunlight is studied in chapter 5. This chapter also includes the identification of the products obtained in the photodegradation of metoprolol by HPLC coupled to tandem mass spectrometry (HPLC-UV-ESI-MSⁿ).

At the end, some final remarks and considerations about the work developed will be presented.

1.5. References

- 1 R. Bonnett, in *The Porphyrins Volume I: Structure and Synthesis, Part A*, ed. D. Dolphin, Academic Press, London, 1978, pp. 1–27.
- 2 L. R. Milgrom, *The colours of life — an introduction to the chemistry of porphyrins and related compounds*, Oxford University Press, Oxford, 2002.
- 3 D. Dolphin and T. Wijesekera, in *Metalloporphyrins in Catalytic Oxidations*, ed. R. A. Sheldon, Marcel Dekker, Basel, 1994, pp. 193–293.
- 4 J. E. Merritt and K. L. Loening, *Pure Appl. Chem.*, 1979, **51**, 2251–2304.
- 5 G. P. Moss, *Pure Appl. Chem.*, 1987, **59**, 779–832.
- 6 T. R. Janson and J. J. Katz, in *The Porphyrins IV: Physical Chemistry, Parte B*, ed. D. Dolphin, Academic Press, London, 1979, pp. 12–16.
- 7 M. Gouterman, *J. Mol. Spectrosc.*, 1961, **6**, 138–163.
- 8 R. Giovannetti, in *Macro To Nano Spectroscopy*, ed. J. Uddin, InTech, Rijeka, 2012, pp. 87–109.
- 9 J. M. Thomas and R. Raja, *Annu. Rev. Mater. Res.*, 2005, **35**, 315–350.
- 10 J. M. Thomas and R. Raja, *Catal. Today*, 2006, **117**, 22–31.
- 11 R. A. Sheldon, *Chem. Commun.*, 2008, 3352–3365.
- 12 R. A. Sheldon, *Green Chem.*, 2017, **19**, 18–43.
- 13 J. Piera and J.-E. Bäckvall, *Angew. Chemie Int. Ed.*, 2008, **47**, 3506–3523.
- 14 Z. Shi, C. Zhang, C. Tang and N. Jiao, *Chem. Soc. Rev.*, 2012, **41**, 3381–3430.
- 15 E. Roduner, W. Kaim, B. Sarkar, V. B. Urlacher, J. Pleiss, R. Gläser, W.-D. Einicke, G. A. Sprenger, U. Beifuß, E. Klemm, C. Liebner, H. Hieronymus, S.-F. Hsu, B. Plietker and S. Laschat, *ChemCatChem*, 2013, **5**, 82–112.
- 16 R. A. Sheldon, in *Organic Peroxygen Chemistry. Topics in Current Chemistry*, ed. W. A. Herrmann, Springer, Berlin, Heidelberg, 1993, vol. 164, pp. 21–43.
- 17 R. A. Sheldon, *Green Chem.*, 2005, **7**, 267–278.
- 18 A. Scarso and G. Strukul, in *Handbook of Advanced Processes in Oxidation Catalysis: From Laboratory to Industry*, eds. D. Duprez and F. Cavani, Imperial College Press, London, 2014, pp. 679–766.
- 19 R. W. Estabrook, *FASEB J.*, 1996, **10**, 202–204.
- 20 S. Rendic and F. J. Di Carlo, *Drug Metab. Rev.*, 1997, **29**, 413–580.

- 21 F. P. Guengerich and Q. Cheng, *Pharmacol. Rev.*, 2011, **63**, 684–699.
- 22 S. Rendic and F. P. Guengerich, *Chem. Res. Toxicol.*, 2015, **28**, 38–42.
- 23 M. Sono, M. P. Roach, E. D. Coulter and J. H. Dawson, *Chem. Rev.*, 1996, **96**, 2841–2887.
- 24 D. Mansuy, *Comp Biochem Physiol C*, 1998, **121**, 5–14.
- 25 F. P. Guengerich, *Chem. Res. Toxicol.*, 2001, **14**, 611–650.
- 26 W. Lohmann and U. Karst, *Anal. Bioanal. Chem.*, 2008, **391**, 79–96.
- 27 B. Meunier and J. Bernadou, in *Structure and Bonding*, ed. B. Meunier, Springer, 2000.
- 28 T. M. Makris, I. Denisov, I. Schlichting and S. G. Sligar, in *Cytochrome P450 Structure, Mechanism, and Biochemistry*, ed. P. R. O. de Montellano, Kluwer Academic/Plenum, New York, 3rd edn., 2005, pp. 149–182.
- 29 B. Meunier, S. P. de Visser and S. Shaik, *Chem. Rev.*, 2004, **104**, 3947–3980.
- 30 B. Meunier and J. Bernadou, *Top. Catal.*, 2002, **21**, 47–54.
- 31 F. P. Guengerich, *ACS Catal.*, 2018, **8**, 10964–10976.
- 32 M. Pereira, L. D. Dias and M. J. F. Calvete, *ACS Catal.*, 2018, **8**, 10784–10808.
- 33 K. Auclair, Z. Hu, D. M. Little, P. R. O. De Montellano and J. T. Groves, *J. Am. Chem. Soc.*, 2002, **124**, 6020–6027.
- 34 X. Huang and J. T. Groves, *Chem. Rev.*, 2018, **118**, 2491–2553.
- 35 K. D. Dubey and S. Shaik, *Acc. Chem. Res.*, 2019, **52**, 389–399.
- 36 A. D. N. Vaz, E. S. Roberts and M. J. Coon, *J. Am. Chem. Soc.*, 1991, **113**, 5886–5887.
- 37 A. D. N. Vaz, S. J. Pernecky, G. M. Raner and M. J. Coon, *Proc. Natl. Acad. Sci. USA*, 1996, **93**, 4644–4648.
- 38 Y. Watanabe, *J. Biol. Inorg. Chem.*, 2001, **6**, 846–856.
- 39 A. D. N. Vaz, D. F. McGinnity and M. J. Coon, *Proc. Natl. Acad. Sci. USA*, 1998, **95**, 3555–3560.
- 40 P. H. Toy, M. Newcomb, M. J. Coon and A. D. N. Vaz, *J. Am. Chem. Soc.*, 1998, **120**, 9718–9719.
- 41 B. Meunier, *Chem. Rev.*, 1992, **92**, 1411–1456.
- 42 D. Dolphin, T. G. Traylor and L. Y. Xie, *Acc. Chem. Res.*, 1997, **30**, 251–259.
- 43 D. Mansuy, *Pure Appl. Chem.*, 1994, **66**, 737–744.

-
- 44 J. Bernadou and B. Meunier, *Chem. Commun.*, 1998, 2167–2173.
- 45 J. Bernadou and B. Meunier, *Adv. Synth. Catal.*, 2004, **346**, 171–184.
- 46 J. T. Groves, R. C. Haushalter, M. Nakamura, T. E. Nemo and B. J. Evans, *J. Am. Chem. Soc.*, 1981, **103**, 2884–2886.
- 47 S. Shaik, M. Filatov, D. Schröder and H. Schwarz, *Chem. Eur. J.*, 1998, **4**, 193–199.
- 48 F. Ogliaro, S. P. de Visser, S. Cohen, J. Kaneti and S. Shaik, *ChemBioChem*, 2001, **2**, 848–851.
- 49 J. T. Groves and G. A. McClusky, *J. Am. Chem. Soc.*, 1976, **98**, 859–861.
- 50 T. J. Volz, D. A. Rock and J. P. Jones, *J. Am. Chem. Soc.*, 2002, **124**, 9724–9725.
- 51 M. J. Gunter and P. Turner, *Coord. Chem. Rev.*, 1991, **108**, 115–161.
- 52 D. Mansuy, *Comptes Rendus Chim.*, 2007, **10**, 392–413.
- 53 C. Che and J. Huang, *Chem. Commun.*, 2009, 3996–4015.
- 54 M. M. Q. Simões, R. De Paula, M. G. P. M. S. Neves and J. A. S. Cavaleiro, *J. Porphyr. Phthalocyanines*, 2009, **13**, 589–596.
- 55 J. C. Barona-Castaño, C. C. Carmona-Vargas, T. J. Brocksom and K. T. De Oliveira, *Molecules*, 2016, **21**, 310.
- 56 M. M. Q. Simões, C. M. B. Neves, S. M. G. Pires, M. G. P. M. S. Neves and J. A. S. Cavaleiro, *Pure Appl. Chem.*, 2013, **85**, 1671–1681.
- 57 P. Zucca, C. M. B. Neves, M. M. Q. Simões, M. D. G. P. M. S. Neves, G. Cocco and E. Sanjust, *Molecules*, 2016, **21**, 1–40.
- 58 M. M. Q. Simões, S. M. G. Pires, M. G. P. M. S. Neves and J. A. S. Cavaleiro, in *Handbook of Porphyrin Science: with Applications to Chemistry, Physics, Materials Science, Engineering, Biology and Medicine*, eds. K. M. Kadish, K. M. Smith and R. Guilard, World Scientific Publishing, Singapore, 2016, pp. 197–306.
- 59 B. Akagah, A. T. Lormier, A. Fournet and B. Figadère, *Org. Biomol. Chem.*, 2008, **6**, 4494–4497.
- 60 J. T. Groves, T. E. Nemo and R. S. Myers, *J. Am. Soc.*, 1979, **101**, 1032–1033.
- 61 J. T. Groves and W. J. Kruper, *J. Am. Chem. Soc.*, 1979, **101**, 7613–7615.
- 62 C. L. Hill and B. C. Schardt, *J. Am. Chem. Soc.*, 1980, **102**, 6374–6375.
- 63 J. T. Groves, W. J. Kruper and R. C. Haushalter, *J. Am. Chem. Soc.*, 1980, **102**, 6375–6377.
- 64 D. Mansuy, J.-F. Bartoli, J.-C. Chottard and M. Lange, *Angew. Chemie Int. Ed.*,

- 1980, **19**, 909–910.
- 65 P. S. Traylor, D. Dolphin and T. G. Traylor, *J. Chem. Soc. Chem. Commun.*, 1984, 279–280.
- 66 M. J. Nappa and C. A. Tolman, *Inorg. Chem.*, 1985, **24**, 4711–4719.
- 67 J. F. Bartoli, O. Brigaud, P. Battioni and D. Mansuy, *J. Chem. Soc. Chem. Commun.*, 1991, 440–442.
- 68 A. M. d’A. R. Gonsalves, M. M. Pereira, A. C. Serra, R. A. W. Johnstone and M. L. P. G. Nunes, *J. Chem. Soc. Perkin Trans. 1*, 1994, 2053–2057.
- 69 Z. Gross and L. Simkhovich, *Tetrahedron Lett.*, 1998, **39**, 8171–8174.
- 70 A. A. Guedes, A. C. M. A. Santos and M. D. Assis, *Kinet. Catal.*, 2006, **47**, 555–563.
- 71 F. G. Doro, J. R. L. Smith, A. G. Ferreira and M. D. Assis, *J. Mol. Catal. A Chem.*, 2000, **164**, 97–108.
- 72 G. R. Friedermann, M. Halma, K. A. D. F. Castro, F. L. Benedito, F. G. Doro, S. M. Drechsel, A. S. Mangrich, M. das D. Assis and S. Nakagaki, *Appl. Catal. A Gen.*, 2006, **308**, 172–181.
- 73 J. T. Groves and W. J. Kruper, *Isr. J. Chem.*, 1985, **25**, 148–154.
- 74 T. G. Traylor and A. R. Miksztal, *J. Am. Chem. Soc.*, 1989, **111**, 7443–7448.
- 75 T. Młodnicka and B. R. James, *Metalloporphyrins Catalyzed Oxidations*, Kluwer Academic Publishers, Dordrecht, 1994.
- 76 T. Naota, H. Takaya and S.-I. Murahashi, *Chem. Rev.*, 1998, **98**, 2599–2660.
- 77 R. A. Baglia, J. P. T. Zaragoza and D. P. Goldberg, *Chem. Rev.*, 2017, **117**, 13320–13352.
- 78 B. Meunier, E. Guilmet, M.-E. de Carvalho and R. Poilblanc, *J. Am. Chem. Soc.*, 1984, **106**, 6668–6676.
- 79 Z. Solati, M. Hashemi and L. Ebrahimi, *Catal. Lett.*, 2011, **141**, 163–167.
- 80 W. Nam, S.-Y. Oh, M. H. Lim, M.-H. Choi, S.-Y. Han and G.-J. Jhon, *Chem. Commun.*, 2000, 1787–1788.
- 81 M. J. F. Calvete, M. Piñeiro, L. D. Dias and M. M. Pereira, *ChemCatChem*, 2018, **10**, 3615–3635.
- 82 I. Tabushi, *Coord. Chem. Rev.*, 1988, **86**, 1–42.
- 83 C.-A. Guo, M.-F. Chu, Q. Liu, Y. Liu, D.-C. Guo and X.-Q. Liu, *Appl. Catal. A Gen.*, 2003, **246**, 303–309.

-
- 84 J. T. Groves and Y. Watanabe, *Inorg. Chem.*, 1986, **25**, 4808–4810.
- 85 T. G. Traylor and J. P. Ciccone, *J. Am. Chem. Soc.*, 1989, **111**, 8413–8420.
- 86 W. Nam, H. J. Han, S.-Y. Oh, Y. J. Lee, M.-H. Choi, S.-Y. Han, C. Kim, S. K. Woo and W. Shin, *J. Am. Chem. Soc.*, 2000, **122**, 8677–8684.
- 87 S. Banfi, M. Cavazzini, F. Coppa, S. V. Barkanova and O. L. Kaliya, *J. Chem. Soc., Perkin Trans. 2*, 1997, 1577–1583.
- 88 J. T. Groves and M. K. Stern, *J. Am. Chem. Soc.*, 1987, **109**, 3812–3814.
- 89 N. A. Stephenson and A. T. Bell, *J. Am. Chem. Soc.*, 2005, **127**, 8635–8643.
- 90 K. Yamaguchi, Y. Watanabe and I. Morishima, *Inorg. Chem.*, 1992, **31**, 156–157.
- 91 K. Yamaguchi, Y. Watanabe and I. Morishima, *J. Am. Chem. Soc.*, 1993, **115**, 4058–4065.
- 92 N. A. Stephenson and A. T. Bell, *J. Mol. Catal. A Chem.*, 2007, **272**, 108–117.
- 93 W. Nam, M. H. Lim, H. J. Lee and C. Kim, *J. Am. Chem. Soc.*, 2000, **122**, 6641–6647.
- 94 W. Nam, H. J. Lee, S.-Y. Oh, C. Kim and H. G. Jang, *J. Inorg. Biochem.*, 2000, **80**, 219–225.
- 95 S. L. H. Rebelo, M. M. Pereira, M. M. Q. Simões, M. G. P. M. S. Neves and J. A. S. Cavaleiro, *J. Catal.*, 2005, **234**, 76–87.
- 96 J.-P. Renaud, P. Battioni, J. F. Bartoli and D. Mansuy, *J. Chem. Soc. Chem. Commun.*, 1985, 888–889.
- 97 P. Battioni, J. P. Renaud, J. F. Bartoli, M. Reina-Artiles, M. Fort and D. Mansuy, *J. Am. Chem. Soc.*, 1988, **110**, 8462–8470.
- 98 P. L. Anelli, S. Banfi, F. Montanari and S. Quici, *J. Chem. Soc. Chem. Commun.*, 1989, 779–780.
- 99 A. M. d’A. R. Gonsalves, R. A. W. Johnstone, M. M. Pereira and J. Shaw, *J. Chem. Soc. Perkin Trans. 1*, 1991, 645–649.
- 100 A. Thellend, P. Battioni and D. Mansuy, *J. Chem. Soc. Chem. Commun.*, 1994, **202**, 1035–1036.
- 101 J. Dawson, *Science*, 1988, **240**, 433–439.
- 102 S. Nakagaki, G. K. B. Ferreira, A. L. Marçal and K. J. Ciuffi, *Curr. Org. Synth.*, 2014, **11**, 67–88.
- 103 T. Tatsumi, M. Nakamura and H. Tominaga, *Catal. Today*, 1989, **6**, 163–170.

- 104 K. A. D. F. Castro, S. M. G. Pires, M. A. Ribeiro, M. M. Q. Simões, M. G. P. M. S. Neves, W. H. Schreiner, F. Wypych, J. A. S. Cavaleiro and S. Nakagaki, *J. Colloid Interface Sci.*, 2015, **450**, 339–352.
- 105 M. Halma, K. A. D. F. Castro, C. Taviot-Gueho, V. Prévot, C. Forano, F. Wypych and S. Nakagaki, *J. Catal.*, 2008, **257**, 233–243.
- 106 C. Freire, C. Pereira and S. Rebelo, in *Catalysis: Volume 24*, eds. J. J. Spivey and M. Gupta, Royal Society of Chemistry, Cambridge, 2012, pp. 116–203.
- 107 M. J. F. Calvete, M. Silva, M. M. Pereira and H. D. Burrows, *RSC Adv.*, 2013, **3**, 22774–22789.
- 108 H. Nur, H. Hamid, S. Endud, H. Hamdan and Z. Ramli, *Mater. Chem. Phys.*, 2006, **96**, 337–342.
- 109 A. A. Costa, G. F. Ghesti, J. L. De Macedo, V. S. Braga, M. M. Santos, J. A. Dias and S. C. L. Dias, *J. Mol. Catal. A Chem.*, 2008, **282**, 149–157.
- 110 J. Połtowicz, E. M. Serwicka, E. Bastardo-Gonzalez, W. Jones and R. Mokaya, *Appl. Catal. A Gen.*, 2001, **218**, 211–217.
- 111 Z. Li, C.-G. Xia and X.-M. Zhang, *J. Mol. Catal. A Chem.*, 2002, **185**, 47–56.
- 112 A. K. Rahiman, K. Rajesh, K. S. Bharathi, S. Sreedaran and V. Narayanan, *Appl. Catal. A Gen.*, 2006, **314**, 216–225.
- 113 A. K. Rahiman, K. Rajesh, K. S. Bharathi, S. Sreedaran and V. Narayanan, *Inorganica Chim. Acta*, 2009, **362**, 1491–1500.
- 114 A. Kalilur Rahiman, K. S. Bharathi, S. Sreedaran, K. Rajesh and V. Narayanan, *Inorganica Chim. Acta*, 2009, **362**, 1810–1818.
- 115 A. Kalilur Rahiman, S. Sreedaran, K. S. Bharathi and V. Narayanan, *J. Porous Mater.*, 2010, **17**, 711–718.
- 116 I. L. V. Rosa, C. M. C. P. Manso, O. A. Serra and Y. Iamamoto, *J. Mol. Catal. A Chem.*, 2000, **160**, 199–208.
- 117 A. W. van der Made, J. W. H. Smeets, R. J. M. Nolte and W. Drenth, *J. Chem. Soc., Chem. Commun.*, 1983, 1204–1206.
- 118 D. Wöhrle, J. Gitzel, G. Krawczyk, E. Tsuchida, H. Ohno, I. Okura and T. Nishisaka, *J. Macromol. Sci. Part A - Chem.*, 1988, **25**, 1227–1254.
- 119 T. G. Traylor, Y. S. Byun, P. S. Traylor, P. Battioni and D. Mansuy, *J. Am. Chem. Soc.*, 1991, **113**, 7821–7823.

-
- 120 P. Battioni, J. F. Bartoli, D. Mansuy, Y. S. Byun and T. G. Traylor, *J. Chem. Soc. Chem. Commun.*, 1992, **5**, 1051–1053.
- 121 M. A. Martinez-Lorente, P. Battioni, W. Kleemiss, J. F. Bartoli and D. Mansuy, *J. Mol. Catal. A Chem.*, 1996, **113**, 343–353.
- 122 M. das Dores Assis and J. R. L. Smith, *J. Chem. Soc. Perkin Trans. 2*, 1998, 2221–2226.
- 123 F. L. Benedito, S. Nakagaki, A. A. Saczk, P. G. Peralta-Zamora and C. M. M. Costa, *Appl. Catal. A Gen.*, 2003, **250**, 1–11.
- 124 B. Gao, R. Wang and Y. Zhang, *J. Appl. Polym. Sci.*, 2009, **112**, 2764–2772.
- 125 M. Ghiaci, F. Molaie, M. E. Sedaghat and N. Dorostkar, *Catal. Commun.*, 2010, **11**, 694–699.
- 126 A. L. Faria, T. O. C. Mac Leod, V. P. Barros and M. D. Assis, *J. Braz. Chem. Soc.*, 2009, **20**, 895–906.
- 127 J. S. dos Santos, A. L. Faria, P. M. da S. Amorin, F. M. La Luna, K. L. Caiado, D. O. C. Silva, P. P. C. Sartoratto and M. D. Assis, *J. Braz. Chem. Soc.*, 2012, **23**, 1411–1420.
- 128 A. Molinari, A. Maldotti, A. Bratovcic and G. Magnacca, *Catal. Today*, 2011, **161**, 64–69.
- 129 S. Tangestaninejad and V. Mirkhani, *J. Chem. Res.*, 1998, 788–789.
- 130 E. Brulé, Y. R. De Miguel and K. Kuok, *Tetrahedron*, 2004, **60**, 5913–5918.
- 131 E. Brulé and Y. R. De Miguel, *Tetrahedron Lett.*, 2002, **43**, 8555–8558.
- 132 R. De Paula, I. C. M. S. Santos, M. M. Q. Simões, M. G. P. M. S. Neves and J. A. S. Cavaleiro, *J. Mol. Catal. A Chem.*, 2015, **404–405**, 156–166.
- 133 P. R. Cooke and J. R. L. Smith, *J. Chem. Soc. Perkin Trans. 1*, 1994, 1913–1923.
- 134 C. Gilmartin and J. R. L. Smith, *J. Chem. Soc. Perkin Trans. 2*, 1995, 243–251.
- 135 P. Zucca, C. Vinci, A. Rescigno, E. Dumitriu and E. Sanjust, *J. Mol. Catal. A Chem.*, 2010, **321**, 27–33.
- 136 S. Maeno, Q. Zhu, M. Sasaki, T. Miyamoto and M. Fukushima, *J. Mol. Catal. A Chem.*, 2015, **400**, 56–63.
- 137 M. Bagherzadeh and A. Mortazavi-Manesh, *J. Coord. Chem.*, 2015, **68**, 2347–2360.
- 138 N. Makoto, T. Takashi and T. Hiro-o, *Bull. Chem. Soc. Jpn.*, 1990, **63**, 3334–3336.
- 139 P. Battioni, R. Iwanejko and D. Mansuy, *J. Mol. Catal. A Chem.*, 1996, **109**, 91–98.

- 140 M. Silva, M. E. Azenha, M. M. Pereira, H. D. Burrows, M. Sarakha, C. Forano, M. F. Ribeiro and A. Fernandes, *Appl. Catal. B Environ.*, 2010, **100**, 1–9.
- 141 M. Madadi and R. Rahimi, *React. Kinet. Mech. Catal.*, 2012, **107**, 215–229.
- 142 F. Bedioui, *Coord. Chem. Rev.*, 1995, **144**, 39–68.
- 143 G. S. Machado, P. B. Groszewicz, K. A. D. F. Castro, F. Wypych and S. Nakagaki, *J. Colloid Interface Sci.*, 2012, **374**, 278–86.
- 144 A. Nuzzo and A. Piccolo, *J. Mol. Catal. A Chem.*, 2013, **371**, 8–14.
- 145 M. Moghadam, S. Tangestaninejad, M. H. Habibi and V. Mirkhani, *J. Mol. Catal. A Chem.*, 2004, **217**, 9–12.
- 146 M. Moghadam, S. Tangestaninejad, V. Mirkhani, I. Mohammadpoor-Baltork and H. Kargar, *Bioorg. Med. Chem.*, 2005, **13**, 2901–2905.
- 147 R. Rahimi, S. Z. Ghoreishi and M. G. Dekamin, *Monatshefte für Chemie*, 2012, **143**, 1031–1038.
- 148 P. Battioni, J. P. Lallier, L. Barloy and D. Mansuy, *J. Chem. Soc., Chem. Commun.*, 1989, **01**, 1149–1151.
- 149 F. G. Doro, J. R. L. Smith, A. G. Ferreira and M. D. Assis, *J. Mol. Catal. A Chem.*, 2000, **164**, 97–108.
- 150 A. A. Guedes, J. R. L. Smith, O. R. Nascimento, D. F. C. Guedes and M. D. D. Assis, *J. Braz. Chem. Soc.*, 2005, **16**, 835–843.
- 151 M. A. Schiavon, Y. Iamamoto, O. R. Nascimento and M. D. D. Assis, *J. Mol. Catal. A Chem.*, 2001, **174**, 213–222.
- 152 S. Evans and J. R. Lindsay Smith, *J. Chem. Soc. Perkin Trans. 2*, 2000, 1541–1552.
- 153 S. L. H. Rebelo, A. R. Gonçalves, M. M. Pereira, M. M. Q. Simões, M. G. P. M. S. Neves and J. A. S. Cavaleiro, *J. Mol. Catal. A Chem.*, 2006, **256**, 321–323.
- 154 K. A. D. F. Castro, M. M. Q. Simões, M. G. P. M. S. Neves, J. A. S. Cavaleiro, F. Wypych and S. Nakagaki, *Catal. Sci. Technol.*, 2014, **4**, 129–141.
- 155 K. A. D. F. Castro, M. M. Q. Simões, M. G. P. M. S. Neves, J. A. S. Cavaleiro, R. R. Ribeiro, F. Wypych and S. Nakagaki, *Appl. Catal. A Gen.*, 2015, **503**, 9–19.
- 156 T. Heberer and T. Heberer, *Toxicol. Lett.*, 2002, **131**, 5–17.
- 157 V. Calisto and V. I. Esteves, *Chemosphere*, 2009, **77**, 1257–1274.
- 158 R. P. Schwarzenbach, B. I. Escher, K. Fenner, T. B. Hofstetter, C. A. Johnson, U. von Gunten and B. Wehrli, *Science*, 2006, **313**, 1072–1077.

-
- 159 L. H. M. L. M. Santos, A. N. Araújo, A. Fachini, A. Pena, C. Delerue-Matos and M. C. B. S. M. Montenegro, *J. Hazard. Mater.*, 2010, **175**, 45–95.
- 160 R. Rodil, J. B. Quintana, E. Concha-Graña, P. López-Mahía, S. Muniategui-Lorenzo and D. Prada-Rodríguez, *Chemosphere*, 2012, **86**, 1040–1049.
- 161 A. Jelic, M. Gros, A. Ginebreda, R. Cespedes-Sánchez, F. Ventura, M. Petrovic and D. Barcelo, *Water Res.*, 2011, **45**, 1165–1176.
- 162 R. Salgado, R. Marques, J. P. Noronha, J. T. Mexia, G. Carvalho, A. Oehmen and M. A. M. Reis, *Environ. Pollut.*, 2011, **159**, 2359–2367.
- 163 R. Loos, G. Locoro, S. Comero, S. Contini, D. Schwesig, F. Werres, P. Balsaa, O. Gans, S. Weiss, L. Blaha, M. Bolchi and B. M. Gawlik, *Water Res.*, 2010, **44**, 4115–4126.
- 164 T. V. Madureira, J. C. Barreiro, M. J. Rocha, E. Rocha, Q. B. Cass and M. E. Tiritan, *Sci. Total Environ.*, 2010, **408**, 5513–5520.
- 165 R. Loos, B. M. Gawlik, G. Locoro, E. Rimaviciute, S. Contini and G. Bidoglio, *Environ. Pollut.*, 2009, **157**, 561–568.
- 166 W. Hua, E. R. Bennett and R. J. Letcher, *Water Res.*, 2006, **40**, 2259–2266.
- 167 D. Bendz, N. A. Paxéus, T. R. Ginn and F. J. Loge, *J. Hazard. Mater.*, 2005, **122**, 195–204.
- 168 A. L. Boreen, W. A. Arnold and K. McNeill, *Aquat. Sci.*, 2003, **65**, 320–341.
- 169 T. A. Ternes, *Water Res.*, 1998, **32**, 3245–3260.
- 170 B. Halling-Sorensen, S. N. Nielsen, P. F. Lanzky, F. Ingerslev, H. C. H. Liitzhofl and S. E. Jorgensen, *Chemosphere*, 1998, **36**, 357–393.
- 171 F. Pomati, S. Castiglioni, E. Zuccato, R. Fanelli, D. Vigetti, C. Rossetti and D. Calamari, *Environ. Sci. Technol.*, 2006, **40**, 2442–2447.
- 172 F. Pomati, C. Orlandi, M. Clerici, F. Luciani and E. Zuccato, *Toxicol. Sci.*, 2008, **102**, 129–137.
- 173 S. Schnell, N. C. Bols, C. Barata and C. Porte, *Aquat. Toxicol.*, 2009, **93**, 244–252.
- 174 B. Quinn, F. Gagné and C. Blaise, *Sci. Total Environ.*, 2009, **407**, 1072–1079.
- 175 O. A. H. Jones, N. Voulvoulis and J. N. Lester, *Environ. Technol.*, 2001, **22**, 1383–1394.
- 176 J. Wilkinson, P. S. Hooda, J. Barker, S. Barton and J. Swinden, *Environ. Pollut.*, 2017, **231**, 954–970.

- 177 P. K. Jjemba, *Ecotoxicol. Environ. Saf.*, 2006, **63**, 113–130.
- 178 A. Y. C. Tong, B. M. Peake and R. Braund, *Environ. Int.*, 2011, **37**, 292–298.
- 179 L. Wollenberger, B. Halling-Sorensen and K. O. Kusk, *Chemosphere*, 2000, **40**, 723–730.
- 180 I. K. Konstantinou, D. G. Hela and T. A. Albanis, *Environ. Pollut.*, 2006, **141**, 555–570.
- 181 A. K. Sarmah, M. T. Meyer and A. B. A. Boxall, *Chemosphere*, 2006, **65**, 725–759.
- 182 G. M. Lalumera, D. Calamari, P. Galli, S. Castiglioni, G. Crosa and R. Fanelli, *Chemosphere*, 2004, **54**, 661–668.
- 183 J. F. Leal, M. G. P. M. S. Neves, E. B. H. Santos and V. I. Esteves, *Rev. Aquac.*, 2018, **10**, 281–295.
- 184 D. G. J. Larsson, C. De Pedro and N. Paxeus, *J. Hazard. Mater.*, 2007, **148**, 751–755.
- 185 J. Wang and S. Wang, *J. Environ. Manage.*, 2016, **182**, 620–640.
- 186 C. Afonso-Olivares, Z. Sosa-Ferrera and J. J. Santana-Rodríguez, *Sci. Total Environ.*, 2017, **599–600**, 934–943.
- 187 D. Dąbrowska, A. Kot-Wasik and J. Namieśnik, *Polish J. Environ. Stud.*, 2004, **13**, 617–626.
- 188 E. R. Christensen and A. Li, *Physical and Chemical Processes in the Aquatic Environment*, Wiley & Sons, Inc., Hoboken, 2014.
- 189 C. K. Remucal, *Environ. Sci. Process. Impacts*, 2014, **16**, 628–653.
- 190 P. Bartels and W. Von Tümpling Jr., *Sci. Total Environ.*, 2007, **374**, 143–155.
- 191 B. Mathon, J.-M. Choubert, C. Miege and M. Coquery, *Sci. Total Environ.*, 2016, **551–552**, 712–724.
- 192 D. B. Miklos, C. Remy, M. Jekel, K. G. Linden, J. E. Drewes and U. Hübner, *Water Res.*, 2018, **139**, 118–131.
- 193 D. Kanakaraju, B. D. Glass and M. Oelgemöller, *J. Environ. Manage.*, 2018, **219**, 189–207.
- 194 W. H. Glaze, J. Kang and D. H. Chapin, *Ozone Sci. Eng.*, 1987, **9**, 335–352.
- 195 R. Thiruvenkatachari, S. Vigneswaran and I. S. Moon, *Korean J. Chem. Eng.*, 2008, **25**, 64–72.
- 196 D. Pei and J. Luan, *Int. J. Photoenergy*, 2012, **2012**, 1–13.

-
- 197 M. C. DeRosa and R. J. Crutchley, *Coord. Chem. Rev.*, 2002, **233–234**, 351–371.
- 198 A. C. Herath, R. M. G. Rajapakse, A. Wicramasinghe and V. Karunaratne, *Environ. Sci. Technol.*, 2009, **43**, 176–180.
- 199 L. Shao, G. Xing, W. Lv, H. Yu, M. Qiu, X.-M. Zhang and C. Qi, *Polym. Int.*, 2013, **62**, 289–294.
- 200 E. Silva, M. M. Pereira, H. D. Burrows, M. E. Azenha, M. Sarakha and M. Bolte, *Photochem. Photobiol. Sci.*, 2004, **3**, 200–204.
- 201 C. J. P. Monteiro, M. M. Pereira, M. E. Azenha, H. D. Burrows, C. Serpa, L. G. Arnaut, M. J. Tapia, M. Sarakha and P. Wong-wah-chung, *Photochem. Photobiol. Sci.*, 2005, **4**, 617–624.
- 202 E. Pepe, O. Abbas, C. Rebufa, M. Simon, S. Lacombe and M. Julliard, *J. Photochem. Photobiol. A Chem.*, 2005, **170**, 143–149.
- 203 J.-H. Cai, J.-W. Huang, P. Zhao, Y.-H. Zhou, H.-C. Yu and L.-N. Ji, *J. Mol. Catal. A Chem.*, 2008, **292**, 49–53.
- 204 G. Yao, J. Li, Y. Luo and W. Sun, *J. Mol. Catal. A Chem.*, 2012, **361–362**, 29–35.
- 205 V. Héquet, P. Le Cloirec, C. Gonzalez and B. Meunier, *Chemosphere*, 2000, **41**, 379–386.
- 206 S. L. H. Rebelo, A. Melo, R. Coimbra, M. E. Azenha, M. M. Pereira, H. D. Burrows and M. Sarakha, *Environ. Chem. Lett.*, 2007, **5**, 29–33.
- 207 G. Granados-Oliveros, E. A. Páez-Mozo, F. M. Ortega, C. Ferronato and J.-M. Chovelon, *Appl. Catal. B Environ.*, 2009, **89**, 448–454.
- 208 M. Silva, M. E. Azenha, M. M. Pereira, H. D. Burrows, M. Sarakha, M. F. Ribeiro, A. Fernandes, P. Monsanto and F. Castanheira, *Pure Appl. Chem.*, 2009, **81**, 2025–2033.
- 209 S. Murphy, C. Saurel, A. Morrissey, J. Tobin, M. Oelgemöller and K. Nolan, *Appl. Catal. B Environ.*, 2012, **119–120**, 156–165.
- 210 H. Kim, W. Kim, Y. MacKeyev, G.-S. Lee, H.-J. Kim, T. Tachikawa, S. Hong, S. Lee, J. Kim, L. J. Wilson, T. Majima, P. J. J. Alvarez, W. Choi and J. Lee, *Environ. Sci. Technol.*, 2012, **46**, 9606–9613.

CHAPTER 2

Synthesis of new second-generation porphyrins bearing potential anchorage units to be used as catalysts in oxidation reactions

Chapter 2. Synthesis of new second-generation porphyrins bearing potential anchorage units to be used as catalysts in oxidation reactions

In this chapter, after a short introduction concerning the synthetic methodologies to obtain 5,10,15,20-tetraarylporphyrins, the work developed to obtain this type of porphyrins bearing potential anchorage units will be discussed. The preparation of the Mn(III) complexes used in the catalytic studies described in chapter 3 will also be presented here.

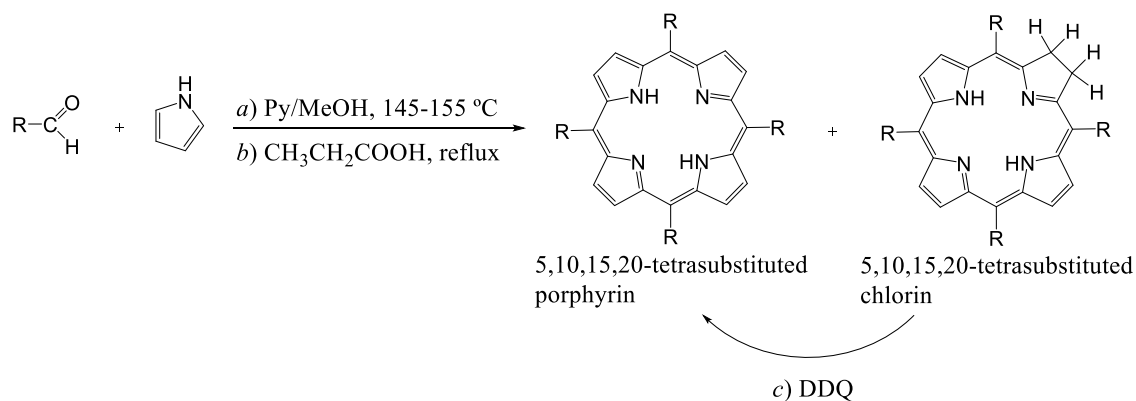
2.1. Synthetic methodologies to obtain 5,10,15,20-tetraarylporphyrins

Most of the porphyrinic ligands used in catalysis are based on 5,10,15,20-tetraarylporphyrins as already discussed in the first chapter. In general, the access to this sort of macrocycles involves condensation reactions between aldehydes and pyrroles or dipyrromethanes and other similar precursors.¹ In this section, only methods involving the simple polymerization of pyrrole with aldehydes will be revised, since this was the methodology followed in the preparation of the ligands described in this thesis.

Most of the methodologies used to prepare 5,10,15,20-tetraarylporphyrins are based on synthetic improvements of the landmark Rothmund reaction. In 1935, Rothmund described for the first time that the simple condensation of pyrrole with an aldehyde (e.g. formaldehyde, acetaldehyde and furaldehyde) affords the corresponding 5,10,15,20-tetrasubstituted porphyrin. These reactions were performed in pyridine/methanol at 145-155 °C in a sealed tube under anaerobic conditions (**Scheme 2.1-a**).^{2,3} In 1939, the same author used this approach to obtain 25 new porphyrins by using adequate aliphatic, aromatic and heterocyclic aldehydes.⁴ In all these works, the yields reported were always low, being the best results obtained in the synthesis of 5,10,15,20-tetraphenylporphyrin (10%).⁵ Another limitation of this approach was the presence of a contaminant^{4,5} that was posteriorly identified by Calvin and co-workers as being the corresponding 5,10,15,20-tetrasubstituted chlorin (**Scheme 2.1**).^{6,7}

In 1967 Adler and co-workers implemented some important changes to the Rothmund's conditions by carrying out the reaction in acidic medium and in the presence of oxygen (**Scheme 2.1-b**).⁸ Although important improvements in the porphyrin yields were described under these conditions, the presence of the corresponding chlorin was still a limitation.⁸ In 1979 Smith and co-workers reported that the treatment of the reactional mixture with 2,3-dichloro-5,6-dicyanobenzoquinone (DDQ) allows obtaining the

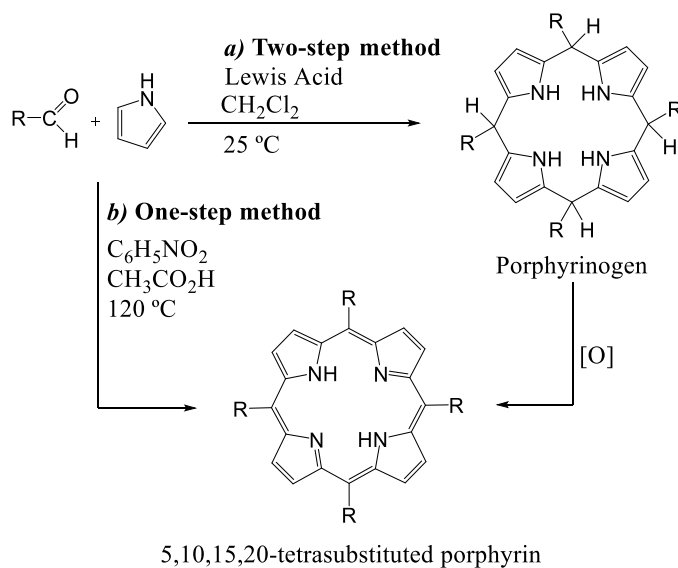
porphyrin free of the chlorin (**Scheme 2.1-c**).⁹ Although the Adler's methodology permits to enhance substantially the porphyrin yields, the approach is limited to aldehydes that are not sensitive to the refluxing acidic conditions.



Scheme 2.1. Synthesis of 5,10,15,20-tetrasubstituted porphyrins: a) Rothemund's conditions; b) Adler's conditions; c) Smith oxidation procedure.

Important contributions allowing the preparation of porphyrins from aldehydes that could not support the Adler's refluxing acidic conditions were reported by the Gonsalves and the Lindsey groups in the 1980's (**Scheme 2.2-a**).¹⁰⁻¹² In both cases the tetramerization of the monomeric units were accomplished in chlorinated solvents at room temperature, in the absence of both oxygen and light, and using trifluoroacetic acid (TFA) or BF₃ as catalysts in order to maximize the formation of the porphyrinogen, followed by the oxidative step with DDQ or *p*-chloranil. In 1985 Gonsalves and Pereira used this two-step approach to prepare 5,10,15,20-tetraalkylporphyrins,¹⁰ and soon after Lindsey and co-workers extended the methodology to the synthesis of 5,10,15,20-tetraarylporphyrins.^{11,12} Under these conditions, and doing the reactions at moderate dilution (10⁻² M), was possible to obtain porphyrins from sensitive aldehydes in yields ranging from 30 to 40%.¹²

Lindsey also tried to promote the synthesis of 5,10,15,20-tetrasubstituted porphyrins in just one-step by doing the condensation in the presence of the oxidant.¹³ Nevertheless, the yields were lower than those obtained using the two-step strategy.



Scheme 2.2. Synthesis of 5,10,15,20-tetrasubstituted porphyrins: *a)* using the two-step approach developed by the Gonsalves and the Lindsey groups; *b)* using the oxidative one-step approach developed by Gonsalves and Pereira.

The Lindsey's method is considered a very important achievement in the synthesis of 5,10,15,20-tetrasubstituted porphyrins, since this type of macrocycles free of the corresponding chlorins can be obtained usually in higher yields than under the other approaches. The major weakness of this method is the use of very expensive quinones in the oxidation step.

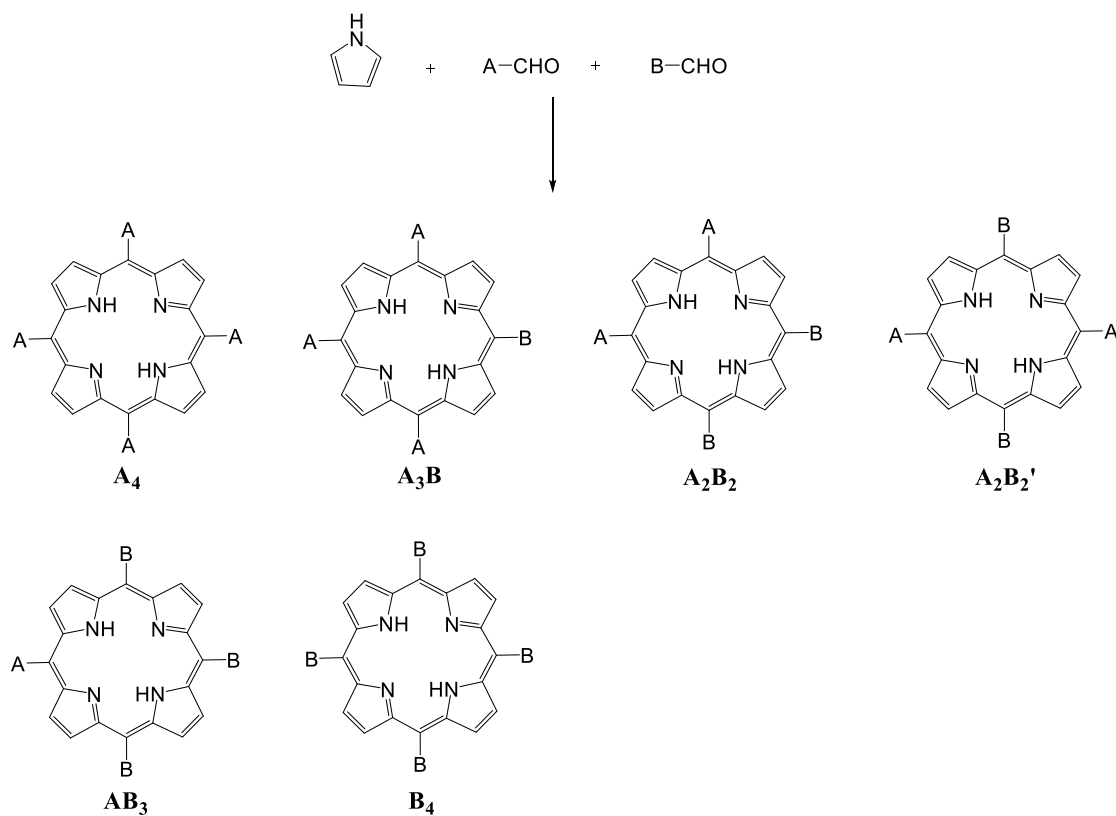
In order to avoid the use of expensive quinones, in 1991 Gonsalves and co-workers reported the condensation between the pyrrole and the aldehyde in a mixture of acetic acid and nitrobenzene, thus obtaining the desired porphyrin free of the corresponding chlorin (**Scheme 2.2-b**).¹⁴ In general, the use of nitrobenzene as the oxidant allows the synthesis of the desired porphyrin in just one-step in acceptable yields. Moreover, in some cases, the porphyrin crystallizes directly from the reaction media, thus avoiding extra purification procedures.

Posteriorly, Sharghi and Nejad reported the synthesis of a series of porphyrins also in just one step, by carrying out the condensation of pyrrole with the adequate aldehyde at room temperature in the presence of equimolar amounts of PCl_5 or $\text{CF}_3\text{SO}_2\text{Cl}$ and in the presence of air.^{15,16} Under these reaction conditions, the authors were able to obtain several tetraarylporphyrins in yields ranging from 20 to 65%.

In the last few years, some authors have reported the synthesis of porphyrins under microwave (MW) irradiation.^{17–25} The MW synthesis usually involves the adaptation of the classical condensation of the pyrrole and the aldehyde, based on Adler or Gonsalves methodologies. Recently, Henriques *et al.* obtained 5,10,15,20-tetraaryl- and 5,10,15,20-tetraalkylporphyrins in good yields under MW irradiation, using water simultaneously as solvent and acid catalyst.²⁵ This methodology avoids the use of organic solvents, catalysts and oxidants which are frequently toxic and expensive.

In general, the main gains related to the use of MW irradiation in the synthesis of 5,10,15,20-tetraarylsubstituted porphyrins are the significant reduction in the reaction time, and, in many cases, the decrease of the volume of solvent used. The yields obtained for various 5,10,15,20-tetraarylsubstituted porphyrins were improved when MW irradiation was used; however, this was not observed for the 5,10,15,20-tetrakis(2,6-dichlorophenyl)porphyrin whose reported yield was near or lower than that obtained by conventional heating.^{19,21,25}

The approaches discussed before can be extended to the use of more than one aldehyde and afford the so-called asymmetric porphyrins. When two different aldehydes are used, depending on the molar amount and reactivity of the aldehydes, six different porphyrins **A₄**, **A₃B**, **A₂B₂** ('*cis*' disubstituted porphyrin), **A₂B₂'** ('*trans*' disubstituted porphyrin), **AB₃** and **B₄** can be obtained (**Scheme 2.3**).^{26–28} In practical terms the use of more than two aldehydes is not viable. This process of synthesis allows obtaining porphyrins with specific groups without the need for an extra functionalization step. Such porphyrins may be very important for subsequent immobilization on solid supports. Depending on the support we can choose the most suitable aldehyde to obtain the porphyrin with the functionality that allows, for example, its covalent attachment to the support. In other cases, it is necessary to perform additional functionalization steps such as the introduction of sulfonic or nitro groups, the last one being usually reduced to the corresponding amino groups. Another example is the nucleophilic aromatic substitution of the *para*-F atoms of the pentafluorophenyl groups in the 5,10,15,20-tetrakis(pentafluorophenyl)porphyrin by nitrogen, oxygen or sulfur-containing nucleophiles, providing electron-donating substituents that allow the subsequent immobilization on a solid support.²⁹



Scheme 2.3. The possible six porphyrins that can be obtained using two different aldehydes.

2.2. The new second-generation porphyrins bearing potential anchorage units prepared in this work

In the last years, the use of heterogeneous catalysts based on metalloporphyrins has been explored, specially due to the possibility of their recovery and reuse.^{30–37} Most of those studies are based on 5,10,15,20-tetraarylporphyrins of the so-called first- and second-generations, having suitable groups to covalently graft them to a support.³⁸ In some cases, the introduction of extra functionalities such as sulfonic or amino groups on the porphyrin core is required in order to allow its attachment to a support.³⁹ Taking the advantage that 3,5-dichloro-4-pyridinecarboxaldehyde is commercially available and that the pyridine unit has electron-withdrawing and bulky substituents at adequate positions to protect the porphyrin ligand from oxidative degradation or inactivation, it was envisaged that porphyrins built from that aldehyde would afford stable catalysts with excellent features for further immobilization through the pyridine unit(s). So, in the present work, two second-generation porphyrins containing 3,5-dichloropyridyl substituent(s) at the *meso* position(s), as well as their manganese(III) complexes, were prepared and characterized for the first time: the symmetric 5,10,15,20-tetrakis(3,5-dichloropyridin-4-yl)porphyrin (**H₂TDCPyP**), and the asymmetric 5,10,15-tris(2,6-dichlorophenyl)-20-(3,5-dichloropyridin-4-yl)porphyrin (**H₂mono-DCPyP**) (**Figure 2.1 A**). The manganese(III) complexes of **H₂TDCPyP** and **H₂mono-DCPyP** were tested as catalysts for the oxidation of alkenes and the results will be described in chapter 3.

Under the same target of developing porphyrins with potential anchorage units, a different strategy was considered in order to obtain porphyrins **P1-5** (**Figure 2.1 A**) with imidazole units. These porphyrins were obtained by the sequential nucleophilic substitution of the *para*-F atoms in the 5,10,15,20-tetrakis(pentafluorophenyl)porphyrin (**H₂TF₅PP**) (**Figure 2.1 B**) by imidazole units. It was envisaged that these derivatives would also give rise to robust catalysts capable of being immobilized onto suitable solid supports *via* the imidazole substituent(s). In this work, constrained by the calendar, the synthesis of the porphyrin metal complexes and their immobilization onto solid supports, in order to study their catalytic performances, was not possible. However, they are expected to exhibit catalytic activities very close to those of the robust **H₂TF₅PP**, which

may be particularly advantageous in a context of heterogeneous catalysis. It will be extremely relevant to carry out these studies in a future work.

During the present work was also necessary to synthesize the 5,10,15,20-tetrakis(2,6-dichlorophenyl)porphyrin (**H₂TDCPP**), the 5,10,15-tris(2,6-dichlorophenyl)-20-(pyridin-4-yl)porphyrin (**H₂DC-mono-4PyP**) (**Figure 2.1 B**) and the corresponding manganese(III) complexes to be used in oxidative catalysis for comparative purposes with the novel catalysts prepared.

In the following sections, the following topics will be discussed:

- i) The synthesis of the new porphyrins and of the known porphyrins that were used as catalysts during the development of this work;
- ii) The complete characterization of the novel porphyrins;
- iii) The experimental details to obtain the porphyrins used in the present work.

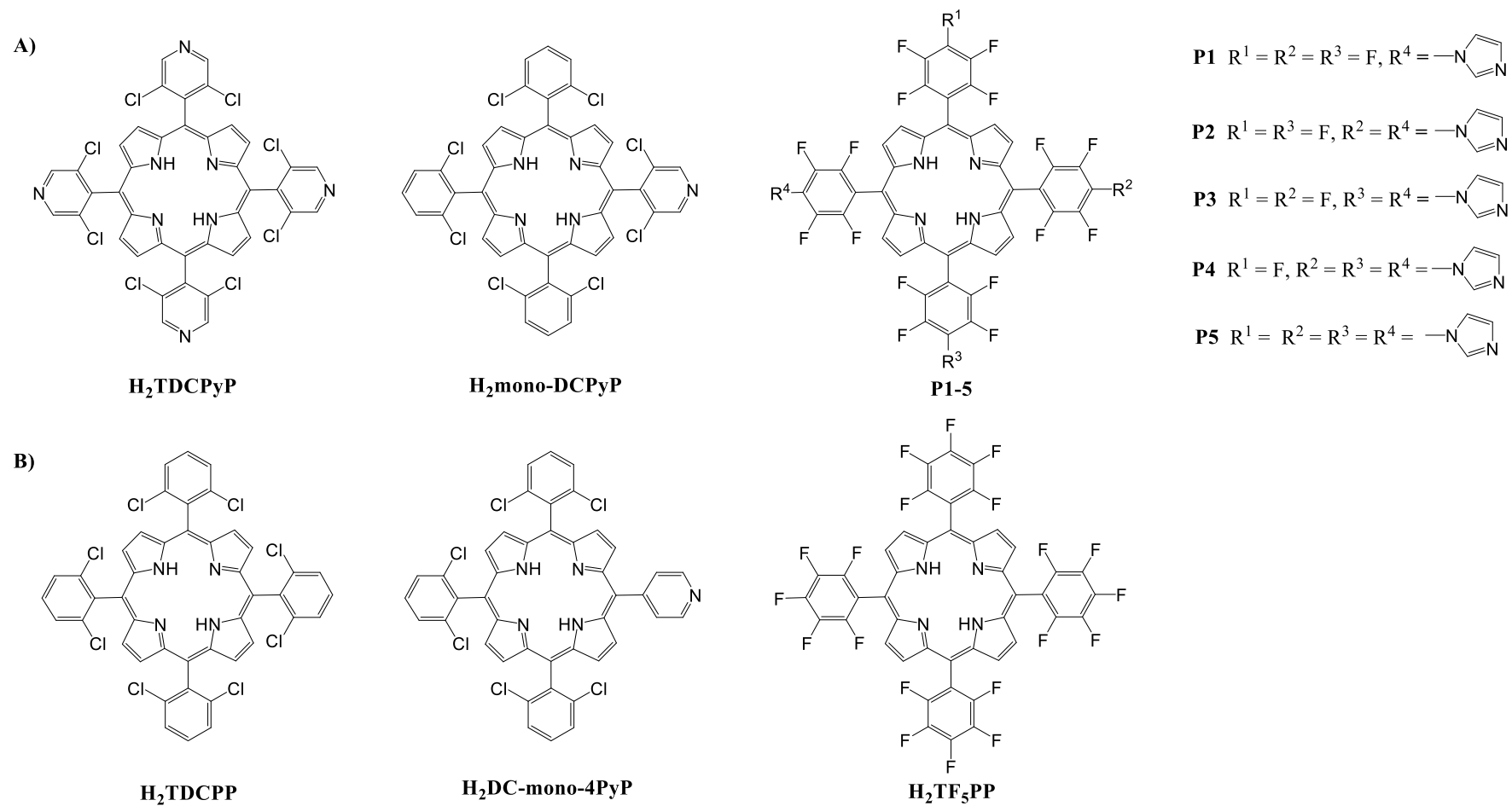
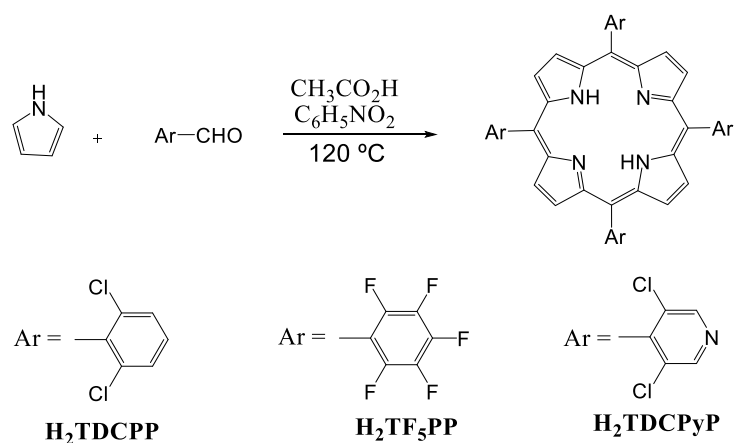


Figure 2.1. The structures of **A)** the novel free-base porphyrins and **B)** other free-base porphyrins prepared in the present work.

2.2.1. Synthesis of the free-base porphyrins

The symmetric free-base porphyrins **H₂TDCPP**, **H₂TF₅PP** and **H₂TDCPyP** were synthesized according to the method developed by Gonsalves *et al.* and previously described.¹⁴ The methodology consists in the condensation of pyrrole with the corresponding aldehyde in a mixture of acetic acid and nitrobenzene at 120 °C, for a period of 45 minutes, as described in **Scheme 2.4**.



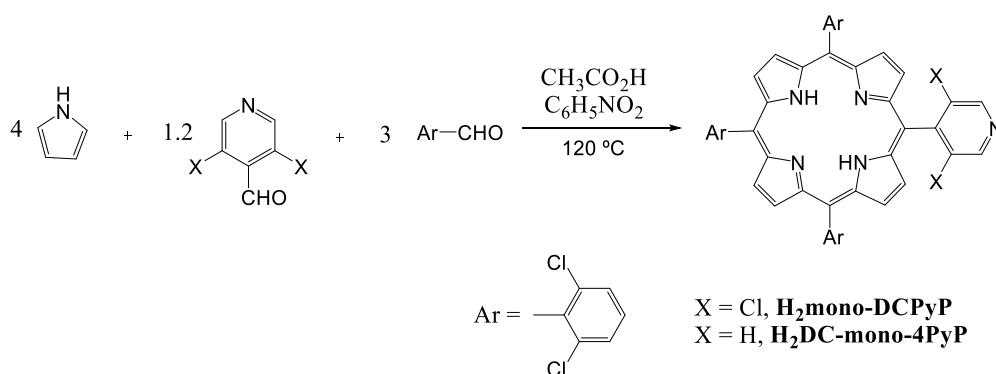
Scheme 2.4. Synthetic strategy to obtain the symmetric free-base porphyrins.

The reactions were monitored by thin layer chromatography (TLC) and by UV-Vis spectrophotometry; the latter technique allowed to confirm the formation of the porphyrins due to the presence of the typical Soret band and the Q-bands in the reactional mixture spectra. At the end of the reaction the well-known **H₂TDCPP** was obtained pure directly from the reaction medium by precipitation with methanol, in 5% yield. In the case of **H₂TF₅PP** was necessary to distil the acetic acid and the nitrobenzene under reduced pressure and then to purify the organic residue by column chromatography (please see the details in the experimental part). After crystallization, **H₂TF₅PP** was obtained pure in 11% yield.

H₂TDCPyP was synthesized for the first time in the present work and, in this case, was also required to distil the solvents of the reaction under reduced pressure before the purification step by silica column chromatography. The fraction containing the porphyrin was identified by UV-Vis spectrophotometry and further purification by TLC was required in order to obtain the desired pure porphyrin. During these studies was verified that this

porphyrin was not very stable in solution, which can partially justify the low yield obtained in the synthesis (0.2%).

The same approach was used to prepare the asymmetric free-base porphyrins **H₂mono-DCPyP** and **H₂DC-mono-4PyP**. The condensation between pyrrole, 2,6-dichlorobenzaldehyde and the suitable aldehyde bearing the pyridine unit was accomplished by using the adequate molar amount of the aldehydes that could favour the formation of the desired porphyrins just with one pyridine unit (**Scheme 2.5**).



Scheme 2.5. Synthetic strategy to obtain the asymmetric free-base porphyrins.

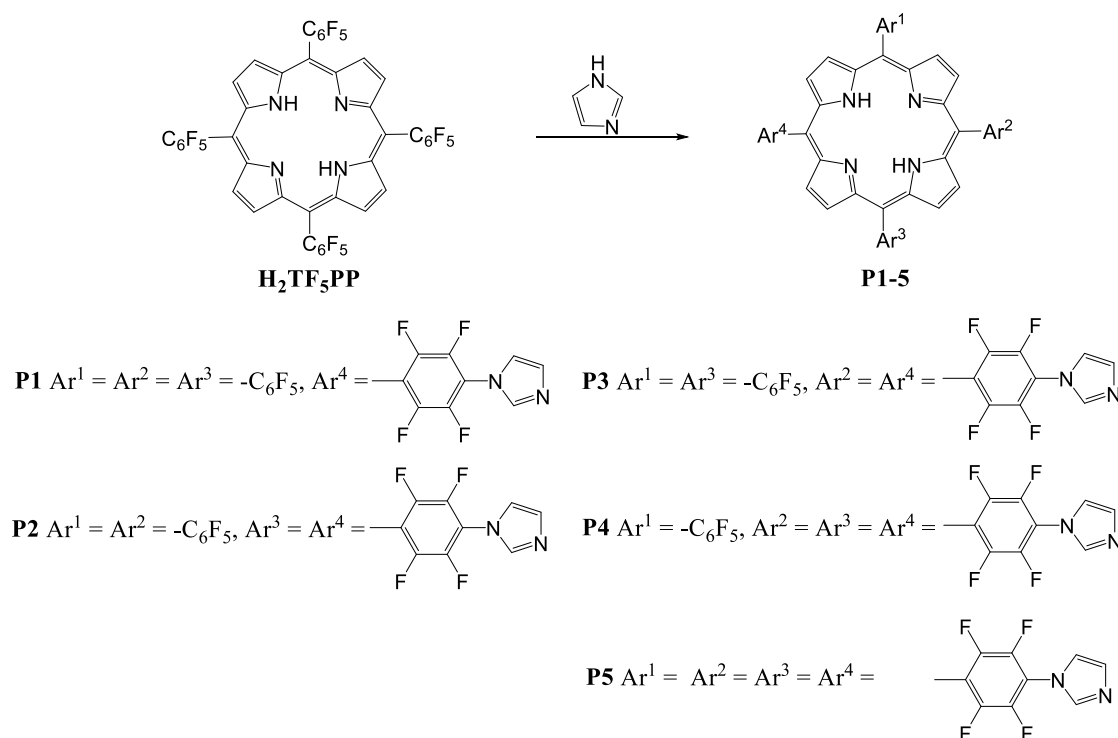
In both cases, at the end of the reaction the solvents were distilled at reduced pressure and the asymmetric porphyrins were purified by column chromatography. After crystallization, **H₂mono-DCPyP** and **H₂DC-mono-4PyP** were obtained pure in 2.6% and 1.7% yield, respectively.

As already mentioned, when two aldehydes are used a mixture of porphyrins is expected, which is related to the possible combinations of the aldehydes. The formation of a desired porphyrin can be favored by controlling the ratio between the selected aldehydes. As mentioned above, to promote the formation of **H₂mono-DCPyP** and **H₂DC-mono-4PyP** the proportion 3:1.2 of 2,6-dichlorobenzaldehyde and 3,5-dichloro-4-pyridinecarboxaldehyde (for **H₂mono-DCPyP**) or 4-pyridinecarboxaldehyde (for **H₂DC-mono-DCPyP**) was used. Even so, and in addition to the desired porphyrin, other porphyrins were isolated.

So, in the synthesis of the desired **H₂DC-mono-4PyP**, also the **H₂TDCPP** and the porphyrins with two, three or four 4-pyridyl units were obtained. In the case of the **H₂mono-DCPyP**, was possible to isolate also **H₂TDCPP**, but no other porphyrins were detected. The absence of other porphyrins resulting from the combination of two, three or

four units of 3,5-dichloro-4-pyridinecarboxaldehyde may be due to the lower reactivity of this aldehyde if compared to 2,6-dichlorobenzaldehyde. Therefore, a higher amount of **H₂TDCPP** and of mono-substituted derivative would be predictable. It is noteworthy that, in the synthesis of the symmetrical porphyrin **H₂TDCPyP**, a low yield was also obtained which corroborates these results and the low reactivity of the aldehyde.

Before discussing the work developed in the synthesis of porphyrins bearing imidazole units (**Scheme 2.6**), is important to refer that the main goal was to obtain porphyrin **P1**, with just one imidazole unit, and porphyrin **P5**, with four imidazole units. The different reaction conditions tested, in order to improve the yields for these two derivatives, such as type and volume of solvent, reaction temperature and molar ratio of the reagents are summarized in **Table 2.1**.



Scheme 2.6. Synthetic strategy to obtain the porphyrins **P1-5**. Different experimental conditions were studied (e.g., solvent, temperature, molar ratio of the reagents, the presence of a base) to obtain **P1** or **P5** as the major products. The results of such studies can be seen in **Table 2.1**.

The studies were initiated using tetrahydrofuran (THF) as solvent and 6 equivalents (eq) of imidazole to promote the formation of the tetra-substituted derivative **P5**, adapting the conditions from literature procedures.⁴⁰ The results show that, at room temperature

(23 °C) and without adding a base (cesium carbonate), no reaction occurred even after 62 h (**Table 2.1**, Entry 1). Therefore, we decided to perform the reaction using 5 eq of imidazole and the same molar amount of cesium carbonate, in order to improve the imidazole nucleophilicity (**Table 2.1**, Entry 2). The reaction was monitored by TLC, showing the formation of 5 compounds, later on identified as porphyrins **P1-5**. Since no significant changes were detected in the TLC after 48 h, the reaction was stopped. Under these conditions, although the starting porphyrin **H₂TF₅PP** was almost totally consumed, the desired tetra-substituted porphyrin **P5** was isolated in a non-satisfactory yield (7.7%). Under these conditions, the porphyrin isolated with a better yield was **P4** (22.3%), followed by **P3** (18.2%), **P1**(15.4%) and finally **P2** (7.5%). Trying to improve the yield of **P5**, the reaction was repeated but at THF refluxing temperature (65 °C) (**Table 2.1**, Entry 3). There was a considerable improvement in the yield of **P5** (15.7%), that was isolated as the second most abundant derivative, following **P4**, and the reaction time needed to completely transform **H₂TF₅PP** was reduced to 9 h (**Table 2.1**, Entry 3). However, under these conditions, some degradation compounds were observed at the bottom of the TLC plate. In an attempt to minimize the decomposition of the desired products, the reaction was repeated using more diluted conditions (4 mL vs 2 mL of solvent) (**Table 2.1**, Entry 4). The yield of **P5** was not improved and no decrease on the formation of more polar compounds was detected.

When the amount of imidazole was reduced to 1.5 eq and the reaction was done in THF at 65 °C and in the presence of cesium carbonate, the mono-substituted porphyrin **P1** was obtained as the major product (33.3% yield) followed by **P3** (14.0%), **P4** (9.8%) and **P2** (6.7%) (**Table 2.1**, Entry 6). Under these conditions the formation of **P5** was not detected.

The change of THF for dimethylformamide (DMF) (**Table 2.1**, Entries 7-10) allowed to improve some aspects of the previous reactions. The reactions were carried out at room temperature (\approx 23 °C), which allowed minimizing the formation of the degradation products and the reaction time was reduced to 4 h. Moreover, using this solvent and 5 eq of imidazole and base, the yield of the tetra-substituted porphyrin **P5** was enhanced to 29.7%, being the main product obtained (**Table 2.1**, Entry 7). In the same conditions and using 1.5 eq of imidazole and base, the major product obtained was the mono-substituted porphyrin **P1** (32% yield) and the formation of porphyrins **P4** and **P5** was not observed (**Table 2.1**,

Entry 8). The yield of the desired products did not change significantly when the amount of the reagents was doubled (**Table 2.1**, Entries 5, 9 and 10).

From the reaction conditions studied, the best to obtain the porphyrins **P1** and **P5** are: DMF as solvent at room temperature in the presence of cesium carbonate, using 1.5 or 5 eq of imidazole and base to obtain **P1** or **P5**, respectively.

Table 2.1. Nucleophilic aromatic substitution of **H₂TF₅PP** with imidazole.

Entry	H ₂ TF ₅ PP (mg)	Imidazole (eq)	Base ^(a) (eq)	Solvent (mL)	Time (h)	Yield %				
						P1	P2	P3	P4	P5
1	50	6	0	THF (2) ^(b)	62	-	-	-	-	-
2	50	5	5	THF (2) ^(b)	48	15.4	7.5	18.2	22.3	7.7
3	50	5	5	THF (2) ^(c)	9	5.7	4.4	8.7	21.6	15.7
4	50	5	5	THF (4) ^(c)	9	10.7	3.2	6.7	21.6	13.7
5	100	5	5	THF (4) ^(c)	9	4.2	3.8	7.2	18.5	15.4
6	50	1.5	1.5	THF (2) ^(c)	9	33.3	6.7	14.0	9.8	-
7	50	5	5	DMF (2) ^(b)	4	7.2	3.6	6.7	26.1	29.7
8	50	1.5	1.5	DMF (2) ^(b)	4	32	7.7	14.4	-	-
9	100	5	5	DMF (4) ^(b)	4	1.3	2.8	6.0	25.5	25.1
10	100	1.5	1.5	DMF (4) ^(b)	4	30.0	5.8	14.1	-	-

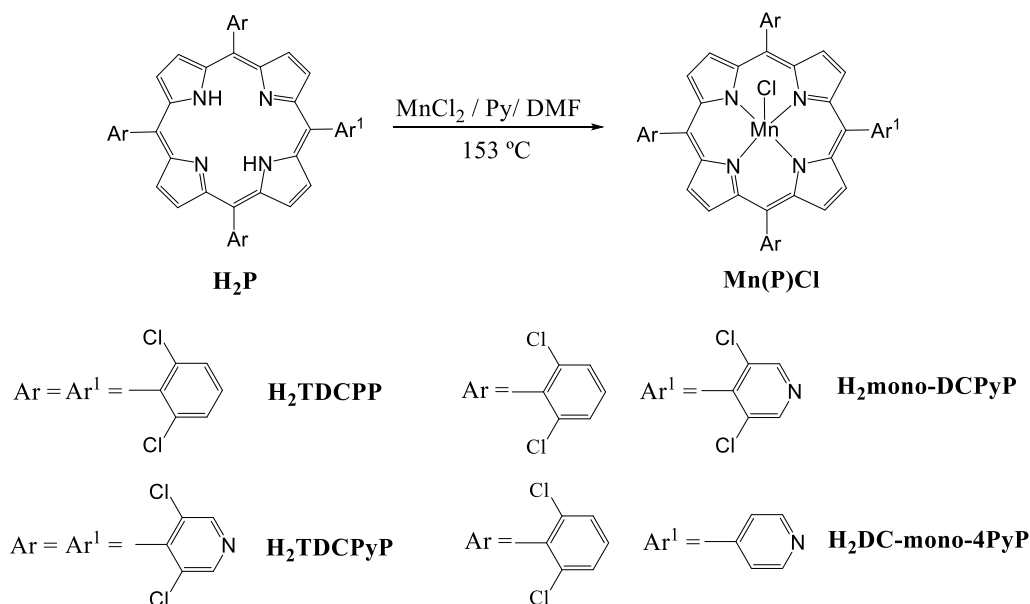
^(a) Cesium carbonate

^(b) Reactions were carried out at room temperature (≈ 23 °C)

^(c) Reactions were carried out at 65 °C

2.2.2. Synthesis of the manganese(III) complexes

The free-base porphyrins **H₂TDCPP**, **H₂TDCPyP**, **H₂mono-DCPyP** and **H₂DC-mono-4PyP** were metalated according to Adler's conditions, using 10 equivalents of the metal salt, MnCl₂·4H₂O, pyridine and DMF at 153 °C (**Scheme 2.7**).⁴¹



Scheme 2.7. Synthetic strategy to obtain the manganese(III) complexes.

The metalations were monitored by TLC and by UV-Vis spectrophotometry. Throughout the reaction, when dichloromethane was used as eluent, the disappearance of the free-base porphyrin spot that elutes in the front of the TLC plate and the appearance of the manganese complex spot at the base of the TLC was observed. Notwithstanding, UV-Vis spectrophotometry is the most effective method to unambiguously observe that the complexation is complete. As previously mentioned in chapter 1, the UV-Vis spectrum of a free-base porphyrin presents a Soret band at $\lambda \approx 390\text{-}425$ nm and can display up to four Q-bands at $\lambda \approx 480\text{-}700$ nm. After manganese complexation, the bathochromic shift of the Soret band, the change in the number, position and intensity of the Q-bands and the presence of the transition bands at $\lambda \approx 320\text{-}400$ nm confirmed the success of manganese insertion (see **Figures 2.4** and **2.8** for the manganese insertion in **H₂TDCPyP** and **H₂mono-DCPyP**, respectively and the sections 2.2.3 and 2.3.2 for further details).

After complexation, the solvent was removed in the rotary evaporator, under vacuum, and the organic residue was washed with water to remove the excess of metal salt. The complexes were crystallized using a mixture of dichloromethane/hexane, leading to pure manganese(III) porphyrins in quantitative yields.

2.2.3. Structural characterization

The structures of all the synthesized compounds were confirmed by adequate spectroscopic techniques, namely UV-Vis spectrophotometry, NMR and mass spectrometry. In this section, only the spectroscopic data of the new compounds prepared will be discussed. The characterization of the other porphyrins, already known from the literature, is summarized in the experimental section.

The ^1H NMR spectrum of the free-base porphyrin **H₂TDCPyP** (Figure 2.2), presents the characteristic high field signal at $\delta = -2.66$ ppm relative to the resonance of the inner NH protons of the porphyrin, while it is possible to identify two singlets in the aromatic region, one at $\delta = 8.68$ ppm, corresponding to the eight protons of the β -pyrrolic positions and the other one at $\delta = 9.04$ ppm due to the resonance of the eight protons of the *meso*-3,5-dichloropyridyl rings.

The HRMS-ESI spectrum of **H₂TDCPyP** (Figure 2.3) shows the mass of the most abundant peak at m/z 894.9168, with the isotope pattern of the chlorine atoms corresponding to the molecular ion $[\text{M}+\text{H}]^+$, which is consistent with the expected molecular formula $[\text{C}_{40}\text{H}_{18}\text{Cl}_8\text{N}_8]$.

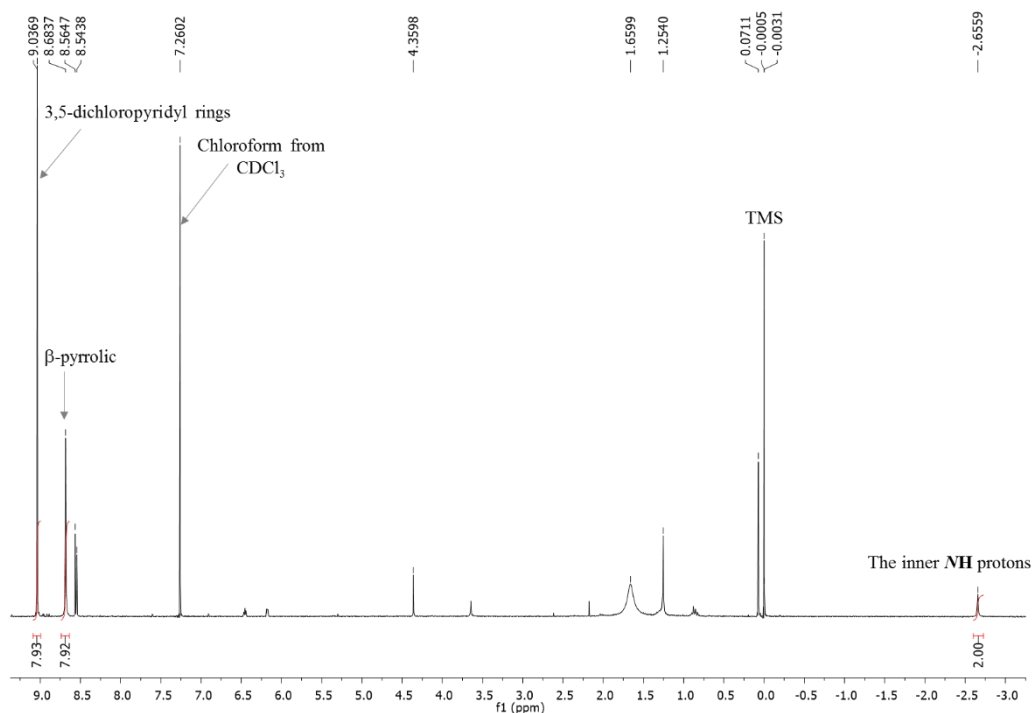


Figure 2.2. ^1H NMR spectrum of **H₂TDCPyP**, using CDCl_3 as solvent.

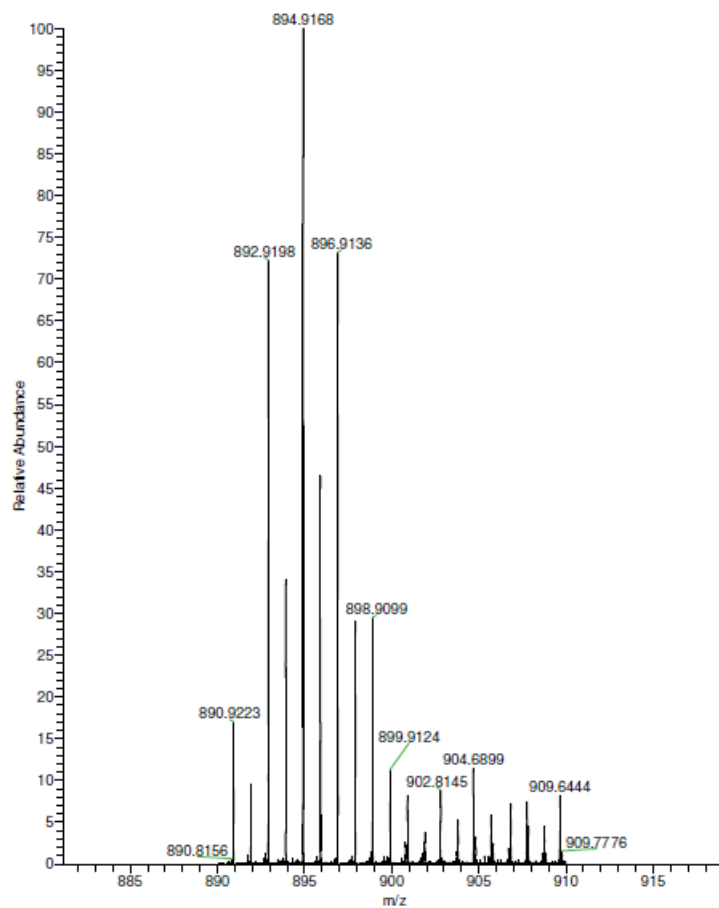


Figure 2.3. Mass spectrum (HRMS-ESI) of **H₂TDCPyP**.

The UV-Vis spectrum of **H₂TDCPyP** in chloroform presents the characteristic Soret band at $\lambda_{\text{max}} = 417$ nm and two Q-bands are detected at $\lambda_{\text{max}} = 510$ and 586 nm (**Figure 2.4**).

In the case of **Mn(TDCPyP)Cl**, its UV-Vis spectrum in methanol is consistent with the insertion of the metal, showing the Soret band shifted to a higher wavelength ($\lambda_{\text{max}} = 459$ nm), two Q-bands at $\lambda_{\text{max}} = 504$ and 555 nm and the manganese transition bands at $\lambda \approx 320$ –400 nm (**Figure 2.4**).

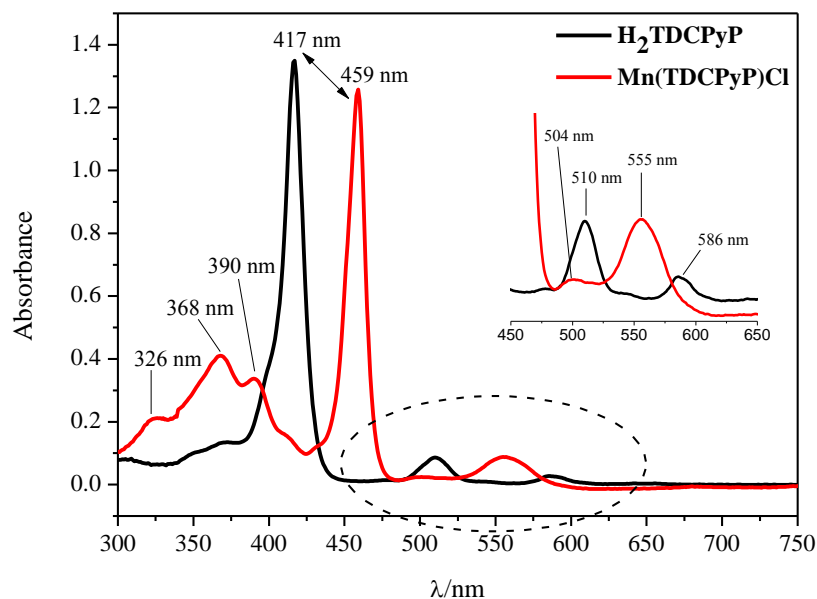


Figure 2.4. UV-Vis spectra of H_2TDCPyP and $\text{Mn}(\text{TDCPyP})\text{Cl}$. The spectra were obtained using chloroform as solvent for the free-base porphyrin and methanol for the Mn(III) complex.

The HRMS-ESI spectrum of $\text{Mn}(\text{TDCPyP})\text{Cl}$ (Figure 2.5) shows the most abundant peak at m/z 946.8317 with the isotope pattern of the chlorine atoms confirming with the molecular ion $[\text{M}]^+$, which is consistent with the expected molecular formula $[\text{C}_{40}\text{H}_{16}\text{Cl}_8\text{MnN}_8]$.

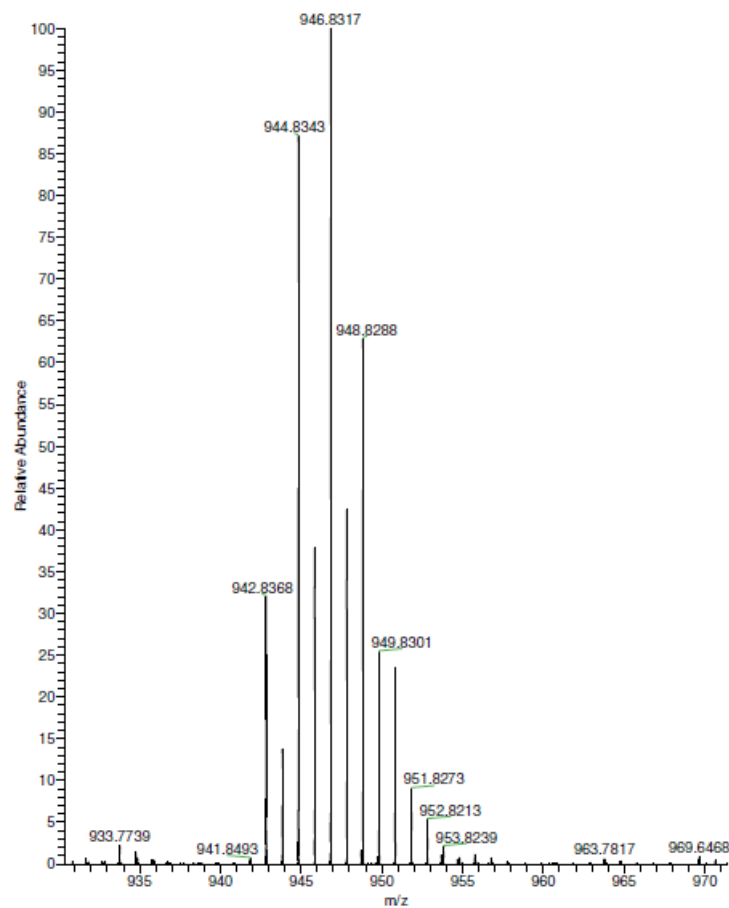


Figure 2.5. Mass spectrum (HRMS-ESI) of Mn(TDCPyP)Cl.

In the ^1H NMR spectrum of **H₂mono-DCPyP** (Figure 2.6), the presence of the 3,5-dichloropyridyl moiety was easily identified by the singlet at $\delta = 9.00$ ppm due to the resonance of its two protons. In this case, as a result of the macrocycle asymmetry, the signals due to the resonance of the β -pyrrolic protons appear as two doublets ($J = 4.4$ Hz) at $\delta = 8.61$ and 8.70 ppm and as singlet at $\delta = 8.68$ ppm. The doublets were assigned to the four β -pyrrolic protons near the 3,5-dichloropyridyl ring while the singlet was identified as being due to the remaining β -pyrrolic protons less affected by the asymmetry induced by the pyridine unit. The resonances of the protons of the 2,6-dichlorophenyl units appear as two multiplets at $\delta = 7.69$ - 7.73 ppm for the three protons of the *para* positions and at $\delta = 7.79$ - 7.81 ppm for the six protons of the *meta* positions. The resonance of the inner NH protons appears as a singlet at $\delta = -2.57$ ppm.

The HRMS-ESI spectrum of **H₂mono-DCPyP** (Figure 2.7) shows the most abundant peak at m/z 891.9311, with the isotope pattern of the chlorine atoms

corresponding to the molecular ion $[M+H]^+$, which is in accordance with the expected molecular formula $[C_{43}H_{21}Cl_8N_5]$.

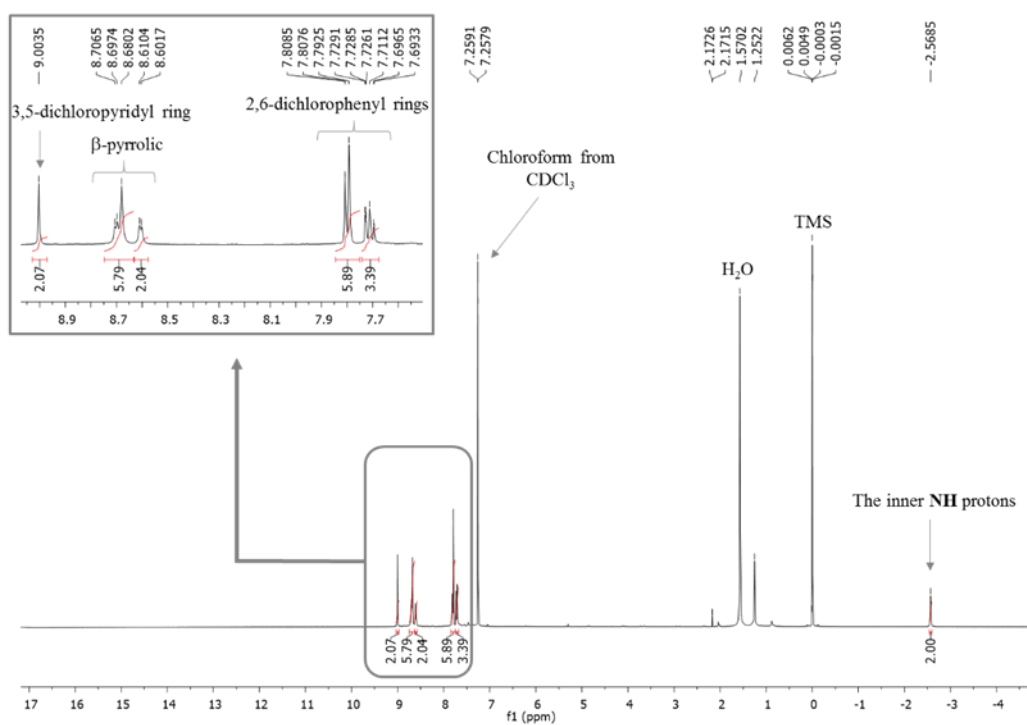


Figure 2.6. ^1H NMR spectrum of $\text{H}_2\text{mono-DCPyP}$, using CDCl_3 as solvent.

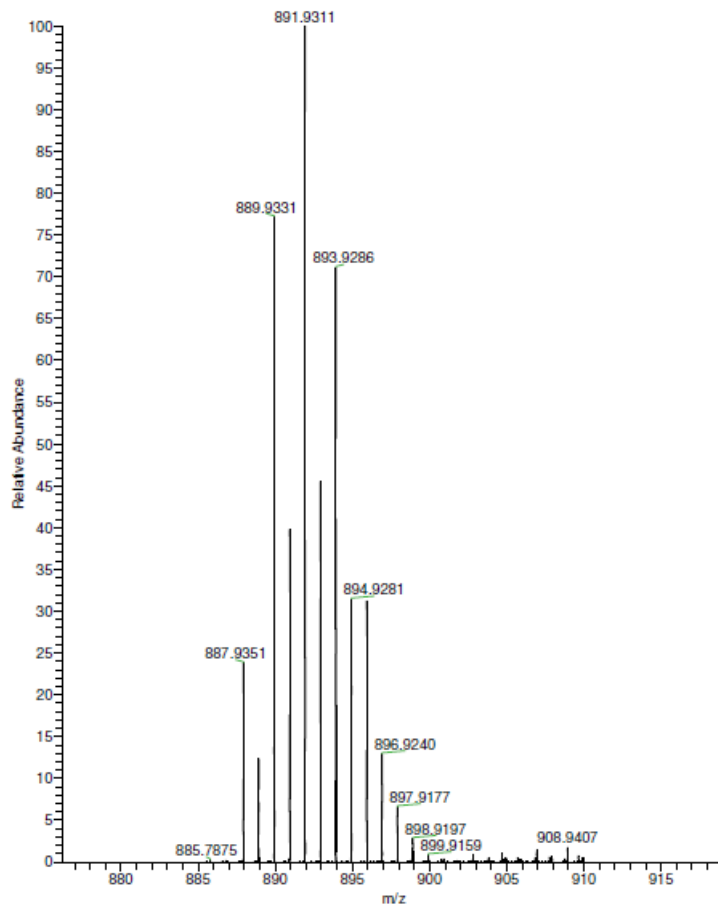


Figure 2.7. Mass spectrum (HRMS-ESI) of **H₂mono-DCPyP**.

The UV-Vis spectrum of **H₂mono-DCPyP** in chloroform is very similar to the **H₂TDCPyP** UV-Vis spectrum, showing the Soret band at $\lambda_{\text{max}} = 417$ nm and two Q-bands at $\lambda_{\text{max}} = 511$ and 587 nm (**Figure 2.8**).

The UV-Vis spectrum of **Mn(TDCPyP)Cl** in methanol displays the Soret band at $\lambda_{\text{max}} = 462$ nm, two Q-bands at $\lambda_{\text{max}} = 504$ and 555 nm and the manganese transition bands at $\lambda \approx 320$ -400 nm, in accordance with the insertion of the metal (**Figure 2.8**).

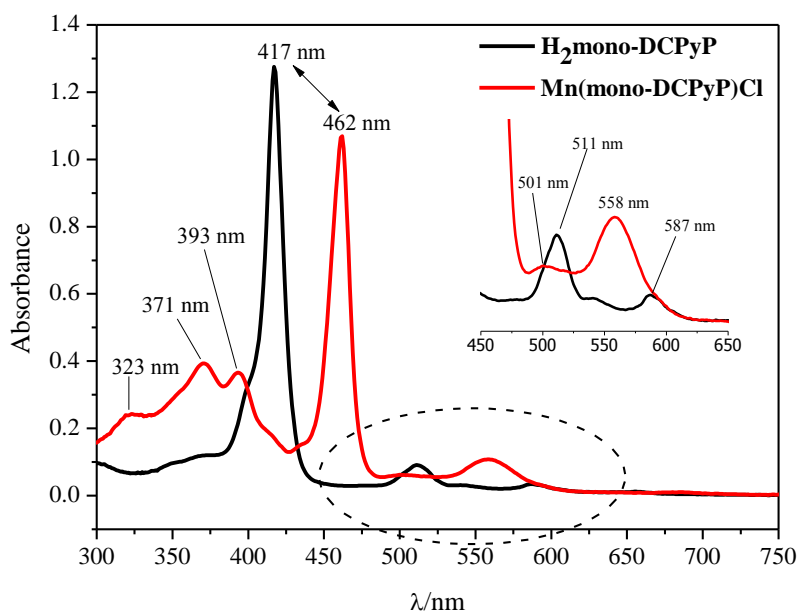


Figure 2.8. UV-Vis spectra of the **H₂mono-DCPyP** and of **Mn(mono-DCPyP)Cl**. The spectra were obtained by using chloroform as solvent for the free-base porphyrin and methanol for the Mn(III) complex.

The HRMS-ESI spectrum of **Mn(mono-DCPyP)Cl** (**Figure 2.9**) shows the most abundant peak at m/z 943.8459, with the isotope pattern of the chlorine atoms in accordance with the molecular ion $[M]^{+}$, which is consistent with the molecular formula $[C_{43}H_{19}Cl_8MnN_5]$.

Considering the characterization of the porphyrins bearing imidazole units, a special attention will be given to the desired porphyrins **P1** and **P5**. The 1H NMR spectrum of the mono-substituted porphyrin **P1** (**Figure 2.10**) shows the signal at $\delta = -2.89$ ppm due to the resonance of the inner NH protons of the porphyrin. In the low field region, six of the β -pyrrolic protons appear as a multiplet at $\delta = 8.94$ -8.96 ppm and the other two protons as a doublet ($J = 4.8$ Hz) at 9.00 ppm. The signals due to the resonances of the three protons of the imidazole moiety appear as three broad singlets at $\delta = 7.47$, $\delta = 7.61$ and $\delta = 8.18$ ppm.

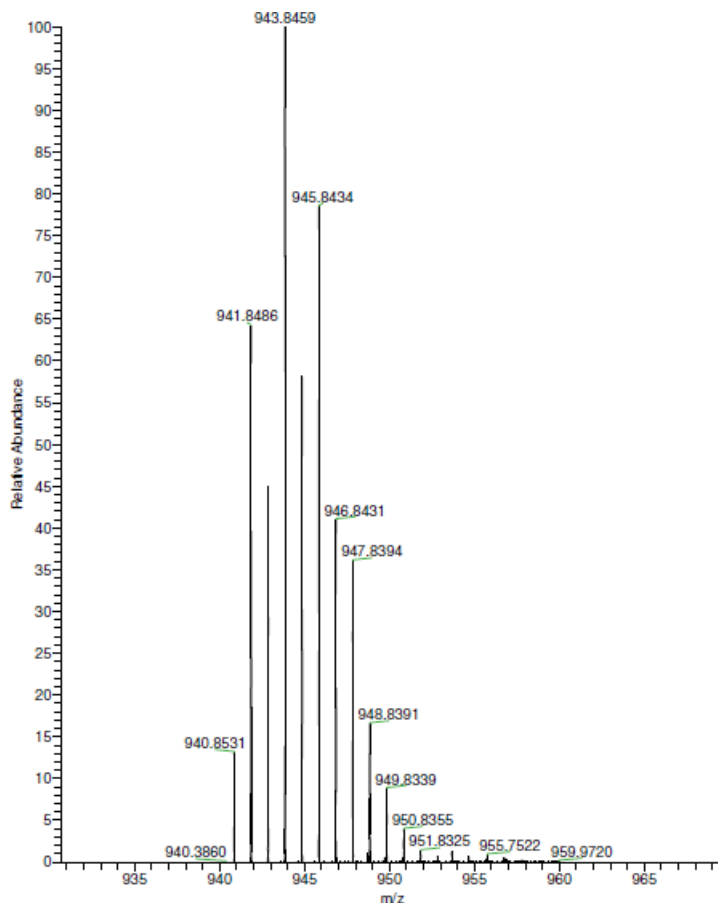


Figure 2.9. Mass spectrum (HRMS-ESI) of Mn(mono-DCPyP)Cl.

The ^{19}F NMR spectrum of this mono-substituted porphyrin **P1** (**Figure 2.11**) shows a multiplet at $\delta = -157.82$ to -157.63 ppm integrating to 6 fluorine atoms, which is assigned to the resonance of the *meta* fluorine atoms of the non-substituted pentafluorophenyl rings. Due to the asymmetry of the porphyrin, the *para* fluorine atoms of the 10-pentafluorophenyl and the *para* fluorine atoms of the 5- and 15-pentafluorophenyl are not equivalent and therefore the resonance of these fluorine atoms appears as two triplets, which are overlapped, since the chemical environment is very similar. The triplet corresponding to the resonance of the *para* fluorine atom of the 10-pentafluorophenyl ring appears at $\delta = -147.59$ ppm ($J = 21.0$ Hz) and the triplet due to the resonance of the *para* fluorine atoms of 5- and 15-pentafluorophenyl rings appears at $\delta = -147.56$ ppm ($J = 20.9$ Hz). The double duplet at $\delta = -144.73$ ppm ($J = 10.3$ and 23.0 Hz) is attributed to the resonance of the two *meta* fluorine atoms of the substituted pentafluorophenyl ring. The signal appears as a double duplet due to the coupling with the *ortho* fluorine atoms, which although being chemically equivalent are magnetically non-equivalent. For the same

reason, the signal of the *ortho* fluorine atoms of the non-substituted pentafluorophenyl rings appears as a doublet at $\delta = -132.98$ ppm ($J = 6.6$ and 23.8 Hz). The doublet at $\delta = -131.49$ ppm corresponds to the resonance of the two *ortho* fluorine atoms of the substituted pentafluorophenyl ring ($J = 10.3$ and 23.0 Hz).

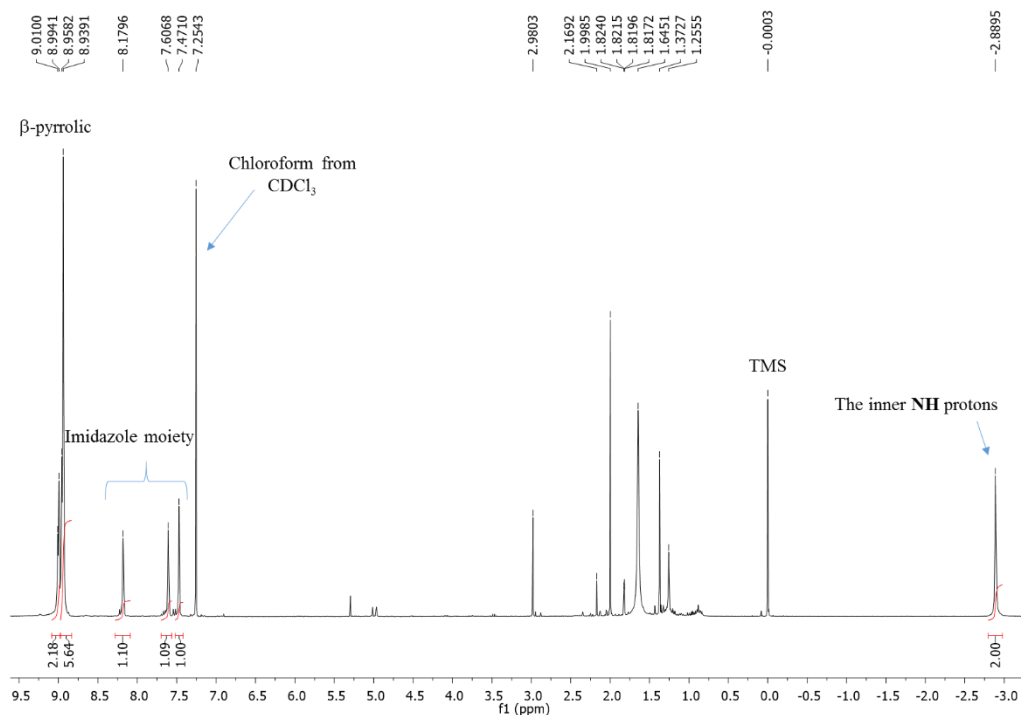
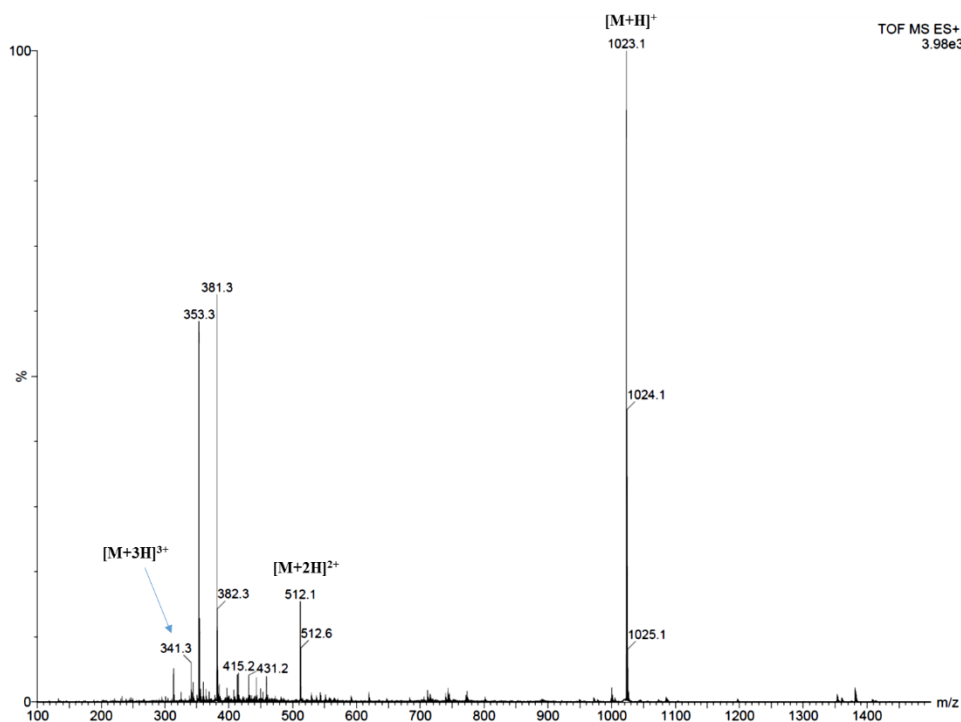
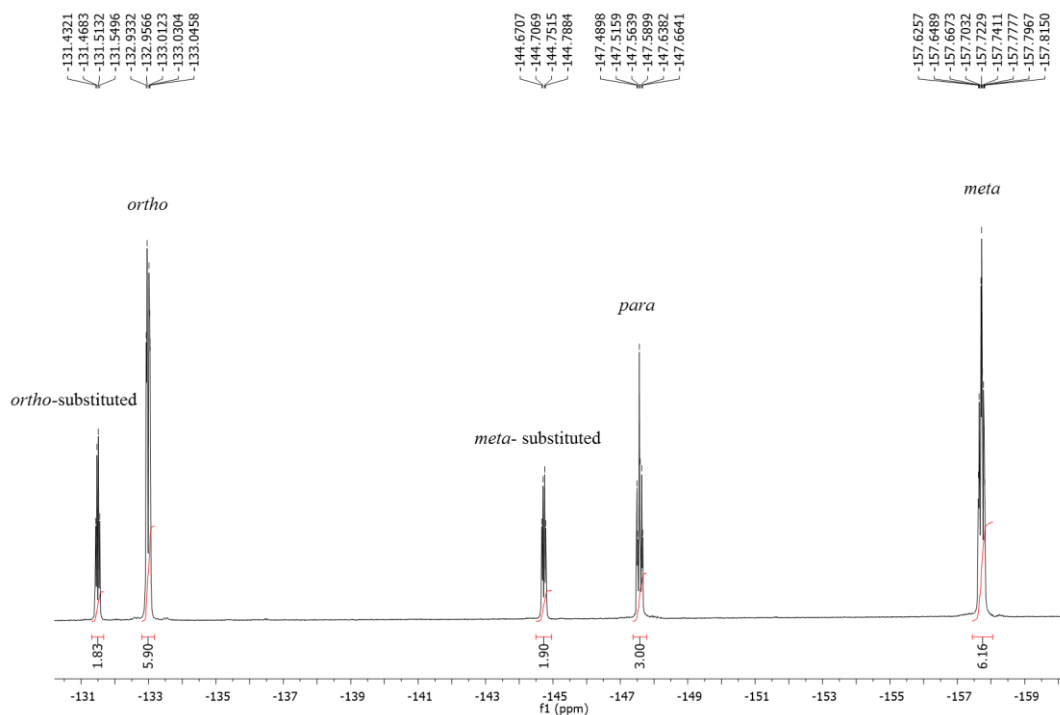


Figure 2.10. ^1H NMR spectrum of **P1** using CDCl_3 as solvent.



The electrospray ionization mass spectrum of the mono-substituted porphyrin **P1** (Figure 2.12) shows the mass of the molecular ion $[\text{M}+\text{H}]^+$ at m/z 1023.1, which is in accordance with the expected molecular formula $[\text{C}_{47}\text{H}_{13}\text{F}_{19}\text{N}_6]$. The spectrum also shows

the mass of the double charged ion $[M+2H]^{2+}$ at m/z 512.1 and the mass of the triple charged ion $[M+3H]^{3+}$ at m/z 341.3.

The ^1H NMR spectrum of the tetra-substituted porphyrin **P5** (**Figure 2.13**) shows a broad singlet at $\delta = 9.16$ ppm corresponding to the resonance of the 8 β -pyrrolic protons. The three broad singlets at $\delta = 7.54$, $\delta = 7.79$ and $\delta = 8.52$ ppm are due to the resonances of the imidazole moiety protons. In order to dissolve the tetra-substituted porphyrin **P5** was necessary to add deuterated methanol; for this reason, the typical resonance of the inner NH protons does not appear in the spectrum.

The ^{19}F NMR spectrum of the tetra-substituted porphyrin **P5** (**Figure 2.14**) shows two double doublets, integrating both to 8 fluorine atoms, which indicates the total substitution of the *para* fluorine atoms by imidazole. The double duplet at $\delta = -141.20$ ppm is assigned to the resonance of the *meta* fluorine atoms. They appear as a double duplet due to the coupling with the *ortho* fluorine atoms ($J = 9.5$ and 22.2 Hz). The double duplet at $\delta = -128.16$ ppm is attributed to the resonance of the *ortho* fluorine atoms.

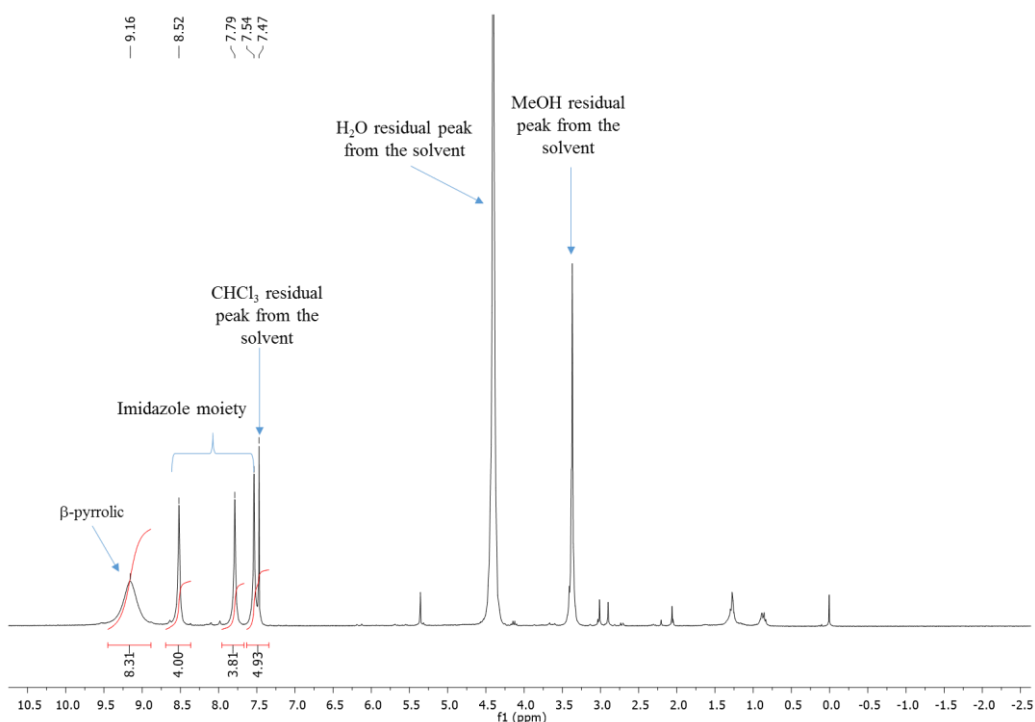


Figure 2.13. ^1H NMR spectrum of **P5**, using $\text{CDCl}_3/\text{CD}_3\text{OD}$ as solvent.

The electrospray ionization mass spectrum of the tetra-substituted porphyrin **P5** (**Figure 2.15**) shows the mass of the molecular ion $[M+H]^+$ at m/z 1167.2, which is in accordance with the expected molecular formula $[\text{C}_{56}\text{H}_{22}\text{F}_{16}\text{N}_{12}]$. As in the case of

porphyrin **P1**, the spectrum of **P5** also shows the mass of the double charged ion $[M+2H]^{2+}$ at m/z 584.1 and the mass of the triple charged ion $[M+3H]^{3+}$ at m/z 389.7.

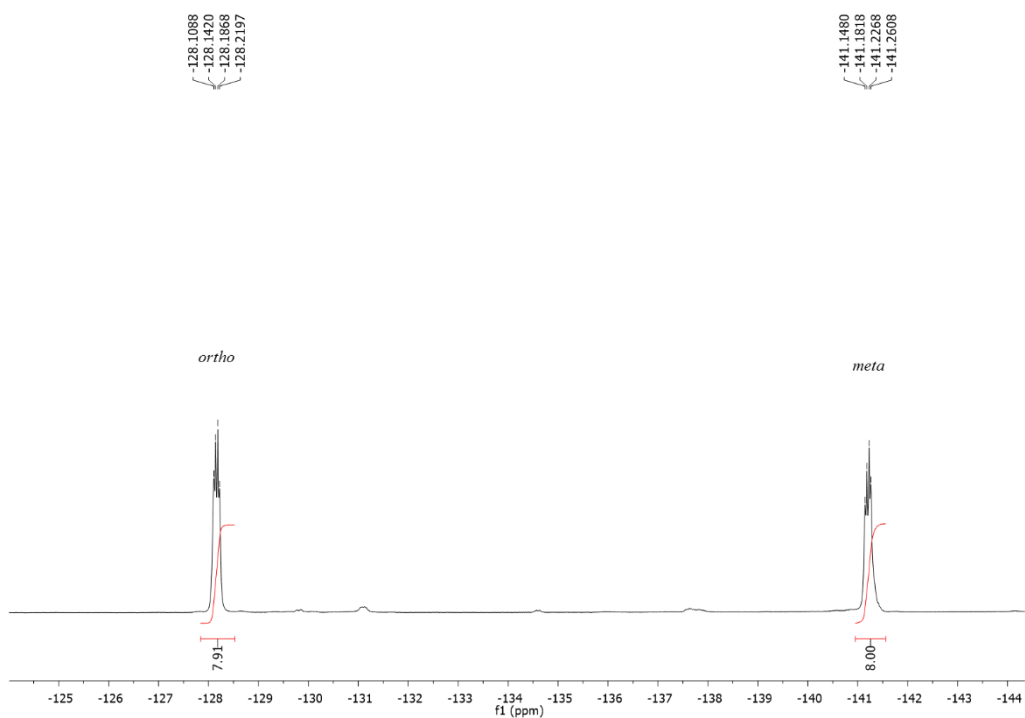


Figure 2.14. ^{19}F NMR spectrum of **P5**, using $\text{CDCl}_3/\text{CD}_3\text{OD}$ as solvent.

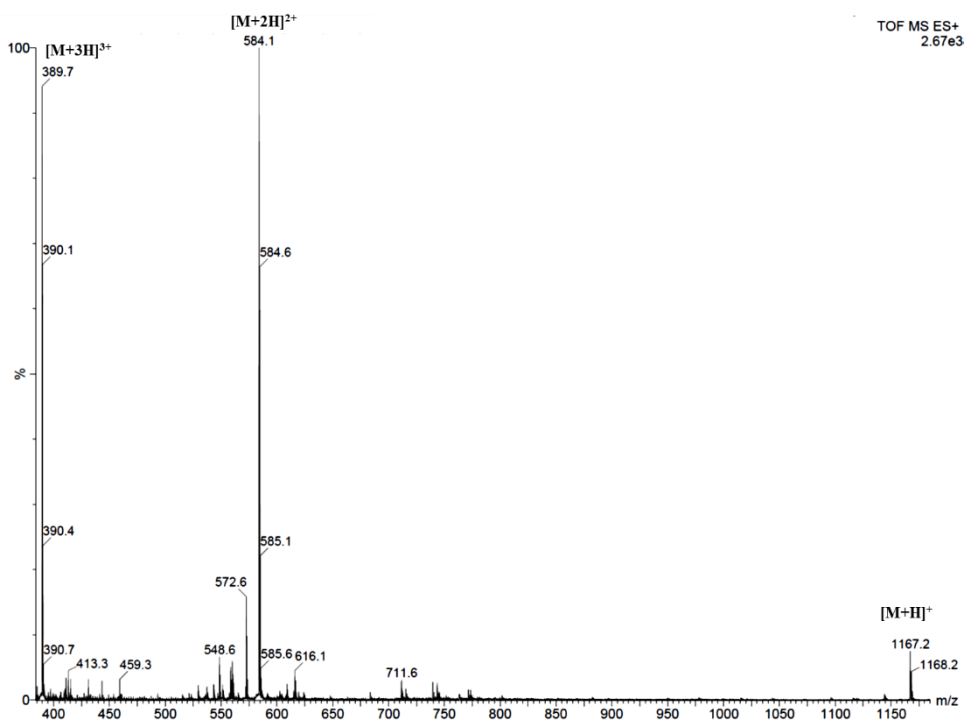


Figure 2.15. Electrospray ionization mass spectrum (ESI-MS) of **P5**.

2.3. Experimental

The porphyrins were synthesized using reagents and solvents with high purity. Pyrrole used in the synthesis of the free-base porphyrins was purchased from Sigma-Aldrich and was previously distilled. Nitrobenzene was acquired from Acros, 2,6-dichlorobenzaldehyde and 3,5-dichloro-4-pyridinecarboxaldehyde were both purchased from Sigma-Aldrich, while the 2,3,4,5,6-pentafluorobenzaldehyde was acquired from Fluka. The manganese(II) chloride.4H₂O was purchased from Merck. The reactions were monitored using TLC sheets coated with silica gel 60 without indicator from Merck. In the column chromatographic purification of the compounds, the stationary phase used was silica gel 60, with 0.063-0.200 nm of porosity from Merck. In the case of the preparative TLC, the glass plates (20 × 20 cm) were degreased and then coated with a 0.5 mm layer of silica gel G60 without indicator from Merck and were activated in the oven at 115 °C for 12 hours before use.

The ¹H and ¹⁹F NMR spectra were recorded on a Bruker Avance 300 spectrometer operating at 300.13 and 282.38 MHz, respectively, using CDCl₃ as solvent and tetramethylsilane (TMS) as internal reference. In the case of **H₂mono-DCPyP**, the ¹H and ¹³C NMR spectra were obtained on an Avance III HD 500 spectrometer at 500.13 and 125.76 MHz. The chemical shifts are reported in δ (ppm) and the coupling constants (*J*) in hertz (Hz). The mass spectra of **H₂TDCPyP** and **Mn(TDCPyP)Cl** were obtained in a 4800 mass spectrometer Maldi TOF/TOF, Applied Biosystems 4700 Proteomics Analyser 66, without matrix. The electrospray mass spectrometry (ESI-MS) spectra in positive ion mode were acquired in a Q-TOF 2 instrument (Micromass, Manchester, UK). For the acquisition of the mass spectra, the needle voltage was set at 3000 V with the ion source at 80 °C and cone voltage at 30 V. High-mass-resolving ESI-MS were conducted in a Q-Exactive® hybrid quadrupole Orbitrap® mass spectrometer (Thermo Fisher Scientific, Bremen, Germany). The instrument was operated in positive mode, with a spray voltage at 3000 V and interfaced with a HESI II ion source. The analyses were performed through direct infusion of the prepared solutions at a flow rate of 10 μL min⁻¹ into the ESI source, and the operating conditions were as follows: sheath gas (nitrogen) flow rate 5 (arbitrary units); auxiliary gas (nitrogen) 1 (arbitrary units); capillary temperature 320 °C, and S-lens rf level 50. Spectra were analysed using the acquisition software Xcalibur ver. 4.0 (Thermo Scientific, San Jose, CA, USA). The UV-Visible spectra were acquired on a dual beam

spectrophotometer Shimadzu UV-2501-PC, in 1 cm glass cells. Diffuse reflectance spectra were registered on Jasco V-560 spectrophotometer, using MgO as reference.

2.3.1. Synthesis of the free-base porphyrins

General procedure

In a two necked round bottom flask (1 L) equipped with a reflux condenser and a dropping funnel, the glacial acetic acid and the nitrobenzene were mixed and heated under stirring in an oil bath at 120 °C. Then the aldehyde or the mixture of aldehydes were added and, after total dissolution, the pyrrole was slowly added through the dropping funnel. The reaction was maintained at 120 °C under stirring and protected from light for 45 min.

2.3.1.1. Symmetric porphyrins

5,10,15,20-Tetrakis(2,6-dichlorophenyl)porphyrin (H₂TDCPP)

The reaction was carried out according to the general procedure, using 105 mL of glacial acetic acid, 75 mL of nitrobenzene, 2 mL (0.02883 mol) of pyrrole, and 5.04 g (0.02883 mol) of 2,6-dichlorobenzaldehyde. After cooling, the porphyrin was crystallized directly from the reaction medium by the addition of 200 mL of methanol. The reaction flask was left in the dark overnight and, in the next day, the formation of a powder was observed, which was filtered through a normal glass funnel with cotton wool. The cotton wool with the powder was washed with methanol to remove the black tars and then the purple porphyrin retained in the cotton wool was dissolved with dichloromethane into a round bottom flask (250 mL). The solvent was concentrated in the rotary evaporator, and then methanol was added. The purple crystals obtained were filtered under vacuum, in a Hirsch funnel with a membrane filter 0.2 µm NL16 (Schleicher & Schuell), washed with methanol and dried in the oven (55 °C). The porphyrin was obtained pure in 5% yield.

¹H NMR (300.13 MHz, CDCl₃) δ (ppm): -2.54 (2H, s-broad, NH); 7.67-7.81 (12H, m, H-Ar); 8.67 (8H, s, H-β). UV-Vis (CHCl₃) λ_{max} nm (%): 417 (100), 512 (6), 587 (2), 656 (0.5). The results are in agreement with those described in the literature.^{42,43}

5,10,15,20-Tetrakis(3,5-dichloropyridin-4-yl)porphyrin (H₂TDCPyP)

The reaction was carried out according to the general procedure, using 105 mL of glacial acetic acid, 75 mL of nitrobenzene, 5.00 g (0.0284 mol) of 3,5-dichloro-4-

pyridinecarboxaldehyde and 1.97 mL (0.0284 mol) of pyrrole. After the end of the reaction, the acetic acid and the nitrobenzene were removed by distillation under reduced pressure. The black residue obtained was subjected to purification by a silica gel column chromatography, first using hexane to remove traces of nitrobenzene, then dichloromethane to elute some orange and red coloured fractions and finally with a mixture of dichloromethane/methanol (3%) to elute the fraction which contained the porphyrin. This fraction required further purification by TLC, where a mixture of dichloromethane/methanol (3%) was used as eluent. Then, the porphyrin was crystallized using a mixture of dichloromethane and hexane (1:5). The crystals were filtered under vacuum in a Hirsch funnel with a membrane filter 0.2 μm NL16 (Schleicher & Schuell), washed with hexane and dried in the oven (55 $^{\circ}\text{C}$). The porphyrin was obtained pure in 0.2% yield. All these steps were performed with the minimum exposure to light.

$^1\text{H NMR}$ (300.13 MHz, CDCl_3) δ /ppm: -2.66 (2H, s-broad, NH); 8.68 (8H, s, H- β pyrrolic); 9.04 (8H, s, H-3,5-dichloropyridyl rings). **UV-Vis** (CHCl_3) λ_{max} nm (log ϵ): 417 (5.34), 510 (4.29), 586 (3.81). **MALDI (TOF/TOF)-MS** (m/z , %): 890 (15), 891 (32), 892 (53), 893 (87), 894 (80), 895 (100), 896 (72), 897 (69), 898 (51), 899 (34), 900 (27), 901 (11), 902 (5), 903 (3) assigned as isotope $[\text{M}+\text{H}]^+$, consistent with the expected molecular formula $[\text{C}_{40}\text{H}_{18}\text{Cl}_8\text{N}_8]$. **HRMS-ESI** analysis presented the most abundant peak at 894.9168 Da assigned as $[\text{M}+\text{H}]^+$, also consistent with the expected molecular formula.

5,10,15,20-Tetrakis(pentafluorophenyl)porphyrin ($\text{H}_2\text{TF}_5\text{PP}$)

The reaction was carried out following the general procedure, using 160 mL of glacial acetic acid, 120 mL of nitrobenzene, 2 mL (0.0288 mol) of pyrrole and 3.56 mL (0.0288 mol; 5.65 g) of pentafluorobenzaldehyde. At the end of the reaction, the acetic acid and the nitrobenzene were removed by distillation under reduced pressure. The residue obtained was submitted to purification by a silica gel column chromatography, first with hexane to remove traces of nitrobenzene and then with a mixture of hexane/dichloromethane (3:1) to elute the fraction which contained the porphyrin. The solvent was removed in the rotary evaporator and then the porphyrin was crystallized in a mixture of dichloromethane and methanol (1:5), protected from light. The crystals were filtered under vacuum in a Hirsch funnel with a membrane filter 0.2 μm NL16 (Schleicher

& Schuell), washed with methanol and dried in the oven at 55 °C. The porphyrin was obtained pure in 11% yield.

¹H NMR (300.13 MHz, CDCl₃) δ/ppm: -2.92 (2H, s-broad, NH); 8.92 (8H, s, H-β-pyrrolic). ¹⁹F NMR (282.38 MHz, CDCl₃) δ/ppm: -157.89 to -157.70 (8F, m, *meta*); -147.69 (4F, t, *J* = 20.9 Hz, *para*); -130.00 (8F, dd, *J* = 7.3 and 23.9 Hz, *ortho*). UV-Vis (CHCl₃) λ_{max} nm (%): 412 (100), 505 (7), 583 (2), 637 (1). The results are in agreement with those described in the literature.^{42,44–47}

2.3.1.2. Asymmetric porphyrins

5,10,15-Tris(2,6-dichlorophenyl)-20-(3,5-dichloropyridin-4-yl)porphyrin (H₂mono-DCPyP)

The reaction was carried out according to the general procedure using 160 mL of glacial acetic acid, 120 mL of nitrobenzene, 2 mL (4 eq; 0.02883 mol) of pyrrole, 3.78 g (3 eq; 0.0216 mol) of 2,6-dichlorobenzaldehyde and 1.52 g (1.2 eq; 0.0086 mol) of 3,5-dichloro-4-pyridinecarboxaldehyde. At the end of the reaction, the acetic acid and the nitrobenzene were removed by distillation under reduced pressure and the residue obtained was subjected to purification by a silica gel column chromatography. The first eluent used was hexane in order to remove traces of nitrobenzene, then a mixture of dichloromethane/hexane (5:1) was used to elute a fraction containing an orange compound and the symmetric porphyrin **H₂TDCPP** and finally using dichloromethane the **H₂mono-DCPyP** was removed from the column. The porphyrin was crystallized and recrystallized with dichloromethane/hexane (1:5), protected from light. The crystals were filtered under vacuum in a Hirsch funnel with a membrane filter 0.2 μm NL16 (Schleicher & Schuell), washed with hexane and dried overnight in the oven (55 °C). The porphyrin was obtained pure in 2.6% yield.

¹H NMR (500.13 MHz, CDCl₃) δ/ppm: -2.57 (2H, s-broad, NH); 7.69-7.73 (3H, m, H-*para*-2,6-dichlorophenyl rings); 7.79-7.81 (6H, m, H-*meta*-2,6-dichlorophenyl rings); 8.61 (2H, d, *J* = 4.4 Hz, H-β pyrrolic); 8.68 (4H, s, H-β pyrrolic); 8.70 (2H, d, *J* = 4.4 Hz, H-β pyrrolic); 9.00 (2H, s, H-3,5-dichloropyridyl ring). ¹³C NMR (125.76 MHz, CDCl₃) δ/ppm: 110.6, 114.7, 114.9, 127.89 (C-*meta*-2,6-dichlorophenyl), 127.90 (C-*meta*-2,6-dichlorophenyl), 130.71 (C-*para*-2,6-dichlorophenyl), 130.73 (C-*para*-2,6-

dichlorophenyl), 135.8 (C-3 and C-5 of 3,5-dichloropyridyl ring), 138.7, 139.21, 139.25, 147.45 (C-2 and C-6 of 3,5-dichloropyridyl ring). **UV-Vis** (CHCl_3) λ_{max} nm (log ϵ): 417 (5.33), 511 (4.24), 587 (3.88). **ESI-MS** (m/z , %): 888 (31), 889 (21), 890 (87), 891 (45), 892 (100), 893 (44), 894 (65), 895 (29), 896 (27), 897 (13), 898 (9), 899 (4) assigned as isotope $[\text{M}+\text{H}]^+$, consistent with the expected molecular formula $[\text{C}_{43}\text{H}_{21}\text{Cl}_8\text{N}_5]$. **HRMS-ESI** analysis provided the most abundant peak at $m/z = 891.9311$ Da assigned as $[\text{M}+\text{H}]^+$, also consistent with the expected molecular formula.

5,10,15-tris(2,6-dichlorophenyl)-20-(pyridin-4-yl)porphyrin ($\text{H}_2\text{DC-mono-4PyP}$)

The reaction was carried out as described for the synthesis of the **H₂mono-DCPyP** using 2 mL (4 eq; 0.02883 mol) of pyrrole, 3.78 g (3 eq; 0.0216 mol) of 2,6-dichlorobenzaldehyde and 0.81 mL (1.2 eq; 0.0086 mol) of 4-pyridinecarboxaldehyde. After removal of the solvents by distillation under reduced pressure, the obtained residue was subjected to purification by a silica gel column chromatography. The first eluent used was hexane in order to remove traces of nitrobenzene, then a mixture of dichloromethane/hexane (10%) was used to elute a fraction containing the **H₂TDCPP** together with other non-porphyrinic compounds. Then, using the same eluent a fraction containing the **H₂DC-mono-4PyP** was removed from the column. The porphyrin was crystallized and recrystallized with dichloromethane/hexane (1:5), protected from light. The crystals were filtered under vacuum in a Hirsch funnel with a membrane filter 0.2 μm NL16 (Schleicher & Schuell), washed with hexane and dried overnight in the oven (55 °C).

¹H NMR (300.13 MHz, CDCl_3) δ /ppm: -2.60 (2H, s-broad, NH); 7.70-7.84 (9H, m, 2,6-dichlorophenyl rings); 8.66-8.71 (8H, m, H- β pyrrolic); 8.80 (2H, d, $J = 5.6$ Hz, H-3 and H-5 of pyridyl ring); 9.14 (2H, d, $J = 5.6$ Hz, H-2 and H-6 of pyridyl ring). **UV-Vis** (CH_3Cl) λ_{max} nm (%): 417 (100), 512 (6), 586 (3), 640 (1). **ESI-MS** (m/z , %): 820 (42), 821 (27), 822 (100), 823 (35), 824 (76), 825 (25), 826 (29), 827 (10), 828 (7), 829 (3) assigned as isotope $[\text{M}+\text{H}]^+$, consistent with the expected molecular formula $[\text{C}_{43}\text{H}_{23}\text{Cl}_6\text{N}_5]$. The results are in agreement with those described in the literature.⁴⁸ The porphyrin was obtained pure in 1.7% yield.

Porphyrins P1-5 obtained from the reaction of H₂TF₅PP with imidazole

a) General procedure for the reactions performed in THF

In a 25 mL round bottom flask, 50 mg of **H₂TF₅PP** were dissolved in 2 mL of THF p.a. grade. After total dissolution of the porphyrin, the adequate amounts of imidazole and cesium carbonate were added, depending on the desired porphyrin (1.5 eq for **P1** and 5 eq for **P5**). The mixture was stirred at 65 °C, protected from light and under nitrogen atmosphere. After 9 h, the TLC control confirmed that the starting porphyrin was substantially transformed and the reaction was ended. After reaching the room temperature, the reaction mixture was washed with distilled water and the products were extracted with dichloromethane. The organic solution was dried (Na₂SO₄) and concentrated under reduced pressure. The products were purified by preparative TLC using dichloromethane/methanol (5%) as eluent. The compounds were dissolved in chloroform and crystallized with hexane.

a) General procedure for the reactions performed in DMF

When DMF was used as solvent, the reactions were carried out at room temperature (approximately 23 °C) and the starting porphyrin was totally consumed after 4 h approximately. At the end of the reaction, DMF was removed under reduced pressure on the rotary evaporator, using toluene to facilitate its evaporation. The organic residue was dissolved in dichloromethane and washed with distilled water. The following steps proceeded as already described for the reactions carried out with THF as solvent. The yields of the different isolated porphyrins are summarized in **Table 2.1**.

Mono-substituted porphyrin (P1)

¹H NMR (300.13 MHz, CDCl₃) δ/ppm: -2.89 (2H, s-broad, NH); 7.47 (1H, s-broad, H-imidazole); 7.61 (1H, s-broad, H-imidazole); 8.18 (1H, s-broad, H-imidazole); 8.94-8.96 (6H, m, H-β-pyrrolic); 9.00 (2H, d, *J* = 4.8 Hz). **¹⁹F NMR** (282.38 MHz, CDCl₃) δ/ppm: -157.82 to -157.63 (6F, m, F-*meta*); -147.59 (1F, t, *J* = 21.0 Hz, F-*para*-10-pentafluorophenyl); -147.56 (2F, t, *J* = 21.0 Hz, F-*para*-5-pentafluorophenyl and F-*para*-15-pentafluorophenyl) -144.73 (2F, dd, *J* = 10.3 and 23.0 Hz, F-*meta*-substituted); -132.98 (6F, dd, *J* = 6.6 and 23.8 Hz, F-*ortho*); -131.49 (2F, dd, *J* = 10.3 and 23.0 Hz, F-*ortho*-substituted). **UV-Vis** (CHCl₃) λ_{max} nm (log ε): 414 (5.40), 507 (4.28), 583 (3.81), 637

(1.95). **ESI-MS** (m/z): 1023.1 $[M+H]^+$, 512.1 $[M+2H]^{2+}$, 341.3 $[M+3H]^{3+}$, consistent with the expected molecular formula $[C_{47}H_{13}F_{19}N_6]$. **HRMS-ESI** analysis provided the peak at $m/z = 1023.1012$ Da assigned as $[M+H]^+$, also consistent with the expected molecular formula.

Di-substituted porphyrin (P2)

1H NMR (300.13 MHz, $CDCl_3$) δ /ppm: -2.88 (2H, s-broad, NH); 7.48 (2H, s-broad, imidazole); 7.61 (2H, s-broad, imidazole); 8.18 (2H, s-broad, imidazole); 8.95 (4H, d, $J = 4.7$ Hz, H- β -pyrrolic); 9.00 (4H, d, $J = 4.7$ Hz, H- β -pyrrolic). **^{19}F NMR** (282.38 MHz, $CDCl_3$) δ /ppm: -157.2 to -157.54 (4F, m, F-*meta*); -147.42 (2F, t, $J = 21.0$ Hz, F-*para*); -144.67 (4F, dd, $J = 10.4$ and 23.3 Hz, F-*meta*-substituted); -132.98 (4F, dd, $J = 7.6$ and 23.1 Hz, F-*ortho*); -131.48 (4F, dd, $J = 10.4$ and 23.3 Hz, F-*ortho*-substituted). **UV-Vis** ($CHCl_3$) λ_{max} nm (log ϵ): 414 (5.43), 507 (4.30), 584 (3.83), 637 (1.99). **ESI-MS** (m/z): 1071.2 $[M+H]^+$, 536.1 $[M+2H]^{2+}$, consistent with the expected molecular formula $[C_{50}H_{16}F_{18}N_8]$. **HRMS-ESI** analysis provided the peak at $m/z = 1071.1321$ Da assigned as $[M+H]^+$, also consistent with the expected molecular formula.

Di-substituted porphyrin (P3)

1H NMR (300.13 MHz, $CDCl_3/5\%$ CD_3OD) δ /ppm: 7.37 (2H, s-broad, imidazole); 7.93 (2H, s-broad, imidazole); 8.08 (2H, s-broad, imidazole); 8.85-9.25 (8H, m, H- β -pyrrolic). **^{19}F NMR** (282.38 MHz, $CDCl_3/5\%$ CD_3OD) δ /ppm: -157.80 to -157.62 (4F, m, F-*meta*); -147.56 (2F, t, $J = 20.8$ Hz, F-*para*); -143.90 (4F, dd, $J = 8.6$ and 21.2 Hz, F-*meta*-substituted); -133.05 (4F, dd, $J = 7.5$ and 23.0 Hz, F-*ortho*); -130.25 (4F, dd, $J = 8.6$ and 21.2 Hz, F-*ortho*-substituted). **UV-Vis** ($CHCl_3/5\%$ CH_3OH) λ_{max} nm (log ϵ): 414 (5.37), 507 (4.31), 583 (3.83), 636 (1.98). **ESI-MS** (m/z): 1071.2 $[M+H]^+$, 536.1 $[M+2H]^{2+}$, consistent with the expected molecular formula $[C_{50}H_{16}F_{18}N_8]$. **HRMS-ESI** analysis provided the peak at $m/z = 1071.1329$ Da assigned as $[M+H]^+$, also consistent with the expected molecular formula.

Tri-substituted porphyrin (P4)

1H NMR (300.13 MHz, $CDCl_3/5\%$ CD_3OD) δ /ppm: 7.45 (3H, s-broad, imidazole); 7.66 (3H, s-broad, imidazole); 7.90 (3H, s-broad, imidazole); 8.96-9.35 (8H, m, H- β -

pyrrolic). ^{19}F NMR (282.38 MHz, $\text{CDCl}_3/5\% \text{CD}_3\text{OD}$) δ/ppm : -154.62 to 154.38 (2F, m, F-*meta*); -144.35 (1F, t, $J = 20.8$ Hz, F-*para*); -141.05 to -140.98 (6F, m, F-*meta*-substituted); -129.77 (2F, dd, $J = 7.0$ and 22.2 Hz, F-*ortho*); -127.80 (6F, dd, $J = 9.8$ and 22.1 Hz, F-*ortho*-substituted). UV-Vis ($\text{CHCl}_3/5\% \text{CH}_3\text{OH}$) λ_{max} nm (log ϵ): 414 (5.36), 509 (4.28), 586 (3.82), 638 (1.96). ESI-MS (m/z): 1119.2 $[\text{M}+\text{H}]^+$, 560.1 $[\text{M}+2\text{H}]^{2+}$, 373.3 $[\text{M}+3\text{H}]^{3+}$, consistent with the expected molecular formula $[\text{C}_{53}\text{H}_{19}\text{F}_{17}\text{N}_{10}]$. HRMS-ESI analysis provided the peak at $m/z = 1119.1653$ Da assigned as $[\text{M}+\text{H}]^+$, also consistent with the expected molecular formula.

Tetra-substituted porphyrin (P5)

^1H NMR (300.13 MHz, $\text{CDCl}_3/5\% \text{CD}_3\text{OD}$) δ/ppm : 7.54 (4H, s-broad, imidazole); 7.79 (4H, s-broad, imidazole); 8.52 (4H, s-broad, imidazole); 9.16 (8H, s-broad, H- β). ^{19}F NMR (282.38 MHz, $\text{CDCl}_3/5\% \text{CD}_3\text{OD}$) δ/ppm : -141.20 (8F, dd, $J = 9.5$ and 22.2 Hz, F-*meta*); -128.16 (8F, dd, $J = 9.5$ and 22.2 Hz, F-*ortho*). UV-Vis ($\text{CHCl}_3/5\% \text{CH}_3\text{OH}$) λ_{max} nm (log ϵ): 414 (5.45), 509 (4.32), 586 (3.81), 638 (2.00). ESI-MS (m/z): 1167.2 $[\text{M}+\text{H}]^+$, 584.1 $[\text{M}+2\text{H}]^{2+}$, 389.7 $[\text{M}+3\text{H}]^{3+}$, consistent with the expected molecular formula $[\text{C}_{56}\text{H}_{22}\text{F}_{16}\text{N}_{12}]$. HRMS-ESI analysis provided the peak at $m/z = 1167.1974$ Da assigned as $[\text{M}+\text{H}]^+$, also consistent with the expected molecular formula.

2.3.2. Manganese(III) porphyrins

In a 25 mL round bottom flask equipped with a reflux condenser and a magnetic bar, 50 mg of the free-base porphyrin were dissolved in 5.0 mL of DMF. The solution was refluxed in the dark, under a nitrogen atmosphere and then 0.5 mL of pyridine and 10 equivalents of manganese(II) chloride ($\text{MnCl}_2 \cdot 4\text{H}_2\text{O}$) were added. The progress of the reaction was monitored by UV-Vis spectrophotometry (an aliquot of the reaction mixture was diluted in CH_3CN) and by TLC (using CH_2Cl_2 as eluent). The UV-Vis spectrum shows a Soret band shift to a higher wavelength, thereby confirming the presence of the complex. The transition bands of manganese at $\lambda_{\text{max}} = 320\text{-}400$ nm can also be observed. The reaction normally takes 2 h to be complete. The heating was switched off and the reaction mixture was kept under stirring overnight, in open air and protected from light. The solvent was removed by distillation in the rotary evaporator and the obtained residue was dissolved in dichloromethane and washed 2-3 times with water in a separating funnel,

and finally with a saturated sodium chloride solution. The organic phase was passed through a glass funnel with cotton wool and anhydrous sodium sulphate to remove traces of water. The manganese complexes were crystallized in hexane, after dissolution in a minimal amount of dichloromethane. The crystals were filtered under vacuum using a Hirsch funnel with a membrane filter 0.2 μm NL16 (Schleicher & Schuell), washed several times with hexane and placed in the oven (55 $^{\circ}\text{C}$). The yield, based on the porphyrin, was higher than 90%.

Chloro[5,10,15,20-Tetrakis(2,6-dichlorophenyl)porphyrinate]manganese(III)

Mn(TDCPP)Cl

UV-Vis (CH_2Cl_2) λ_{max} , nm (%): 364 (66); 474 (100); 573 (12).

Chloro[5,10,15,20-tetrakis(3,5-dichloropyridin-4-

yl)porphyrinate]manganese(III) Mn(TDCPyP)Cl

UV-Vis (CH_3OH) λ_{max} nm (log ϵ): 326 (4.27), 368 (4.51), 390 (4.42), 459 (5.00), 504 (3.61), 555 (3.96). **MALDI (TOF/TOF)-MS** (m/z , %): 943 (29), 944 (19), 945 (90), 946 (43), 947 (100), 948 (54), 949 (72), 950 (34), 951 (32), 952 (14), 953 (9), 954 (6) assigned as isotope $[\text{M}]^{+}$, consistent with the expected molecular formula $[\text{C}_{40}\text{H}_{16}\text{Cl}_8\text{MnN}_8]$. **HRMS-ESI** analysis provided the most abundant peak at $m/z = 946.8317$ Da assigned as $[\text{M}]^{+}$, also consistent with the expected molecular formula.

Chloro[5,10,15-tris(2,6-dichlorophenyl)-20-(pyridin-4-

yl)porphyrinate]manganese(III) - Mn(DC-mono-4PyP)Cl

UV-Vis (CH_3OH) λ_{max} , nm (%): 373 (40), 395 (39), 463 (100), 502 (5), 558 (10), (CH_3CN) λ_{max} , nm (%): 369 (47), 474 (100), 577 (10), 608 (6).

Chloro[5,10,15,-tris(2,6-dichlorophenyl)-20-(3,5-dichloropyridin-

4yl)porphyrinate]manganese(III) - Mn(mono-DCPyP)Cl

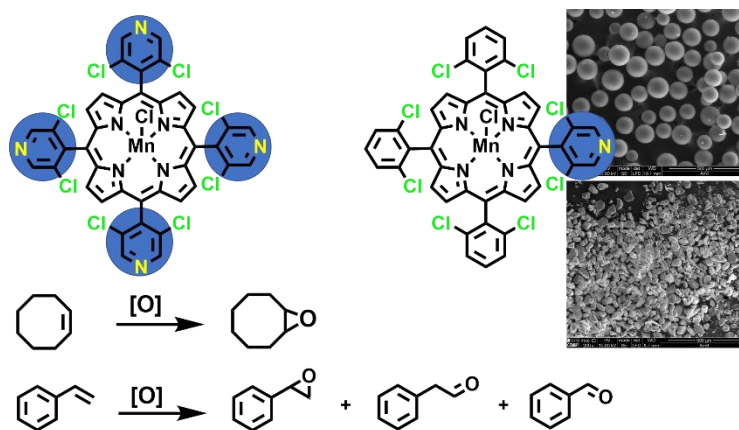
UV-Vis (CH_3OH) λ_{max} nm (log ϵ): 323 (4.40), 371 (4.61), 393 (4.58), 462 (5.04), 501 (3.83), 558 (4.07). **ESI-MS** (m/z , %): 940 (28), 941 (13), 942 (88), 943 (32), 944 (100), 945 (33), 946 (58), 947 (18), 948 (19), 949 (7), 950 (5), 951 (2) assigned as isotope $[\text{M}]^{+}$, consistent with the expected molecular formula $[\text{C}_{43}\text{H}_{19}\text{Cl}_8\text{MnN}_5]$. **HRMS-ESI** analysis provided the most abundant peak at $m/z = 943.8459$ Da assigned as $[\text{M}]^{+}$, also consistent with the expected molecular formula.

2.4. References

- 1 S. Shanmugathan, C. Edwards and R. W. Boyle, *Tetrahedron*, 2000, **56**, 1025–1046.
- 2 P. Rothmund, *J. Am. Chem. Soc.*, 1935, **57**, 2010–2011.
- 3 P. Rothmund, *J. Am. Chem. Soc.*, 1936, **58**, 625–627.
- 4 P. Rothmund, *J. Am. Chem. Soc.*, 1939, **61**, 2912–2915.
- 5 P. Rothmund and A. R. Menotti, *J. Am. Chem. Soc.*, 1941, **63**, 267–270.
- 6 S. Aronoff and M. Calvin, *J. Org. Chem.*, 1943, **8**, 205–223.
- 7 M. Calvin, R. H. Ball and S. Aronoff, *J. Am. Chem. Soc.*, 1943, **65**, 2259.
- 8 A. D. Adler, F. R. Longo, J. D. Finarelli, J. Goldmacher, J. Assour and L. Korsakoff, *J. Org. Chem.*, 1967, **32**, 476.
- 9 G. H. Barnett, M. F. Hudson and K. M. Smith, *J. Chem. Soc., Perkin Trans.*, 1975, **1**, 1401–1403.
- 10 A. M. d'A. R. Gonsalves and M. M. Pereira, *J. Heterocycl. Chem.*, 1985, **22**, 931–933.
- 11 J. S. Lindsey, H. C. Hsu and I. C. Schreiman, *Tetrahedron Lett.*, 1986, **27**, 4969–4970.
- 12 J. S. Lindsey, I. C. Schreiman, H. C. Hsu, P. C. Kearney and A. M. Marguerettaz, *J. Org. Chem.*, 1987, **52**, 827–836.
- 13 J. S. Lindsey, K. A. MacCrum, J. S. Tyhonas and Y. Y. Chuang, *J. Org. Chem.*, 1994, **59**, 579–587.
- 14 A. M. d'A. R. Gonsalves, J. M. T. B. Varejão and M. M. Pereira, *J. Heterocycl. Chem.*, 1991, **28**, 635–640.
- 15 H. Sharghi and A. H. Nejad, *Helv. Chim. Acta*, 2003, **86**, 408–414.
- 16 H. Sharghi and A. H. Nejad, *Tetrahedron*, 2004, **60**, 1863–1868.
- 17 M. O. Liu, C. H. Tai, W. Y. Wang, J. R. Chen, A. T. Hu and T. H. Wei, *J. Organomet. Chem.*, 2004, **689**, 1078–1084.
- 18 S. M. S. Chauhan, B. B. Sahoo and K. A. Srinivas, *Synth. Commun.*, 2001, **31**, 33–37.
- 19 B. F. O. Nascimento, M. Pineiro, A. M. d'A. R. Gonsalves, M. R. Silva, A. M. Beja and J. A. Paixão, *J. Porphyr. Phthalocyanines*, 2007, **11**, 77–84.
- 20 A. Mikus, M. E. Bielińska, T. Lipińska and S. Ostrowski, *Synth. Commun.*, 2011, **41**, 3703–3713.
- 21 B. F. O. Nascimento, A. M. d'A. R. Gonsalves and M. Pineiro, *Inorg. Chem. Commun.*, 2010, **13**, 395–398.

-
- 22 R. De Paula, M. A. F. Faustino, D. C. G. A. Pinto, M. G. P. M. S. Neves and J. A. S. Cavaleiro, *J. Heterocycl. Chem.*, 2008, **45**, 453–459.
- 23 R. Lucas, J. Vergnaud, K. Teste, R. Zerrouki, V. Sol and P. Krausz, *Tetrahedron Lett.*, 2008, **49**, 5537–5539.
- 24 B. Boëns, P.-A. Faugeras, J. Vergnaud, R. Lucas, K. Teste and R. Zerrouki, *Tetrahedron*, 2010, **66**, 1994–1996.
- 25 C. A. Henriques, S. M. A. Pinto, G. L. B. Aquino, M. Pineiro, M. J. F. Calvete and M. M. Pereira, *ChemSusChem*, 2014, **7**, 2821–2824.
- 26 J. A. Anton and P. A. Loach, *J. Heterocycl. Chem.*, 1975, **12**, 573–576.
- 27 L. R. Milgrom, *J. Chem. Soc. Perkin Trans. 1*, 1984, 1483–1487.
- 28 P. Laszlo and J. Luchetti, *Chem. Lett.*, 1993, **22**, 449–452.
- 29 J. I. T. Costa, A. C. Tomé, M. G. P. M. S. Neves and J. A. S. Cavaleiro, *J. Porphyr. Phthalocyanines*, 2011, **15**, 1116–1133.
- 30 S. L. H. Rebelo, A. R. Gonçalves, M. M. Pereira, M. M. Q. Simões, M. G. P. M. S. Neves and J. A. S. Cavaleiro, *J. Mol. Catal. A Chem.*, 2006, **256**, 321–323.
- 31 S. M. G. Pires, R. De Paula, M. M. Q. Simões, M. G. P. M. S. Neves, I. C. M. S. Santos, A. C. Tomé and J. A. S. Cavaleiro, *Catal. Commun.*, 2009, **11**, 24–28.
- 32 R. De Paula, I. C. M. S. Santos, M. M. Q. Simões, M. G. P. M. S. Neves and J. A. S. Cavaleiro, *J. Mol. Catal. A Chem.*, 2015, **404–405**, 156–166.
- 33 M. J. F. Calvete, M. Silva, M. M. Pereira and H. D. Burrows, *RSC Adv.*, 2013, **3**, 22774–22789.
- 34 P. Zucca, C. M. B. Neves, M. M. Q. Simões, M. G. P. M. S. Neves, G. Cocco and E. Sanjust, *Molecules*, 2016, **21**, 1–40.
- 35 S. Nakagaki, K. M. Mantovani, G. S. Machado, K. A. D. F. Castro and F. Wypych, *Molecules*, 2016, **21**, 291.
- 36 C. F. Pereira, M. M. Q. Simões, J. P. C. Tomé and F. A. A. Paz, *Molecules*, 2016, **21**, 1348.
- 37 M. J. F. Calvete, M. Piñeiro, L. D. Dias and M. M. Pereira, *ChemCatChem*, 2018, **10**, 3615–3635.
- 38 E. Brulé and Y. R. de Miguel, *Org. Biomol. Chem.*, 2006, **4**, 599–609.
- 39 M. A. Martinez-Lorente, P. Battioni, W. Kleemiss, J. F. Bartoli and D. Mansuy, *J. Mol. Catal. A Chem.*, 1996, **113**, 343–353.

- 40 S. Fujii, Y. Maki and H. Kimoto, *J. Fluor. Chem.*, 1989, **43**, 131–144.
- 41 A. D. Adler, F. R. Longo, F. Kampas and J. Kim, *J. Inorg. Nucl. Chem.*, 1970, **32**, 2443–2445.
- 42 A. W. van der Made, E. J. H. Hoppenbrouwer, R. J. M. Nolte and W. Drenth, *Recl. des Trav. Chim. des Pays-Bas*, 1988, **107**, 15–16.
- 43 C. M. B. Neves, M. M. Q. Simões, F. M. J. Domingues, M. G. P. M. S. Neves and J. A. S. Cavaleiro, *Quim. Nova*, 2012, **35**, 1477–1481.
- 44 F. R. Longo, M. G. Finarelli and J. B. Kim, *J. Heterocycl. Chem.*, 1969, **6**, 927–931.
- 45 K. M. Kadish, B. C. Han, M. M. Franzen and C. Araullo-McAdams, *J. Am. Chem. Soc.*, 1990, **112**, 8364–8368.
- 46 M. A. C. de Medeiros, S. Cosnier, A. Deronzier and J.-C. Moutet, *Inorg. Chem.*, 1996, **35**, 2659–2664.
- 47 J. P. C. Tomé, M. G. P. M. S. Neves, A. C. Tomé, J. A. S. Cavaleiro, A. F. Mendonça, I. N. Pegado, R. Duarte and M. L. Valdeira, *Bioorg. Med. Chem.*, 2005, **13**, 3878–3888.
- 48 I. C. M. S. Santos, S. L. H. Rebelo, M. S. S. Balula, R. R. L. Martins, M. M. M. S. Pereira, M. M. Q. Simões, M. G. P. M. S. Neves, J. A. S. Cavaleiro and A. M. V. Cavaleiro, *J. Mol. Catal. A Chem.*, 2005, **231**, 35–45.



CHAPTER 3

Catalytic activity evaluation of new second-generation manganese(III) porphyrins in oxidation reactions

Chapter 3. Catalytic activity evaluation of new second-generation manganese(III) porphyrins in oxidation reactions

Oxidation reactions play a very important role both in academia and in the industrial environment. Particularly, epoxidations are very useful in the production of fine chemicals because the resulting epoxides can be used in the synthesis of a wide variety of compounds. The continuous industry demand for new compounds requires the development of more efficient and selective catalysts. Metalloporphyrins have been described as effective homogeneous catalysts in epoxidation reactions. However, the low yield usually obtained in the synthesis of metalloporphyrins, the somewhat low stability in the presence of oxidants and the difficulty of recovery from the reaction medium are limitations for its application as homogeneous catalysts in industrial processes. The immobilization of efficient homogeneous catalysts on solid supports is an interesting strategy to overcome some of these gaps and contribute to more sustainable synthesis processes, since the catalyst is easily separated from the reaction mixture and can be reused.^{1,2} As already mentioned in the introductory chapter, different methods have been used to anchor metalloporphyrins in a wide variety of solid supports such as adsorption, electrostatic binding, covalent bonding, coordinative binding or encapsulation.^{1,3-6} From the aforementioned methods, covalent bonding is the strongest interaction possible between the metalloporphyrin and the solid support, which avoids the leaching of the catalyst during reaction.⁶ Porphyrin ligands whose metal complexes are usually considered as robust catalysts are preferably from the second-generation. However, its covalent bonding to the support usually requires chemical modification of the macrocycle, such as the introduction of NH₂ or SO₃H functionalities.⁷ Part of the work developed in this thesis consisted in developing new catalysts based on second-generation porphyrins containing functionalities that allow its easy immobilization on solid supports [**Mn(TDCPyP)Cl**] and [**Mn(mono-DCPyP)Cl**] (**Figure 3.1 A**). The synthesis and characterization of the novel porphyrin-based catalysts was described in chapter 2. In the present chapter the results obtained in the oxidation reactions in the presence of the new catalysts will be reported.

The following points will be addressed along this chapter:

i) The catalytic activity evaluation of the novel manganese(III) complexes of the porphyrins with 3,5-dichloropyridyl substituents at the *meso* positions [**Mn(TDCPyP)Cl**]

and **[Mn(mono-DCPyP)Cl]** (**Figure 3.1 A**) in the oxidation of cyclooctene using aqueous hydrogen peroxide as oxidant under homogeneous conditions;

ii) The comparison of the catalytic activity between the novel catalysts and the already known counterparts in the epoxidation of cyclooctene: chloro[5,10,15,20-tetrakis(2,6-dichlorophenyl)porphyrinate]manganese(III) **[Mn(TDCPP)Cl]**,^{8,9} chloro[5,10,15,20-tetra(pyridin-4-yl)porphyrinate]manganese(III) **[Mn(T-4PyP)Cl]**,¹⁰ and chloro[5,10,15-tris(2,6-dichlorophenyl)-20-(pyridin-4-yl)porphyrinate]manganese(III) **Mn(DC-mono-4PyP)Cl**,¹¹ (**Figure 3.1 A**);

iii) The catalytic activity evaluation of **Mn(TDCPyP)Cl** in the oxidation of cyclooctene using a mixture of acetonitrile/water as solvent in the presence of different co-catalysts;

iv) The strategy used to anchor **[Mn(mono-DCPyP)Cl]** and **[Mn(DC-mono-4PyP)Cl]** onto the solid supports: 3-bromopropyl silica and Merrifield resin (MR);

v) The characterization of the materials obtained: **CAT-Si**, **CAT-MR** and **CAT-4Py-MR** (**Figure 3.1 B**);

vi) The catalytic activity evaluation of **CAT-Si**, **CAT-MR** and **CAT-4Py-MR** in the epoxidation of cyclooctene;

vii) The catalytic oxidation of styrene under homogeneous and heterogeneous conditions, using the best catalytic system found for cyclooctene.

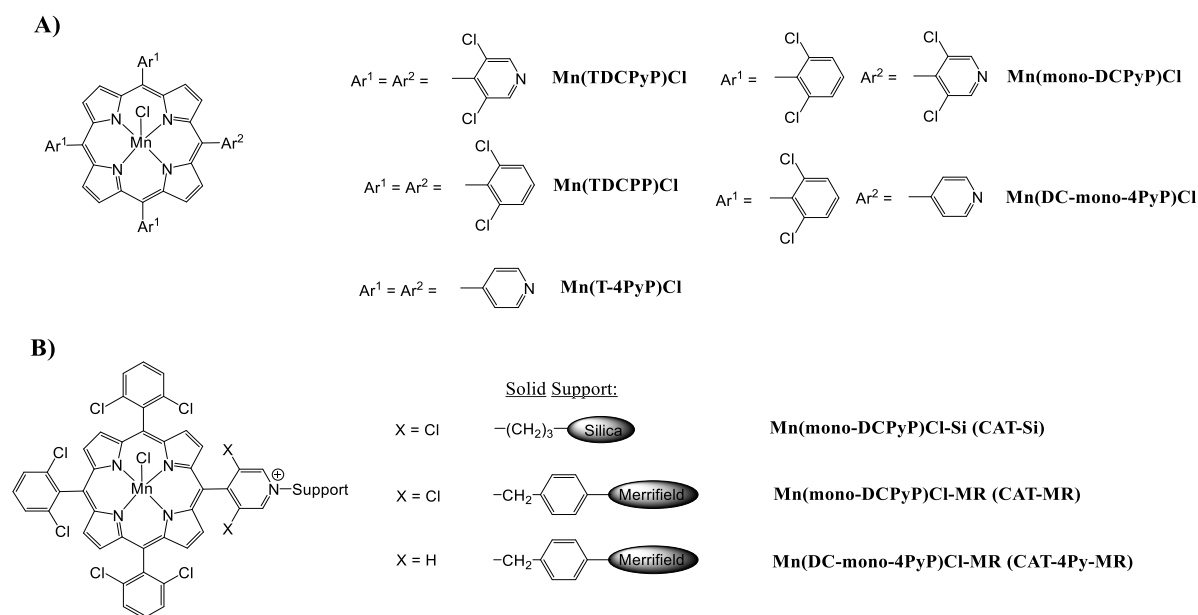


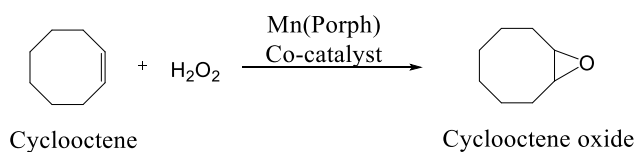
Figure 3.1. The structures of the catalysts used in the present study for oxidation reactions under **A)** homogeneous conditions and **B)** heterogeneous conditions.

3.1. Results and discussion

3.1.1. Oxidation of cyclooctene under homogeneous catalytic conditions

3.1.1.1. Mn(TDCPyP)Cl and Mn(mono-DCPyP)Cl catalytic activity evaluation

To evaluate the catalytic activity of the novel manganese(III) porphyrins, **Mn(TDCPyP)Cl** and **Mn(mono-DCPyP)Cl**, in oxidation reactions, cyclooctene was selected as model substrate and aqueous hydrogen peroxide as oxygen donor, due to our interest in developing environmentally friendly reaction conditions (**Scheme 3.1**).^{9,12–20}



Scheme 3.1. Cyclooctene oxidation reaction in the presence of H₂O₂ catalysed by the Mn(III) porphyrins prepared.

For the preliminary assays, acetonitrile was chosen as solvent whereas ammonium acetate was preferred as co-catalyst, in order to promote the required heterolytic cleavage of H₂O₂.^{8,12,21} Nevertheless, during the preparation of the stock solutions, we found that **Mn(TDCPyP)Cl** was not completely soluble in acetonitrile. To make sure that the right amount of catalyst was used, **Mn(TDCPyP)Cl** was weighed directly into the glass reactor and 2 mL of acetonitrile were added. Interestingly, when the required amount of ammonium acetate was added to the suspension of **Mn(TDCPyP)Cl** in the 2 mL of acetonitrile, and after 3 min under strong stirring, the catalyst was totally solubilized. However, longer stirring without adding the oxidant led to the precipitation of the catalyst, which resulted in a lower conversion of the substrate. Thus, after complete solubilization of the catalyst, H₂O₂ was added and the evolution of the reaction was monitored by GC-FID, along with the epoxide formation with gradual addition of the oxidant. Under these conditions, for a substrate/catalyst (S/C) molar ratio of 150, almost total conversion of cyclooctene (98.8%) to cyclooctene oxide (selectivity > 99%) was obtained after 90 min of reaction (**Figure 3.2 A** and **Table 3.1**).

In the case of **Mn(mono-DCPyP)Cl** no problems associated with its solubility in acetonitrile or with its precipitation, after adding ammonium acetate, were observed. Therefore, a stock solution was prepared in acetonitrile and kept in the fridge for later use. The amount of catalyst needed for each assay was added to the reactor and the final volume was completed with acetonitrile. With the **Mn(mono-DCPyP)Cl** asymmetric catalyst, in acetonitrile, using ammonium acetate as co-catalyst and the same S/C molar ratio of 150, accompanied by the addition of 0.5 equivalents (eq) of H_2O_2 at every 15 min, almost total conversion (98.8%) of cyclooctene to cyclooctene oxide (selectivity > 99%) was obtained after 60 min of reaction (**Figure 3.2 B** and **Table 3.1**).

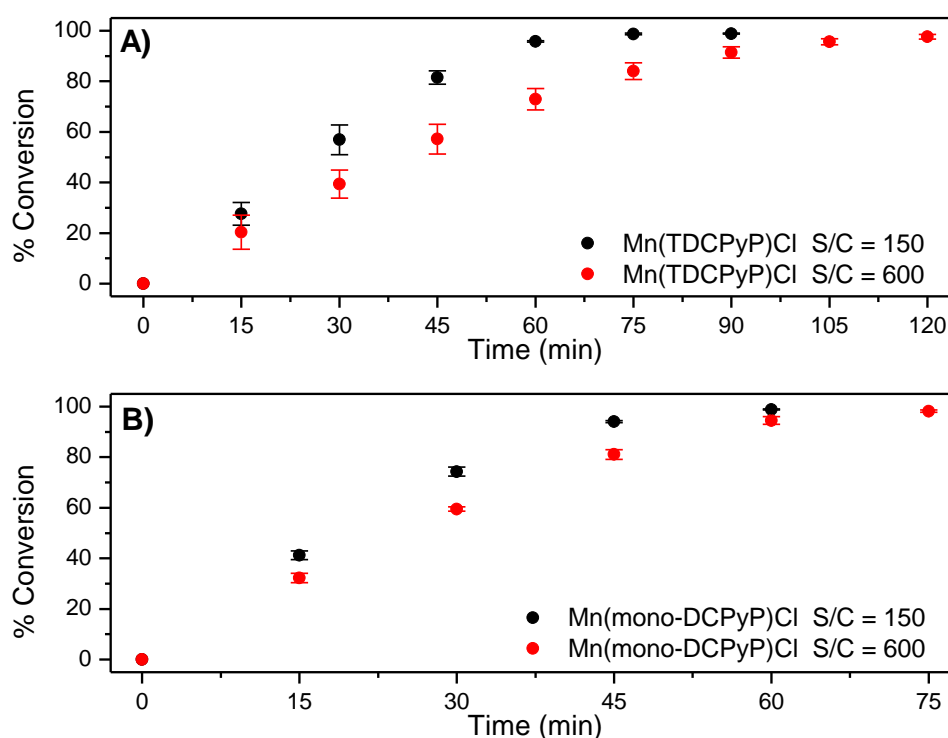


Figure 3.2 Comparison of the catalytic efficiency for the oxidation of cyclooctene with H_2O_2 catalysed by **A) Mn(TDCPyP)Cl** and **B) Mn(mono-DCPyP)Cl**. Data correspond to mean values of at least three non-simultaneous replicates and the vertical bars correspond to standard deviations.

The excellent behaviour of both catalysts under the conditions tested (high conversion of cyclooctene and good stability of the catalysts confirmed by UV-Vis spectrophotometry) led us to test a S/C molar ratio of 600 (**Table 3.1**). Under these conditions, the oxidation of cyclooctene in the presence of **Mn(TDCPyP)Cl** was slightly

slower (**Figure 3.2 A**), but still a high conversion of the substrate was achieved after 120 min of reaction (97.6%). In the case of **Mn(mono-DCPyP)Cl**, the efficiency of the catalyst was roughly maintained with a substrate conversion of 98.2% after 75 min of reaction (**Figure 3.2 B**).

3.1.1.2. Comparison between the novel catalysts and analogous Mn(III) porphyrins

Taking into account the results obtained with the two novel metalloporphyrins, **Mn(mono-DCPyP)Cl** and **Mn(TDCPyP)Cl**, it seems important to compare its catalytic activity with that of already known porphyrins having related structural features (**Figure 3.1 A**):

i) the highly efficient homogeneous catalyst chloro[5,10,15,20-tetrakis(2,6-dichlorophenyl)porphyrinate]manganese(III), **Mn(TDCPP)Cl**, having all the *meso* positions substituted by 2,6-dichlorophenyl units;

ii) the chloro[5,10,15,20-tetra(pyridin-4-yl)porphyrinate]manganese(III), **Mn(T-4PyP)Cl**, with all the *meso* positions substituted by pyridine units;

iii) the chloro[5,10,15-tri(2,6-dichlorophenyl)-20-(pyridin-4-yl)porphyrinate]manganese(III), **Mn(DC-mono-4PyP)Cl**, with one *meso* position substituted by a pyridine unit and the other three *meso* positions by the 2,6-dichlorophenyl groups.

The results obtained using both S/C molar ratios of 150 and 600 are summarized in **Table 3.1**. To facilitate the discussion, the evolution of the conversion of cyclooctene at those S/C molar ratios during the reaction course for all the catalysts are depicted in **Figures 3.3** and **3.4**.

The results show that the newly synthesized catalyst **Mn(mono-DCPyP)Cl** and the well-known and highly efficient catalyst **Mn(TDCPP)Cl** exhibit similar activity, even when a S/C molar ratio of 600 is used. **Mn(mono-DCPyP)Cl** was also more efficient than its analogue **Mn(DC-mono-4PyP)Cl** that, despite achieving high cyclooctene conversion for the S/C molar ratio of 150 (98.8% after 90 min), when the S/C molar ratio was increased to 600 the conversion decreased to 40.1% only (**Table 3.1**).

Table 3.1. Results obtained for the oxidation of cyclooctene with H₂O₂ using CH₃CN as solvent and ammonium acetate as co-catalyst, in the presence of different Mn(III) porphyrins^(a)

Catalyst	S/C molar ratio	H ₂ O ₂ (eq)	Conversion (%)	Time (min)
Mn(TDCPyP)Cl	150	3	98.8	90
	600	4	97.6	120
Mn(mono-DCPyP)Cl	150	2	98.8	60
	600	2.5	98.2	75
Mn(TDCPP)Cl	150	2	98.3	60
	600	2.5	98.6	75
Mn(DC-mono-4PyP)Cl	150	3	98.8	90
	600	2.5	40.1	75
Mn(T-4PyP)Cl	150	3	25.4	90

^(a) 7.5×10^{-5} mol of cyclooctene; 5×10^{-7} mol of the catalyst in the case of the S/C molar ratio of 150 and 1.25×10^{-7} mol in the case of the S/C molar ratio of 600. The co-catalyst: 0.2 mmol (≈ 15 mg) of ammonium acetate. The final volume of 2 mL was completed with CH₃CN and the reaction mixture was kept protected from light, under stirring at 30 ± 1 °C. The oxidant used was aqueous H₂O₂ (30% w/w) diluted 1:5 in CH₃CN and was added at regular intervals of 15 min, each oxidant addition corresponding to half of the initial amount of the substrate (3.75×10^{-5} mol).

The new catalyst **Mn(TDCPyP)Cl** was also very efficient in the oxidation of cyclooctene. Its performance was much better than that of its tetrapyrrolyl analogue **Mn(T-4PyP)Cl**, which proved to be the least efficient of all, not exceeding 25.4 % of conversion for a S/C molar ratio of 150 (**Table 3.1** and **Figure 3.3**). In fact, after 30 min of reaction, its UV-Vis spectrum (**Figure 3.5 E**) shows the absence of the Soret band of the Mn(III) species at $\lambda_{\max} = 465$ nm. Due to its low efficiency when using a S/C molar ratio of 150, **Mn(T-4PyP)Cl** was not tested for the S/C molar ratio of 600. A different situation was observed with the other catalysts (**Figure 3.5 A-D**). After the addition of H₂O₂, besides the Soret band relative to the Mn(III) species, a band at $\lambda_{\max} \approx 425 \pm 1$ nm is observed. This band has been attributed to an Mn(IV)-OH species and results from the Mn(V)=O species, which may be the main responsible for the oxidation process, but due to its instability is not easily detected.²²⁻²⁸ When a S/C molar ratio of 600 was used, the catalytic activity of **Mn(TDCPyP)Cl** was lower, however a conversion of 97.6% was achieved after 120 min of reaction, its activity being higher than that achieved using **Mn(DC-mono-4PyP)Cl** (**Figure 3.4** and **Table 3.1**). These results highlight the great importance of the presence of the chlorine atoms in the pyridyl substituents at the *meso* positions of the porphyrins on their stability and the consequent efficiency as catalysts.

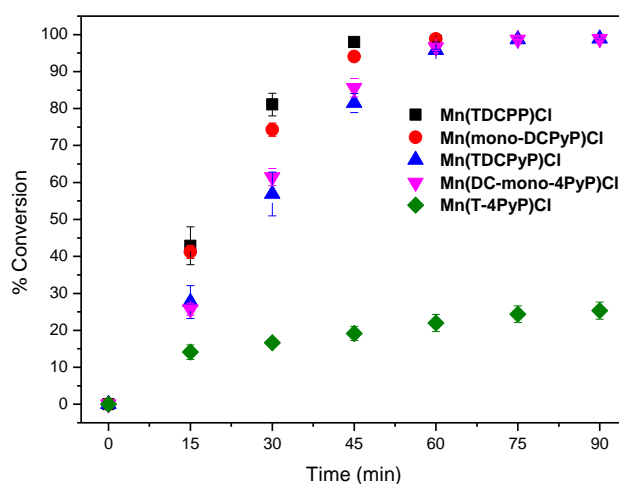


Figure 3.3. Cyclooctene conversion in the oxidation reactions catalysed by different Mn(III) porphyrin catalysts vs time for a S/C molar ratio of 150. Data correspond to mean values of at least three non-simultaneous replicates and the vertical bars correspond to standard deviations.

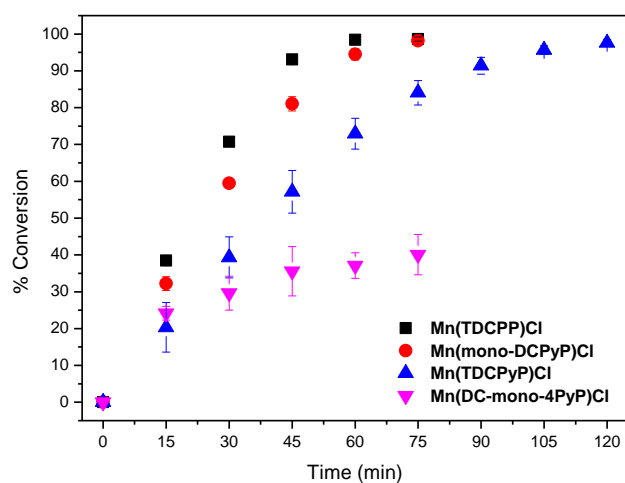


Figure 3.4. Cyclooctene conversion in the oxidation reactions catalysed by different Mn(III) porphyrin catalysts vs time for a S/C molar ratio of 600. Data correspond to mean values of at least three non-simultaneous replicates and the vertical bars correspond to standard deviations.

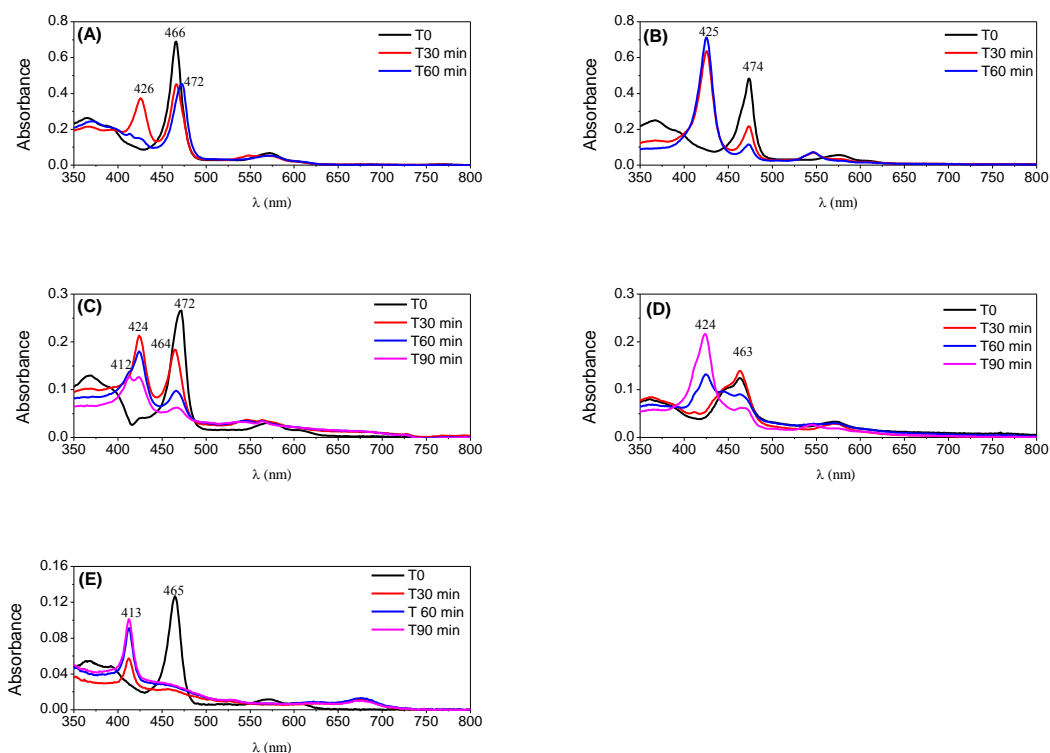


Figure 3.5. UV-Vis monitoring of the catalysts along cyclooctene oxidation reactions for the S/C molar ratio of 150: (A) Mn(TDCPP)Cl; (B) Mn(mono-DCPyP)Cl; (C) Mn(DC-mono-4PyP)Cl; (D) Mn(TDCPyP)Cl; (E) Mn(T-4PyP)Cl.

3.1.1.3. Catalytic activity of Mn(TDCPyP)Cl using a mixture acetonitrile/water

Since Mn(TDCPyP)Cl was scarcely soluble in acetonitrile alone, we tried to dissolve this catalyst in a mixture of acetonitrile/water and to prepare a stock solution. The amount of water used in the reaction mixture may not exceed 20% due to the substrate and internal standard poor solubility in water. Thus, a stock solution of this catalyst was prepared in a mixture of acetonitrile/water (1:1), the amount of catalyst required was added to the reactor and the final volume filled with acetonitrile, thus the final mixture being about 10% of water. First, cyclooctene oxidation reactions were carried out as previously described for the reactions in acetonitrile, using ammonium acetate as co-catalyst with additions of 0.5 eq H₂O₂ every 15 min and the S/C molar ratio of 150. Under these conditions, the conversion of cyclooctene into the corresponding epoxide was accompanied by the precipitation of the catalyst and no evolution was detected after 210 min of reaction (**Table 3.2**, Entry 1). Catalyst precipitation was considered the main reason for its limited catalytic activity under the conditions described above (80.2% conversion, with selectivity to the epoxide > 99%). It was verified that the precipitate was only soluble in water or dimethyl sulfoxide (DMSO) and its UV-Vis spectrum in DMSO was fully coincident with the UV-Vis spectrum of Mn(TDCPyP)Cl, with the Soret band at $\lambda = 458$ nm (**Figure 3.6**). This result led us to admit the possibility of protonation of the pyridine units in the manganese porphyrin due to the putative presence of acetic acid (from ammonium acetate) in the reaction medium. However, when the assay was repeated with acetic acid instead of ammonium acetate, no precipitation occurred, and the catalyst revealed to be totally inefficient (**Table 3.2**, Entry 2). Aiming to improve the performance of the catalyst in the mixture of acetonitrile/water, the next assays were performed using ammonium formate or ammonium benzoate as co-catalyst, instead of ammonium acetate (**Table 3.2**, Entries 3 and 4). In both cases, the Mn(III) porphyrin seemed to be very stable and no precipitation was observed. The best performance was registered in the presence of ammonium benzoate, where full conversion of cyclooctene was registered after 120 min of reaction. The absence of precipitation of the catalyst in the presence of ammonium formate is also responsible for its superior catalytic activity when compared with the ammonium acetate assays (95% conversion after 180 min of reaction with ammonium formate vs 80% after 210 min with ammonium acetate). The evolution of cyclooctene conversion in the presence of the three co-catalysts is compared in **Figure 3.7**. It seems that the distinction

between the efficiency of ammonium formate and ammonium acetate is more notable after 90 min of reaction, when the precipitation of the catalyst with ammonium acetate starts to be strongly limitative. After 45 min of reaction, a cyclooctene conversion of *ca* 20% was obtained in the presence of ammonium acetate and ammonium formate, while with ammonium benzoate, after the same time of reaction, its superiority was already patent with a conversion close to 70%.

Table 3.2. Results obtained for the oxidation of cyclooctene with H₂O₂ catalysed by Mn(TDCPyP)Cl in the presence of different co-catalysts for a S/C molar ratio of 150 using a mixture of CH₃CN/H₂O as solvent.^(a)

Entry	Co-catalyst	H ₂ O ₂ (eq)	Conversion (%)	Time (min)
1	Ammonium acetate	7	80.2	210
2	Acetic acid	3.5	0	105
3	Ammonium formate	6	94.7	180
4	Ammonium benzoate	4	100	120
5	No co-catalyst	7	0	210

^(a) 7.5×10^{-5} mol of cyclooctene; 5×10^{-7} mol of catalyst (taken from a stock solution previously prepared in a mixture of CH₃CN/H₂O 1:1). The co-catalyst: 0.2 mmol (\approx 15 mg) of ammonium acetate or 0.42 mmol (24 μ L) of acetic acid or 0.2 mmol (\approx 12.6 mg) of ammonium formate or 0.2 mmol (\approx 27.8 mg) of ammonium benzoate. The final volume of 2 mL was completed with CH₃CN and the reaction mixture was kept protected from light, under stirring at 30 ± 1 °C. The oxidant used was aqueous H₂O₂ (30% w/w) diluted 1:5 in CH₃CN, and was added at regular intervals of 15 min, each addition corresponding to half of the initial amount of substrate (3.75×10^{-5} mol).

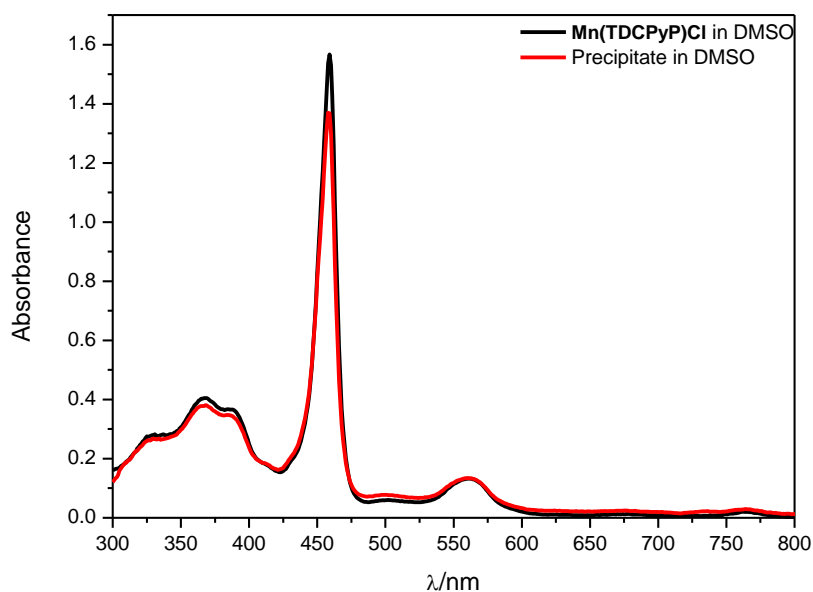


Figure 3.6. Comparison of the UV-Vis spectrum of Mn(TDCPyP)Cl in DMSO with that of the precipitate which is obtained during the oxidation reaction of cyclooctene in a mixture of acetonitrile/water using ammonium acetate as co-catalyst.

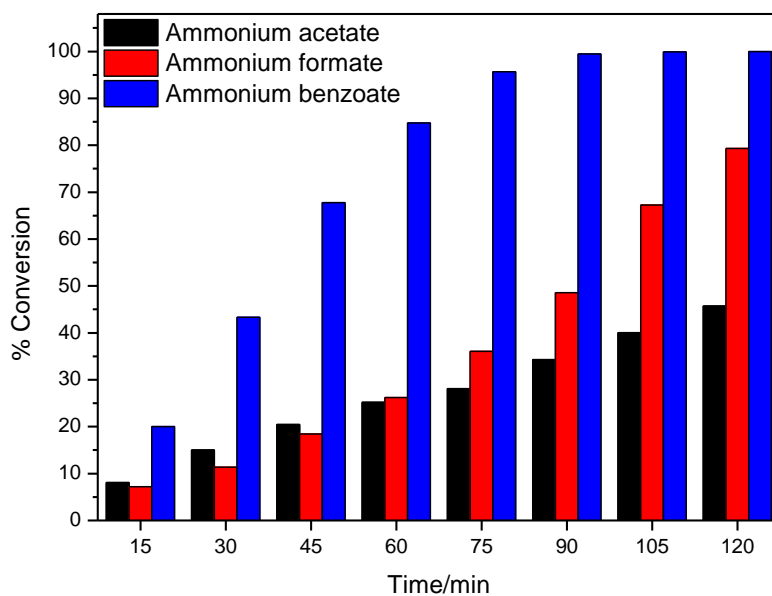
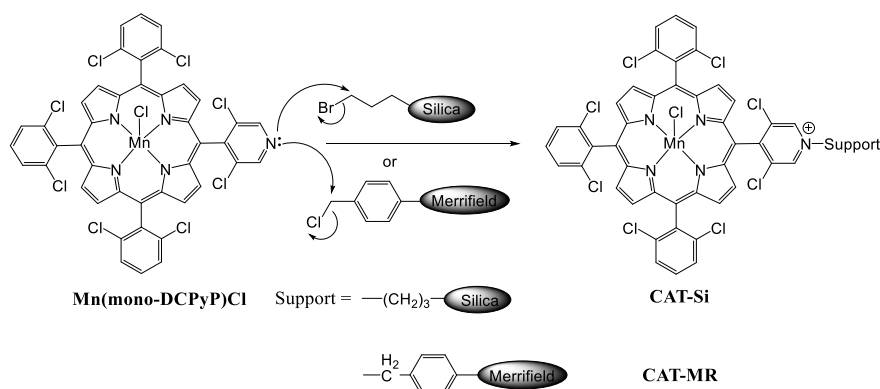


Figure 3.7. Conversion obtained for the epoxidation of cyclooctene with H_2O_2 in the presence of different co-catalysts and catalysed by Mn(TDCPyP)Cl in a mixture of $\text{CH}_3\text{CN}/\text{H}_2\text{O}$ for a S/C molar ratio of 150.

3.1.2. Synthesis and characterization of the heterogeneous catalysts

3.1.2.1. Immobilization of Mn(mono-DCPyP)Cl under classic heating

The metalloporphyrin **Mn(mono-DCPyP)Cl** was immobilized by the covalent anchorage of the pyridine moiety present in the metalloporphyrin (**Scheme 3.4**) to 3-bromopropyl-functionalized silica and Merrifield resin (MR) supports (commercially available).



Scheme 3.4. Strategy used to covalently immobilize **Mn(mono-DCPyP)Cl** to 3-bromopropyl-functionalized silica and Merrifield resin supports.

The first immobilization reaction was made with the MR support, at 155 °C, using dry DMF as solvent and based on previous works.^{29,30} After 4 h of reaction, the solution still had a dark brown colour thus indicating the presence of the metalloporphyrin. A small amount of the resin was removed from the reaction medium and, after washing with DMF, the resin remained white showing that the anchorage of the metalloporphyrin to the support was not occurring. The immobilization was also carried out with a high amount of manganese porphyrin but, even after 48 h, there was almost no immobilization of the metalloporphyrin. In a different assay, trying to improve the reactivity of the MR support, NaI was added to the reaction medium in order to substitute chlorine atoms by iodine atoms. After 24 h, the resin became brown and the solid was filtered and washed with DMF, CH₃CN and dichloromethane (previously passed through an aluminum oxide column). However, the UV-Vis spectrum of the reaction medium (**Figure 3.8**) presented, besides the Soret band of the manganese complex, another band at 417 nm. A similar profile was observed in the diffuse reflectance spectrum of the obtained solid material (**Figure 3.8**), indicating a probable demetallation, which was confirmed by TLC. These

problems may be related with the formation of decomposition products from DMF, often obtained at high temperatures. By using DMF as solvent in the porphyrin immobilization process, an extra complexation step would be necessary to ensure that all the porphyrin was metallated.

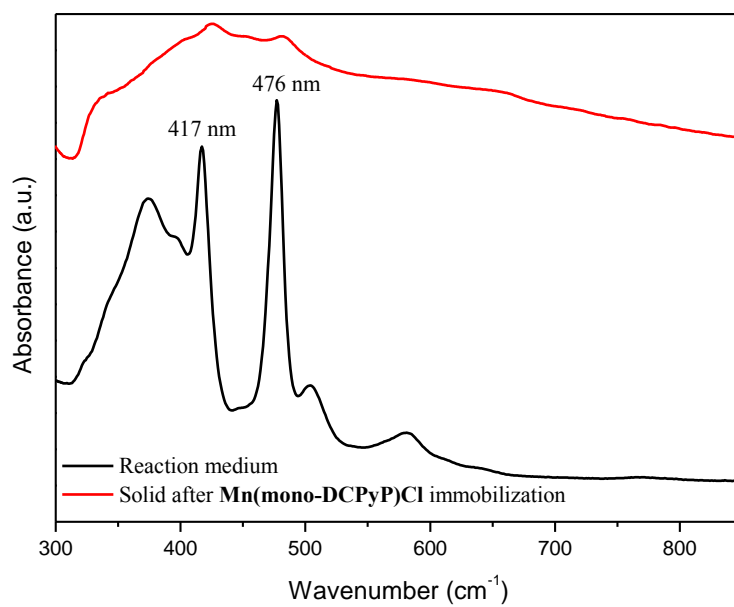
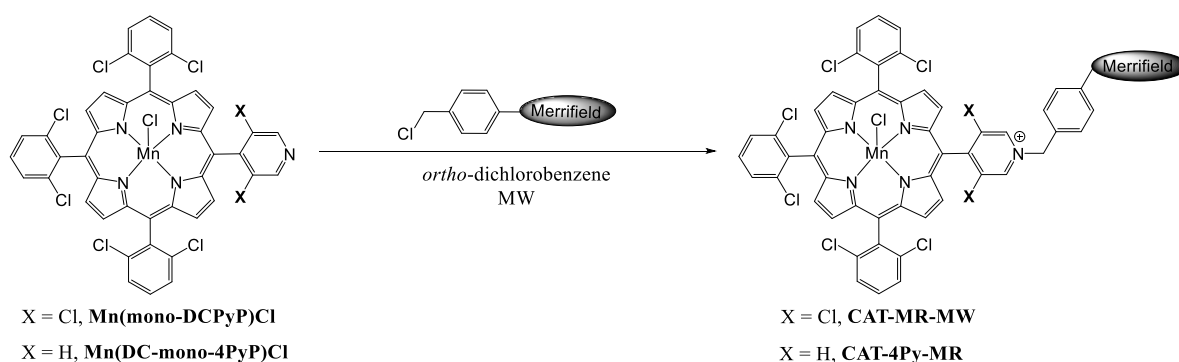


Figure 3.8. UV-Vis spectrum of the reaction medium in the immobilization of **Mn(mono-DCPyP)Cl** on MR using DMF as solvent and diffuse reflectance UV-Vis spectrum of the obtained solid.

Aiming to circumvent the problems resulting from the use of DMF and to improve the loading of the catalyst, the immobilization was carried out following a procedure developed by our group,³¹ using *ortho*-dichlorobenzene as solvent. The reaction was left at 190 °C in a sand bath, being followed by UV-Vis. Although some metalloporphyrin was still present in solution, the reaction was stopped after 96 h. The obtained solid was filtered, washed with *ortho*-dichlorobenzene, CH₃CN and dichloromethane (previously passed through an aluminum oxide column) and dried. The loading of catalyst immobilized was calculated by elemental analysis based on the amount of nitrogen present in the sample. Using these conditions, a loading of 7.2 μmol/g was obtained for the immobilization of **Mn(mono-DCPyP)Cl** on MR. The same approach was applied to anchor the manganese porphyrin onto the functionalized silica leading to a loading of 17.8 μmol/g.

3.1.2.2. Immobilization of Mn(mono-DCPyP)Cl and Mn(DC-mono-4PyP)Cl on Merrifield resin under microwave assisted irradiation

In order to improve the loading of catalyst, to decrease the reaction time and to work in more sustainable conditions, we decided to test the microwave (MW) assisted irradiation as a heating source in the immobilization of the catalysts on MR (**Scheme 3.5**).



Scheme 3.5. Immobilization of the manganese(III) porphyrins on MR using MW-assisted irradiation.

Initially, a multimode MW equipment was used and the immobilization was tested with Mn(DC-mono-4PyP)Cl using different irradiation conditions in a closed vessel (**Scheme 3.5** and **Table 3.4**). The reactions were started by using a power of 600 watt for 45 min with a restriction for the maximum temperature of 200 °C, since the boiling point of *ortho*-dichlorobenzene is 180 °C and MR may not be stable at higher temperatures. Under these conditions, a loading of 9.7 $\mu\text{mol/g}$ was obtained (**Table 3.4**, Entry 1). Trying to obtain higher catalyst loadings, the power was increased to 800 watt with a maximum temperature restriction of 200 °C (**Table 3.4**, Entry 2); however, the temperature reached 200 °C after 4 min, which automatically lowered the power. Using these conditions, a catalyst loading of 11.4 $\mu\text{mol/g}$ was obtained after 45 min. Then, two experiments were carried out with the power of 800 watt without temperature restriction (**Table 3.4**, Entry 3 and 4) and the temperature did not exceed 216 °C. Therefore, keeping the power at 800 watt it was possible to carry out the reaction and to get a loading of 9.4 $\mu\text{mol/g}$ in 30 min (**Table 3.4**, Entry 4). At the end of the reactions, even in the situations where the loading was higher, a large amount of unreacted porphyrin was always present in solution. So, we decided to use a larger amount of MR, using a power of 800 watt and without temperature

restriction, trying to have less porphyrin in solution (**Table 3.4**, Entry 5). In addition, we would have a larger amount of heterogeneous catalyst with the same porphyrin loading. However, in this case a sudden increase in the temperature occurred and the irradiation had to be stopped after 10 min since a very high temperature had been reached. The reaction was allowed to cool and was irradiated for further 9 min but was stopped because the temperature was too high and could destroy the MR. In this case the porphyrin loading was considerably lower. To obtain a higher amount of catalyst with the same porphyrin loading, we decided to repeat the immobilization reaction with 250 mg of resin with 800 watt of power for 30 min without restriction of temperature (**Table 3.4**, Entry 4). The porphyrin loading was lower, nevertheless two batches with loading of 7.3 and 7.4 $\mu\text{mol/g}$ were obtained.

The latter conditions were used in the immobilization of **Mn(mono-DCPyP)Cl**. In this case the porphyrin loading was 4.4 $\mu\text{mol/g}$ (**Table 3.5**, Entry 1), which was considerably lower than that obtained in the immobilization of **Mn(DC-mono-4PyP)Cl**. In fact, the presence of the chlorine atoms in the pyridine ring may cause a less nucleophilic character of the nitrogen, thus resulting in lower reactivity of **Mn(mono-DCPyP)Cl**. Aiming to improve these results, a single-mode MW apparatus was used, where the reactions are usually faster. The reactions in the single-mode MW equipment were carried out in a closed vessel for 30 min with a restriction for maximum temperature of 200 °C and the power was variable. Under these conditions, the power was always lower than 300 watt and a loading of 18.8 $\mu\text{mol/g}$ was attained for **Mn(DC-mono-4PyP)Cl** (**Table 3.4**, Entry 6) and 11.4 $\mu\text{mol/g}$ was achieved in the case of **Mn(mono-DCPyP)Cl** (**Table 3.5**, Entry 2). The reactions were repeated, and the same results were obtained.

Table 3.4. MW irradiation conditions used to immobilize **Mn(DC-mono-4PyP)Cl** on Merrifield resin (MR) and manganese(III) porphyrin loading obtained.^(a)

Entry	MR (mg)	MW device	Power (watt)	Time (min)	Temperature restriction (°C)	Final temperature (°C)	Loading (μmol/g) ^(b)
1	250	Multimode	600	45	200	176	9.7
2	250	Multimode	800	45	200	200 ^(c)	11.4
3	250	Multimode	800	8	No	212	4.5
4 ^(d)	250	Multimode	800	30	No	216	9.4
5	500	Multimode	800	19 (10+9)	No	270; 300	5.9
6	250	Single-mode	-	30	200	200	18.8

^(a) 5 mg of **Mn(DC-mono-4PyP)Cl** and 4 mL of *ortho*-dichlorobenzene were used in all the reactions.

^(b) Porphyrin loading was calculated by elemental analysis, based on the % mass of nitrogen.

^(c) The temperature was 200 °C after 4 min.

^(d) The reaction was repeated two times and loadings of 7.3 and 7.4 μmol/g were obtained.

Table 3.5. MW irradiation conditions used to immobilize **Mn(mono-DCPyP)Cl** on Merrifield resin (MR) and manganese(III) porphyrin loading obtained.^(a)

Entry	MR (mg)	MW device	Power (watt)	Time (min)	Temperature restriction (°C)	Final temperature (°C)	Loading (μmol/g) ^(b)
1	250	Multimode	800	30	No	250	4.4
2	250	Single-mode	-	30	200	200	11.4

^(a) 5 mg of **Mn(mono-DCPyP)Cl** and 4 mL of *ortho*-dichlorobenzene.

^(b) Porphyrin loading was calculated by elemental analysis, based on the % mass of nitrogen.

The use of MW assisted irradiation as a source of heat in the immobilization of manganese(III) porphyrins in MR has some advantages over the conventional heating. First, we have shortened the reaction time from 96 h to just 30 min using both the available MW equipments. It was also possible to increase the porphyrin loading on immobilized catalyst and better results with the single-mode MW equipment were obtained.

3.1.2.3. Structural characterization of the immobilized porphyrin materials

The solid material resulting from the immobilization of **Mn(mono-DCPyP)Cl** with 3-bromopropyl-functionalized silica (**CAT-Si**) have a pale green colour (**Figure 3.9** left), whereas the solids obtained with the immobilization of **Mn(mono-DCPyP)Cl** and **Mn(DC-mono-4PyP)Cl** with MR (**CAT-MR** and **CAT-4Py-MR**, respectively) have a light brown colour (**Figure 3.9** right - illustrated for **CAT-MR**).

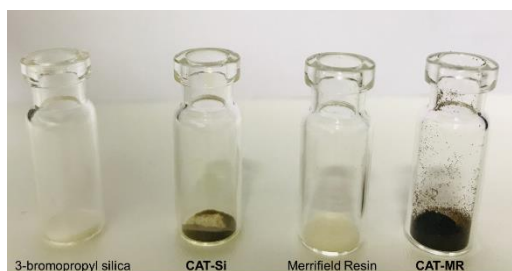


Figure 3.9. Appearance of the starting materials 3-bromopropylsilica and MR and of the solids obtained after **Mn(mono-DCPyP)Cl** immobilization, **CAT-Si** and **CAT-MR**.

The supported porphyrin materials were analysed by diffuse reflectance (**Figure 3.10**). The UV-Vis spectrum of the **Mn(mono-DCPyP)Cl** powder (**Figure 3.10 – a**) shows the Soret band at around 479 nm and the Q-bands at 583 nm and 623 nm. The UV-Vis spectrum of the **Mn(DC-mono-4PyP)Cl** powder (**Figure 3.10 – b**) shows the Soret band at 473 nm and the Q-bands at 578 nm and 620 nm. The presence of the Soret and the Q-bands in the UV-Vis spectra of the immobilized porphyrin materials (**Figure 3.10 – c, d, e**) confirms the presence of the corresponding porphyrin.

The solids were also analysed by ATR infrared spectroscopy (**Figure 3.11**); however, in the spectra of **CAT-Si** (c), **CAT-MR** (e) and **CAT-4Py-MR** (f) the bands due to the metalloporphyrin were not seen due to the low concentration of porphyrin if compared with the solid supports and, therefore, the silica and the Merrifield bands overlap the metalloporphyrin bands. For the same reason, the powder X-ray diffraction spectra of **CAT-Si**, **CAT-MR** and **CAT-4Py-MR** (data not shown) display a halo in the region of 20-30° (2θ), typical of amorphous samples, similar to the starting materials.

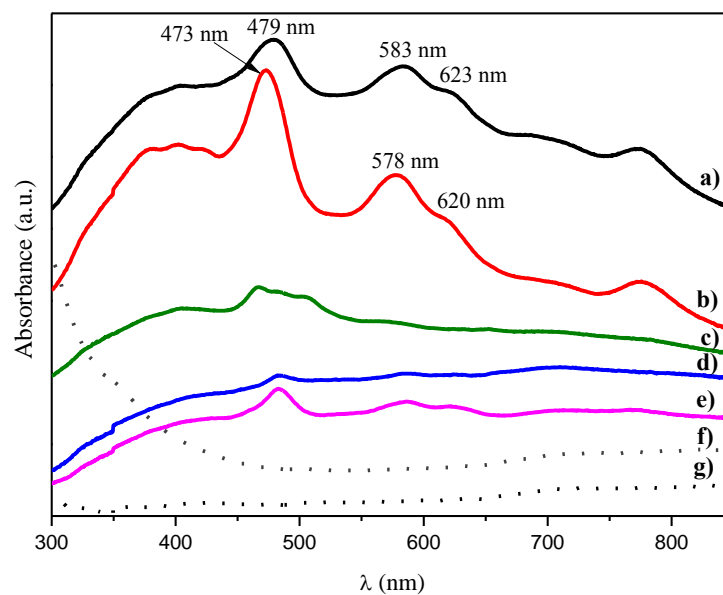


Figure 3.10. Diffuse reflectance UV-Vis spectra obtained for: a) Mn(mono-DCPyP)Cl powder, b) Mn(DC-mono-4PyP)Cl powder, c) CAT-Si, d) CAT-MR, e) CAT-4Py-MR, f) MR, g) 3-bromopropylsilica.

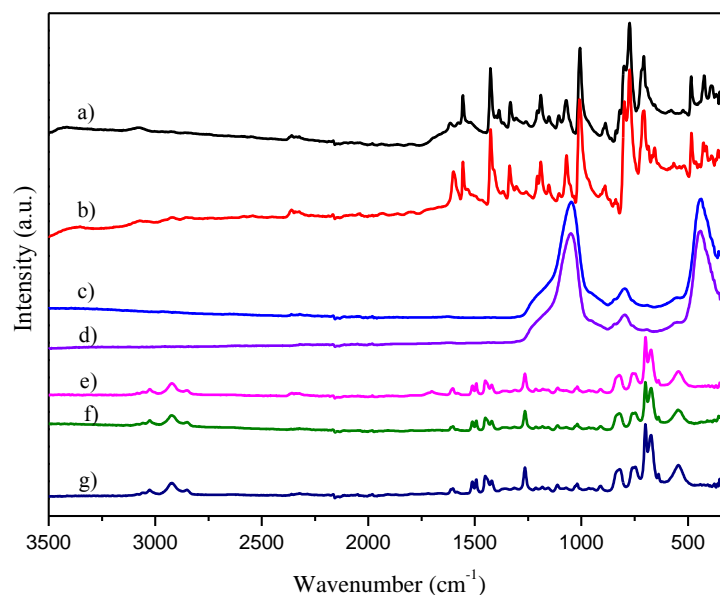


Figure 3.11. ATR spectra of a) Mn(mono-DCPyP)Cl, b) Mn(DC-mono-4PyP)Cl, c) CAT-Si, d) 3-bromo-propyl silica, e) CAT-MR, f) CAT-4Py-MR, g) MR.

The morphology of **CAT-MR** (classic heating), **CAT-MR-MW** (4.4 $\mu\text{mol/g}$ of loading calculated by elemental analysis, **Table 3.5**, Entry 1) and **CAT-Si** was studied by the SEM technique and compared with the starting materials (**Figures 3.12** and **3.13**). The images show that there are no major changes in the morphology of the immobilized porphyrin materials when compared with the original MR and silica supports, which means that the characteristics of the original materials are maintained after immobilization. In the case of **CAT-MR** (**Figure 3.12** b, c, f, g, h) a small change in the surface was observed, after immobilization, at various points presenting some roughness, which is more pronounced in the sample of **CAT-MR-MW** (**Figure 3.12** h). This roughness should result from functionalization reaction. In the case of the material obtained by immobilization of **Mn(mono-DCPyP)Cl** on silica, this type of surface change is less evident (**Figure 3.13**).

The EDS analysis of **CAT-Si** shows the presence of chlorine (**Figure 3.14 B**), which was not present in the starting silica sample (**Figure 3.14 A**) and confirms the anchoring of the porphyrin onto the solid support. In the case of the materials resulting from the immobilization of **Mn(mono-DCPyP)Cl** and **Mn(DC-mono-4PyP)Cl** on the MR support, no changes were observed in the EDS spectra before and after the immobilization onto the starting material.

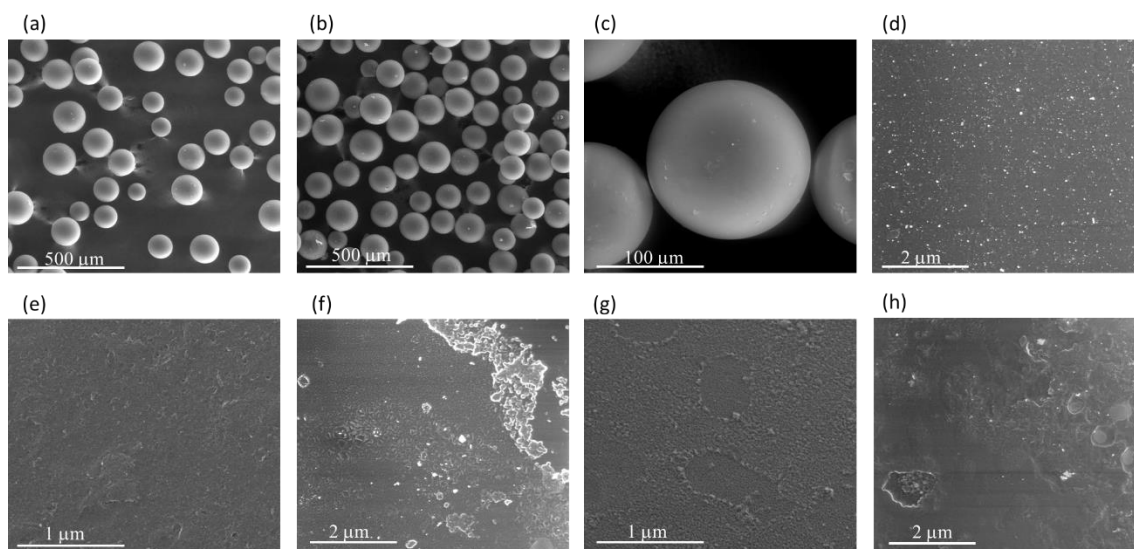


Figure 3.12. SEM micrographs of (a) starting MR ($\times 200$), (b) **CAT-MR** obtained by classic heating ($\times 200$), (c) **CAT-MR** obtained by classic heating ($\times 1000$), (d) starting MR ($\times 40000$), (e) starting MR ($\times 100000$), (f) **CAT-MR** obtained by classic heating ($\times 40000$), (g) **CAT-MR** obtained by classic heating ($\times 100000$), (h) **CAT-MR-MW** ($\times 40000$).

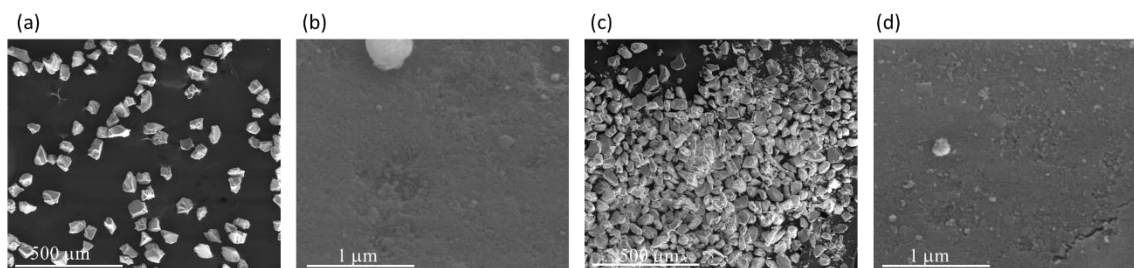


Figure 3.13. SEM micrographs of (a) starting silica ($\times 200$), (b) starting silica ($\times 100000$), (c) **CAT-Si** ($\times 200$), (d) **CAT-Si** ($\times 100000$).

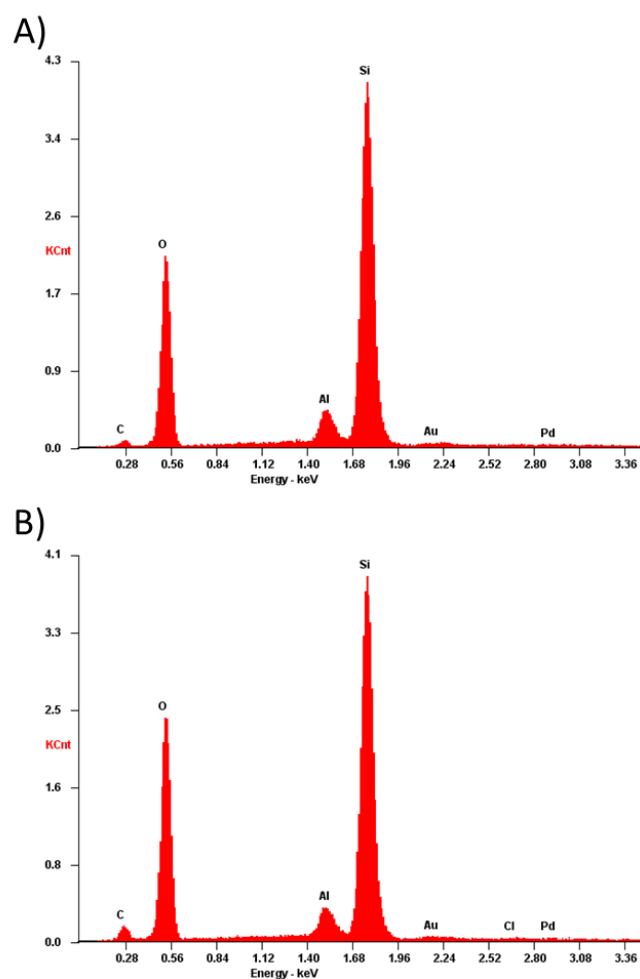


Figure 3.14. EDS spectra of **A)** the starting 3-bromopropyl functionalized silica and **B)** the solid material obtained after immobilization of **Mn(mono-DCPyP)Cl** onto the silica (**CAT-Si**).

The composition of the heterogeneous catalysts was determined by X-ray photoelectron spectroscopy (XPS) and was compared with the starting materials. The elemental atomic percentages are summarized in **Table 3.6**.

In the case of the solid material obtained by immobilization of **Mn(mono-DCPyP)Cl** on silica, **CAT-Si**, the presence of nitrogen and chlorine and the increase in the atomic percentage of C 1s are in accordance with the anchorage of the manganese(III) porphyrin (**Table 3.6**, Entry 2). In addition, the decrease in the atomic percentage of bromine indicates the occurrence of the nucleophilic substitution. The decrease in bromine is, however, higher than expected for the immobilization of metalloporphyrin when compared to the increase in nitrogen and chlorine. The possible reason for the lower atomic percentage is because bromine can be lost during the immobilization due to the high temperature and/or by reaction with water present in the atmosphere. The manganese is not detected due to the low atomic percentage expected (at the detection limit level). In the case of the solid materials obtained by **Mn(mono-DCPyP)Cl** and **Mn(DC-mono-4PyP)Cl** immobilization on the MR (**CAT-MR**, **CAT-MR-MW** and **CAT-4Py-MR**), the increase in the atomic percentage of chlorine and the presence of nitrogen and manganese are the main evidences of metalloporphyrin anchorage (**Table 3.6**, Entries 4-6).

Table 3.6. Surface atomic percentages for **CAT-Si**, **CAT-MR**, **CAT-MR-MW** and **CAT-4Py-MR** obtained by XPS.^(a)

Entry	Material	Atomic (%)						
		C 1s	N 1s	O 1s	Si 2p	Cl 2p	Br 3d	Mn 2p3
1	3-bromopropylsilica	15.4	-	59.1	24.0	-	1.4	-
2	CAT-Si	17.0	0.5	56.4	25.0	0.4	0.7	n.d.
3	MR	93.4	-	5.6	-	1.1	-	-
4	CAT-MR	88.9	0.7	7.0	-	3.3	-	0.06
5	CAT-MR-MW	88.6	0.8	6.7	-	3.6	-	Traces
6	CAT-4Py-MR	86.3	0.7	9.5	-	3.4	-	0.1

^(a) Determined by the areas of the respective bands in high resolution XPS.
n.d. - Not Detected

The high-resolution spectra of the elements present in the **CAT-Si** and in the starting 3-bromopropyl functionalized silica are depicted in **Figure 3.15**.

The XPS high-resolution spectra in the C 1s region of 3-bromopropyl silica (**Figure 3.15 A**) and **CAT-Si** (**Figure 3.15 B**) were deconvoluted into three components. The peak at 285.0 eV is attributed to the C–Si,³² and to the aliphatic C–C bonds that appear overlaid, the peak at 286.6 eV is ascribed to C–Br bonds and the peak at 288.4 eV is due to “adventitious carbon” contamination. “Adventitious” contamination is commonly present in samples exposed to air atmosphere. As in silica materials the amount of carbon is low, the carbon contamination due to “adventitious carbon”, which normally arises at approximately 284.8 eV, 286 eV and 288.5 eV becomes significant. For this reason, the bands present in the high-resolution C 1s spectra of silica and of **CAT-Si** have also a contribution of this contamination. In the spectrum of **CAT-Si**, the main peak at 285.0 eV corresponds to C–Si bonds, which overlaps with the aliphatic C–C bonds and the aromatic C=C bonds of the metalloporphyrin, the peak at 286.4 eV is ascribed to the C–Br bonds together with the C–N and C–Cl bonds of the metalloporphyrin and the peak at 288.1 eV is attributed to “adventitious carbon” contamination. The band at 286.4 eV is less intense in **CAT-Si** than in the starting silica due to the loss of bromine. The decrease in band intensity does not result only from the loss of bromine during the nucleophilic substitution, because the C–N and C–Cl bonds from the porphyrin, that appear at the same binding energy (B.E.), compensate for this decrease. Instead, bromine can be lost during the immobilization by reaction with the water.

The O 1s high-resolution spectrum of 3-bromopropylsilica (**Figure 3.15 A**) was deconvoluted into four bands. The main peak observed at 533.0 eV is assigned to Si–O–Si bonds and the peak at 533.9 eV is ascribed to O–Si and O–C bonds. The peak at 531.0 eV can be attributed to “adventitious” material and the peak at 535.2 eV is due to the presence of adsorbed water.³³ The O 1s high-resolution spectrum of **CAT-Si** (**Figure 3.15 B**) shows an identical profile and can be deconvoluted into the same four bands with binding energies very close to those obtained for 3-bromopropylsilica. The peak at 533.4 eV attributed to O–Si and O–C bonds increases in the **CAT-Si** material probably due to the nucleophilic substitution of bromine by water.

The Si 2p high-resolution spectra of the starting 3-bromopropylsilica (**Figure 3.15 A**) and of the **CAT-Si** (**Figure 3.15 B**) were deconvoluted into three components (doublets

for 2p orbitals) and the B.E. of the Si 2p components of **CAT-Si** do not differ significantly from the original silica. The bands at 103.5 eV ($2p_{3/2}$) and 104.1 ($2p_{1/2}$) eV are assigned to Si–O–Si bonds and the peaks at 102.0 eV ($2p_{3/2}$) and 102.6 eV ($2p_{1/2}$) are attributed to Si–C bonds. The bands at 104.5 eV ($2p_{3/2}$) and 105.1 eV ($2p_{1/2}$) may be attributed to Si–Br–O bonds, which might result from a possible nucleophilic substitution of the silica Si–O–Si groups by Br^- and further oxidation.

The Br 3d high-resolution spectra of the starting 3-bromopropylsilica (**Figure 3.15 A**) and of the **CAT-Si** (**Figure 3.15 B**) were fitted with three main components (doublets for 3d orbitals). In the Br 3d high-resolution spectrum of **CAT-Si** the preeminent peaks at 70.6 eV ($3d_{5/2}$) and 71.6 eV ($3d_{3/2}$) are assigned to Br–C bonds and the peaks at 68.7 eV ($3d_{5/2}$) and 69.7 eV ($3d_{3/2}$) are attributed to Br^- ions.³⁴ Regarding the peaks at 71.8 eV ($3d_{5/2}$) and 72.8 eV ($3d_{3/2}$), since there are no studies of XPS reported in the literature, the assignment to Br-Si-O is proposed, in coherence with the assignments made in the high resolution spectrum Si 2p.

The N 1s high-resolution spectrum of **CAT-Si** (**Figure 3.15 B**) was deconvoluted into two bands. The band at 400.3 eV is attributed to the central porphyrin nitrogen bonds, in accordance with reported works.^{35–38} The peak at 402.4 eV is attributed to the nitrogen bonds of the pyridine moieties, in accordance with that described for protonated nitrogen atoms in pyridines.^{38–40} This also indicates that the manganese(III) porphyrin is covalently bonded to the silica support through the nitrogen atom of the pyridine moiety.

The Cl 2p high-resolution spectrum of **CAT-Si** (**Figure 3.15 B**) presents the doublet band at 200.9 eV and 202.5 eV attributed to the C–Cl bonds of the metalloporphyrin.

The high-resolution spectra in the relevant regions of MR, **CAT-MR**, **CAT-MR-MW** and **CAT-4Py-MR** are presented in **Figure 3.16**.

The C 1s high-resolution spectra of the starting MR (**Figure 3.16 A**) and of the Merrifield-supported materials (**Figure 3.16 B**, illustrated for the case of **CAT-MR**) were fitted with five components. The peak centred at 284.9–285.0 eV corresponds to sp^2 carbons (aromatic bonds) and the π system of the metalloporphyrin, while the peak at 285.6–285.7 eV is due to sp^3 carbons. The peak at 286.7–286.8 eV is attributed to C–Cl bonds of Merrifield overlaid with C–N and C–Cl bonds of the metalloporphyrin and the peak at 283.2–283.4 eV may be ascribed to a contamination already present in the starting

material. The band at 291.5-291.8 eV (≈ 6.8 eV above the main C 1s peak) corresponds to a shake-up satellite of π - π^* transitions of the aromatic rings.⁴¹

The Cl 2p high-resolution spectrum of MR (**Figure 3.16 A**) was deconvoluted into two components with the corresponding doublet bands. The main peaks at 200.4 eV ($2p_{3/2}$) and 202.0 eV ($2p_{1/2}$) are due to C-Cl bonds and the peaks at 198.7 eV ($2p_{3/2}$) and 200.3 eV ($2p_{1/2}$) correspond to Cl^- ions. The high-resolution spectra of the Merrifield supported materials (**Figure 3.16 B**) have an additional component attributed to C-Cl bonds of the metalloporphyrin at ≈ 201.4 eV ($2p_{3/2}$) and ≈ 203.0 eV ($2p_{1/2}$).

The N 1s high-resolution spectra of the Merrifield immobilized materials (**Figure 3.16 B and C**, for **CAT-MR** and **CAT-MR-MW**, respectively) present a band at 400.2-400.6 eV attributed to the central porphyrin nitrogen bonds. In the case of **CAT-MR** and **CAT-4Py-MR** it was not possible to identify the band at about 402 eV that was present in the **CAT-Si** material corresponding to protonated nitrogen atoms. As the signal is very low due to the low loading of metalloporphyrin, the noise is very high and, therefore, we cannot state that this band is not present and that the immobilization did not occur by covalent bonding. However, in the Merrifield supported materials we cannot discard the possibility of the immobilization to occur through π - π stacking interaction between the aromatic rings. In the case of **CAT-MR-MW** the presence of a band at 401.3 eV attributed to protonated nitrogen atoms may indicate covalent bonding.

The Mn 2p high-resolution spectra of the Merrifield supported materials also present a high noise due to the low loading of porphyrin. However, it was possible to identify a doublet with a band at about 642 eV ($2p_{3/2}$), in agreement with a Mn(III) porphyrin (**Figure 3.16 D**, displayed for **CAT-4Py-MR**).⁴²⁻⁴⁵

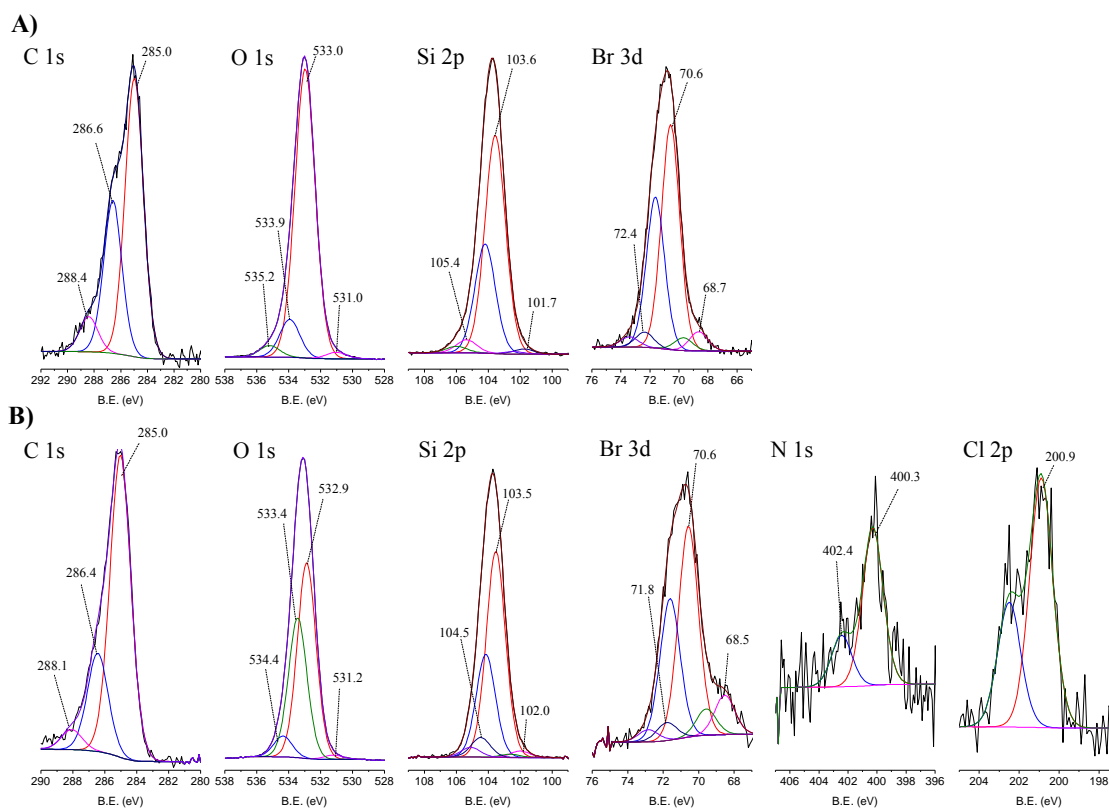


Figure 3.15. High-resolution XPS spectra in the C 1s, O 1s, Si 2p, Br 3d, N 1s and Cl 2p regions with the corresponding fits for **A)** 3-bromopropylsilica and **B)** CAT-Si.

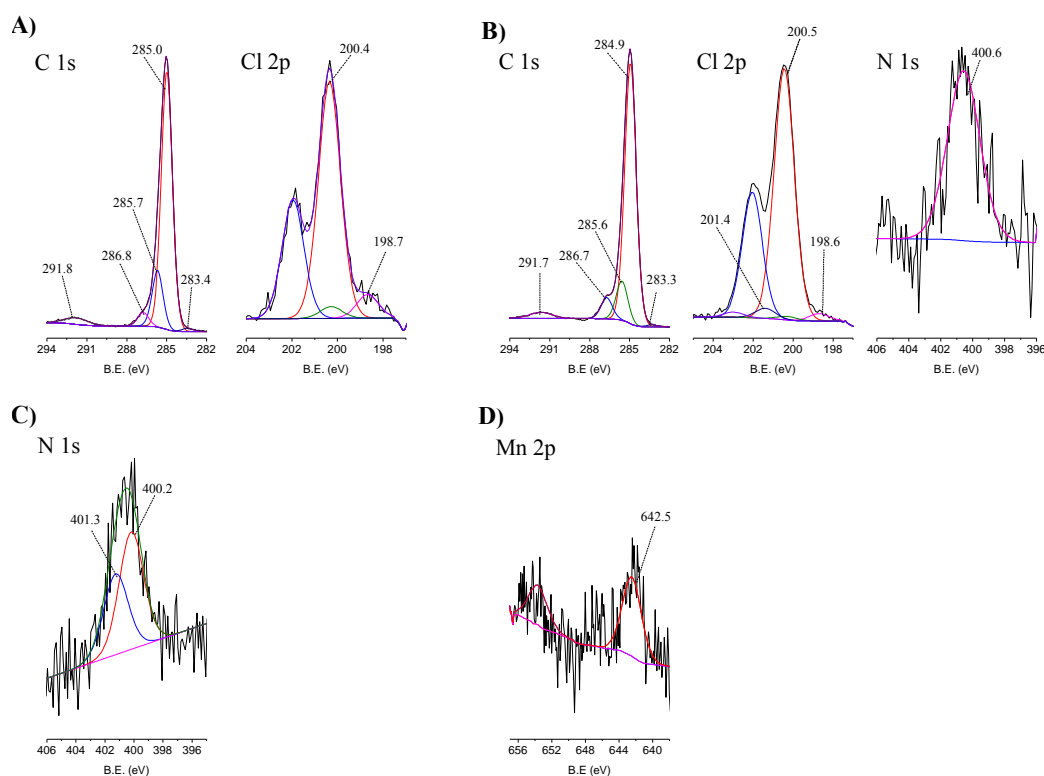


Figure 3.16. High-resolution XPS spectra in the relevant regions with the corresponding fits for A) MR, B) CAT-MR, C) CAT-MR-MW, D) CAT-4Py-MR.

3.1.3. Oxidation of cyclooctene under heterogeneous catalysis

3.1.3.1. Silica *versus* Merrifield Resin and the choice of the oxidant

The good catalytic performance of **Mn(mono-DCPyP)Cl** in the oxidation of cyclooctene under homogeneous conditions led us to evaluate the catalytic activity of the solid materials obtained by its immobilization on MR and functionalized silica, respectively **CAT-MR** and **CAT-Si**. To evaluate the catalytic activity of the new heterogeneous materials, the oxidation of cyclooctene was performed using H_2O_2 and *tert*-butyl hydroperoxide (TBHP) as oxidants, ammonium acetate as co-catalyst and acetonitrile as solvent. The results obtained are summarized in **Table 3.7**.

Both catalysts revealed to be effective in the epoxidation of cyclooctene. **CAT-MR** was less efficient when H_2O_2 was used as oxygen donor, notwithstanding how it was added. In the first cycle, after 24 h of reaction the conversion of cyclooctene was acceptable, being possible to reach 65.6% when the oxidant was diluted (1:5) in

acetonitrile and the additions were 0.5 eq every 15 min. On the other hand, 74.3% of conversion were registered when 30% (w/w) H₂O₂ was used directly with additions of 4 eq every 2 h (**Table 3.7**). However, a drastic drop in the conversion of cyclooctene was observed in the second cycle (**Figure 3.17**).

Better results were obtained using TBHP as oxidant with additions of 0.5 eq every 15 min, reaching 88.6% of conversion after 6 h, in the first catalytic cycle. Moreover, using this oxidant, the Merrifield-supported catalyst presented a high level of recyclability, with five cycles (**Figure 3.18**). In the fifth cycle, the reaction was slower, but was still possible to obtain a cyclooctene conversion of 41.5% after 6 h. The conversion of cyclooctene was negligible using **CAT-MR** without the addition of oxidant or in the presence of the starting **MR** using TBHP as oxidant, with additions of 0.5 eq every 15 min, thus revealing that the incorporation of the metalloporphyrin in the support and the presence of TBHP is essential for the oxidation reaction to occur.

Table 3.7. Results obtained for the oxidation of cyclooctene catalysed by **CAT-MR**, **CAT-4Py-MR** or **CAT-Si**.^(a)

Catalyst	Oxidant	Cycle	Oxidant (eq)	Time (h)	Conversion (%)
CAT-MR ^(b)	$\text{H}_2\text{O}_2^{(e)}$	1 st	14 (15)	7 (24)	58.9 (65.6)
		2 nd			10.8 (16.7)
	$\text{H}_2\text{O}_2^{(f)}$	1 st	12	6 (24)	46.6 (74.3)
		2 nd			10.9 (33.4)
	TBHP ^(g)	1 st	12	6	88.6
		2 nd			86.3
		3 rd			79.2
		4 th			69.4
		5 th			41.5
	Without	-	12	6	9.8
CAT-4Py-MR ^(c)	TBHP ^(g)	1 st	10	5	92.8
		2 nd			72.0
		3 rd			54.4
	Without	-	10	5	10.3
MR	TBHP ^(g)	-	12	6	6.3
CAT-Si ^(d)	$\text{H}_2\text{O}_2^{(e)}$	1 st	4.5	2.5	98.2
		2 nd			38.4
	TBHP ^(g)	1 st	8	4	93.5
		2 nd			37.8

^(a) 7.5×10^{-5} mol of cyclooctene, 7.5×10^{-5} mol of the internal standard (chlorobenzene), 5.0×10^{-7} mol of catalyst (S/C molar ratio of 150), the co-catalyst (≈ 15 mg of ammonium acetate) and CH_3CN (final volume of 0.5 mL). The reaction mixture was kept under stirring at $30 \text{ }^\circ\text{C} \pm 1$ and protected from light.

^(b) Obtained by classic heating (loading of $7.2 \text{ } \mu\text{mol/g}$ determined by elemental analysis).

^(c) Obtained by MW heating (loading of $7.3 \text{ } \mu\text{mol/g}$).

^(d) Obtained by classic heating (loading of $17.8 \text{ } \mu\text{mol/g}$).

^(e) H_2O_2 (30% w/w aqueous solution) diluted 1:5 in acetonitrile with additions of 0.5 eq every 15 min.

^(f) H_2O_2 (30% w/w aqueous solution) with additions of 4 eq every 2 h.

^(g) TBHP (5.0-6.0 M in decane) with additions of 0.5 eq every 15 min.

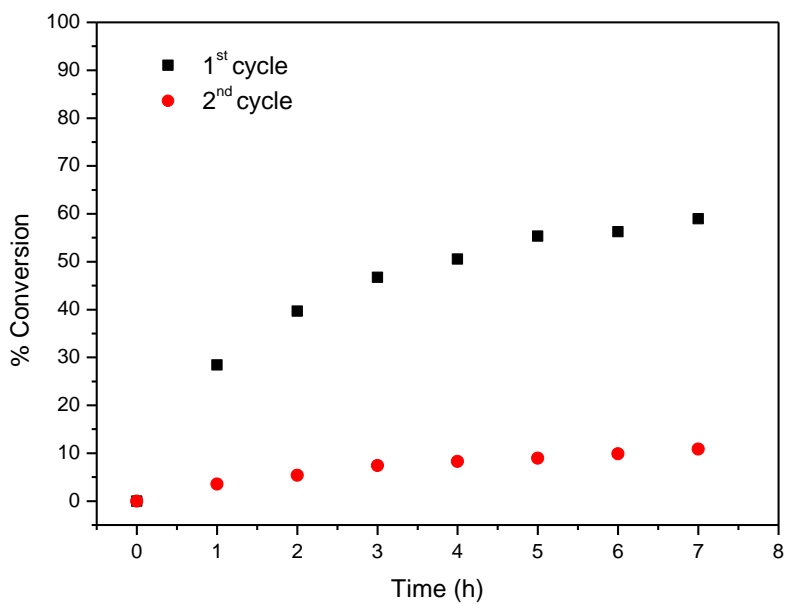


Figure 3.17. Oxidation of cyclooctene using **CAT-MR** as catalyst and diluted (1:5) H_2O_2 as oxidant with additions of 0.5 eq every 15 min.

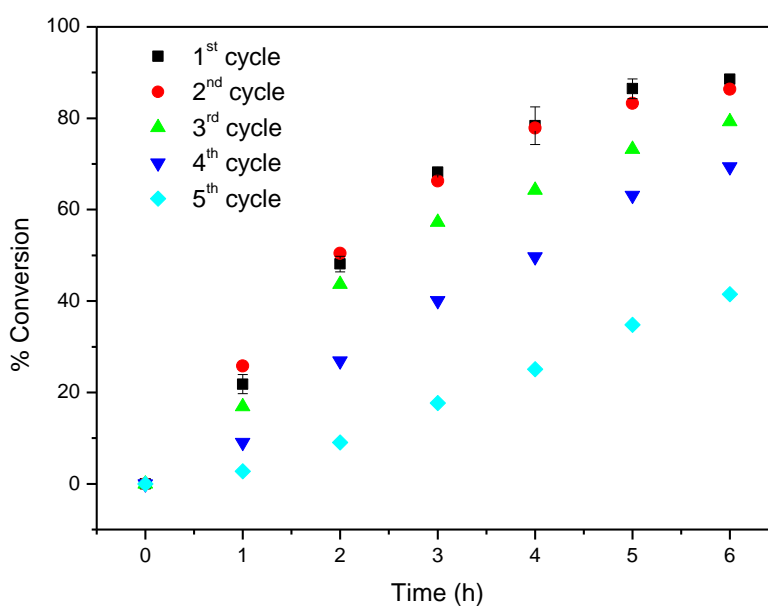


Figure 3.18. Oxidation of cyclooctene using **CAT-MR** as catalyst and TBHP as oxidant with additions of 0.5 eq every 15 min.

In the first cycle **CAT-Si** was highly efficient in the epoxidation of cyclooctene leading to excellent substrate conversion using both H_2O_2 and TBHP (**Figures 3.19** and **3.20**). Using H_2O_2 as oxidant (0.5 eq every 15 min), 98.2% of substrate conversion was obtained after only 2.5 h and using TBHP a conversion of 93.5% was achieved after 4 h. However, in the second cycle a drastic drop in substrate conversion was obtained in both cases (38.4%, after 5 h for H_2O_2 and 37.8%, after 6 h for TBHP).

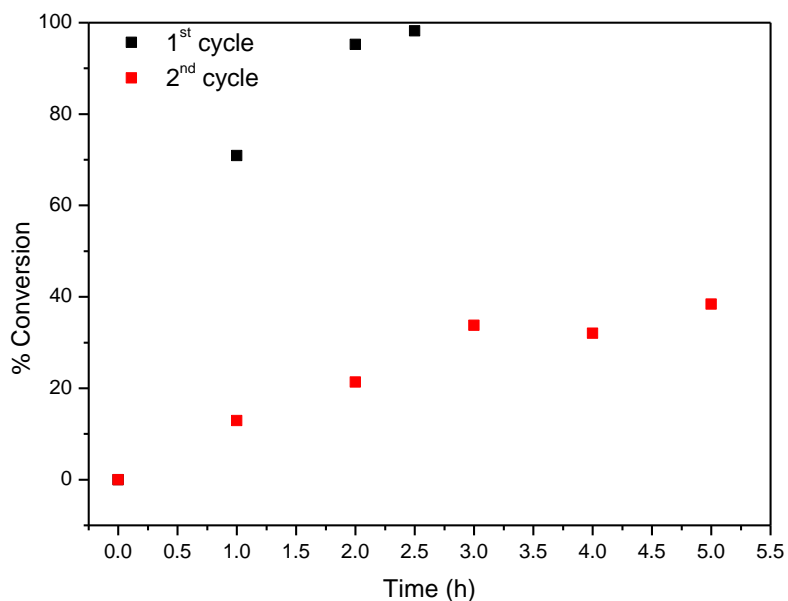


Figure 3.19. Oxidation of cyclooctene using **CAT-Si** as catalyst and diluted (1:5) H_2O_2 as oxidant with additions of 0.5 eq every 15 min.

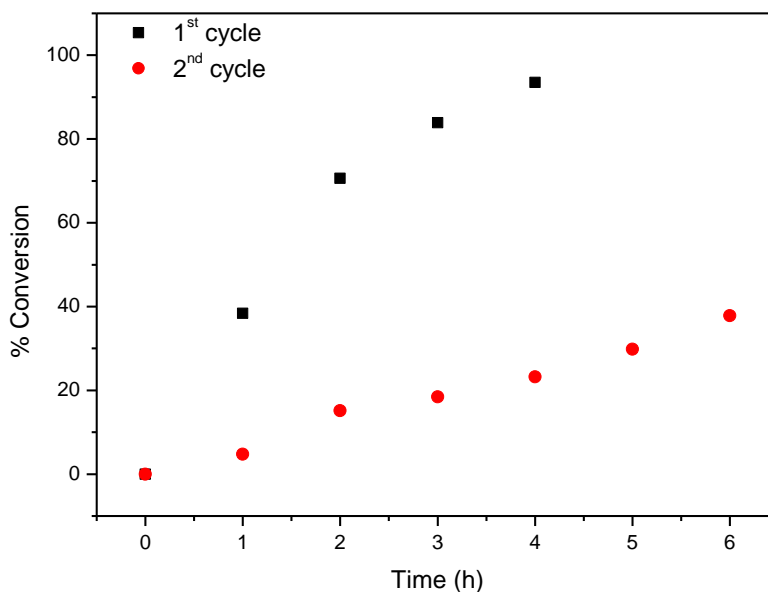


Figure 3.20. Oxidation of cyclooctene using **CAT-Si** as catalyst and TBHP as oxidant with additions of 0.5 eq every 15 min.

The morphology of the solid materials after oxidation reactions were examined by SEM technique (**Figures 3.21-3.24**) and the elemental composition of the solids was determined by XPS and is summarized in **Table 3.8**.

In the case of **CAT-MR**, after oxidation, using both H_2O_2 (**CAT-MR-H₂O₂**) and TBHP (**CAT-MR-TBHP**), the SEM images reveal a greater fragmentation in relation to the **CAT-MR** material before oxidation and the formation of deposits in the surface of the material (**Figure 3.21 a**, **Figure 3.22 a** and see **Figure 3.12 b**). In the case of **CAT-Si** after oxidation (**CAT-Si-H₂O₂** and **CAT-Si-TBHP**), the fragmentation is less evident when compared to the material before oxidation (**Figure 3.23 a**, **Figure 3.24 a** and see **Figure 3.13 c**).

The higher magnification images reveal that the **CAT-MR** surface is more polished after oxidation (**Figure 3.21 b-d** and **Figure 3.22 b-d**) which may be due to a possible oxidation of surface structures. This surface change is much more evident in **CAT-MR-H₂O₂**, however, the detection of manganese and chlorine by XPS in **CAT-MR-H₂O₂** in the same amount as in **CAT-MR** before oxidation reactions (**Table 3.8**) indicates that the metalloporphyrin is still present in the sample and therefore, the inefficiency of **CAT-MR** in the second catalytic cycle may also be due to metalloporphyrin bleaching. In the case of

CAT-MR-TBHP, it was not possible to detect manganese and there is a decrease in the atomic percentage of Cl 2p and C 1s. In contrast, in this sample a considerable increase of the N 1s is observed. This result is probably due to a deposition of ammonium acetate which is used as co-catalyst in the oxidation reactions and may have not been efficiently removed. In fact, in the fifth catalytic cycle using TBHP as oxidant, **CAT-MR** has a lower efficiency, probably as a result of the leaching of the catalyst from the support.

In the higher magnification SEM images of **CAT-Si-H₂O₂** and **CAT-Si-TBHP** the changes in the surface of the solid materials are less pronounced (**Figure 3.23 b-d** and **Figure 3.24 b-d**). On the other hand, the XPS analysis of **CAT-Si-H₂O₂** (**Table 3.8**), shows the presence of manganese and a decrease in the atomic percentage of C 1s, N 1s and Cl 2p, which indicates that the manganese porphyrin may be present in the support but in a catalytically inactive form due to bleaching. In the case of **CAT-Si-TBHP**, the absence of manganese and the decrease in the atomic percentage of C 1s and Cl 2p shows a leaching of the catalyst, which justifies the loss of efficiency in the second catalytic cycle. In this case N 1s is also increased, possibly due to deposition of ammonium acetate.

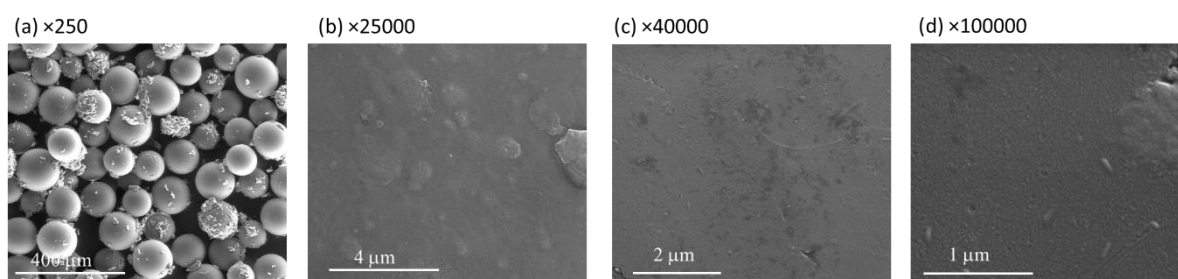


Figure 3.21. SEM micrographs of **CAT-MR-H₂O₂** after 2 cycles oxidation reaction using H₂O₂ as oxidant.

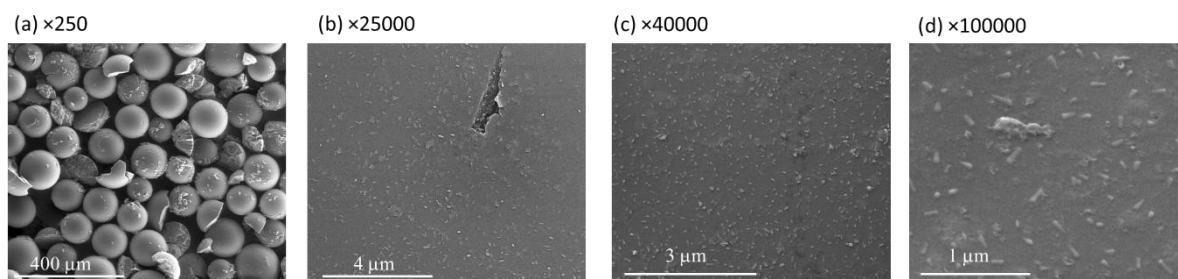


Figure 3.22. SEM micrographs of **CAT-MR-TBHP**, after 5 cycles oxidation reaction using TBHP as oxidant.

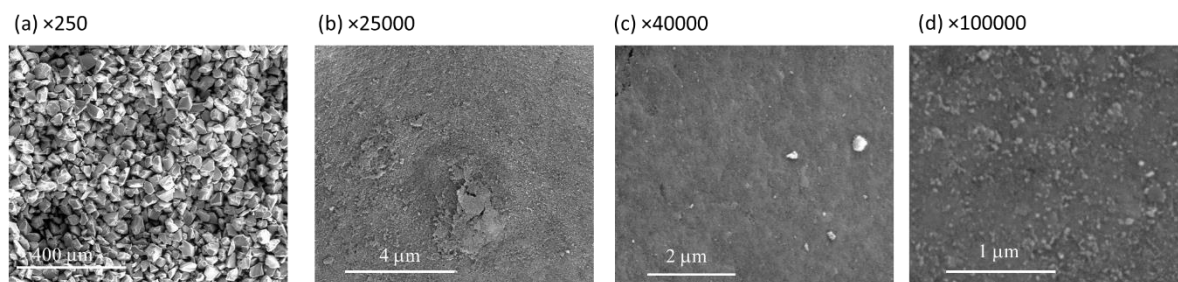


Figure 3.23. SEM micrographs of **CAT-Si-H₂O₂**, after 2 cycles oxidation reaction using H₂O₂ as oxidant.

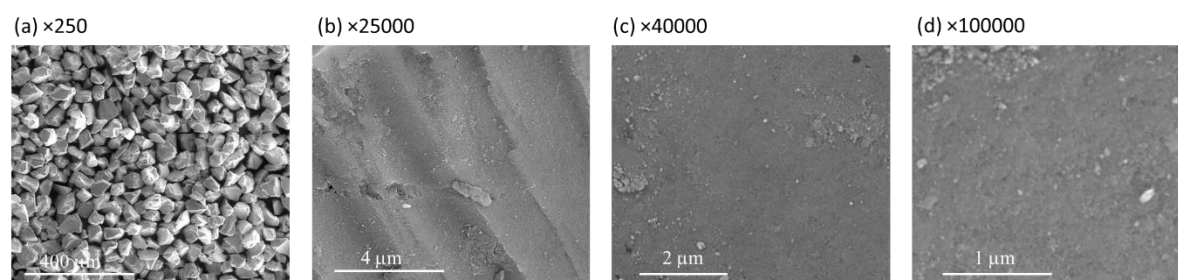


Figure 3.24. SEM micrographs of **CAT-Si-TBHP**, after 2 cycles oxidation reaction using TBHP as oxidant.

Table 3.8. Comparison of the surface atomic percentages obtained by XPS of **CAT-MR**, **CAT-Si** with the obtained materials after catalysis **CAT-MR-H₂O₂**, **CAT-MR-TBHP**, **CAT-Si-H₂O₂** and **CAT-Si-TBHP**.^(a)

Sample	Atomic (%)						
	C 1s	N 1s	O 1s	Si 2p	Cl 2p	Br 3d	Mn 2p
CAT-MR	88.9	0.7	7.0	-	3.3	-	0.06
CAT-MR-H₂O₂	91.7	0.5	4.5	-	3.2	-	0.05
CAT-MR-TBHP	81.0	3.7	14.5	-	0.9	-	n.d.
CAT-Si	17.0	0.5	56.4	25.0	0.4	0.7	n.d.
CAT-Si-H₂O₂	16.6	0.4	56.7	24.7	0.1	1.4	0.07
CAT-Si-TBHP	16.7	0.8	58.2	22.9	0.2	1.1	n.d.

^(a) Determined by the areas of the respective bands in high resolution XPS.
n.d. - Not Detected

3.1.3.2. Comparison of CAT-MR and CAT-4Py-MR catalytic activity

The results obtained in the oxidation of cyclooctene under homogeneous catalysis indicate that **Mn(mono-DCPyP)Cl** exhibits higher catalytic activity relatively to **Mn(mono-DC-4PyP)Cl**. However, after its immobilization onto the MR, the porphyrin core may be more protected from the common deactivation/destruction due to the presence of the oxidant. So, the catalytic activity of **CAT-4Py-MR** was evaluated in the oxidation of cyclooctene using TBHP as oxidant, under the same conditions previously used for **CAT-MR** (Table 3.7 and Figure 3.25). In the first cycle 92.8% of cyclooctene conversion was obtained after 5 h of reaction, with cyclooctene oxide being the only product formed. This result was surprisingly better than that obtained using **CAT-MR** as catalyst (88.6% of conversion after 6 h). However, in the second and third catalytic cycles a catalytic activity decrease was observed, with cyclooctene conversion of 72.0% and 54.4%, respectively, after 5 h of reaction (Table 3.7 and Figure 3.25). In the case of **CAT-MR** its catalytic efficiency is maintained in the second cycle and in the third and fourth cycles the conversion of cyclooctene is still higher than 60% (Table 3.7 and Figure 3.18). The absence of the chlorine atoms at the *ortho* positions of the pyridyl moiety in **CAT-4Py-MR** may facilitate the access of the co-catalyst, oxidant and substrate to the metal, which may justify the better result in the first catalytic cycle. On the other hand, the porphyrin nucleus is also more exposed to the oxidant, which may justify the decrease of the catalytic activity in the following catalytic cycles.

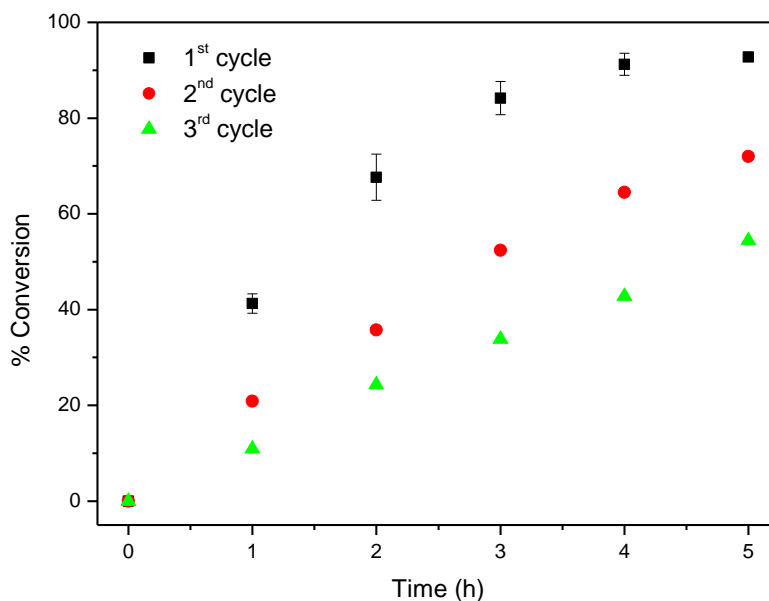


Figure 3.25. Oxidation of cyclooctene using **CAT-4Py-MR** as catalyst and TBHP as oxidant with additions of 0.5 eq every 15 min.

After 5 h, with additions of 0.5 eq of oxidant every 15 min, we have 10 eq of oxidant relatively to the substrate, which is a large excess of oxidant in the reaction medium that may degrade/deactivate the manganese(III) porphyrin, thereby prejudicing its activity. Thus, the mode of addition of TBHP was studied using **CAT-4Py-MR** as catalyst and cyclooctene as substrate, in order to try to use less oxidant (**Table 3.9** and **Figure 3.26**). When TBHP was added in the amount of 0.5 eq per hour, the oxidation of cyclooctene was slower, requiring a further two hours to achieve a conversion close to that obtained with additions of 0.5 eq of TBHP every 15 min. In the same way, when 1 eq per hour was used, the oxidation of cyclooctene, though slightly faster, still required an additional hour to achieve a conversion equal to that obtained with 0.5 eq every 15 min. When 4 eq of TBHP were added at once at the beginning, the reaction was faster at an initial stage, reaching 46.6% conversion after 1 h, while when 0.5 eq of the oxidant were added every 15 min, for the same reaction time a conversion of 39.8% was obtained after 1 h. However, as the oxidant is consumed, the reaction becomes slower and after 5 h a conversion of 78.9% has been achieved. The reaction is not expected to progress significantly as the oxidant becomes less and less available. It is noteworthy that when 0.5 eq of TBHP were added each hour, after 5 h of reaction, which corresponds to 2.5 eq of oxidant added, we had

already achieved 79.2% of cyclooctene conversion. Furthermore, after 7 h it was also possible to achieve a conversion of cyclooctene close to that obtained using 0.5 eq every 15 min but using less amount of oxidant.

To verify if the addition of less oxidant resulted in a better efficiency, the catalyst from the reaction using 0.5 eq of TBHP per hour was recovered and reused under the same conditions. We expected that using less oxidant would result in lower porphyrin degradation leading to a catalytic performance very close to that obtained in the first cycle and, therefore, more cycles could be done. However, the results indicate that there is no advantage for catalyst recycling when using less oxidant (**Figure 3.27**). In the second catalytic cycle, using 0.5 eq of TBHP each hour, after 7 h of reaction (3.5 eq of TBHP added in each cycle), loss of catalytic activity is observed and conversion of cyclooctene very close to that reached after 5 h using 0.5 eq every 15 min (10 eq of TBHP added in each cycle) was obtained. This shows that not only the amount of oxidant added is important for catalyst activity, but also the time of contact between the porphyrin and the oxidant has a determining role.

Table 3.9. Effect of the oxidant mode of addition in the oxidation of cyclooctene using **CAT-4Py-MR** as catalyst.^(a)

Entry	Oxidant mode of addition	TBHP (eq)	Time (h)	Conversion (%)
1	0.5 eq/15 min	10	5	92.8
2	0.5 eq/h	3.5	7	89.4
3	1 eq/h	6	6	91.2
4	4 eq at the beginning	4	5	78.9

^(a) Conditions: 7.5×10^{-5} mol of cyclooctene, 7.5×10^{-5} mol of the internal standard (chlorobenzene), 5.0×10^{-7} mol of **CAT-4Py-MR** (for a S/C molar ratio of 150), the co-catalyst (≈ 15 mg of ammonium acetate) and acetonitrile until attaining a final volume of 0.5 mL. The reaction mixture was kept under stirring at 30 ± 1 °C and protected from light.

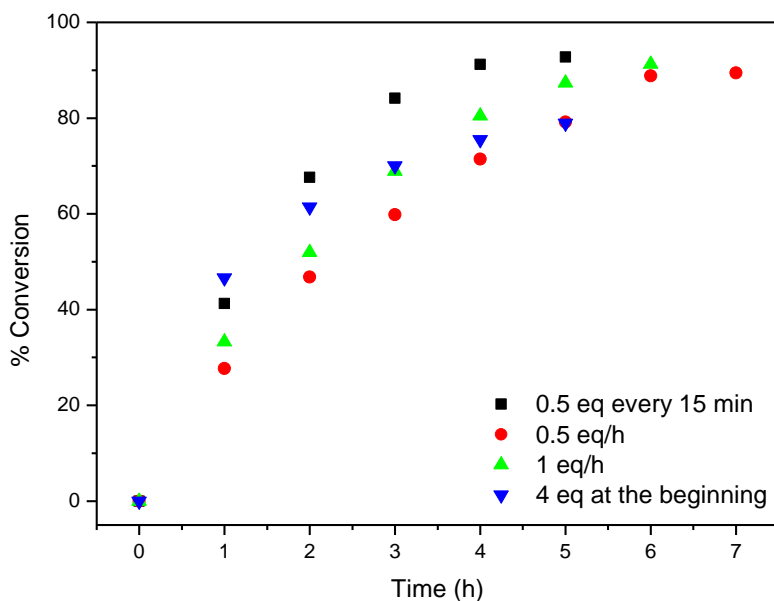


Figure 3.26. Effect of TBHP mode of addition on cyclooctene oxidation using **CAT-4Py-MR** as catalyst.

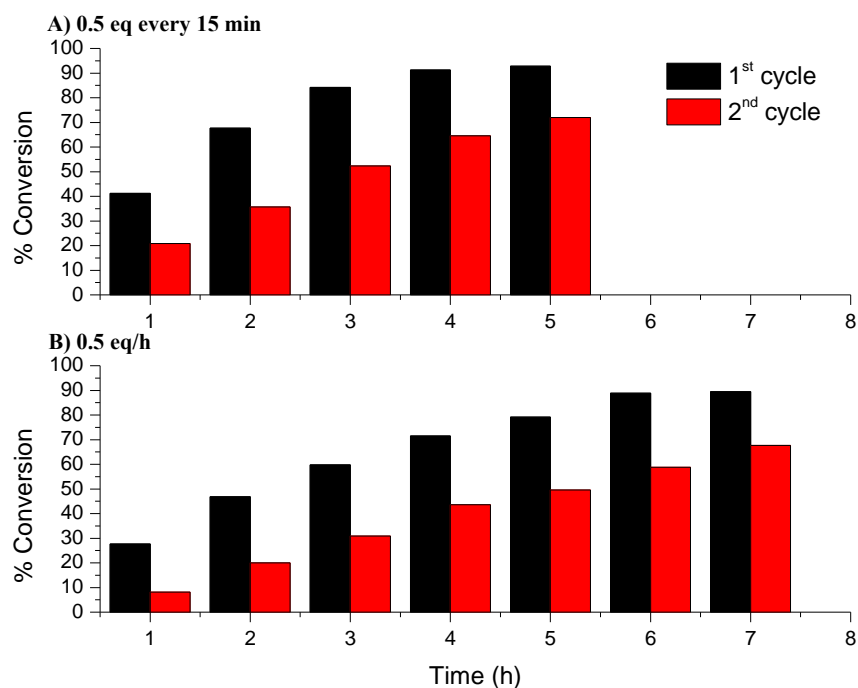


Figure 3.27. Influence of the mode of addition of TBHP on the efficiency of **CAT-4Py-MR** recycling. **A)** Additions of 0.5 eq of TBHP every 15 min and **B)** additions of 0.5 eq of TBHP every hour.

In order to investigate whether there is manganese(III) porphyrin leaching from the support throughout the oxidation reactions, leaching tests were carried out for **CAT-MR** and **CAT-4Py-MR** using cyclooctene as substrate with additions of 0.5 eq of TBHP every 15 min. After 1 h of reaction (\approx 20% of cyclooctene conversion using **CAT-MR** and \approx 41% of cyclooctene conversion using **CAT-4Py-MR**) the catalyst was filtered, and the supernatant was allowed to react, ongoing the addition of oxidant for a further 5 h. During this time, for both catalysts, the conversion of cyclooctene was negligible and no increase in the product or formation of other products was observed.

3.1.4. Oxidation of styrene

Styrene is a substrate commonly used to test catalysts' activity in oxidation reactions.^{46–49} Since styrene is a terminal olefin, different products can be found depending on the reaction conditions and the catalyst used (**Scheme 3.6**).

The mechanism of formation of phenylacetaldehyde is a subject of great discussion (**Scheme 3.7**). Many studies have shown that phenylacetaldehyde is not formed by isomerization of styrene epoxide.^{16,46,50–52} Other authors, on the contrary, state that phenylacetaldehyde should result from the isomerization of the resulting styrene epoxide.⁵³ The hypervalent manganese(V)-oxo porphyrin species (**1**) has been suggested as the oxidant species in these catalytic processes.^{21,25,54,55} Arasasingham *et al.* proposed a charge-transfer complex (**2**) as the rate-determining step for the oxygen atom transfer from oxometalloporphyrins to alkenes.⁵⁴ Studies with iron and manganese porphyrins support the hypothesis of the involvement of cationic or radical species such as (**4**) and (**5**) in the production of phenylacetaldehyde.^{46,50,51,56–58} Collman *et al.* proposed the involvement of two regioisomeric metallaoxetanes (**7**) and (**8**) resulting from the addition of styrene to the manganese-oxo porphyrin complex as possible intermediates in the competitive formation of phenylacetaldehyde or styrene epoxide.⁵² According to these authors, phenylacetaldehyde should result from metallaoxetane (**7**) by a rearrangement involving the migration of H, formation of the carbon-oxygen double bond, and cleavage of the metal-carbon bond. On the other hand, steric hindrance would greatly destabilize metallaoxetane (**7**) resulting in a drastic decrease or absence of phenylacetaldehyde and a higher selectivity to the epoxide, which should result mainly from the intervention of the metallaoxetane (**8**).⁵² De Paula *et al.* also proposed a concerted reaction starting from an

3.1.4.1. Oxidation of styrene using Mn(mono-DCPyP)Cl or Mn(TDCPyP)Cl and hydrogen peroxide as oxidant under homogeneous conditions

The manganese(III) porphyrins containing 3,5-dichloropyridyl substituents at the *meso* positions were tested in the oxidation of styrene using a S/C molar ratio of 600, acetonitrile as solvent, ammonium acetate as co-catalyst and H₂O₂ as oxidant. For comparative purposes, the reactions were also carried out in the presence of the highly efficient second-generation catalyst **Mn(TDCPP)Cl**, using similar conditions. The results summarized in **Table 3.10** confirm the high efficiency of the newly prepared catalysts in terms of conversion and selectivity for the epoxide. In the presence of **Mn(mono-DCPyP)Cl** an excellent conversion of 99.0% after 105 min of reaction was obtained, with 65.6% selectivity for the epoxide. With **Mn(TDCPyP)Cl** the high selectivity for the epoxide was maintained (67.6%), accompanied by excellent styrene conversion (97.6%) after 150 min of reaction. In the presence of **Mn(TDCPP)Cl**, the total conversion of styrene after 75 min of reaction gave rise to a slight lower selectivity for the epoxide (62.7%). In all these reactions the formation of styrene epoxide was accompanied by a significant amount of phenylacetaldehyde (30.3-36.7%) and traces of benzaldehyde (0.6-2.1%) (**Table 3.10**).

Table 3.10. Results obtained for the oxidation of styrene with H₂O₂ using CH₃CN as solvent and ammonium acetate as co-catalyst^(a)

Catalyst	Time (min)	H ₂ O ₂ (eq)	Conversion (%)	Selectivity (%)		
				Benzaldehyde	Phenylacetaldehyde	Styrene epoxide
Mn(TDCPyP)Cl	150	5	97.6	2.1	30.3	67.6
Mn(mono-DCPyP)Cl	105	3.5	99.0	1.7	32.7	65.6
Mn(TDCPP)Cl	75	2.5	100	0.6	36.7	62.7
No catalyst	150	5	—	—	—	—

^(a) 7.5×10^{-5} mol of styrene; 1.25×10^{-7} mol of the catalyst (S/C molar ratio of 600). The co-catalyst: 0.2 mmol (\approx 15 mg) of ammonium acetate. The final volume of 2 mL was completed with CH₃CN and the reaction mixture was kept protected from light, under stirring at 30 ± 1 °C. The oxidant used was aqueous H₂O₂ (30% w/w) diluted 1:5 in CH₃CN and was added at regular intervals of 15 min, each oxidant addition corresponding to half of the initial amount of the substrate (3.75×10^{-5} mol).

3.1.4.2. Oxidation of styrene catalysed by CAT-MR using TBHP as oxidant

Since **Mn(mono-DCPyP)Cl** showed to be efficient in the oxidation of styrene in the presence of H_2O_2 under homogeneous conditions, and given the good oxidation results for cyclooctene in the presence of **CAT-MR** as catalyst and TBHP as oxidant, it was decided to study this catalytic system in the oxidation of styrene. Therefore, the reactions were carried out using 5×10^{-7} mol of **CAT-MR** (S/C molar ratio of 150) with additions of 0.5 eq of TBHP at regular intervals of 15 min, ammonium acetate as co-catalyst and acetonitrile as solvent. After 6 h of reaction, 96.2% of conversion was observed, styrene epoxide being the main product (81.3%) along with benzaldehyde formation (18.7%), whereas no phenylacetaldehyde was detected (**Figure 3.28**).

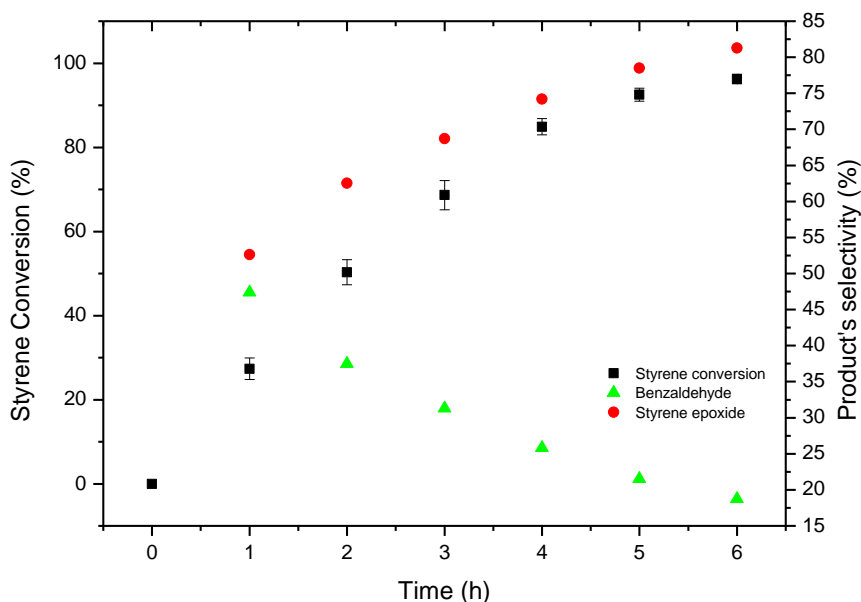


Figure 3.28. Oxidation of styrene catalysed by **CAT-MR** using TBHP as oxidant with additions of 0.5 eq every 15 min.

The absence of phenylacetaldehyde may be related with the steric hindrance provided by the support, which disfavours the formation of the intermediate leading to phenylacetaldehyde. There is also a considerable increase of benzaldehyde (18.7%) relatively to that observed using the homogeneous catalyst [**Mn(mono-DCPyP)Cl**] and H_2O_2 (after 105 min, 1.7% of benzaldehyde, for a conversion of 99%, please see **Table**

3.10). It should be noted that this product may be formed *via* a radical mechanism and therefore a greater amount of benzaldehyde will be obtained for longer reaction times.

3.2. Conclusions

The symmetric chloro[5,10,15,20-tetrakis(3,5-dichloropyridin-4-yl)porphyrinate]manganese(III) [**Mn(TDCPyP)Cl**] and the asymmetric chloro[5,10,15-tris(2,6-dichlorophenyl)-20-(3,5-dichloropyridin-4-yl)porphyrinate]manganese(III) [**Mn(mono-DCPyP)Cl**] were tested as catalysts in the oxidation of cyclooctene, using aqueous hydrogen peroxide as oxidant. In the oxidation of cyclooctene, using acetonitrile as solvent and ammonium acetate as co-catalyst for a substrate/catalyst (S/C) molar ratio of 600, in the presence of **Mn(TDCPyP)Cl**, 97.6% of conversion was obtained after 120 min whereas using the **Mn(mono-DCPyP)Cl** 98.2% of conversion was attained after 75 min. The catalytic activity of **Mn(mono-DCPyP)Cl** is very similar to that obtained with the well-known second-generation catalyst **Mn(TDCPP)Cl**. On the other hand, **Mn(mono-DCPyP)Cl** showed to be more efficient than its analogue **Mn(DC-mono-4PyP)Cl**. **Mn(TDCPyP)Cl** and **Mn(mono-DCPyP)Cl** also exhibited high stability during the oxidation reactions. The presence of electron-withdrawing chlorine atoms in the substituents at the *meso* positions of the metalloporphyrins are responsible for preventing the macrocycle oxidation resulting in higher stability of the catalyst.

Mn(TDCPyP)Cl was also tested as catalyst in the oxidation of cyclooctene in the presence of different co-catalysts using a mixture of acetonitrile/water. Under these conditions, ammonium benzoate showed to be the best co-catalyst with total conversion of cyclooctene to the corresponding epoxide in 120 min.

Mn(mono-DCPyP)Cl was successfully immobilized on MR and 3-bromopropylsilica supports as evidenced by the various characterization techniques presented and discussed. **Mn(mono-DCPyP)Cl** and **Mn(DC-mono-4PyP)Cl** were also immobilized on MR using MW heating. MW heating was more advantageous than conventional heating, resulting in a considerable reduction of the reaction time from 96 h to 30 min only. In addition, when the single-mode MW equipment was used, the loading of porphyrin increased significantly.

CAT-MR and **CAT-Si** showed to be efficient catalysts in the epoxidation of cyclooctene. The best results were obtained with the Merrifield-supported catalyst,

CAT-MR, using TBHP as oxidant with additions of 0.5 eq every 15 min, allowing five catalytic cycles. **CAT-Si** exhibited high catalytic activity using both H₂O₂ and TBHP as oxidant in the first catalytic cycle, however in the second cycle its activity strongly decreased. The SEM and XPS analysis of the solid materials after oxidation shows leaching and bleaching of the manganese porphyrin, which justifies the less efficiency observed in the last catalytic cycles.

CAT-4Py-MR was also highly efficient in the oxidation of cyclooctene, although presenting less robustness when compared to **CAT-MR**, allowing only three catalytic cycles. The higher recycling capacity of **CAT-MR** is probably due to the presence of the two extra chlorine atoms in the pyridyl substituent affording higher protection to the porphyrin nucleus relatively to the oxidizing reaction medium. Using **CAT-4Py-MR** and adding less oxidant, a similar cyclooctene conversion was reached, however the reaction was slower and no improvement in catalyst recycling was observed.

In the oxidation of styrene, for a S/C molar ratio of 600, high conversion was obtained using both **Mn(TDCPyP)Cl** (97.6% after 150 min) and **Mn(mono-DCPyP)Cl** (99.0% after 105 min) under homogeneous conditions with H₂O₂ as oxidant. High selectivity to the corresponding epoxide (67.6% and 65.6%, respectively) was obtained, similarly to the oxidation in the presence of **Mn(TDCPP)Cl**. Beyond the formation of styrene epoxide, phenylacetaldehyde (30.3-36.7%) and traces of benzaldehyde (0.6-2.1%) were also obtained. A different situation was observed using the solid **CAT-MR** as catalyst and TBHP as oxidant, since no phenylacetaldehyde was formed, thus resulting in higher selectivity to styrene epoxide (81.3%) along with the formation of benzaldehyde (18.7%). The absence of phenylacetaldehyde may be related with difficulties in the formation of the intermediate responsible for its production due to steric hindrance caused by the solid support.

3.3. Experimental

3.3.1. Reagents and Methods

The Merrifield resin (MR, 100-200 mesh, 3.5-4.5 mmol Cl/g, 1% cross-linked) and the 3-bromopropylsilica (200-400 mesh, extent of labelling: 1.5 mmol/g loading) were purchased from Sigma-Aldrich.

The DMF used as solvent in the immobilization of **Mn(mono-DCPyP)Cl** was dried over molecular sieves previously activated in the muffle furnace at 350 °C for 4 h.

Ammonium acetate, ammonium formate and ammonium benzoate were acquired from Sigma-Aldrich. Aqueous hydrogen peroxide (30% w/w) was purchased from Riedel-de-Haën whilst *tert*-butyl hydroperoxide (TBHP) (5.0-6.0 M in decane), cyclooctene and styrene were obtained from Aldrich. Chlorobenzene was obtained from Carlo Erba and used as internal standard for the GC analyses.

Two different equipment were used for the immobilizations using MW heating. For the first reactions a Milestone MW device was used, which operates at fixed frequency (2450 MHz) in multimode (run up to 12 flasks simultaneously). The last reactions were carried out in a CEM Discover SP, a single-mode MW apparatus.

Diffuse reflectance spectra were registered on a Jasco V-560 spectrophotometer, using MgO as reference. Attenuated total reflectance (ATR) FT-IR spectra were measured on a Bruker optics Tensor 27 equipped with a Specac Golden Gate Mk II ATR accessory having a diamond top plate and KRS-5 focusing lenses (resolution 4 cm⁻¹, 256 scans). Routine Powder X-ray Diffraction (PXRD) data for all the prepared materials were collected at ambient temperature on a Empyrean PANalytical diffractometer (Cu K_{α1,2} X-radiation, λ₁ = 1.540598 Å; λ₂ = 1.544426 Å), equipped with an PIXcel 1D detector and a flat-plate sample holder in a Bragg-Brentano para-focusing optics configuration (45 kV, 40 mA). Intensity data were collected by the step-counting method (step 0.03°), in continuous mode, in the ca. 5° ≤ 2θ ≤ 60° range.

The SEM/EDS analyses were performed using a High-resolution (Schottky) Environmental Scanning Electron Microscope with X-Ray Microanalysis and Electron Backscattered Diffraction analysis: Quanta 400 FEG ESEM / EDAX Genesis X4M.

Samples were coated with an Au/Pd thin film, by sputtering, using the SPI Module Sputter Coater equipment.

X-ray photoelectron spectroscopy (XPS) was performed at “Centro de Materiais da Universidade do Porto” (CEMUP, Porto, Portugal) in a VG Scientific ESCALAB 200A spectrometer using non-monochromatized Al K α radiation (1486.6 eV). The powdered samples were pressed into pellets prior to the XPS studies. Binding energies were calibrated relative to the base C 1s peak at 285.0 eV. The raw XPS spectra were deconvoluted by curve fitting peak components using the software CASAXPS (version 2.3.12) with no preliminary smoothing. Symmetric GaussianLorentzian product functions were used to approximate the line shapes of the fitting components after a Shirley-type background subtraction. Atomic ratios were calculated from experimental intensity ratios and normalized by atomic sensitivity factors.

3.3.2. Synthesis of the heterogeneous catalysts

Classic heating

In a Schlenk flask 5 mg of **Mn(mono-DCPyP)Cl** were dissolved in 4 mL of 1,2-dichlorobenzene and, after total dissolution, 250 mg of MR or 3-bromopropylsilica were added. Using a sand bath and a magnetic stirrer, the mixture was stirred at 190 °C, being kept under nitrogen atmosphere and protect from light for 96 h.

Microwave heating

In a MW reactor 5 mg of porphyrin [**Mn(mono-DCPyP)Cl** or **Mn(DC-mono-4PyP)Cl**] were dissolved in 4 mL of 1,2-dichlorobenzene and, after total dissolution, 250 mg of MR were added. The reactions were carried out under magnetic stirring for 30 min at 800 watt, without temperature control, but with the maximum temperature value set at 250 °C.

In both approaches, and after cooling, the material was filtered under vacuum, using a Hirsch funnel with a membrane filter 0.2 μ m NL16 (Schleicher & Schuell), washed several times with *ortho*-dichlorobenzene, CH₃CN and dichloromethane (previously passed through an aluminum oxide column) and dried overnight in the oven (55 °C). The loading of immobilized catalyst was determined by elemental analysis based on the nitrogen amount present in the sample.

3.3.3. Oxidation reactions

Homogeneous catalysis

In a glass reactor with a stopper, the catalyst (variable amounts according to the S/C molar ratio used: 5×10^{-7} mol in the case of the S/C molar ratio 150 and 1.25×10^{-7} mol in the case of the S/C molar ratio 600), acetonitrile (up to a 2 mL reaction mixture volume), the substrate (7.5×10^{-5} mol), the internal standard (7.5×10^{-5} mol of chlorobenzene), and the co-catalyst (0.2 mmol; 15 mg of ammonium acetate) were added in this order. In the case of **Mn(TDCPP)Cl**, **Mn(DC-mono-4PyP)Cl** and **Mn(mono-DCPyP)Cl** a catalyst stock solution in acetonitrile was previously prepared and kept in the fridge protected from light until use. Due to the low solubility of **Mn(TDCPyP)Cl** and **Mn(T-4PyP)Cl** in acetonitrile, the preparation of the stock solutions in this solvent was not possible. Therefore, for these latter catalysts was necessary to weigh the amount required for each assay directly to the glass reactor or to prepare the stock solution in a mixture of acetonitrile/water (1:1). For the first situation, after addition of the co-catalyst, the solution was maintained under stirring for 3 min before the first addition of oxidant to ensure a complete solubilization of the metalloporphyrins.

For the oxidation reactions in acetonitrile/water a stock solution of **Mn(TDCPyP)Cl** was prepared in a mixture of acetonitrile/water (1:1) and 5×10^{-7} mol (S/C ratio of 150) of catalyst were added to the reactor and the final volume of 2 mL completed with acetonitrile, thus the final mixture being about 10% of water. The work-up of these reactions was carried out as described for the reactions in acetonitrile and several co-catalysts were tested (0.2 mmol/15 mg of ammonium acetate; or 0.42 mmol/24 μ L of acetic acid; or 0.2 mmol/12.6 mg of ammonium formate; or 0.2 mmol/27.8 mg of ammonium benzoate). The reaction mixtures were kept under stirring at 30 ± 1 °C and protected from light. The oxidant used was 30% (w/w) aqueous hydrogen peroxide diluted 1:5 in acetonitrile, with additions of 0.5 eq at regular intervals of 15 min. Every 15 min, immediately before the addition of H₂O₂, 10 μ L of the reaction mixture were taken for analysis by GC-FID. The stability of the catalysts was checked by UV-Vis spectrophotometry.

Heterogeneous catalysis

In a glass reactor with a stopper, 7.5×10^{-5} mol of substrate, the internal standard (7.5×10^{-5} mol of chlorobenzene), the catalyst (5.0×10^{-7} mol for a S/C molar ratio of 150), the co-catalyst (0.2 mmol; 15 mg of ammonium acetate) and acetonitrile were added until a reaction mixture final volume of 0.5 mL. The reaction mixtures were kept under stirring at 30 ± 1 °C and protected from light. The reactions were monitored by GC-FID. At the end of the reaction the catalyst was recovered by centrifugation and carefully washed using acetonitrile and dichloromethane (previously passed through an aluminum oxide column). The recovered catalyst was dried overnight at 55 °C to further reuse. Since some material is lost between reactions, the recovered catalyst was weighted, and the amount of substrate was recalculated after each cycle, in order to perform the reactions under identical conditions. Leaching tests were carried out using cyclooctene as substrate and maintaining the same reaction conditions. After 1 h of reaction, the catalyst was filtered through a Hirsch funnel with a membrane filter 0.2 μm NL16 (Schleicher & Schuell). The filtrate was transferred to a glass reactor, protected from light, and left under stirring for further 5 h at 30 ± 1 °C, with additions of 0.5 eq of TBHP every 15 min. The evolution of the reaction was monitored by GC-FID.

Monitoring of the oxidation reactions

The reaction products were identified by GC-FID according to their retention times using the chromatographic conditions previously established in our laboratory.¹⁶ The GC-FID analyses were carried out on a Varian 3900 chromatograph using helium as the carrier gas (30 cm/s) equipped with a fused silica capillary DB-5 type column (30 m, 0.25 mm i.d., 0.25 μm film thickness). The GC-FID conditions for cyclooctene oxidation monitoring were as follows: column initial temperature 80 °C for 1 min; column increasing temperature rate of 20 °C/min until 220 °C, which was maintained for 2 min; the injector and detector temperatures were both set at 250 °C. The GC-FID conditions for styrene oxidation monitoring were as follows: column initial temperature 80 °C for 2 min; column increasing temperature rate of 20 °C/min until 220 °C, which was maintained for 3 min; the injector temperature was set at 250 °C and the detector temperature was set at 270 °C.

Conversion (%) for each time (t) was determined by calculation of reacted substrate using the internal standard method, based on the chromatographic peak areas of substrate ($A_{\text{substrate}}$) and of the internal standard ($A_{\text{chlorobenzene}}$) for each chromatogram:

$$\text{Conversion } \%_{(t=x)} = \frac{\left(\frac{A_{\text{substrate}}}{A_{\text{chlorobenzene}}}\right)_{t=0} - \left(\frac{A_{\text{substrate}}}{A_{\text{chlorobenzene}}}\right)_{t=x}}{\left(\frac{A_{\text{substrate}}}{A_{\text{chlorobenzene}}}\right)_{t=0}} \times 100$$

Product's selectivity (%) was calculated as follows:

$$\text{Selectivity } \%_{(\text{Product } A)} = \frac{A_{\text{Product } A}}{\sum A_{\text{Products}}} \times 100$$

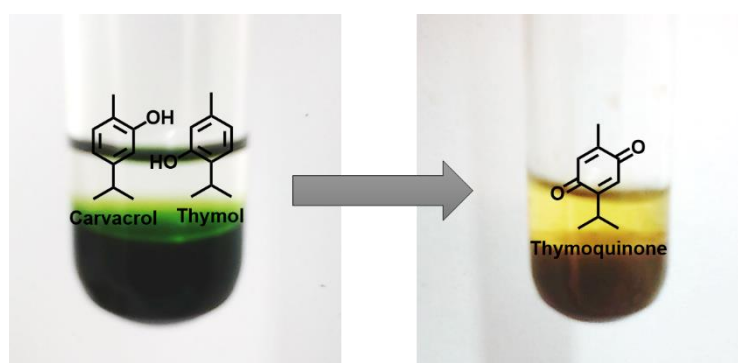
3.4. References

- 1 C. Freire, C. Pereira and S. Rebelo, in *Catalysis: Volume 24*, eds. J. J. Spivey and M. Gupta, Royal Society of Chemistry, Cambridge, 2012, pp. 116–203.
- 2 A. Scarso and G. Strukul, in *Handbook of Advanced Processes in Oxidation Catalysis: From Laboratory to Industry*, eds. D. Duprez and F. Cavani, Imperial College Press, London, 2014, pp. 679–766.
- 3 P. R. Cooke and J. R. L. Smith, *J. Chem. Soc. Perkin Trans. 1*, 1994, 1913–1923.
- 4 E. Brulé and Y. R. de Miguel, *Org. Biomol. Chem.*, 2006, **4**, 599–609.
- 5 M. J. F. Calvete, M. Silva, M. M. Pereira and H. D. Burrows, *RSC Adv.*, 2013, **3**, 22774–22789.
- 6 P. Zucca, C. M. B. Neves, M. M. Q. Simões, M. G. P. M. S. Neves, G. Cocco and E. Sanjust, *Molecules*, 2016, **21**, 1–40.
- 7 M. A. Martinez-Lorente, P. Battioni, W. Kleemiss, J. F. Bartoli and D. Mansuy, *J. Mol. Catal. A Chem.*, 1996, **113**, 343–353.
- 8 A. Thellend, P. Battioni and D. Mansuy, *J. Chem. Soc. Chem. Commun.*, 1994, **202**, 1035–1036.
- 9 M. M. Q. Simões, C. M. B. Neves, S. M. G. Pires, M. G. P. M. S. Neves and J. A. S. Cavaleiro, *Pure Appl. Chem.*, 2013, **85**, 1671–1681.
- 10 H. Nur, H. Hamid, S. Endud, H. Hamdan and Z. Ramli, *Mater. Chem. Phys.*, 2006, **96**, 337–342.
- 11 I. C. M. S. Santos, S. L. H. Rebelo, M. S. S. Balula, R. R. L. Martins, M. M. M. S. Pereira, M. M. Q. Simões, M. G. P. M. S. Neves, J. A. S. Cavaleiro and A. M. V. Cavaleiro, *J. Mol. Catal. A Chem.*, 2005, **231**, 35–45.
- 12 S. L. H. Rebelo, M. M. Q. Simões, M. G. P. M. S. Neves and J. A. S. Cavaleiro, *J. Mol. Catal. A Chem.*, 2003, **201**, 9–22.
- 13 S. L. H. Rebelo, M. M. Q. Simoes, M. G. P. M. S. Neves, A. M. S. Silva, J. A. S. Cavaleiro, A. F. Peixoto, M. M. Pereira, M. R. Silva, J. A. Paixao and A. M. Beja, *European J. Org. Chem.*, 2004, 4778–4787.
- 14 S. L. H. Rebelo, M. M. Q. Simões, M. G. P. M. S. Neves, A. M. S. Silva and J. A. S. Cavaleiro, *Chem. Commun.*, 2004, 608–609.
- 15 S. L. H. Rebelo, A. R. Gonçalves, M. M. Pereira, M. M. Q. Simões, M. G. P. M. S.

- Neves and J. A. S. Cavaleiro, *J. Mol. Catal. A Chem.*, 2006, **256**, 321–323.
- 16 R. De Paula, M. M. Q. Simões, M. G. P. M. S. Neves and J. A. S. Cavaleiro, *J. Mol. Catal. A Chem.*, 2011, **345**, 1–11.
- 17 C. M. B. Neves, M. M. Q. Simões, I. C. M. S. Santos, F. M. J. Domingues, M. G. P. M. S. Neves, F. A. Almeida Paz, A. M. S. Silva and J. A. S. Cavaleiro, *Tetrahedron Lett.*, 2011, **52**, 2898–2902.
- 18 C. M. B. Neves, M. M. Q. Simões, F. M. J. Domingues, M. G. P. M. S. Neves and J. A. S. Cavaleiro, *Quim. Nova*, 2012, **35**, 1477–1481.
- 19 C. M. B. Neves, M. M. Q. Simões, M. R. M. Domíngues, I. C. M. S. Santos, M. G. P. M. S. Neves, F. A. A. Paz, A. M. S. Silva and J. A. S. Cavaleiro, *RSC Adv.*, 2012, **2**, 7427–7438.
- 20 S. M. G. Pires, M. M. Q. Simões, I. C. M. S. Santos, S. L. H. Rebelo, M. M. Pereira, M. G. P. M. S. Neves and J. A. S. Cavaleiro, *Appl. Catal. A Gen.*, 2012, **439–440**, 51–56.
- 21 S. L. H. Rebelo, M. M. Pereira, M. M. Q. Simões, M. G. P. M. S. Neves and J. A. S. Cavaleiro, *J. Catal.*, 2005, **234**, 76–87.
- 22 J. T. Groves, W. J. Kruper and R. C. Haushalter, *J. Am. Chem. Soc.*, 1980, **102**, 6375–6377.
- 23 J. T. Groves and M. K. Stern, *J. Am. Chem. Soc.*, 1987, **109**, 3812–3814.
- 24 J. T. Groves and M. K. Stern, *J. Am. Chem. Soc.*, 1988, **110**, 8628–8638.
- 25 J. T. Groves, J. Lee and S. S. Marla, *J. Am. Chem. Soc.*, 1997, **119**, 6269–6273.
- 26 N. Jin and J. T. Groves, *J. Am. Chem. Soc.*, 1999, **121**, 2923–2924.
- 27 M. J. Camenzind, F. J. Hollander and C. L. Hill, *Inorg. Chem.*, 1982, **21**, 4301–4308.
- 28 R. Zhang, J. H. Horner and M. Newcomb, *J. Am. Chem. Soc.*, 2005, **127**, 6573–6582.
- 29 M. Moghadam, S. Tangestaninejad, M. H. Habibi and V. Mirkhani, *J. Mol. Catal. A Chem.*, 2004, **217**, 9–12.
- 30 R. De Paula, I. C. M. S. Santos, M. M. Q. Simões, M. G. P. M. S. Neves and J. A. S. Cavaleiro, *J. Mol. Catal. A Chem.*, 2015, **404–405**, 156–166.
- 31 S. M. G. Pires, R. De Paula, M. M. Q. Simões, M. G. P. M. S. Neves, I. C. M. S. Santos, A. C. Tomé and J. A. S. Cavaleiro, *Catal. Commun.*, 2009, **11**, 24–28.

- 32 I. M. El-Nahhal, B. A. El-Shetary, A. E.-K. B. Mustafa, N. M. El-Ashgar, J. Livage, M. M. Chehimi and A. Roberts, *Solid State Sci.*, 2003, **5**, 1395–1406.
- 33 M. E. Lipinska, S. L. H. Rebelo and C. Freire, *J. Mater Sci.*, 2014, **49**, 1494–1505.
- 34 S. A. Al-Bataineh, L. G. Britcher and H. J. Griesser, *Surf. Sci.*, 2006, **600**, 952–962.
- 35 D. K. Lavalley, J. Brace and N. Winograd, *Inorg. Chem.*, 1979, **18**, 1776–1780.
- 36 P. G. Gassman, A. Ghosh and J. Almlöf, *J. Am. Chem. Soc.*, 1992, **114**, 9990–10000.
- 37 J. G. Goll, K. T. Moore, A. Ghosh and M. J. Therien, *J. Am. Chem. Soc.*, 1996, **118**, 8344–8354.
- 38 D. M. Sarno, B. Jiang, D. Grosfeld, J. O. Afriyie, L. J. Matienzo and W. E. Jones, *Langmuir*, 2000, **16**, 6191–6199.
- 39 H. Jansen, R. J. J.; van Bekkum, *Carbon N. Y.*, 1995, **33**, 1021–1027.
- 40 S. H. Goh, S. Y. Lee, J. Dai and K. L. Tan, *Polymer*, 1996, **37**, 5305–5308.
- 41 P. van der Heide, *X-Ray Photoelectron Spectroscopy - An Introduction to Principles and Practices*, John Wiley & Sons, Hoboken, 2012.
- 42 Z. Li, C.-G. Xia and X.-M. Zhang, *J. Mol. Catal. A Chem.*, 2002, **185**, 47–56.
- 43 A. Kaplan, E. Korin and A. Bettelheim, *Eur. J. Inorg. Chem.*, 2014, 2288–2295.
- 44 F. Yang, S. Gao, C. Xiong, H. Wang, J. Chen and Y. Kong, *Cuihua Xuebao/Chinese J. Catal.*, 2015, **36**, 1035–1041.
- 45 A. R. Antonangelo, C. Grazia Bezzu, N. B. McKeown and S. Nakagaki, *J. Catal.*, 2019, **369**, 133–142.
- 46 A. A. Guedes, A. C. M. A. Santos and M. D. Assis, *Kinet. Catal.*, 2006, **47**, 555–563.
- 47 J.-Y. Liu, X.-F. Li, Y.-Z. Li, W.-B. Chang and A.-J. Huang, *J. Mol. Catal. A Chem.*, 2002, **187**, 163–167.
- 48 M.-H. Xie, X.-L. Yang and C.-D. Wu, *Chem. Commun.*, 2011, **47**, 5521.
- 49 R. De Paula, M. M. Q. Simões, M. G. P. M. S. Neves and J. A. S. Cavaleiro, *Catal. Commun.*, 2008, **10**, 57–60.
- 50 J. T. Groves and R. S. Myers, *J. Am. Chem. Soc.*, 1983, **105**, 5791–5796.
- 51 D. Mansuy, J. Leclaire, M. Fontecave and P. Dansette, *Tetrahedron*, 1984, **40**, 2847–2857.
- 52 J. P. Collman, T. Kodadek and J. I. Brauman, *J. Am. Chem. Soc.*, 1986, **108**, 2588–

- 2594.
- 53 A. M. d'A. R. Gonsalves and A. C. Serra, *J. Chem. Soc. Perkin Trans. 2*, 2002, 715–719.
- 54 R. D. Arasasingham, G.-X. He and T. C. Bruice, *J. Am. Chem. Soc.*, 1993, **115**, 7985–7991.
- 55 A. M. d'A. R. Gonsalves and A. C. Serra, *J. Mol. Catal. A Chem.*, 2001, **168**, 25–32.
- 56 S. P. de Visser, D. Kumar and S. Shaik, *J. Inorg. Biochem.*, 2004, **98**, 1183–1193.
- 57 D. Kumar, S. P. De Visser and S. Shaik, *Chem. Eur. J.*, 2005, **11**, 2825–2835.
- 58 Y. Liu, H. Zhang, Y. Lu, Y. Cai and X. Liu, *Green Chem.*, 2007, **9**, 1114–1119.
- 59 M. Fontecave and D. Mansuy, *J. Chem. Soc., Chem. Commun.*, 1984, 879–881.
- 60 C. Gilmartin and J. R. L. Smith, *J. Chem. Soc. Perkin Trans. 2*, 1995, 243–251.



CHAPTER 4

Oxidation of monoterpenes and other organic compounds catalysed by a Mn(III) PEG-porphyrin

The major part of this chapter gave rise to the following publication:

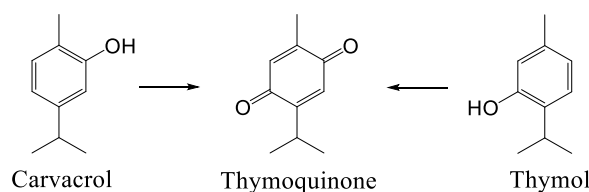
Neves, C. M. B.; Tomé, J. P. C.; Hou, Z.; Dehaen, W.; Hoogenboom, R.; Neves, M. G. P. M. S.; Simões, M. M. Q. Oxidation of Monoterpenes Catalysed by a Water-soluble Mn^{III} PEG-Porphyrin in a Biphasic Medium. *ChemCatChem* **2018**, *10*, 2804-2809. <https://doi.org/10.1002/cctc.201800239>.

Chapter 4. Oxidation of monoterpenes and other organic compounds catalysed by a Mn(III) PEG-porphyrin

There is a growing concern to work with greener and more sustainable technologies in the production of fine chemicals and pharmaceuticals.¹⁻⁴ Particularly, one aspect that has received great attention is the use of alternative reaction media to the usual volatile organic solvents.⁵ In the search for alternative solvents, a relevant aspect is related with the possibility to isolate the catalyst from the products, being able to reuse it several times.⁵ If in heterogeneous catalysis the catalyst is easily recovered because it is usually a solid, in the case of homogeneous catalysis, the catalyst recovery is a much more time-consuming and expensive process. One solution, as discussed in the previous chapter, is the immobilization of the homogeneous catalysts onto solid supports. However, in this process we usually lose one of the main advantages of homogeneous catalysis - the high substrate conversion. Liquid-liquid biphasic catalysis, where the catalyst is soluble in one solvent and the substrate and products are soluble in the other solvent, may be an effective alternative.⁶ This strategy allows the catalyst to be easily separated from the substrate and the reaction products by simple phase separation and, in addition, the usual advantages of homogeneous catalysis are preserved.⁷ It will be particularly attractive from the industrial point of view if the phase containing the catalyst remains in the reactor so that more reactants can be added for a new reaction. These two-phase catalytic systems have been applied in the oxidation of various organic compounds.^{8,9}

It is well established that the transformation of abundant and cheap natural products, such as terpenoids, can produce other more valuable compounds. Oregano is a popular herb widely used in cooking as a spice. Its essential oils are known to present antibacterial, antifungal and antioxidant properties making oregano very attractive for pharmaceutical and food applications.^{10,11} Oregano essential oils are usually rich in carvacrol and thymol (**Scheme 4.1**), which have been identified as the main responsables for the activities described.¹²⁻¹⁵ The oxidation of carvacrol and thymol originates high amounts of thymoquinone, a much more valuable compound that showed a therapeutic effect in numerous diseases but with limited natural occurrence in *Nigella sativa L.* and *Monarda fistulosa L.* plants.¹⁶⁻²² In this sense, the search for processes that can lead to the production

of thymoquinone starting from cheaper and abundant substrates is a subject of great interest.



Scheme 4.1. Structures of the substrates (carvacrol and thymol) and the product (thymoquinone).

Dockal *et al.* prepared thymoquinone by homogeneous oxidation of thymol and carvacrol in DMF using Co(II) salen catalysts, under oxygen flow at low pressure.²³ Thymoquinone was also efficiently obtained by oxidation of thymol and carvacrol in acetonitrile in the presence of homogeneous Mn(III) porphyrins and hydrogen peroxide as oxidant.²⁴ Similar oxidation reactions catalysed by an Y zeolite supported tetracationic Mn(III) porphyrin complex led to < 25% conversion of carvacrol and < 18% conversion of thymol after 24 h of reaction, in acetonitrile, with 100% selectivity towards thymoquinone.²⁵ The leaching of the Mn(III) porphyrin complex to the reaction solution in the presence of H₂O₂, accompanied by the partial collapse and changes of the crystalline structure, causing irreversible deactivation, led to a complete loss of activity when it was recycled.²⁵ A mixture of thymoquinone, thymohydroquinone, and other benzoquinones was obtained when the oxidation of carvacrol was performed in the presence of zeolite-encapsulated metal-*N,N'*-bis(salicylidene)propane-1,3-diamine complexes [M(salpn)-NaY; M = Cr, Fe, Zn, Ni, Bi] as catalysts and hydrogen peroxide as oxidant, in acetonitrile.²⁶ The oxidation of carvacrol and thymol in the presence of Keggin-type heteropolyanions and hydrogen peroxide, in acetonitrile at reflux, was also less selective, affording a mixture of benzoquinones as products, in moderate conversion.²⁷ Recently, the oxidation of thymol and carvacrol was studied by using potassium peroxymonosulfate (KHSO₅) as oxidant in the presence of Fe(III) phthalocyanine tetrasulfonate (FePcTS) and a mixture of methanol:water (8:1) as solvent.²⁸ The selectivity for thymoquinone was lower than 34% for carvacrol and lower than 21% for thymol. When H₂O₂ or *tert*-butyl hydroperoxide (TBHP) were used as oxidants, the yield of thymoquinone was < 1 %. Moreover, by recycling the catalyst, FePcTS, the authors observed that both thymol and carvacrol conversions dropped to < 5% in the second cycle.²⁸ Milos compared the catalytic

efficiency of the Fe(III) complexes of 5,10,15,20-tetraphenylporphyrin and of phthalocyanine in the oxidation of an oregano essential oil using KHSO_5 or H_2O_2 as oxidant, in acetonitrile.²⁹ The essential oil was rich in thymol and carvacrol (47.6% and 25.1%), *p*-cymene (21.4%), γ -terpinene (2.0%), among other constituents (< 1%). Both catalysts were efficient using KHSO_5 with a complete or almost complete conversion of carvacrol and thymol within 1 h (19.1–63.3% yields for thymoquinone), and the co-catalyst, ammonium acetate, did not influence the catalytic process. When H_2O_2 was used as oxidant, a relatively slower conversion and lower yields for thymoquinone were observed and the presence of ammonium acetate affected the oxidation profile with both catalysts, while *p*-cymene and γ -terpinene remained unchanged.²⁹

The following topics will be discussed below:

i) The synthesis and characterization of a water-soluble Mn(III) PEG-porphyrin to be used as catalyst in a water/hexane (1:1) biphasic medium for the oxidation of monoterpenes and other organic compounds;

ii) The preliminary oxidation studies with the Mn(III) complex of the 5,10,15,20-tetraphenylporphyrin [**Mn(TPP)acac**] on the oxidation of carvacrol in order to find the best catalytic conditions to be applied with the Mn(III) PEG-porphyrin as catalyst in a biphasic medium;

iii) The oxidation of carvacrol and thymol using Mn(III) PEG-porphyrin as catalyst in a liquid-liquid biphasic medium, and the recycling ability of the catalyst;

iv) The oxidation studies with an oregano essential oil, rich in thymol and carvacrol, and the monitoring of the chemical composition of the oil, before and after the oxidation reaction, by GC-MS;

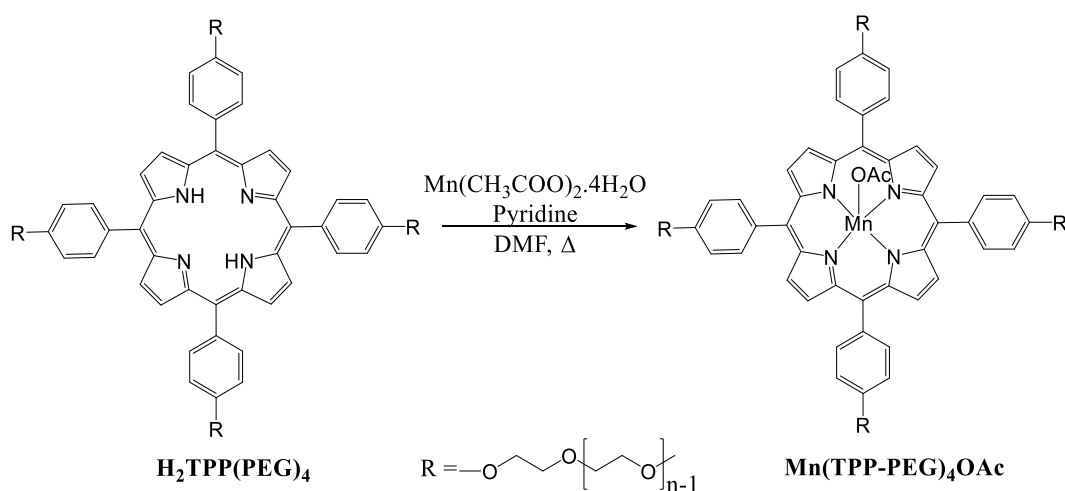
v) The extension of the oxidation studies to other organic compounds.

4.1. Results and discussion

4.1.2. Synthesis and characterization of **MnTPP(PEG)₄OAc**

In the present study, taking advantage of the high water-solubility of porphyrins functionalized with polyethylene glycol (PEG) chains,³⁰ the Mn(III) complex of **H₂TPP(PEG)₄** was prepared (**Scheme 4.2**) to be tested as catalyst for oxidation reactions in a biphasic medium. The free-base porphyrin **H₂TPP(PEG)₄** was synthesized by the

Supramolecular Chemistry Group from the Center of Macromolecular Chemistry of the Ghent University, as previously described.³¹ The incorporation of the metal in the porphyrin core was performed by using a well established literature procedure and involved the reaction of **H₂TPP(PEG)₄** with manganese(II) acetate, as explained in the experimental part (section 4.3.2).



Scheme 4.2. The synthetic strategy to obtain the **MnTPP(PEG)₄OAc** from the **H₂TPP(PEG)₄**.

After the work-up, the obtained manganese complex **MnTPP(PEG)₄OAc** was characterized by UV-Vis (**Figure 4.1**), size exclusion chromatography (SEC; **Figure 4.2**) and MALDI-TOF MS (**Figure 4.3**). **Figure 4.1** compares the UV-Vis spectra of the free-base porphyrin **H₂TPP(PEG)₄** with the corresponding manganese complex, **MnTPP(PEG)₄OAc**. The manganese complexation of the free-base porphyrin resulted in a pronounced change in the Q bands region, with the disappearance of two of the Q bands. In addition, a bathochromic shift (to higher wavelengths) of the Soret band and the presence of the metal transition bands at 350-450 nm were observed. SEC revealed that the **MnTPP(PEG)₄OAc** has a narrow molar mass distribution with a dispersity value below 1.15. Additionally, the successfully loading of manganese in the core of the porphyrin was also confirmed from the MALDI-TOF MS spectra (**Figure 4.3**) revealing the expected increase in the molar mass after de Mn(III) coordination.

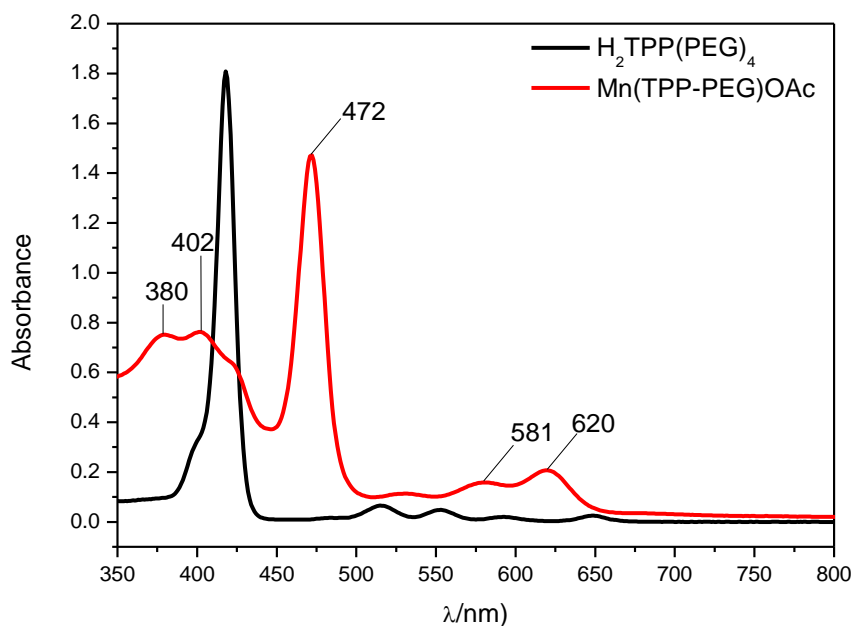


Figure 4.1. UV-Vis spectra of the free-base porphyrin ($H_2TPP(PEG)_4$) and after manganese complexation ($MnTPP(PEG)_4OAc$) using acetonitrile as solvent.

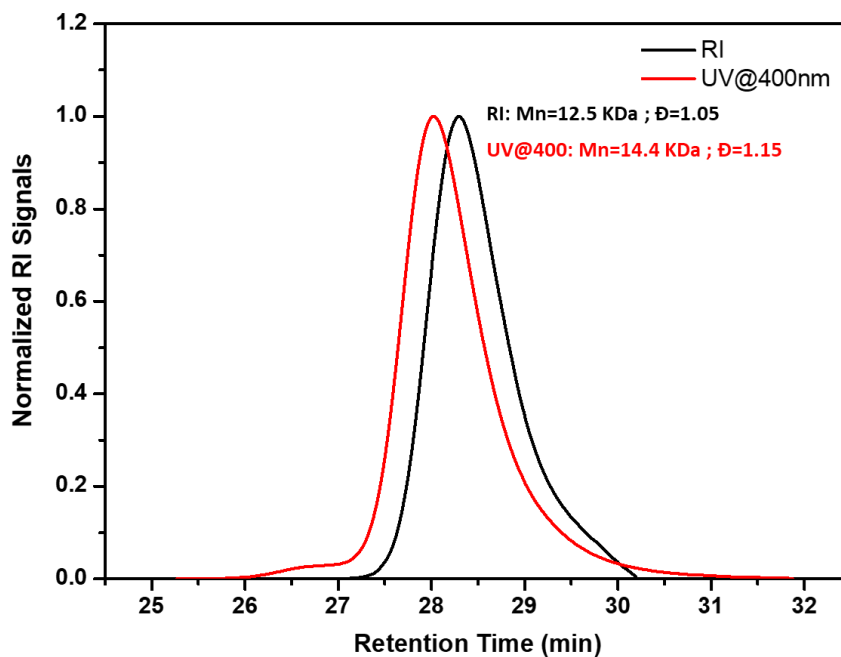


Figure 4.2. SEC traces of $MnTPP(PEG)_4OAc$ obtained with a differential refractive index detector (RI) and a UV-detector at 400 nm placed in series.

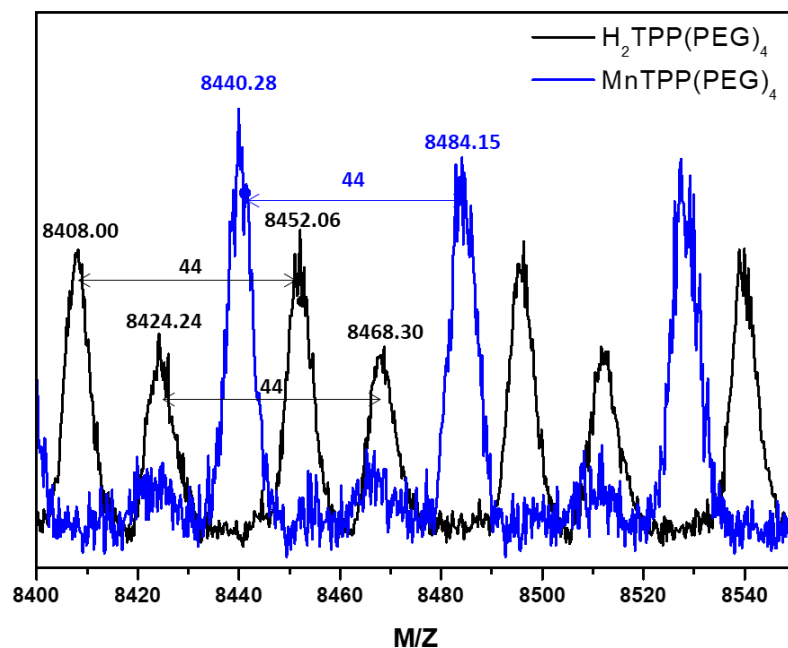


Figure 4.3. Comparison of zoomed in MALDI-TOF MS spectra of **MnTPP(PEG)₄OAc** and the free-base **H₂TPP(PEG)₄** {[H₂TPP(PEG)₄+Na]⁺: 8408.00/8452.06; [H₂TPP(PEG)₄+K]⁺: 8424.24/8468.30; [MnTPP(PEG)₄+H]⁺: 8440.28/8484.15}.

4.1.2. Catalytic oxidation of monoterpenes

The oxidation reactions were planned to be carried out in a biphasic medium. The solvent used was a water/hexane (1:1) mixture and the substrates selected were carvacrol and thymol, due to their high solubility in hexane and low solubility in water. In this way, it was possible to develop a biphasic system in which the catalyst is water-soluble, and the substrate is soluble in the organic solvent. The product obtained is also poorly soluble in water, thereby allowing an easy separation of the catalyst from the substrate and/or product by a simple phase separation. Other solvent mixtures, such as water/acetone and water/ethyl acetate were tested, but in these cases no oxidation of the substrates was observed.

4.1.2.1. Catalytic oxidation of carvacrol under homogeneous conditions

Before investigating the proposed biphasic catalysis, the best reaction conditions, namely the substrate/catalyst (S/C) molar ratio and the oxidant to be used, were optimized under homogeneous conditions with the more synthetic accessible **Mn(TPP)acac** as catalyst, using carvacrol as substrate, ammonium acetate as co-catalyst and acetonitrile as solvent at ambient temperature. The oxidant was initially added in portions with intervals of 15 min, each addition corresponding to 0.5 eq relatively to the molar amount of the substrate. When H₂O₂ was used as oxidant no oxidation reaction occurred, even for a S/C molar ratio of 25. Additionally, a change in the catalyst colour from green to red/brown was observed after some time, indicating a possible destruction/deactivation of the catalyst with H₂O₂, which was confirmed by UV-Vis spectrophotometry as the Soret band disappeared (**Figure 4.4**).

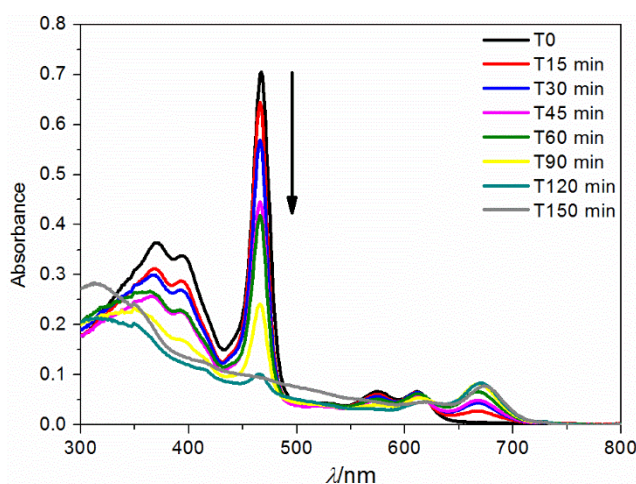


Figure 4.4. UV-Vis monitoring of the **Mn(TPP)acac** catalyst stability in the homogeneous oxidation of carvacrol in acetonitrile using H₂O₂ as oxidant for a S/C molar ratio of 25.

A totally different result was obtained with *tert*-butyl hydroperoxide (TBHP) as oxidant revealing total conversion of the substrate after 45 min and high stability of the catalyst as indicated by UV-Vis spectrophotometry (**Figure 4.5**).

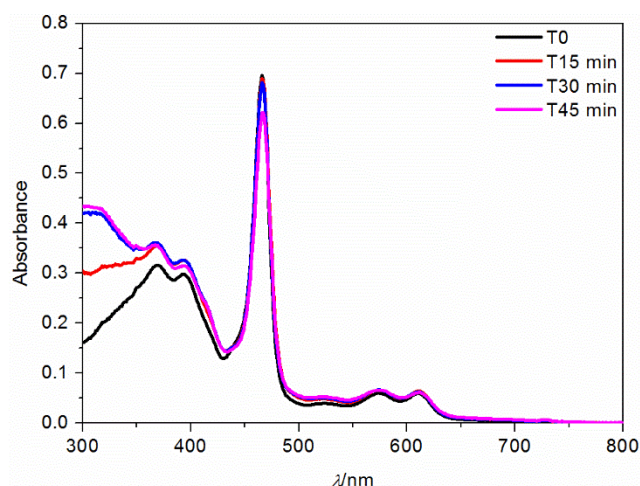


Figure 4.5. UV-Vis monitoring of the **Mn(TPP)acac** catalyst stability in the homogeneous oxidation of carvacrol in acetonitrile using TBHP as oxidant for a S/C molar ratio of 25.

These good results for the homogeneous catalysis with TBHP as oxidant led us to test other S/C molar ratios with a smaller amount of catalyst. Almost total conversion of carvacrol was obtained, after 45 min (**Figure 4.6**), for a S/C molar ratio of 100 (94%), and the efficiency of the catalyst was maintained for a S/C molar ratio of 200 (93% conversion, after 45 min). The same result was obtained using **MnTPP(PEG)₄OAc** as catalyst and acetonitrile as solvent, i.e. under homogeneous conditions (**Figure 4.6**).

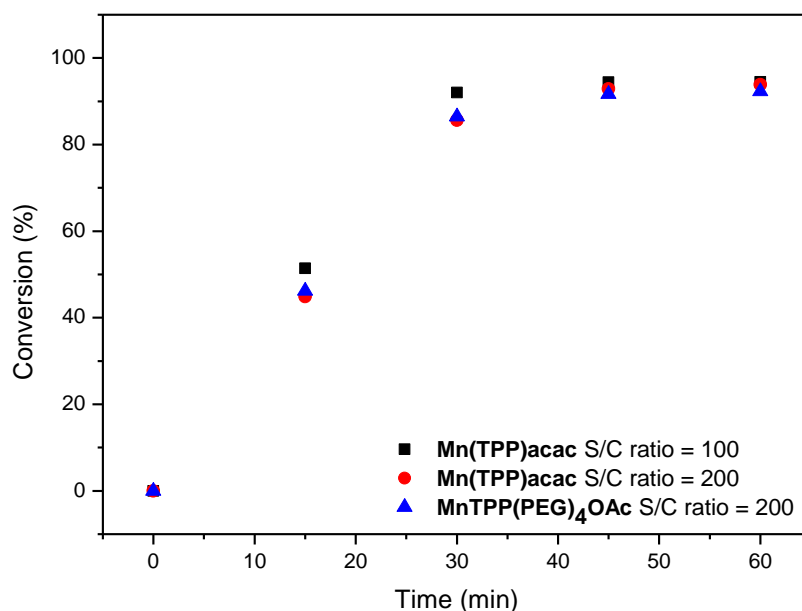


Figure 4.6. Carvacrol conversion using **Mn(TPP)acac** or **MnTPP(PEG)₄OAc** as catalyst, TBHP as oxidant (0.5 eq every 15 min) and acetonitrile as solvent.

4.1.2.2. Catalytic oxidation of carvacrol and thymol with MnTPP(PEG)₄OAc in a biphasic medium

In a next step, the performance of MnTPP(PEG)₄OAc was evaluated using a water/hexane (1:1) biphasic medium, under vigorous stirring. Using this mixture, the substrate (carvacrol or thymol) and the internal standard (chlorobenzene) are soluble in hexane and have low solubility in water and the catalyst is soluble in water (Figure 4.7, left). At the end of reaction, the catalyst is still present in the water phase and the product (thymoquinone) is in the hexane, easily visible due to its yellow colour (Figure 4.7, right), which allows an easy monitoring of the reaction and the separation of the catalyst from the product.

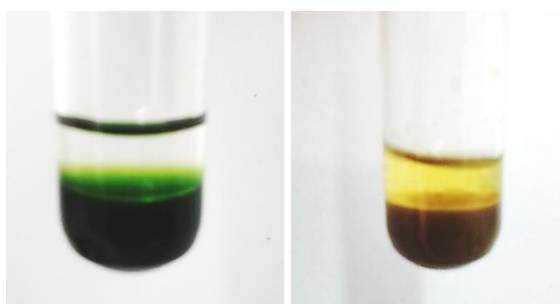


Figure 4.7. Carvacrol oxidation using MnTPP(PEG)₄OAc in the mixture of water/hexane (1:1) as solvent. Before the addition of TBHP the catalyst is completely soluble in water (green colour) and the carvacrol is soluble in the hexane (left); at the end of reaction, the catalyst is still soluble in water and thymoquinone is soluble in the hexane (right).

In this case and using TBHP with additions of 0.5 eq every 15 min, the reaction was slower and after 120 min (4 eq of oxidant added) the conversion of carvacrol was around 70%. The slower reaction was anticipated as the reaction will mainly occur at the interphase between the aqueous and organic phases. The reaction mixture was already in the presence of a large excess of oxidant, since even without adding TBHP, carvacrol continued to be oxidised to thymoquinone. In this case, further additions of oxidant would only lead to the destruction of the catalyst. Therefore, the oxidant was added at once (4 eq of TBHP) and a conversion of 78% was obtained after 300 min (Figure 4.8). The same conditions were used in the oxidation of thymol reaching 94% of conversion after 300 min (Figure 4.8), with thymoquinone being the only product detected. Blank experiments, without adding the catalyst and the co-catalyst were performed and no oxidation was observed.

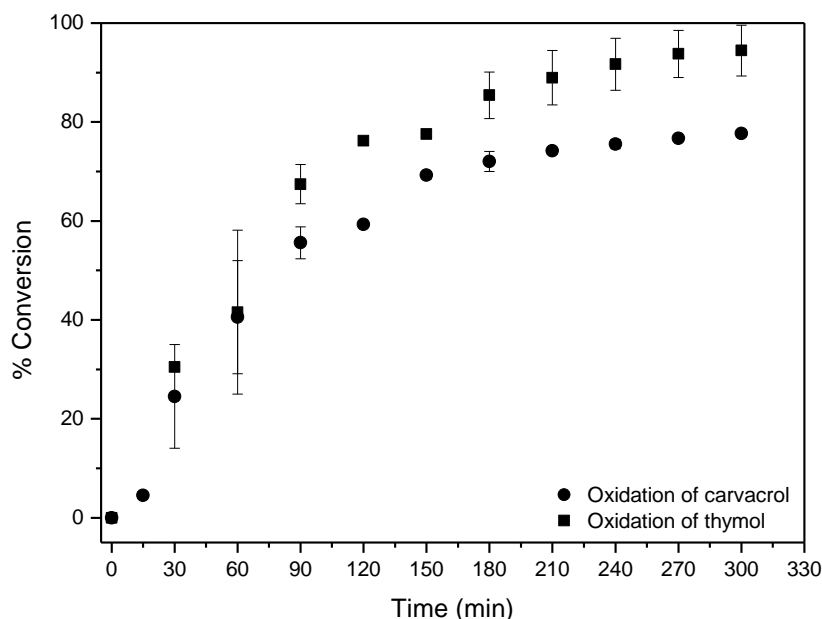


Figure 4.8. Conversion of carvacrol and thymol using **MnTPP(PEG)₄OAc** as catalyst and TBHP as oxidant (4 eq added at once) in a water/hexane (1:1) biphasic medium. Data correspond to mean values and the vertical bars correspond to standard deviations.

Additional assays were performed in order to evaluate if the separation of thymoquinone was not affected by the recycling of the catalyst. These experiments were carried with **MnTPP(PEG)₄OAc** in water-hexane (1:1) by using thymol as substrate and a S/C molar ratio of 50. After each cycle, the catalyst was isolated from the reaction mixture by simple phase separation, for subsequent reuse. The evolution of thymol conversion for each catalytic cycle was monitored by GC-FID and is shown in **Figure 4.9**. The results show that the efficiency of the catalytic biphasic system in the first cycle (99% after 120 min) is maintained in the second catalytic cycle (98% after 150 min). In the third cycle, after 210 min of reaction, a high conversion (83%) is still observed. In the fourth cycle the system was able to convert 50% of thymol after 240 min of reaction. The catalytic activity decrease of the first generation porphyrin metal complexes under oxidative conditions is well known from the literature.^{32,33} Nevertheless, the present biphasic conditions seem to promote the **MnTPP(PEG)₄OAc** stability, allowing its recovery and reuse. In all catalytic cycles the only product obtained was thymoquinone, which was readily and efficiently separated from the catalyst by phase separation, thus allowing us to obtain the

thymoquinone in the organic phase, concomitantly to the easy separation of the catalyst, which remained in the aqueous phase ready for a new run.

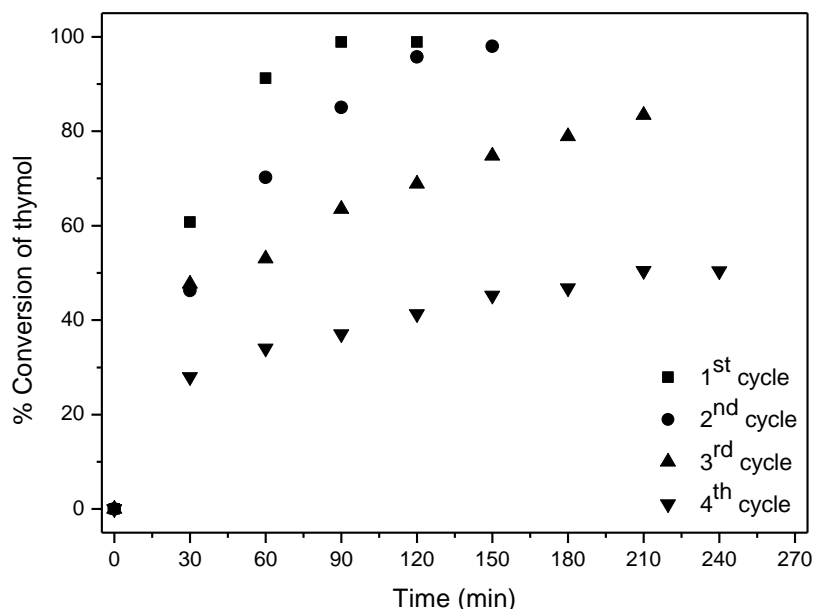


Figure 4.9. Catalyst recycling studies of the $\text{MnTPP(PEG)}_4\text{OAc}$ catalyst using thymol as substrate, TBHP as oxidant and a S/C molar ratio of 50 in a water/hexane (1:1) biphasic medium.

4.1.2.3. Catalytic studies with $\text{MnTPP(PEG)}_4\text{OAc}$ in the oxidation of an oregano essential oil using the biphasic medium

The catalytic system in a biphasic medium previously tested was also used in the oxidation of an essential oil of *Origanum vulgare*. The composition of the essential oil was determined by GC-MS (**Figure 4.10**) revealing carvacrol (33.2%), thymol (17.0%), and *p*-cymene (15.3%) as the main components (**Table 4.1**). Other minor components included terpinen-4-ol (6.6%), *trans*-caryophyllene (5.6%) and β -bisabolene (6.3%). The oxidation reaction was monitored by GC-FID and by GC-MS (**Figure 4.10**) to identify the oxidation products. In line with a previous report by Milos,²⁹ it was observed that the reaction was selective for the oxidation of thymol and carvacrol. After 3 h of reaction, thymol and carvacrol were almost totally converted into thymoquinone (98% and 89%, respectively – **Figure 4.11**) and the other components remained practically intact.

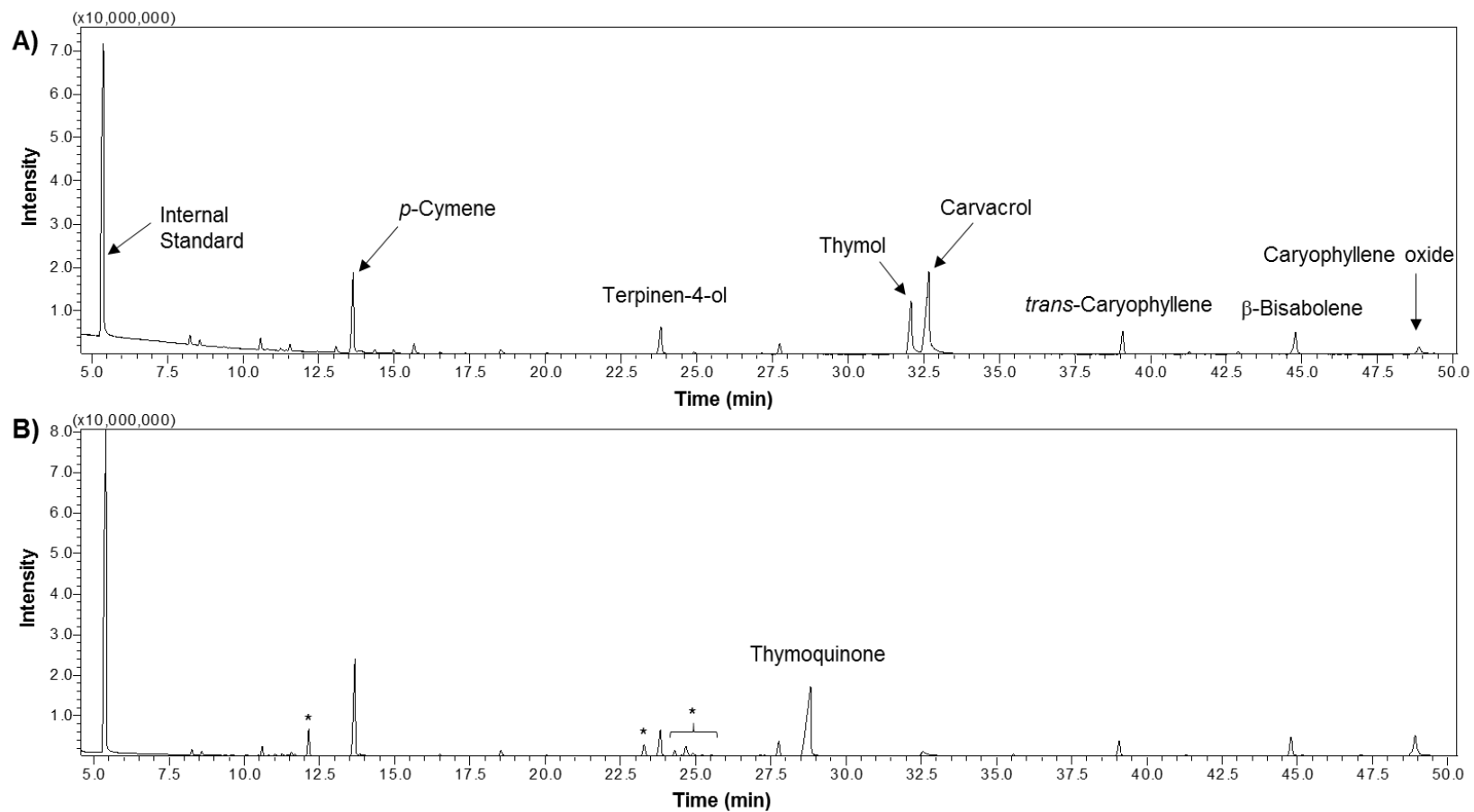
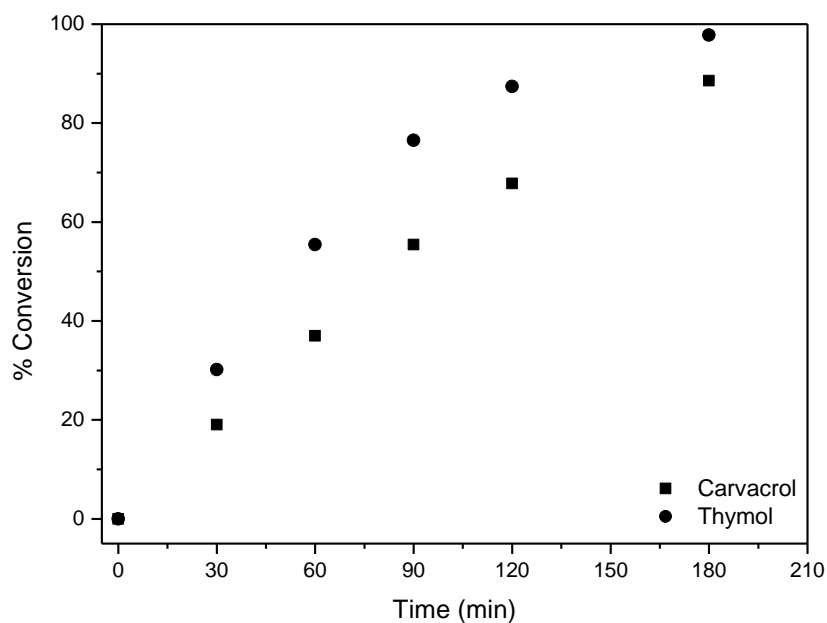


Figure 4.10. GC-MS chromatograms of the essential oil of *Origanum vulgare* (A) before and (B) after 3 h oxidation reaction using MnTPP(PEG)₄OAc as catalyst. The peaks with an asterisk (*) correspond to solvent/contaminants present in the oxidant (*tert*-butyl hydroperoxide solution in decane).

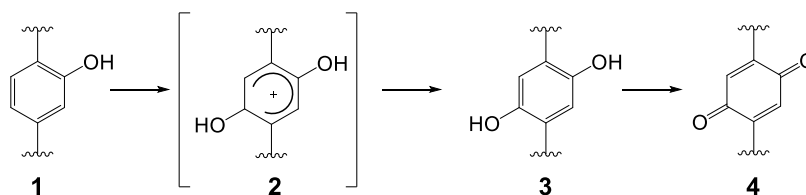
Table 4.1. Volatile compounds present in the composition of the oregano essential oil

Retention time (min)	Compound	%
8.25	α -Thujene	1.3
8.58	α -Pinene	< 1.0
10.58	Sabinene	1.9
11.56	β -Myrcene	1.1
13.08	Terpinolene	1.0
13.64	<i>p</i> -Cymene	15.3
14.36	<i>trans</i> - β -Ocimene	< 1.0
14.99	β -Ocimene	< 1.0
15.66	γ -Terpinene	1.9
18.53	<i>cis</i> -Sabinene hydrate	1.1
23.80	Terpinen-4-ol	6.6
27.74	Carvacrol methyl ether	2.3
32.09	Thymol	17.0
32.68	Carvacrol	33.2
39.08	<i>trans</i> -Caryophyllene	5.6
41.29	α -Humulene	< 1.0
42.91	Germacrene D	< 1.0
44.79	β -Bisabolene	6.3
48.88	Caryophyllene oxide	2.7

**Figure 4.11.** Conversion of carvacrol and thymol in the oxidation of the essential oil of *Origanum vulgare* using $\text{MnTPP(PEG)}_4\text{OAc}$ as catalyst and TBHP as oxidant in a water/hexane (1:1) biphasic medium.

4.1.2.4. Mechanism of thymoquinone formation

The formation of thymoquinone can be justified by a selective hydroxylation of the aromatic ring in the *para* position relatively to the OH group, resulting in a protonated intermediate, the *p*-hydroxylated species **2**, which is stabilised by the OH substituent already present in carvacrol and thymol and originates the hydroquinone **3** (Scheme 4.3).²⁴ The subsequent oxidation of the hydroquinone **3** leads to the corresponding quinone **4** (thymoquinone).²⁴



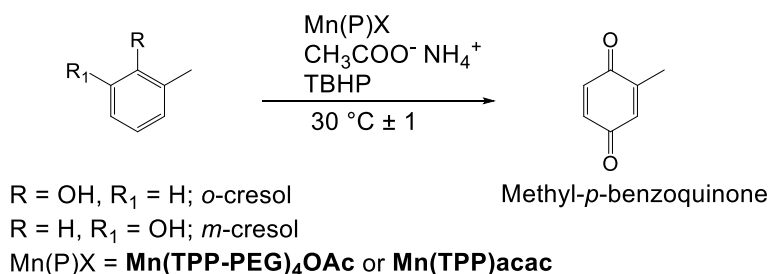
Scheme 4.3. Proposed mechanism for the formation of thymoquinone.

4.1.3. Catalytic oxidation of other organic compounds

Pleased with the results obtained in the oxidation of monoterpenes with Mn(TPP-PEG)₄OAc in biphasic medium, the same catalytic system was also applied to the oxidation of other organic compounds (Table 4.2). The reactions were carried out using TBHP as oxidant, ammonium acetate as co-catalyst and a S/C molar ratio of 200. The catalytic system using Mn(TPP-PEG)₄OAc and the biphasic medium showed to be inefficient in the oxidation of cyclooctene to the corresponding epoxide resulting in only 6% of conversion (Table 4.2, Entry 1). It is known that the metal complexes of 5,10,15,20-tetraphenylporphyrin are easily destroyed in the presence of oxidants, usually resulting in low substrate conversions. However, we expected that the presence of the polyethylene glycol substituents could protect the porphyrin core from the oxidizing medium.

It was considered pertinent to study also the oxidation of *o*-cresol and *m*-cresol (Scheme 4.4) due to their structural similarity with carvacrol and thymol. However, we found that when using Mn(TPP-PEG)₄OAc in the biphasic medium, and after addition of *o*-cresol or *m*-cresol, the porphyrin seems to be encapsulated in a kind of micelles; this behaviour was considered responsible for its low catalytic activity that conducted to low conversions of the substrates (Table 4.2, Entries 2 and 3). In fact, the reason for the inefficiency of Mn(TPP-PEG)₄OAc in the biphasic medium is exclusively due to its encapsulation, since in acetonitrile *m*-cresol was completely converted into methyl-*p*-

benzoquinone in 120 min (Table 4.2, Entry 3). Also, using **Mn(TPP)acac** in acetonitrile almost total conversion of *o*-cresol was obtained (Table 4.2, Entry 2). In the presence of *p*-cymene, **Mn(TPP-PEG)₄OAc** did not form such micelles. However, low conversion (24%) was obtained when **Mn(TPP)acac** was used as catalyst (Table 4.2, Entry 4).



Scheme 4.4. Oxidation of *o*-cresol and *m*-cresol into methyl-*p*-benzoquinone.

Table 4.2. Oxidation of some organic compounds in the presence of Mn(III) porphyrin catalysts, using TBHP as oxidant.^(a)

Entry	Substrate	Catalytic System	Time (min)	Conversion (%)
1		Mn(TPP-PEG)₄OAc /Biphasic	300	6
2		Mn(TPP-PEG)₄OAc /Biphasic	120	12
		Mn(TPP)acac /CH ₃ CN	120	92
3		Mn(TPP-PEG)₄OAc /Biphasic	120	0
		Mn(TPP-PEG)₄OAc /CH ₃ CN	120	100
4		Mn(TPP)acac /CH ₃ CN	120	24

^(a) Conditions: 7.5×10^{-5} mol of substrate, 7.5×10^{-5} mol of the internal standard (chlorobenzene), 3.75×10^{-7} mol of the catalyst (S/C ratio of 200) and 0.2 mmol of the co-catalyst (≈ 15 mg of ammonium acetate). The oxidant used was *tert*-butyl hydroperoxide (TBHP) 5.0-6.0 M solution in decane with a single addition of 4 eq relatively to the molar amount of substrate (3×10^{-4} mol) at the beginning of the reaction.

4.2. Conclusions

In summary, the water-soluble **MnTPP(PEG)₄OAc** is an efficient catalyst for the preparation of thymoquinone by oxidation of carvacrol and thymol in a water/hexane (1:1) biphasic medium, using *tert*-butyl hydroperoxide (TBHP) as oxidant and ammonium acetate as co-catalyst. Recycling studies of the Mn(III) PEG-porphyrin using thymol as substrate showed high conversion values throughout four catalytic cycles. The catalyst is easily isolated and recovered by simple phase separation allowing its reutilization.

The methodology can be applied directly to an oregano essential oil particularly rich in carvacrol and thymol.

MnTPP(PEG)₄OAc in the biphasic medium exhibited low efficiency in the oxidation of other organic compounds such as cyclooctene, *o*-cresol or *m*-cresol. Better results will be expected if more robust second- or third-generation porphyrins are used.

4.3. Experimental

4.3.1. Reagents and Methods

Thymol was purchased from Sigma, whereas carvacrol and *tert*-butyl hydroperoxide (TBHP) 5.0-6.0 M solution in decane were obtained from Aldrich. Ammonium acetate was purchased from Scharlau and chlorobenzene was obtained from Carlo Erba and used as internal standard for the determination of substrates' conversion by GC. The free-base porphyrin **H₂TPP(PEG)₄** was prepared by the Supramolecular Chemistry Group of the Center of Macromolecular Chemistry (CMaC) at the Ghent University.³¹ **Mn(TPP)acac** was prepared by the acetylacetonate method as described in the literature.³⁴ The oregano oil was gently provided by Dr. Susana Cardoso.

The GC-FID analyses were carried out on a Varian 3900 chromatograph using helium as the carrier gas (30 cm/s) equipped with a fused silica capillary DB-5 type column (30 m length, 0.25 mm i.d., 0.25 μm film thickness). The GC-FID chromatographic conditions used for the monitoring of carvacrol, thymol and of the oregano oil were as follows: initial temperature, 100 °C; temperature rate of 10 °C/min up to 200 °C, followed by a new temperature rate of 40 °C/min up to 280 °C which was maintained for 2 min; injector and detector temperatures were both set at 300 °C. The GC-FID chromatographic conditions used for the monitoring of *o*-cresol and *m*-cresol were:

initial temperature, 60 °C; temperature rate of 10 °C/min up to 120 °C, followed by a new temperature rate of 40 °C/min up to 280 °C which was maintained for 2 min; injector and detector temperatures were both set at 300 °C. The GC-FID chromatographic conditions used for the monitoring of *p*-cymene were: initial temperature, 100 °C which was maintained for 1 min; temperature rate of 3 °C/min up to 142 °C, followed by a new temperature rate of 50 °C/min up to 260 °C; injector and detector temperatures were both set at 250 °C. The GC-FID chromatographic conditions used for monitoring cyclooctene reactions were: column initial temperature 80 °C for 1 min; column increasing temperature rate of 20 °C/min to 220 °C, which was maintained for 2 min; injector and detector temperatures were both set at 250 °C.

The GC-MS analyses of the oxidation reaction of the oregano oil were performed using a gas chromatograph mass spectrometer (GC-MS Shimadzu QP2010 Ultra) equipped with an AOC-20i autosampler (Shimadzu, Japan), with the electron impact ionization (EI) at 70 eV and high-performance quadrupole mass filter. The separation of compounds was carried out in a DB-5ms column (30 m length, 0.25 mm i.d., 0.25 µm film thickness) using helium as the carrier gas (40 cm/s). The GC-MS chromatographic conditions were as follows: initial temperature, 50 °C which was maintained for 3 min; temperature rate of 2 °C/min up to 250 °C which was maintained for 10 min; injector temperature, 250 °C. The mass spectrometer was operated over a range of m/z 34-450. The ion source was kept at 230 °C and the interface temperature at 280 °C. Chromatographic peaks were identified by comparing their mass spectra with the equipment mass spectral library (NIST14s MS Library Database or WILEY229 MS Library Database).

Size exclusion chromatography (SEC) was performed on an Agilent 1260-series HPLC system equipped with a 1260 online degasser, a 1260 ISO-Pump, a 1260 automatic liquid sampler, a thermostated column compartment, a 1260 diode array detector (DAD) and a 1260 refractive index detector (RID). Analyses were performed on a PPS Gram 30 column in series with a PPS Gram 1000 column at 50 °C. Dimethylacetamide (DMA) containing 50 mM of LiCl was used as eluent at a flow rate of 0.6 mL/min. The SEC traces were analysed using the Agilent Chemstation software with the GPC add on. Molar mass and PDI values were calculated against PMMA standards.

MALDI-TOF mass spectra were acquired with a Voyager DE-STR (PerSeptive Biosystem) using a simultaneous delay extraction procedure (20 kV applied after 233 ns

with a potential gradient of 2545 V/mm and a wire voltage of 200 V) and detection in reflection mode. The instrument was equipped with a nitrogen laser (emission at 337 nm for 3 ns) and a flash AD converter (time base 2 ns). The *trans*-2-[3-(4-*t*-butylphenyl)-2-methyl-2-propenylidene]malononitrile (DCTB) was used as matrix.

4.3.2. Synthesis of MnTPP(PEG)₄OAc

In a 25 mL round bottom flask, equipped with a reflux condenser and a magnetic stirrer, 50 mg of **H₂TPP(PEG)₄** were dissolved in 5.0 mL of DMF. The solution was refluxed in the dark, under a nitrogen atmosphere and then 0.5 mL of pyridine and 10 equivalents of manganese(II) acetate [Mn(CH₃COO)₂·4H₂O] were added. The progress of the reaction was monitored by UV-Vis. The UV-Vis spectrum shows a Soret band shift to a higher wavelength ($\lambda_{\text{max}} = 472$ nm) and the disappearance of two Q bands of the free-base macrocycle, thereby confirming the presence of the complex (**Figure 4.1**). The absorption bands of manganese at $\lambda_{\text{max}} = 380$ nm and 402 nm can also be observed. The reaction was complete after 4 h. The heating was switched off and the reaction mixture was kept under stirring overnight, in the open air and protected from light. The solvent was evaporated in the rotary evaporator with addition of toluene to facilitate the solvent removal. The residue was dissolved in dichloromethane and the organic phase was washed 2-3 times with water in a separating funnel. The organic phase was passed through a glass funnel with cotton wool and anhydrous sodium sulphate to remove traces of water. The manganese complexes were crystallized in hexane, after dissolution in a minimal amount of dichloromethane. The crystals were filtered under vacuum, using a Hirsch funnel with filter paper, and washed several times with hexane. The yield, based on the porphyrin, was over 90%. UV-Vis (CH₃CN) λ_{max} , nm (%): 380 (51), 402 (52), 472 (100), 581 (11), 620 (14).

4.3.3. General procedure for the oxidation reactions

For the oxidation reactions under homogeneous conditions: a standard solution of the catalyst was previously prepared in acetonitrile and reserved in the fridge protected from light until next use. The volume of catalyst's solution was added to the reactor in accordance to the corresponding substrate/catalyst (S/C) molar ratio. The co-catalyst (0.2 mmol \approx 15 mg of ammonium acetate), the substrate (7.5×10^{-5} mol), the internal standard

(7.5×10^{-5} mol of chlorobenzene) and acetonitrile were added until a final volume of 2 mL. The oxidant was added in aliquots of 0.5 eq relatively to the molar amount of the substrate every 15 min. In the case of cyclooctene, *o*-cresol, *m*-cresol and *p*-cymene, 4 eq of TBHP were added at once at the beginning of the reaction.

For the oxidation reactions under biphasic conditions: the catalyst (3.75×10^{-7} mol; 3.19 mg for a S/C ratio of 200) was dissolved in 1 mL of Milli-Q water, and the co-catalyst (0.2 mmol \approx 15 mg of ammonium acetate) was added. The substrate (7.5×10^{-5} mol) and the internal standard (7.5×10^{-5} mol of chlorobenzene) were dissolved in 1 mL of hexane and added to the aqueous mixture. The oxidant used was TBHP (5.0-6.0 M solution in decane) and 4 eq relatively to the molar amount of substrate (3×10^{-4} mol) were added at the beginning of the reaction. Blank experiments were performed under the same conditions without the catalyst and the co-catalyst.

For the recycling studies, thymol (7.5×10^{-5} mol; 11.3 mg) was chosen as substrate and 1.5×10^{-6} mol of **MnTPP(PEG)₄OAc** (12.7 mg for a S/C ratio of 50) were used under biphasic conditions. The reaction was stopped when the substrate was totally converted or when no significant conversion of the substrate was observed after two successive GC-FID analyses. At the end of the reaction, the organic phase containing the internal standard, the *tert*-butyl hydroperoxide, the thymoquinone and the unreacted thymol was separated from the aqueous phase containing the manganese porphyrin and the co-catalyst. The aqueous phase was washed several times with hexane and controlled by GC-FID to assure that the aqueous phase was deprived of any thymol, thymoquinone or internal standard. The aqueous phase was stored in the freezer protected from light until the next reuse. At each recycling assay, 4 eq of oxidant were added. No further co-catalyst was added in the recycling.

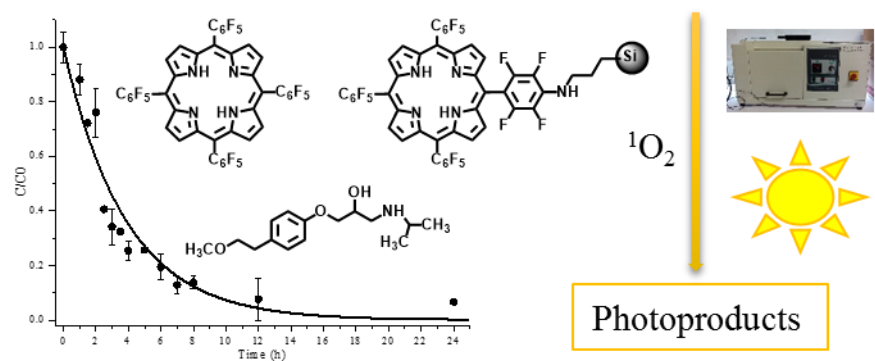
For the oxidation of the oregano oil under biphasic conditions: the catalyst (3.75×10^{-7} mol; 3.19 mg) and the co-catalyst (0.2 mmol; \approx 15 mg of ammonium acetate) were dissolved in 1 mL of Milli-Q water. Next, 20 μ L of the oregano oil and 7.5×10^{-5} mol of the internal standard were dissolved in 1 mL of hexane and added to the aqueous mixture. Finally, 3×10^{-4} mol of TBHP 5.0-6.0 M solution in decane were added to start the reaction.

All the reactions were kept under vigorous stirring at 30 ± 1 °C and protected from light. The conversion of the substrate was monitored by GC-FID and the stability of the catalyst was checked by UV-Vis spectrophotometry.

4.4. References

- 1 P. T. Anastas and M. M. Kirchhoff, *Acc. Chem. Res.*, 2002, **35**, 686–694.
- 2 J. M. Thomas and R. Raja, *Catal. Today*, 2006, **117**, 22–31.
- 3 R. A. Sheldon, *Chem. Commun.*, 2008, 3352–3365.
- 4 R. A. Sheldon, *Green Chem.*, 2017, **19**, 18–43.
- 5 R. A. Sheldon, *Green Chem.*, 2005, **7**, 267–278.
- 6 W. Keim, *Green Chem.*, 2003, **5**, 105–111.
- 7 B. Driessen-Hölscher, *Adv. Catal.*, 1998, **42**, 473–505.
- 8 G.-J. ten Brink, I. W. C. E. Arends and R. A. Sheldon, *Science*, 2000, **287**, 1636–1639.
- 9 N. Ryoji, A. Masao and S. Kazuhiko, *Chem. Commun.*, 2003, 1977–1986.
- 10 M. Milos, J. Mastelic and I. Jerkovic, *Food Chem.*, 2000, **71**, 79–83.
- 11 B. Teixeira, A. Marques, C. Ramos, C. Serrano, O. Matos, N. R. Neng, J. M. F. Nogueira, J. A. Saraiva and M. L. Nunes, *J. Sci. Food Agric.*, 2013, **93**, 2707–2714.
- 12 E. Ipek, H. Zeytinoglu, S. Okay, B. A. Tuylu, M. Kurkcuoglu and K. H. C. Baser, *Food Chem.*, 2005, **93**, 551–556.
- 13 M. Cristani, M. D'Arrigo, G. Mandalari, F. Castelli, M. G. Sarpietro, D. Micieli, V. Venuti, G. Bisignano, A. Saija and D. Trombetta, *J. Agric. Food Chem.*, 2007, **55**, 6300–6308.
- 14 K. H. C. Baser, *Curr. Pharm. Des.*, 2008, **14**, 3106–3120.
- 15 A. Marchese, I. E. Orhan, M. Daglia, R. Barbieri, A. Di Lorenzo, S. F. Nabavi, O. Gortzi, M. Izadi and S. M. Nabavi, *Food Chem.*, 2016, **210**, 402–414.
- 16 H. A. Johnson, L. L. Rogers, M. L. Alkire, T. G. McCloud and J. L. McLaughlin, *Nat. Prod. Lett.*, 1998, **11**, 241–250.
- 17 M. Burits and F. Bucar, *Phyther. Res.*, 2000, **14**, 323–328.
- 18 B. H. Ali and G. Blunden, *Phyther. Res.*, 2003, **17**, 299–305.
- 19 B. Amin and H. Hosseinzadeh, *Planta Med.*, 2016, **82**, 8–16.
- 20 H. Gali-Muhtasib, A. Roessner and R. Schneider-Stock, *Int. J. Biochem. Cell Biol.*, 2006, **38**, 1249–1253.
- 21 C. C. Woo, A. P. Kumar, G. Sethi and K. H. B. Tan, *Biochem. Pharmacol.*, 2012, **83**, 443–451.

- 22 M. A. Khan, M. Tania, S. Fu and J. Fu, *Oncotarget*, 2017, **8**, 51907–51919.
- 23 E. R. Dockal, Q. B. Cass, T. J. Brocksom, U. Brocksom and A. G. Corrêa, *Synth. Commun.*, 1985, **15**, 1033–1036.
- 24 R. R. L. Martins, M. G. P. M. S. Neves, A. J. D. Silvestre, A. M. S. Silva and J. A. S. Cavaleiro, *J. Mol. Catal. A Chem.*, 1999, **137**, 41–47.
- 25 F. C. Skrobot, A. A. Valente, G. Neves, I. Rosa, J. Rocha and J. A. S. Cavaleiro, *J. Mol. Catal. A Chem.*, 2003, **201**, 211–222.
- 26 A. Güneş, O. Bayraktar and S. Yilmaz, *Ind. Eng. Chem. Res.*, 2006, **45**, 54–61.
- 27 I. C. M. S. Santos, M. M. Q. Simões, M. M. M. S. Pereira, R. R. L. Martins, M. G. P. M. S. Neves, J. A. S. Cavaleiro and A. M. V. Cavaleiro, *J. Mol. Catal. A Chem.*, 2003, **195**, 253–262.
- 28 T. Günay, Y. Çimen, R. B. Karabacak and H. Türk, *Catal. Letters*, 2016, **146**, 2306–2312.
- 29 M. Milos, *Appl. Catal. A Gen.*, 2001, **216**, 157–161.
- 30 M. Luciano and C. Brückner, *Molecules*, 2017, **22**, 1–47.
- 31 Z. Hou, W. Dehaen, J. Lyskawa, P. Woisel and R. Hoogenboom, *Chem. Commun.*, 2017, **53**, 8423–8426.
- 32 B. Meunier, *Chem. Rev.*, 1992, **92**, 1411–1456.
- 33 D. Mansuy, *Comptes Rendus Chim.*, 2007, **10**, 392–413.
- 34 J. W. Buchler, in *The Porphyrins Volume I: Structure and Synthesis, Part A*, ed. D. Dolphin, Academic Press, New York, 1978, pp. 389–483.



CHAPTER 5

Photodegradation of metoprolol using a porphyrin as photosensitizer

This chapter gave rise to the following publication:

Neves, C. M. B.; Filipe, O. M. S.; Mota, N.; Santos, S. A. O.; Silvestre, A. J. D.; Santos, E. B. H.; Neves, M. G. P. M. S.; Simões, M. M. Q. Photodegradation of metoprolol using a porphyrin as photosensitizer under homogeneous and heterogeneous conditions. *J. Haz. Mat.* **2019**, *370*, 13-23. <https://doi.org/10.1016/j.jhazmat.2018.11.055>.

Chapter 5. Photodegradation of metoprolol using a porphyrin as photosensitizer

The presence of chemicals in wastewater effluents and in surface and ground waters represents a negative impact on ecosystems and human health. Among the various chemicals commonly found in the aquatic environment, pharmaceuticals were considered emerging contaminants and have aroused great concern, since they are extensively consumed worldwide and reach the environment either by inadequate disposal or by their excretion (unchanged or as metabolites) into sewage waters.¹ In addition, they can be extremely resistant to degradation and often escape intact from conventional sewage treatment plants due to their high chemical stability and low biodegradability.² Therefore, alternative treatments such as the use of photocatalysts must be investigated to complement the existing gaps in the conventional treatment processes.

Porphyrins are known to be highly effective photosensitizers, as they possess triplet states of appropriate energy to allow, under light irradiation, an efficient energy transfer to ground state oxygen, producing high yields of oxygen reactive species such as $^1\text{O}_2$.³ Such properties are responsible for the application of these compounds in different areas such as medical photodynamic therapy (PDT),⁴⁻¹¹ and photodynamic inactivation (PDI) of different microorganisms.¹²⁻¹⁶ These features make porphyrins also good candidates in the photooxidation of organic compounds,¹⁷⁻²⁰ namely as photocatalysts for the degradation of organic pollutants in a water remediation context.^{21,22} In fact, the use of this class of compounds in the treatment of pollutants has been a subject of great attention in the last years, and considerable work has been described in the photodegradation of target molecules such as textile dyes,²³⁻²⁸ chlorophenols,²⁹⁻³⁵ and pesticides.³⁶⁻⁴⁰ However, only a few studies have been reported on the photodegradation of pharmaceuticals.^{41,42}

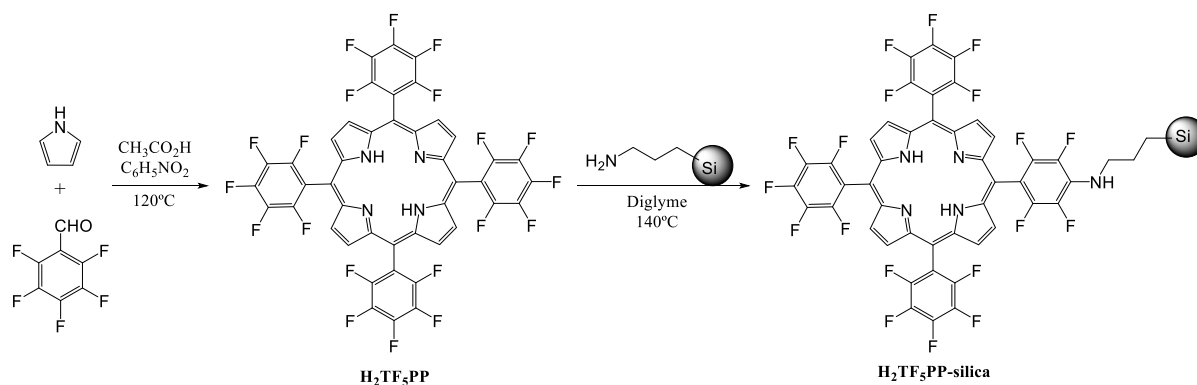
Recently, Mathon *et al.* selected 13 xenobiotics (pharmaceuticals and pesticides) commonly found in secondary effluents to be relevant to sewage polishing treatment.⁴³ Five of the selected xenobiotics were β -blockers, including metoprolol, which can be detected in a range of 5×10^{-3} to $3 \mu\text{g L}^{-1}$. Under direct photolysis, atenolol and metoprolol were classified as slow-photodegradable, and propranolol was classified as medium-photodegradable.⁴³ Direct photolysis of organic micropollutants, specifically β -blockers, may occur by the direct absorbance of photons, when the compound absorption spectrum

overlaps with the solar spectrum but only if the radiation is strong enough.⁴⁴ Thus, since most of the β -blockers only absorb in the UV-C range, their direct photolysis in aquatic environment is not remarkable,^{44,45} but indirect photodegradation may occur induced by photosensitizers present in natural waters, such as humic substances.⁴⁶ However, even when indirect photodegradation may help to reduce β -blockers concentration in natural waters, their discharge should be avoided in the sources, among which outstand the effluents of sewage treatment plants. Given that β -blockers, and specifically metoprolol, are not completely degraded in conventional biological treatments, photocatalytic processes have been tested for their elimination from wastewaters, generally using TiO₂ as photocatalyst.^{47–62} However, a main drawback of this photocatalyst is that solar energy for exciting TiO₂ ($\lambda \leq 387\text{nm}$) accounts for less than 5% of the whole sunlight reaching the surface of Earth.⁶³ Another challenge is its immobilization on solid supports. The immobilization often reduces the photocatalytic efficiency of TiO₂ and the small particle size leads to high filtration costs for the photocatalyst removal.⁶⁴ For this reason, the search for efficient photocatalysts able to use sunlight, in a broader range of wavelengths, associated with an easy and efficient separation after use, is an issue of great importance. In this context, porphyrins are considered promising photocatalysts due to their strong absorption in several wavelengths of the sunlight range, showing in general an intense absorption (Soret band) in the 400–450 nm region and four additional bands (Q-bands) in the 500–800 nm region. A possible side effect, from the environmental point of view, can be the potential phototoxicity of the photocatalyst, which can be minimized by its decomposition in the presence of ¹O₂,³ or alternatively by its immobilization on a solid support. The immobilization of porphyrins onto solid supports has received great attention on the last years due to their practicability in the water purification process, especially their easy removal by filtration and, ultimately, the possibility of reuse.²²

In the present work, the potential of 5,10,15,20-tetrakis(pentafluorophenyl)porphyrin (**H₂TF₅PP**) to be used as photosensitizer, under homogeneous conditions and after its heterogenization on silica (**Scheme 5.1**), was evaluated for the removal of metoprolol in wastewater treatment systems. This porphyrin was selected considering the following aspects: i) easy synthetic accessibility;⁶⁵ ii) high photostability;⁶⁶ iii) high efficiency to generate singlet oxygen;⁶⁷ iv) facile immobilization in solid supports by nucleophilic substitution of *p*-fluorine atoms.^{65,68}

The following topics will be discussed below:

- i) the synthetic approach used to prepare the photocatalysts and its characterization;
- ii) the results obtained during the metoprolol photodegradation experiments in homogeneous medium under simulated solar radiation;
- iii) the photodegradation experiments in the presence of scavengers in order to confirm the type of mechanism involved;
- iv) the results obtained when the studies under simulated solar radiation and also under real solar irradiation were carried out under heterogeneous conditions;
- v) the extension of the studies to a wastewater treatment effluent;
- vi) the identification of the products obtained in the photodegradation of metoprolol by HPLC coupled to tandem mass spectrometry (HPLC-UV-ESI-MSⁿ).



Scheme 5.1. Synthetic strategy to prepare and to attach $\text{H}_2\text{TF}_5\text{PP}$ onto the silica support.^{68,69}

5.1. Results and discussion

5.1.1. Preparation of the photocatalysts

The preparation of the non-immobilized porphyrin $\text{H}_2\text{TF}_5\text{PP}$ and of the immobilized porphyrin $\text{H}_2\text{TF}_5\text{PP-silica}$ (Scheme 5.1) is fully described in section 5.3.2. The porphyrin was prepared by the conventional condensation of pyrrole with pentafluorobenzaldehyde in a mixture of acetic acid and nitrobenzene. After work-up and purification, the spectroscopic data of the non-immobilized $\text{H}_2\text{TF}_5\text{PP}$ (^1H NMR, MS and UV-Vis spectra) were consistent with the literature data (please see details in Chapter 2, section 2.3.1).^{70–74} The immobilization of $\text{H}_2\text{TF}_5\text{PP}$ with 3-aminopropyl-functionalized silica was performed in diglyme at 140°C . After 24 h, the reaction was considered complete and the coloured

solid was thoroughly washed with the adequate solvent and dried. The amount of porphyrin immobilized onto the silica support was $4.9 \mu\text{mol g}^{-1}$; this incorporation was determined by UV-Vis spectrophotometry considering the amount of unreacted porphyrin, as described in section 5.3.2.

The solid material resulting from the immobilization of the porphyrin exhibits a yellowish-brown colour in contrast with the white colour of silica before immobilization (**Figure 5.1**). The supported material was characterized by diffuse reflectance UV-Vis spectrophotometry (**Figure 5.2**), powder X-ray diffraction (**Figure 5.3**) and infrared spectroscopy (**Figure 5.4**). The success of **H₂TF₅PP** incorporation onto the silica support is patent on its diffuse reflectance spectrum. The typical strong Soret band around 410 nm and the three Q-bands between 500 and 650 nm observed in the UV-Vis spectrum of **H₂TF₅PP** in solution and in solid state (see also **Figure 5.2**) were also detected in **H₂TF₅PP-silica**. However, in these two last spectra the relative intensity of the Soret band was largely diminished when compared with the porphyrin spectrum in solution. As expected, no bands were detected in the diffuse reflectance spectrum of the 3-aminopropyl-functionalized silica (**Figure 5.2**).



Figure 5.1. Appearance of the functionalized silica before the immobilization (left) and after the porphyrin immobilization (right).

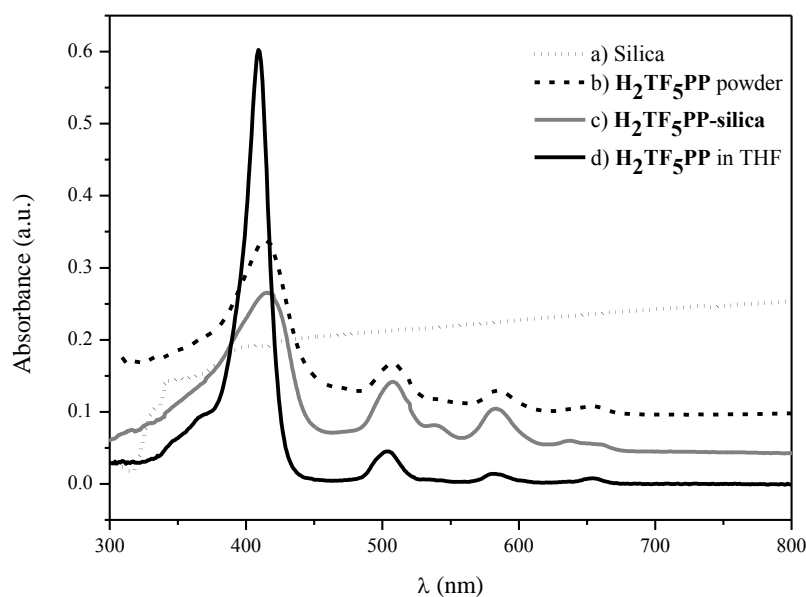


Figure 5.2. Diffuse reflectance UV-Vis spectra obtained for: a) Silica (the 3-aminopropyl-functionalized silica support); b) $\text{H}_2\text{TF}_5\text{PP}$ powder (the non-immobilized $\text{H}_2\text{TF}_5\text{PP}$ solid); c) $\text{H}_2\text{TF}_5\text{PP}$ -silica (the porphyrin immobilized on the silica support). UV-Vis spectrum of d) $\text{H}_2\text{TF}_5\text{PP}$ in solution (dissolved in THF), evidencing the porphyrins' characteristic Soret (around 410 nm) and Q bands (between 500 and 650 nm).

The powder X-ray diffraction patterns of $\text{H}_2\text{TF}_5\text{PP}$ -silica shows a halo in the region of $20\text{-}30^\circ$ (2θ), typical of an amorphous sample, as observed for the amino functionalized silica (**Figure 5.3**); the crystallinity of $\text{H}_2\text{TF}_5\text{PP}$ was not observed in the immobilized solid and this is probably related with the low amount of porphyrin incorporated.

The ATR spectrum of $\text{H}_2\text{TF}_5\text{PP}$ -silica (**Figure 5.4c**) presents the amino functionalized silica characteristic bands at 1051 cm^{-1} and a shoulder around 1200 cm^{-1} , attributed to the asymmetrical Si–O–Si vibration and two other vibration bands related to Si–O–Si at 796 cm^{-1} and 447 cm^{-1} .⁷⁵ The porphyrin characteristic fingerprint bands, such as the band caused by the ring vibration of the porphyrin skeleton ($950\text{-}970\text{ cm}^{-1}$), the bands caused by the out-of-plane bending of the $\beta\text{-H}$ on the pyrrole ring ($772\text{-}805\text{ cm}^{-1}$), the in-plane ($960\text{-}990\text{ cm}^{-1}$) and the out-of-plane ($690\text{-}710\text{ cm}^{-1}$) NH-bending vibrations are engulfed in the broad bands of Si–O–Si vibrations.⁷⁶ Aromatic ring vibrational bands can be observed in the range of $1350\text{-}1700\text{ cm}^{-1}$.⁷⁶

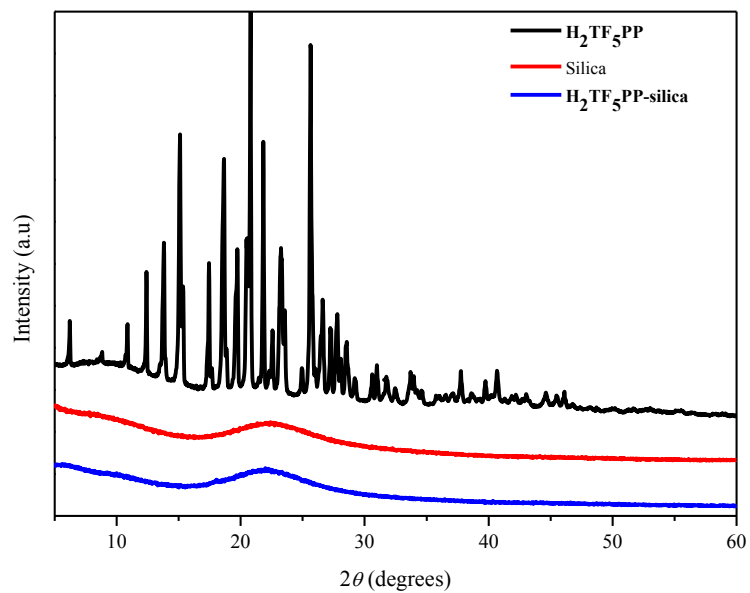


Figure 5.3. Experimental powder X-ray diffraction patterns of H₂TF₅PP, silica and H₂TF₅PP-silica.

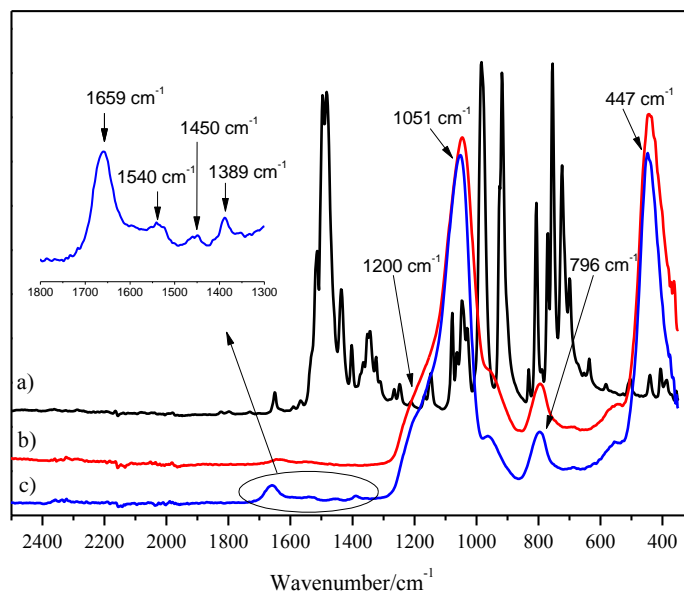


Figure 5.4. ATR spectra of a) H₂TF₅PP, b) silica and c) H₂TF₅PP-silica.

5.1.2. Evaluation of H₂TF₅PP as photosensitizer for metoprolol degradation under homogeneous conditions

The photodegradation experiments under homogeneous conditions were performed in Milli-Q water using a final metoprolol concentration of 50 mg L⁻¹ and 1.0 × 10⁻⁵ mol L⁻¹ of the porphyrin. The irradiations were done under simulated solar radiation, using a Solarbox equipped with a 1500 W arc xenon lamp and outdoor filters that restrict the transmission of light with wavelengths < 290 nm. The first assays were performed in quartz tubes and the evolution of the process was controlled by HPLC analysis (please see section 5.3.7 and discussion below).

The residual percentage of metoprolol remaining in solution after a certain time of irradiation was calculated as

$$\text{Residual percentage of metoprolol} = \frac{C}{C_0} \times 100 \% \quad (\text{Eq 1})$$

where C₀ is the initial metoprolol concentration (calculated from the quantity dissolved for the preparation of the solution) and C is the concentration measured (HPLC analysis) after irradiation.

All the experimental kinetic data obtained in different days were fitted by non-linear regression analysis using the program GraphPadPrism7[®] (Trial version; <http://www.graphpad.com>). The data for the metoprolol photodegradation in the presence of porphyrin under homogeneous conditions were adjusted to the first order kinetics equation,

$$\frac{C}{C_0} = e^{-k_1 t} \quad (\text{Eq 2})$$

where *k₁* is the first order rate constant and *t* is the irradiation time.

Figure 5.5A shows the decrease of metoprolol concentration with the irradiation time in the presence and absence of porphyrin. After 12 h a decrease of *ca* 90% of metoprolol was observed in the presence of porphyrin and, after 24 h, the metoprolol concentration was almost negligible. Without porphyrin, no detectable degradation of metoprolol occurred after 24 h of irradiation. There was also no degradation in the dark control containing porphyrin and metoprolol. The almost complete photodegradation of metoprolol after 24 h of irradiation in the presence of **H₂TF₅PP** is clearly seen in the chromatogram presented in **Figure 5.6**.

The photosensitized degradation of metoprolol follows a pseudo-first order kinetics with $k = 0.262 \pm 0.014 \text{ h}^{-1}$ (95% confidence interval), as confirmed by the good fitting of Eq. (2) to the experimental data values (**Figure 5.5A**).

In order to identify the type of mechanism involved in the metoprolol photodegradation, additional assays were done in the presence of reactive oxygen species scavengers, namely propan-2-ol and sodium azide. While propan-2-ol is a $\cdot\text{OH}$ selective quencher, azide ion is a quencher of both hydroxyl radical ($\cdot\text{OH}$) and singlet oxygen ($^1\text{O}_2$).⁷⁷ The results obtained (**Figure 5.5B**) show that metoprolol degradation in the presence of propan-2-ol follows the same kinetics as in the absence of the scavenger, as confirmed by the coincidence of the experimental points with the pseudo-first order kinetic curve in the absence of the scavenger. A different situation occurred in the presence of sodium azide, where a metoprolol decrease of only 35% was observed after 24 h of irradiation, which lead to the assumption that $^1\text{O}_2$ is the main reactive oxygen species involved in this process.

5.1.3. Metoprolol degradation in the presence of $\text{H}_2\text{TF}_5\text{PP}$ -silica as photosensitizer

Despite the observed efficiency of the porphyrin as photosensitizer in the degradation of metoprolol under homogeneous conditions, the porphyrin has the drawback of being insoluble in water thus requiring its previous solubilization in dimethyl sulfoxide (DMSO) before dilution in water. This fact hampers its large-scale application in wastewater treatment as homogeneous sensitizer. The immobilization of the porphyrin overcomes this problem and allows an easier recovery of the photosensitizer from water after treatment.

The first assays concerning the photodegradation of metoprolol in the presence of **$\text{H}_2\text{TF}_5\text{PP}$ -silica** were carried out in unbuffered solutions without stirring and under simulated solar radiation (see details in section 5.3.4). The kinetic of the photodegradation under these conditions follows an exponential decay, in accordance to Eq. (3), with $k_2 = 0.190 \pm 0.045 \text{ h}^{-1}$ (95% confidence interval, $n = 17$) and $A = 0.586 \pm 0.040$ as shown in **Figure 5.7**.

$$\frac{C}{C_0} = (1 - A)e^{-k_2t} + A \quad (\text{Eq 3})$$

where k_2 is the rate constant and A corresponds to the ratio between C value at infinite time (plateau) and C_0 .

Using these conditions, the residual percentage of metoprolol was $\approx 63\%$ after 12 h of irradiation.

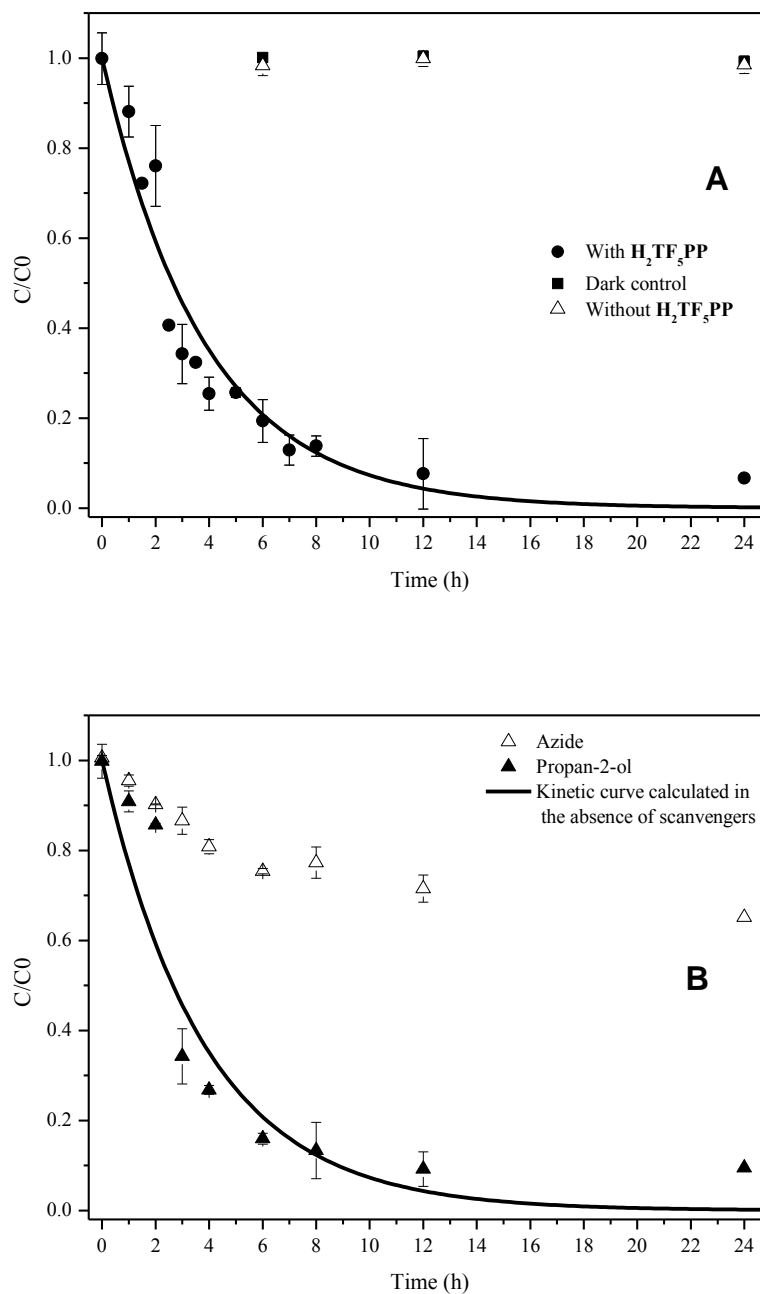


Figure 5.5. Photodegradation of 50 mg L^{-1} metoprolol solutions **A)** in the absence and in the presence of $1.0 \times 10^{-5} \text{ mol L}^{-1}$ of H_2TF_5PP in homogeneous conditions; **B)** in the presence of scavengers. Propan-2-ol was used with a final concentration of 20 mM and sodium azide with a concentration of 2 mM. Data correspond to mean values and the vertical bars correspond to the standard deviations.

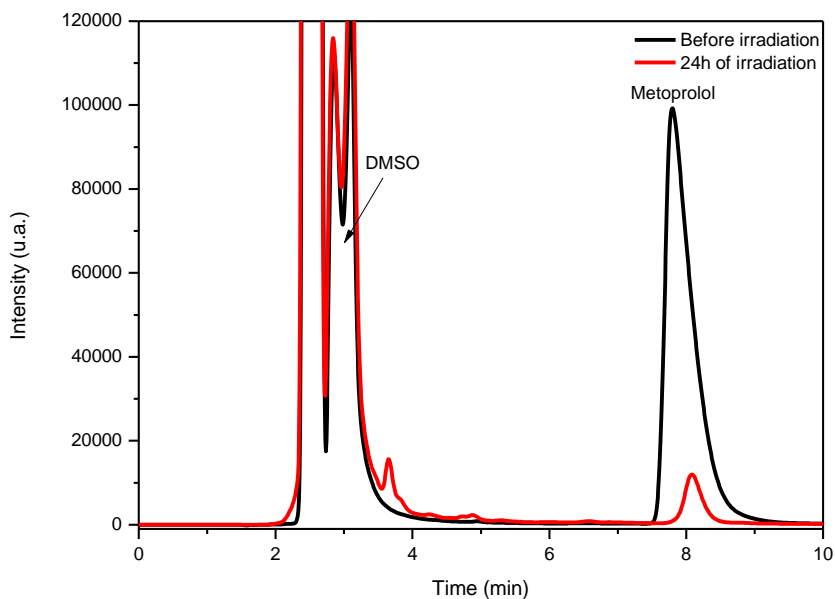


Figure 5.6. HPLC-UV chromatograms operating at 222 nm of 50 mg L⁻¹ metoprolol solutions, in the presence of H₂TF₅PP as photosensitizer, before the irradiation and after 24 h of irradiation, using acetonitrile: water (HCO₂H 0.1%) 20:80 as the mobile phase.

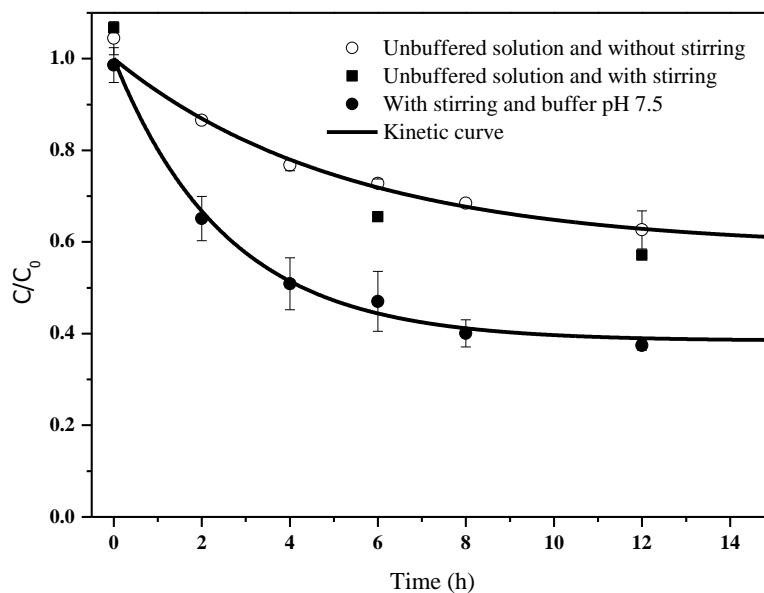


Figure 5.7. Photodegradation of 50 mg L⁻¹ metoprolol solutions catalysed by H₂TF₅PP-silica under different conditions. The vertical bars correspond to the standard deviations.

Since the porphyrin absorbs in the visible range spectrum (Soret band $\lambda_{\max} \approx 410$ nm and the Q bands ranging 500-650 nm), we decided to verify if the efficiency of the photodegradation was the same using glass tubes, which are cheaper than quartz tubes. Since the use of the glass tubes in the irradiation experiments resulted in the same degradation of metoprolol, all the other assays were performed in this type of tubes.

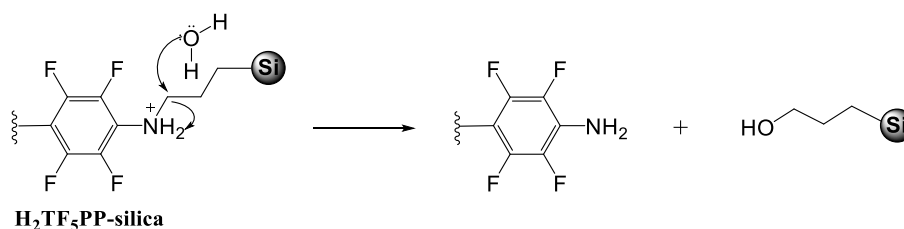
In order to improve the contact of the immobilized photosensitizer with the solution and to avoid some depletion of dissolved oxygen at its surface, extra experiments for 6 h and 12 h of irradiation were done under stirring. The results show an improvement in the photodegradation with a residual percentage of metoprolol of $\approx 65\%$ after 6 h and of $\approx 57\%$ after 12 h (**Figure 5.7**).

Another aspect that merited some attention was the detraction of the yellowish-brown colour of the solid support (**Figure 5.8**), although there was no evidence of the presence of free porphyrin in solution by UV-Vis spectrophotometry. We suspected that this fact was probably due to the photodegradation of the porphyrin either at the solid support or after its release into the solution associated to the alteration of the pH during irradiation.



Figure 5.8. The photocatalyst aspect after 12 h of metoprolol photodegradation without stirring.

In fact, during the assays it was observed that the pH of the solutions decreased from $\text{pH} \approx 6$, before the irradiation, to $\text{pH} \approx 4$ after 12 h of irradiation. The acidic environment of the solutions can give rise to the protonation of the amino group responsible for the linkage of the porphyrin to the solid support and consequently the cleavage of the photocatalyst by a nucleophilic attack would be facilitated (**Scheme 5.2**). In order to minimize this leaching process, the irradiations were carried out in aqueous solutions buffered with 0.01 M phosphate at pH 7.5.



Scheme 5.2. Putative protonation under acidic conditions and cleavage of the covalent bond linking the porphyrin to the support.

The kinetic of the photodegradation of metoprolol, considering the two previous aspects, namely stirring in a buffered solution, follows an exponential decay in accordance to Eq. (3), as shown in **Figure 5.7**. **Table 5.1** compares the kinetic parameters obtained under these conditions with the ones previously obtained (no-stirring in unbuffered solution).

Table 5.1. Kinetic parameters obtained for the photodegradation of 50 mg L⁻¹ metoprolol catalysed by **H₂TF₅PP-silica** under different conditions.

Experimental conditions	k_2 (h ⁻¹)	A ^(c)
Without stirring in unbuffered solutions ^(a)	0.190 ± 0.045	0.586 ± 0.040
With stirring in buffered solutions ^(b)	0.388 ± 0.049	0.384 ± 0.022

^(a) 95% confidence interval, $n = 17$; ^(b) 95% confidence interval, $n = 22$; ^(c) A corresponds to the ratio between C value at infinite time and C₀.

The results show that, in the second conditions, the efficiency of the photosensitizer was improved, and the residual percentage of metoprolol was only $\approx 38\%$ after 12 h of irradiation. Thus, the metoprolol photodegradation at infinite time increased from 41% without stirring in unbuffered solution to 62% in buffered solution under stirring. The considerable improvement in the stability of the photocatalyst was confirmed by diffuse reflectance UV-Vis spectroscopic analysis of the **H₂TF₅PP-silica** material recovered by filtration after 2, 4, 6, 8, and 12 h of irradiation. As can be seen in **Figure 5.9**, the porphyrin's characteristic Soret and Q bands are still present in the **H₂TF₅PP-silica** material, even after 12 h of irradiation, although less intense.

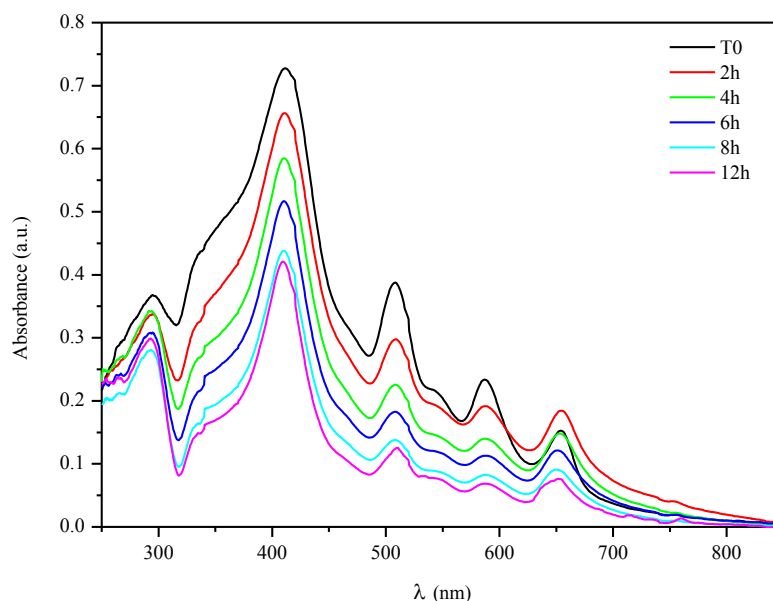


Figure 5.9. Diffuse reflectance UV-Vis spectra of the **H₂TF₅PP-silica** after each period of photo-irradiation, for the experiments using buffered solutions of metoprolol, under stirring.

5.1.4. Metoprolol degradation under real sunlight, photosensitized by H₂TF₅PP-silica

Since the rate constant expressed in h⁻¹ depends on the irradiance of the light source, the irradiation time was converted into energy received by the solutions in order to predict the percentage of degradation under real sunlight. Since the lamp irradiance of the Solarbox was 550 W m⁻², 1 h of irradiation corresponds to 1.98 × 10⁶ J m⁻². Thus, the rate constant 0.388 ± 0.049 h⁻¹ (**Table 5.1**) corresponds to (1.96 ± 0.25) × 10⁻⁷ J⁻¹ m².

Thus, as the energy received by the solutions exposed to real sunlight, calculated as described in section 5.3.5, was 1.43 × 10⁷ J m⁻², and as the exposed area of the irradiated solutions was the same as in the Solarbox, the expected residual metoprolol fraction in solution after sunlight exposition can be calculated as

$$\frac{C}{C_0} = (1 - A)e^{-kE} + A \quad (\text{Eq 4})$$

where $k = 1.96 \times 10^{-7} \text{ J}^{-1} \text{ m}^2$, E , the energy received from the sun, is $1.43 \times 10^7 \text{ J m}^{-2}$ and $A = 0.384 \pm 0.022$ (**Table 5.1**). So, the predicted residual fraction of metoprolol ($\frac{C}{C_0}$) in solution after 6 h of solar exposition ($1.43 \times 10^7 \text{ J m}^{-2}$) is 0.421 ± 0.026 .

From the experiments of metoprolol degradation under real sunlight, the residual fraction of metoprolol obtained after the solar exposition was 0.425 ± 0.022 ($n = 2$), in very good agreement with the predicted value. The results indicate that the kinetic parameters for the degradation of metoprolol photosensitized by **H₂TF₅PP-silica**, obtained under simulated sunlight, can be used to predict the residual fraction of metoprolol obtained in solutions exposed to natural sunlight conditions.

In order to use these data to predict the degradation percentage under other conditions of irradiance and different configurations of the sample containers with different areas of exposition to light, the rate constant was converted into the units $J^{-1} L$ (Eq 5). It was assumed that the solar exposed area corresponds to a half of the cylinder area without the top and the bottom circles (**Figure 5.10** and Eq 6). Taking into account that the volume of solution irradiated was 20 mL and the area exposed to sunlight was $22.6 \times 10^{-4} m^2$ (calculated by Eq 6), then the rate constant $1.96 \times 10^{-7} J^{-1} m^2$ corresponds to $1.73 \times 10^{-6} J^{-1} L$. The predicted residual fraction after solar exposition can be calculated using this rate constant in Eq 4 and replacing E by the energy received per liter of solution. In the present work, the energy received per liter of solution was $1.62 \times 10^6 J L^{-1}$.

$$k(J^{-1}L) = \frac{k(J^{-1}m^2) \times Volume(L)}{Exposed Area (m^2)} \quad (Eq 5)$$

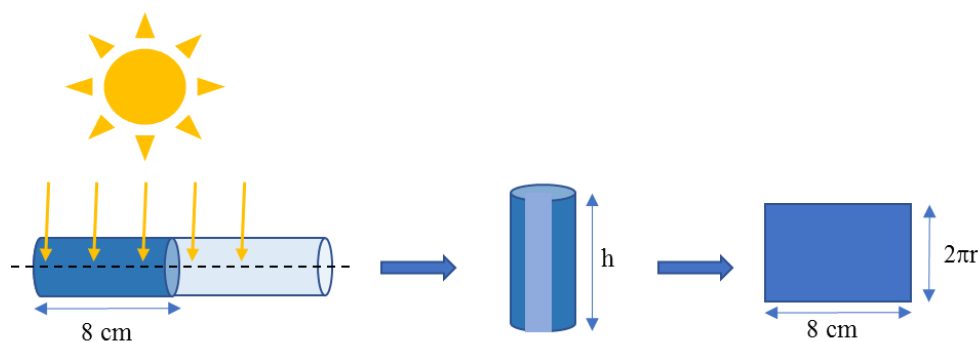


Figure 5.10. Illustration of the area exposed to sunlight.

$$Exposed Area = \frac{2\pi r \times h}{2} \quad (Eq 6)$$

5.1.5. Comparison of metoprolol photodegradation in wastewater treatment effluent and in buffered aqueous solution

The efficacy of **H₂TF₅PP-silica** in metoprolol photodegradation was also evaluated in a sample of the secondary effluent of the municipal wastewater treatment plant (WWTP) located at Gafanha da Encarnação (ETAR de Ílhavo) that was fortified with metoprolol (see details in section 5.3.6). **Figure 5.11** shows the photodegradation of metoprolol in this WWTP effluent and also in buffer solution using a new batch of **H₂TF₅PP-silica**. The results obtained in buffer solution using this new batch of **H₂TF₅PP-silica** are similar to those obtained in the previous assays performed with the first batch of catalyst, as can be seen in **Figure 5.11**, where the individual results which gave rise to the mean values presented in **Figure 5.7** are also shown. Besides, the results obtained in the effluent are almost coincident with those obtained in the buffer solution, using the same batch of **H₂TF₅PP-silica**.

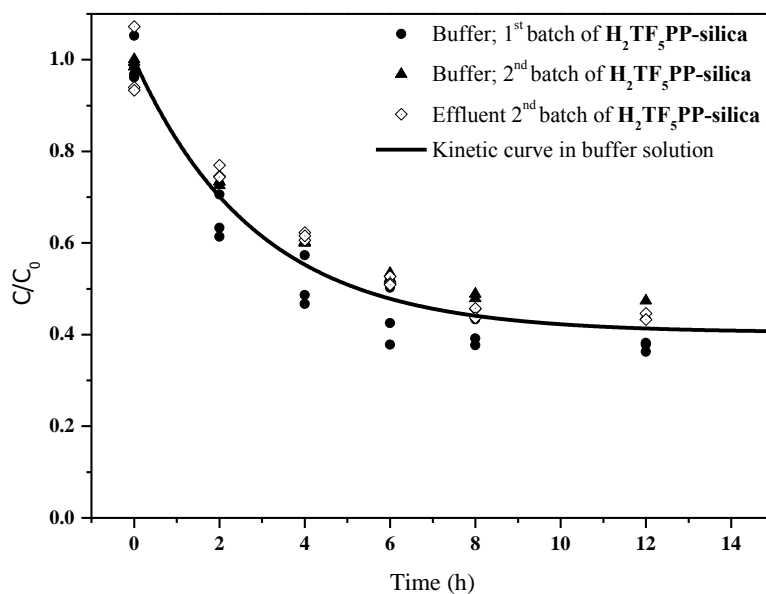


Figure 5.11. Photodegradation of 50 mg L⁻¹ metoprolol solutions prepared in ultrapure water (with buffer) and in WWTP effluent: experimental data and kinetic curve fitted to all the experimental data (with the two batches of immobilized porphyrin) obtained in buffer solution (kinetic parameters $k = 0.347 \pm 0.072 \text{ h}^{-1}$ $A = 0.404 \pm 0.040$).

Thus, it can be stated that the complicated matrix of the effluent did not decrease the efficiency of **H₂TF₅PP-silica** in metoprolol photodegradation. Kim *et al.* also observed a

low effect of the matrices of wastewater treatment effluents on the efficiency of a tin porphyrin immobilized onto silica, for degradation of cimetidine and propranolol.⁴² This is an advantage relatively to photoactive materials capable of generating OH radicals, such as semiconductor based photocatalysts (ex: TiO₂), whose efficiency in pollutants degradation is usually decreased by the components of wastewater matrices.^{42,55} Wastewater components, namely the background organic substances, can compete for reactive oxygen species, and the lower matrix effects observed with porphyrin photosensitizers, relatively to semiconductor based photocatalysts, can be attributed to the higher selectivity of ¹O₂ relatively to OH radicals.

5.1.6. Identification of the photodegradation products by HPLC-UV-ESI-MSⁿ

Figure 5.12A shows the HPLC-UV-ESI-MSⁿ chromatogram obtained with detection at 222 nm when 250 mg L⁻¹ metoprolol solutions in the presence of 1.0 × 10⁻⁵ mol L⁻¹ of **H₂TF₅PP** were irradiated for 12 h. Simultaneously, the samples were analysed using the UV detection in a range of 200-600 nm (**Figure 5.12B**). At least 18 products have been detected and identified based on their [M + H]⁺ ions and on their MSⁿ spectra.

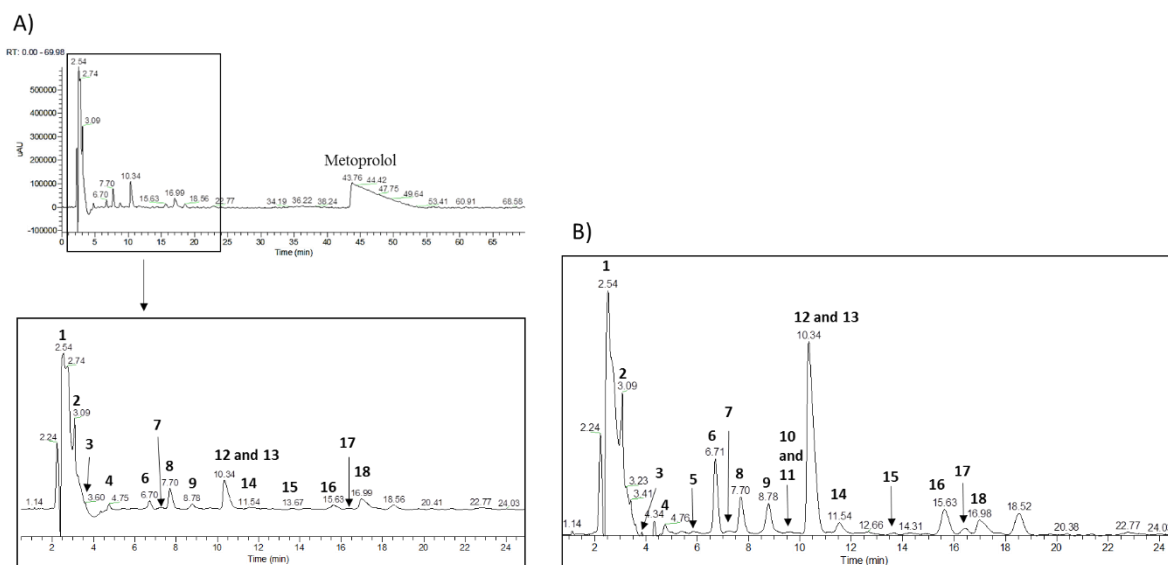
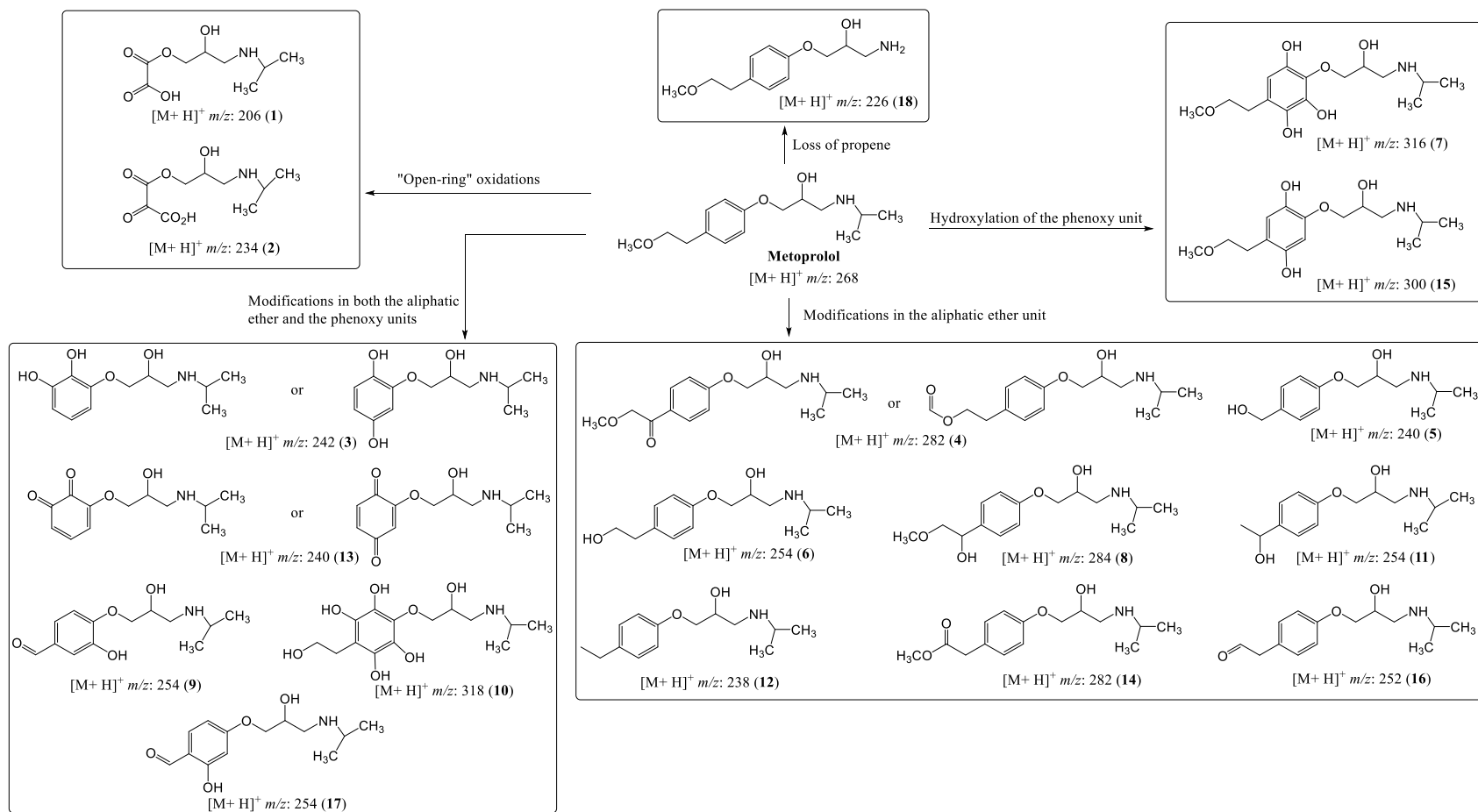


Figure 5.12. **A)** Chromatogram and zoom in the range 1-25 min obtained in HPLC-UV-ESI-MSⁿ operating at 222 nm of 250 mg L⁻¹ metoprolol solutions, in the presence of **H₂TF₅PP** as photosensitizer, after 12 h of irradiation, using acetonitrile: water (HCO₂H 0.1%) 10:90 as the mobile phase. **B)** Zoom in the range 1-25 min of the chromatogram obtained in HPLC-UV-ESI-MSⁿ using diode array detector (200-600 nm) of 250 mg L⁻¹ metoprolol solutions.

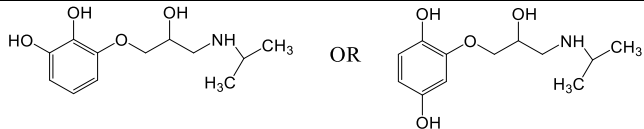
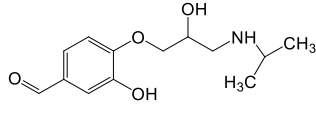
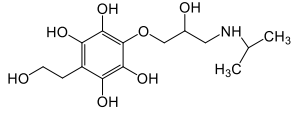
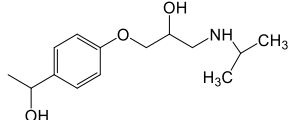
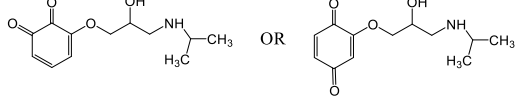
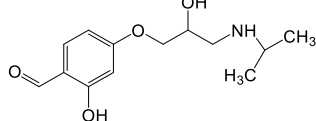
The proposed structures are presented in **Scheme 5.3**. The main products identified here have already been detected by Filipe *et al.* concerning metoprolol photodegradation sensitized by natural fulvic acids, in which the fragmentation pathways of 16 compounds were proposed.⁷⁸ As in the presence of natural fulvic acids, compounds resulting from: ring-opening oxidative processes (**1** and **2**), modifications of the aliphatic ether moiety (**4**, **5**, **6**, **8**, **12**, **14** and **16**), successive hydroxylation reactions of the phenoxy unit (**7** and **15**), and from the loss of propene (**18**), were also detected.

In the presence of the non-immobilized porphyrin, compounds **3**, **9**, **10**, **11**, **13** and **17** were also detected and their structures were proposed based on their MS², MS³ and in some cases MS⁴ spectra (**Table 5.2**). The proposed fragmentation pathways for these compounds are presented in **Schemes 5.4-5.10**. In the presence of the heterogeneous **H₂TF₅PP-silica** only the over oxidized compounds **1**, **7**, **9**, **10**, **13**, **15**, and **17** were not detected. All the other products previously referred were detected. Since in the presence of the heterogeneous porphyrin the photodegradation of metoprolol is lower, the products should appear in lower concentrations and this is probably the reason why the minor degradation products were not detected.



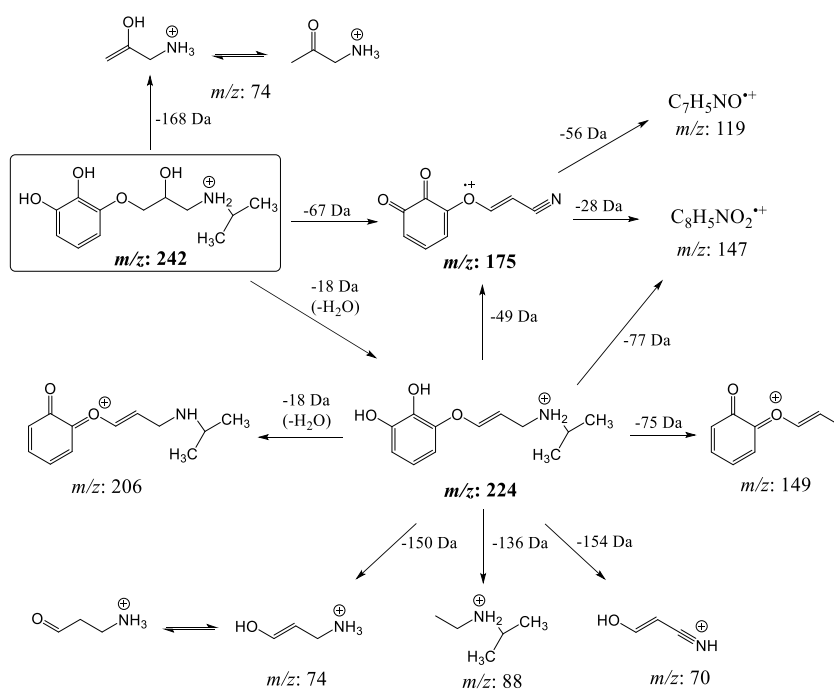
Scheme 5.3. Proposed structures of the main photodegradation products of metoprolol obtained using **H₂TF₅PP** as photosensitizer.

Table 5.2. MSⁿ fragmentation profile of the photodegradation products **3**, **9**, **10**, **11**, **13** and **17**. The MSⁿ fragmentation of the remaining products is in agreement with the structures of the compounds proposed in a previous work.⁷⁸ Only product ions with abundances higher than 5% were considered.

Compound	R _t (min)	[M+H] ⁺ m/z	MS ⁿ m/z (relative abundance, %)	Proposed structure(s)
3	3.6	242	MS ² : 224 (100), 175 (6), 74 (5) MS ³ [224]: 206 (10), 175 (100), 149 (17), 147 (33), 88 (25), 70 (12) MS ³ [175]: 147 (100), 133 (13), 129 (97), 119 (6)	
9	9.1	254	MS ² : 236 (48), 212 (52), 194 (100), 177 (34), 166 (23), 149 (17), 121 (8), 116 (24), 98 (7) MS ³ [212]: 194 (100), 177 (14), 166 (34), 149 (18), 147 (10), 139 (9), 123 (7), 74 (9) MS ³ [194]: 177 (22), 166 (100), 149 (77), 147 (10), 121 (22), 119 (29), 107 (11) MS ³ [177]: 149 (72), 133 (7), 121 (100), 107 (56), 93 (7)	
10	9.9	318	MS ² : 300 (100), 274 (14), 256 (9), 116 (26), 98 (19) MS ³ [300]: 282 (18), 268 (10), 258 (11), 256 (12), 250 (11), 241 (7), 208 (8), 153 (5), 116 (8), 114 (28), 98 (100) MS ⁴ [282]: 149 (100) MS ⁴ [268]: 226 (100), 224 (60), 170 (65), 164 (26)	
11	10.0	254	MS ² : 212 (25), 177 (100), 159 (40), 151(7), 133(6), 116 (23), 98 (8) MS ³ [212]: 194 (16), 177 (100), 159 (52), 121 (5), 74 (14) MS ³ [177]: 159 (100), 133 (40), 105 (42)	
13	10.8	240	MS ² : 222 (30), 198 (80), 180 (13), 163 (100), 151 (8), 135 (17), 116 (14), 105 (25), 98 (10), 74 (8) MS ³ [222]: 163 (100) MS ³ [198]: 180 (25), 163 (30), 125 (100)	
17	16.5	254	MS ² : 212 (52), 195 (8), 177 (100), 149 (11), 139 (10), 121 (9), 116 (62), 98 (6), 74 (5) MS ³ [212]: 194 (6), 177 (100), 149 (11), 139 (25), 74 (30)	

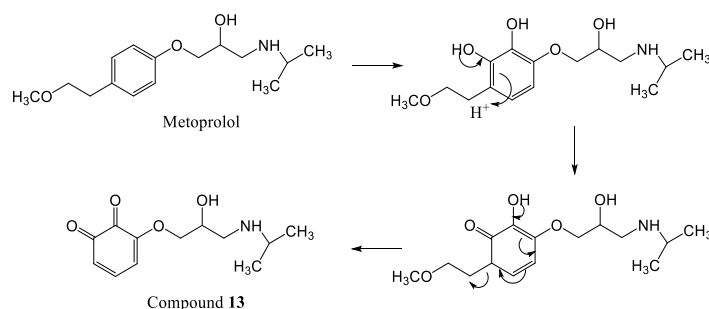
In the MS² spectra of the new compounds (see **Table 5.2** and **Schemes 5.4-5.10**), the presence of the metoprolol characteristic product ions at *m/z* 116, 98 and 74, and the typical losses of 18 Da (H₂O) and 42 Da (CH₃CH=CH₂) indicate that the aminopropanol moiety of metoprolol is unchanged.

In the MSⁿ spectra of **3**, with [M + H]⁺ at *m/z* 242, the absence of the product ions at *m/z* 159 and 133 and the absence of methanol losses means that the phenoxy and ether moieties of metoprolol are changed. Compound **3** was identified as a di-hydroxylated benzene derivative with the OH groups either with a 1,2 and/or 1,4 relative position (**Scheme 5.3**). The MSⁿ fragmentation profile of the compound is consistent with both proposed structures (**Scheme 5.4**, exemplified for the case of the 1,2-dihydroxybenzene derivative).



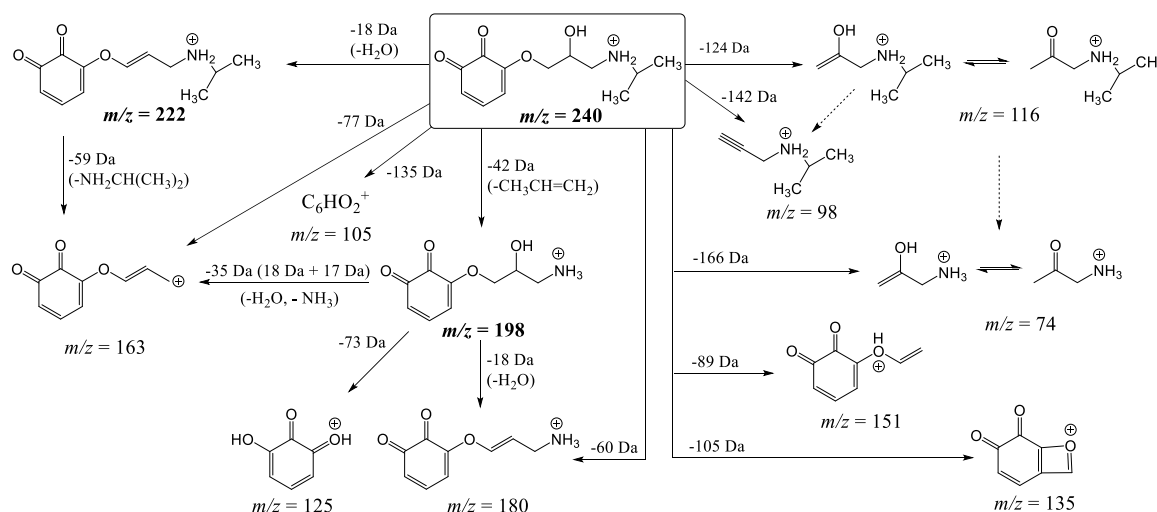
Scheme 5.4. Proposed fragmentation pathways for compound **3** ([M+H]⁺ at *m/z* 242).

The MSⁿ fragmentation of **13** with the molecular ion [M + H]⁺ at *m/z* 240, similarly to **3**, does not generate the product ions at *m/z* 159 and 133. The aminopropanol moiety of metoprolol is maintained, due to the presence of the product ions at *m/z* 116 and 98. The difference of 2 Da in relation to **3** leads us to propose the corresponding 1,2-benzoquinone or 1,4-benzoquinone as the most likely structures of **13** (**Scheme 5.3**) and may result from an oxidation of **3** or directly from metoprolol (**Scheme 5.5**).



Scheme 5.5. Mechanism proposed for the formation of **13** from metoprolol.

The mechanism of formation and the MSⁿ fragmentation profile of the compound are consistent with both proposed structures (**Schemes 5.5** and **5.6**, exemplified for the case of the 1,2-benzoquinone derivative).



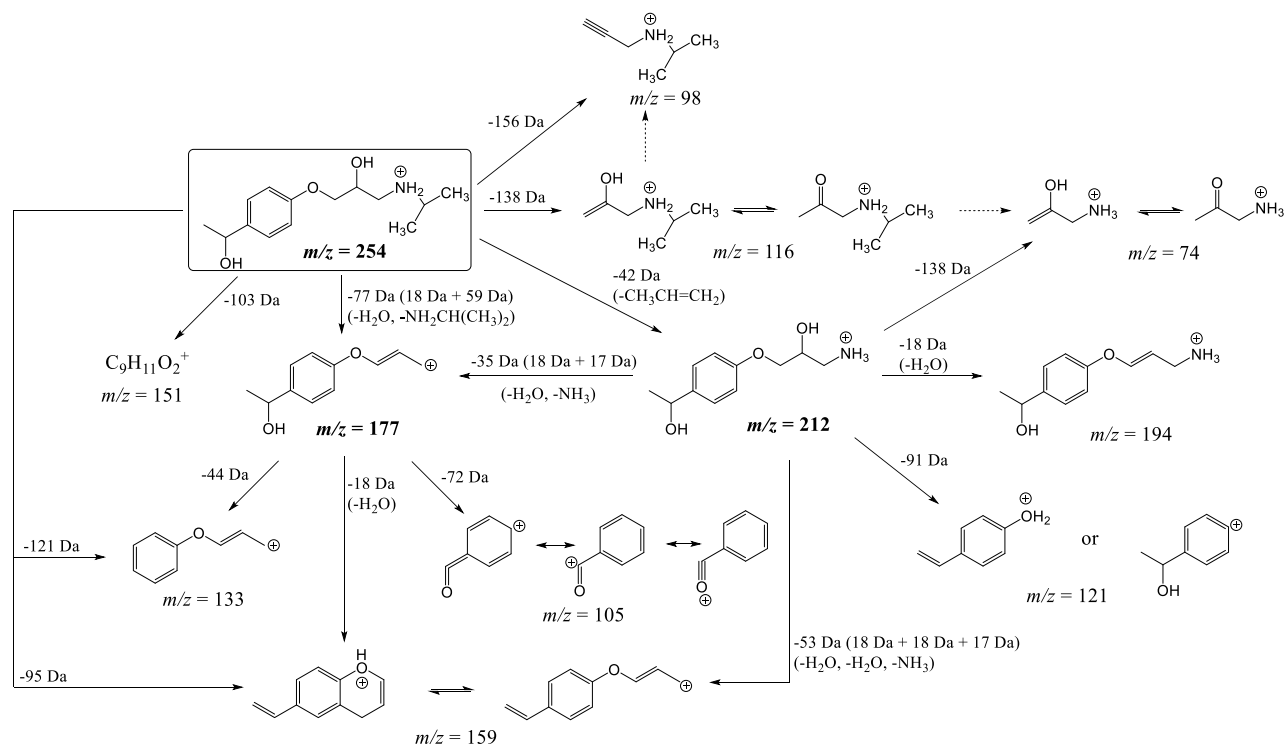
Scheme 5.6. Proposed fragmentation pathways for compound **13** ($[M+H]^+$ at m/z 240).

In addition to **6** already identified in a previous study,⁷⁸ three other derivatives resulting from the photodegradation of metoprolol with $[M + H]^+$ ion at m/z 254 were detected at 9.1 min (**9**), 10.0 min (**11**) and 16.5 min (**17**). Their MS² spectra are similar, however the product ions show different relative abundances and their MSⁿ fragmentation presents some differences. In the MS² spectra of the three compounds, the presence of product ions at m/z 212 (-42 Da, loss of propene) and 177 (-77 Da, loss of water and isopropylamine) can be observed. The absence of methanol losses (32 Da), characteristic of the ether moiety, indicates that a modification occurred in this part of the molecule.

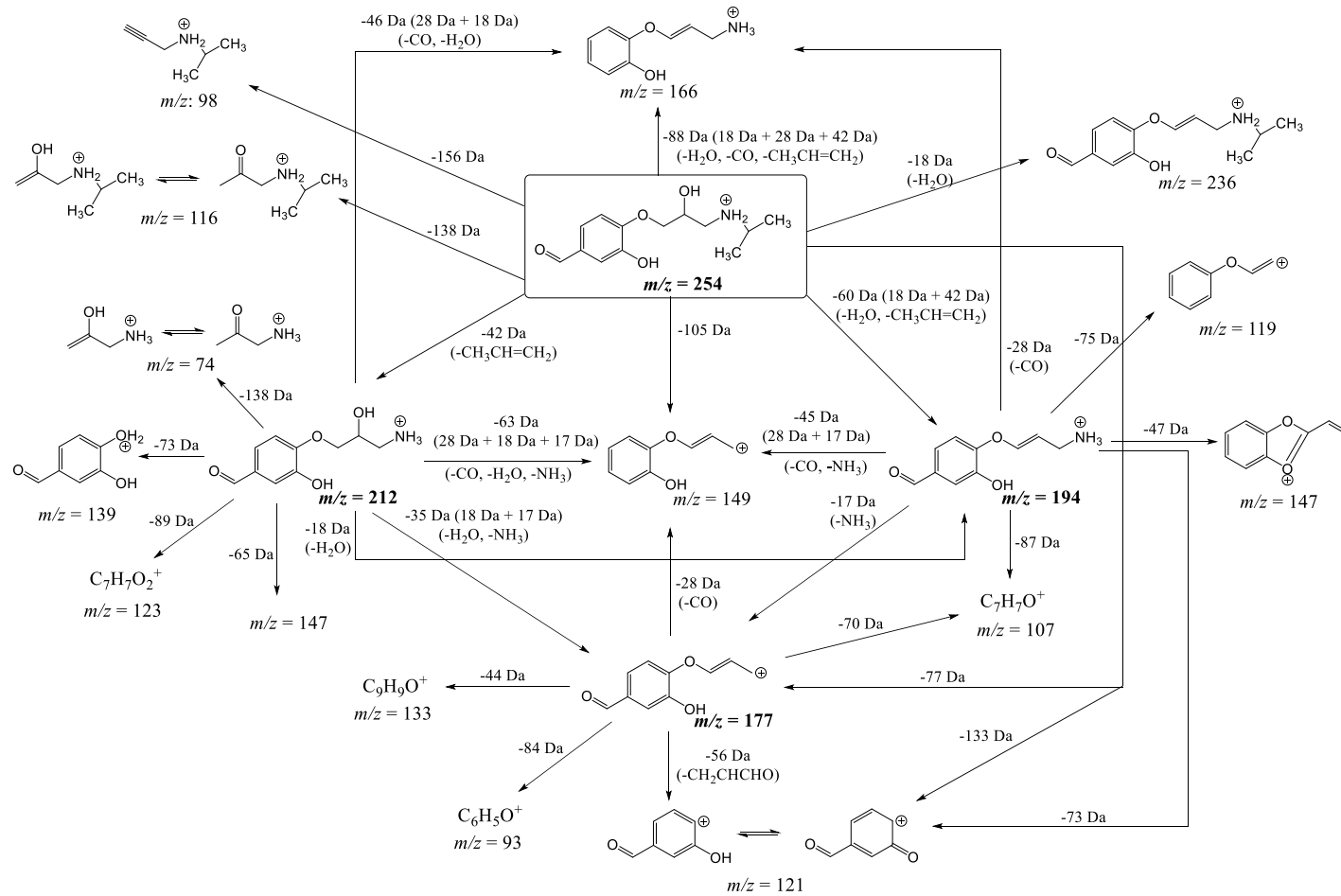
Compound **11** presents a MS² spectrum of the molecular ion at m/z 254 and MS³ fragmentation patterns very similar to **6**, therefore it was identified as 1-[4-(1-

hydroxyethyl)phenoxy]-3-(propan-2-ylamino)propan-2-ol (1-hydroxyethyl isomer of **6**) (Table 5.2 and Scheme 5.7). This compound has already been identified by Armaković *et al.* and their results are in accordance with our MSⁿ spectra fragmentation profile.⁷⁹ In fact, from the MSⁿ fragmentation pattern of [M + H]⁺ ion at *m/z* 254, the presence of product ions at *m/z* = 159, 133 and 105 shows that the aromatic ring of metoprolol is preserved. The loss of two molecules of water and ammonia in the MS³ spectrum of the product ion at *m/z* 212 (product ion at *m/z* 159) suggests the presence of another hydroxyl group. Also, the product ions at *m/z* = 159 and 133 observed in the MS³ spectrum of the product ion at *m/z* 177, resulting from the loss of 18 Da (water) and the loss of 44 Da (CH₃CHO), respectively, are indicative of the presence of a hydroxyethyl moiety.

The MSⁿ fragmentation of [M + H]⁺ ion at *m/z* 254 for **9** is in accordance with the structure of the hydroxy derivative of 4-[2-hydroxy-3-(propan-2-ylamino)propoxy]benzaldehyde (Table 5.2 and Scheme 5.8). This compound has been identified in the photodegradation of atenolol using TiO₂ and photo-Fenton reaction, under natural light.⁸⁰ The same product was also detected in the photodegradation of metoprolol in the presence of TiO₂-based photocatalysts.^{50,79} The presence of the product ion at *m/z* 166 in the MS³ fragmentation pattern of [M + H]⁺ ion at *m/z* 212 (loss of 28 Da and water) and in the MS³ fragmentation pattern of [M + H]⁺ ion at *m/z* 194 (loss of 28 Da) may indicate the presence of a formyl group. In electrospray ionization mass spectrometry, protonated aldehydes can show loss of CO (-28 Da) as a major fragmentation pathway.⁸¹ The presence of the product ion at *m/z* 147 in the MS³ fragmentation patterns of [M + H]⁺ ion at *m/z* 212 and *m/z* 194 may indicate that the hydroxyl group of the aromatic ring should be positioned *meta* to the formyl group.

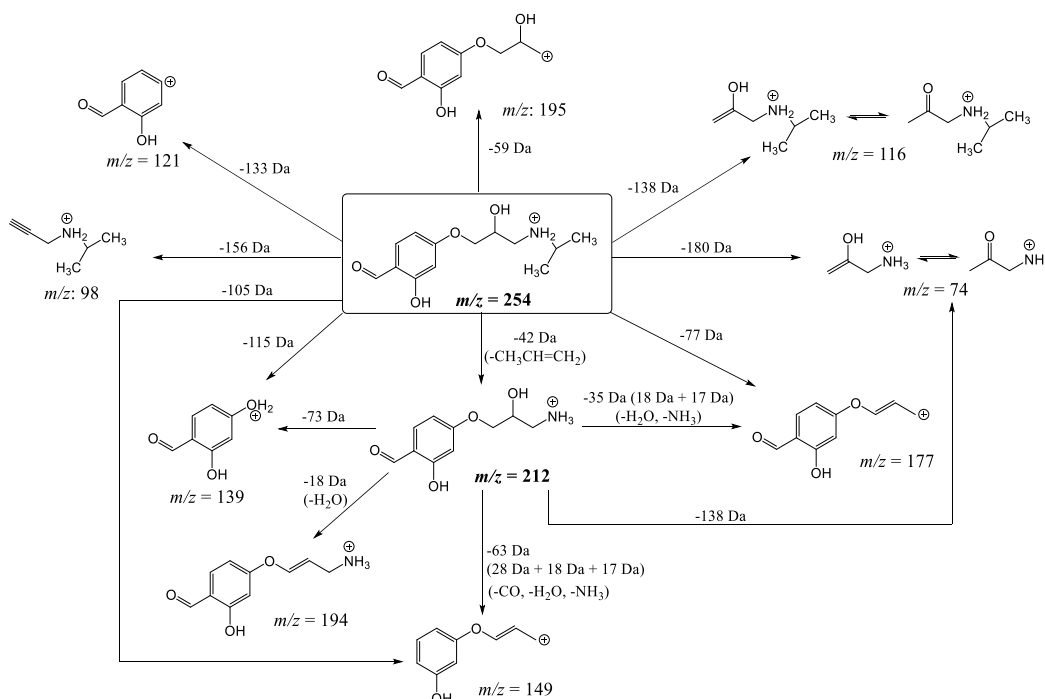


Scheme 5.7. Proposed fragmentation pathways for compound **11** ($[M+H]^+$ at m/z 254).



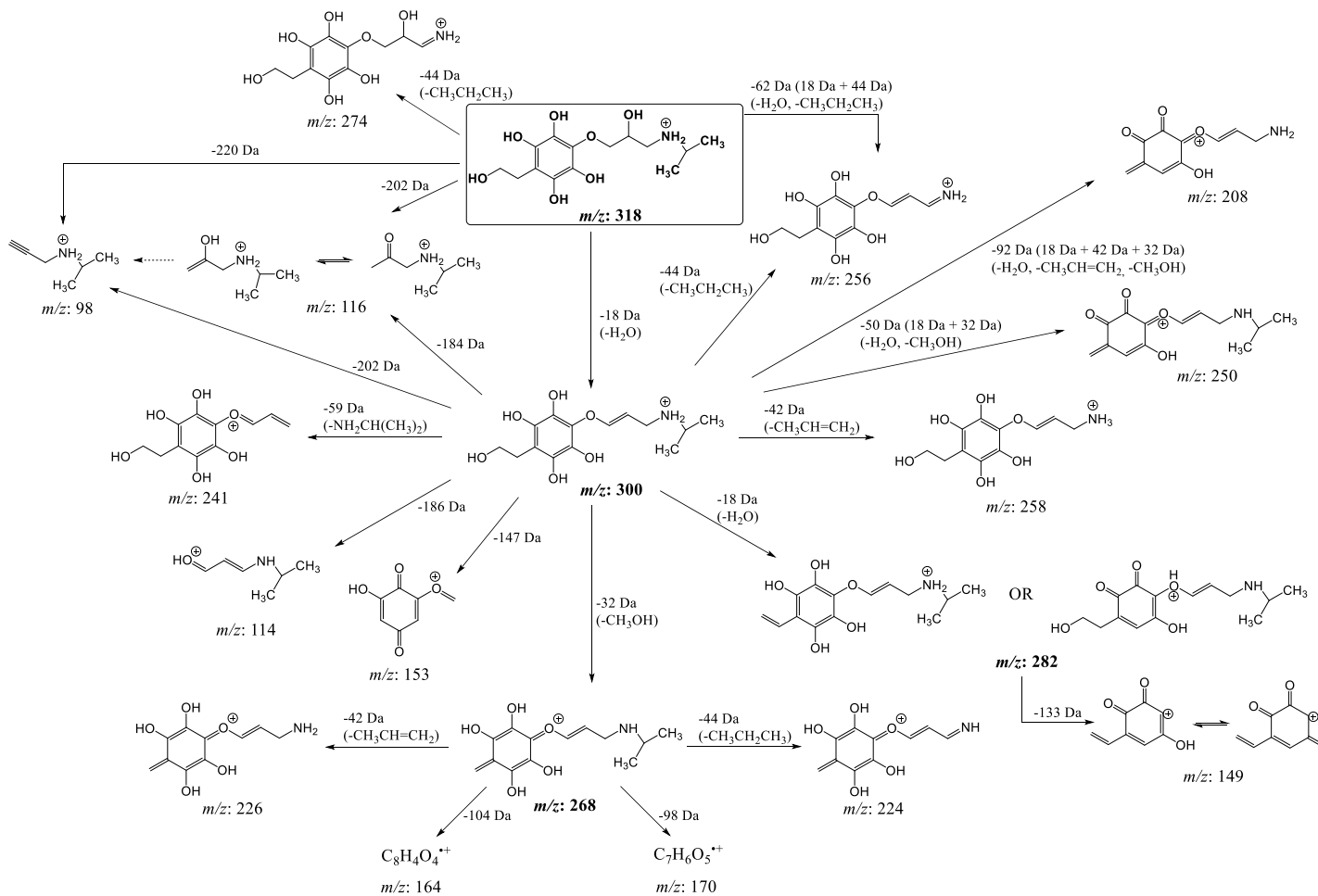
Scheme 5.8. Proposed fragmentation pathways for compound **9** ($[M+H]^+$ at m/z 254).

Compound **17** presents a MS^2 spectrum and MS^3 fragmentation pattern of $[M + H]^+$ ion at m/z 212 similar to **9** and is probably the *ortho*-isomer (**Table 5.2** and **Scheme 5.9**).



Scheme 5.9. Proposed fragmentation pathways for compound **17** ($[M+H]^+$ at m/z 254)

Compound **10**, with $[M + H]^+$ at m/z 318 may result from the hydroxylation of the aromatic ring of metoprolol and demethylation of the ether moiety. In the previous work with fulvic acids a product resulting from the hydroxylation of the aromatic ring of metoprolol was identified (compound with $[M + H]^+$ at m/z 332).⁷⁸ However, in the present study, this compound was only detected in trace amounts, which may indicate that it has been converted into **10**. Compound **10** has a difference of 14 Da with respect to the derivative detected in the work with fulvic acids, which is in accordance with the absence of the methyl group. In addition, in the MS^2 spectrum of **10**, with the molecular ion $[M + H]^+$ at m/z 318, the presence of the product ions at m/z 116 and 98 and the losses observed in the MS^n spectra of 42 Da ($CH_3CH=CH_2$), 44 Da ($CH_3CH_2CH_3$) and 59 Da ($NH_2CH(CH_3)_2$) indicate that the aminopropanol moiety of metoprolol is preserved (**Scheme 5.10**).



Scheme 5.10. Proposed fragmentation pathways for compound **10** ($[\text{M}+\text{H}]^+$ at m/z 318).

5.2. Conclusions

In this study the photodegradation of metoprolol was carried out, for the first time, in the presence of a porphyrin (**H₂TF₅PP**) as photosensitizer, both under homogeneous conditions and immobilized on a silica support.

The main photoproducts formed were identified by HPLC-UV-ESI-MSⁿ. At least 18 products have been tentatively identified based on MSⁿ experiments and fragmentation patterns, including: i) several compounds which have already been previously identified in the work concerning the photodegradation of metoprolol in the presence of natural fulvic acids; ii) the 3 isomeric compounds with m/z 254, previously identified in the literature as being formed by photocatalysis using TiO₂, and iii) 3 new compounds which were tentatively identified for the first time in this work, with m/z 240, m/z 242 and m/z 318.

In homogeneous conditions and under simulated solar light, the degradation of metoprolol follows a pseudo-first order kinetics with a decrease in metoprolol of *ca* 90% after 12 h. The irradiation experiments in the presence of scavengers revealed that singlet oxygen is the main reactive oxygen species involved in the photooxidation process. In the presence of **H₂TF₅PP-silica** in buffered and under stirring conditions, the photodegradation of metoprolol follows an exponential decay with a decrease in metoprolol of *ca* 62% after 12 h. Besides being an improvement over the direct photolysis, there is no need for solvents for its solubilisation and the porphyrin was easily removed. The irradiation time was converted into energy received by the solutions in order to predict the percentage of degradation under real sunlight. The predicted residual fraction of metoprolol in solution using the kinetic parameters obtained under Solarbox irradiation is in accordance with the results obtained under real solar exposition. Finally, studies performed in a sample from the secondary effluent of a wastewater treatment plant fortified with metoprolol revealed that the efficiency of **H₂TF₅PP-silica** was not decreased by the complex matrix of the effluent.

5.3. Experimental

5.3.1. Chemicals and solutions

Nitrobenzene and 2,3,4,5,6-pentafluorobenzaldehyde used in the synthesis of the free-base porphyrin were acquired from Acros and Fluka, respectively. Pyrrole was obtained from Sigma-Aldrich and was previously distilled. Diethylene glycol dimethyl ether (diglyme, $\geq 99\%$) used as solvent for the immobilization of the porphyrin was purchased from Fluka, whereas 3-aminopropyl-functionalized silica gel 9% was obtained from Aldrich.

Metoprolol tartrate salt ($\geq 98\%$), propan-2-ol and sodium azide were acquired from Sigma-Aldrich. Formic acid (HCO_2H , 98%) was obtained from Panreac and acetonitrile (HPLC quality) and dimethyl sulfoxide ($\geq 99,5\%$; DMSO) were purchased from Lab-Scan Analytical Sciences. Potassium dihydrogen phosphate (KH_2PO_4) and sodium hydroxide (NaOH) were obtained from Merck and di-sodium hydrogen phosphate anhydrous (Na_2HPO_4) from Fluka.

The stock solution of **H₂TF₅PP** (1000 mg L⁻¹) was prepared by dissolving the porphyrin in DMSO and the stock solution of metoprolol was prepared by dissolving the compound in ultrapure water (Milli-Q). The stock solutions were protected from light with aluminum foil and stored at 4 °C until use.

The stock solution of phosphate buffer 0.1 M was prepared in 250 mL of Milli-Q water with a mixture of 0.0125 mol of KH_2PO_4 and 0.0125 mol of Na_2HPO_4 . The pH of the solution was adjusted to 7.5 with NaOH solutions (1 M and 0.1 M).

5.3.2. Synthesis of H₂TF₅PP and immobilization on the silica support

The 5,10,15,20-tetrakis(pentafluorophenyl)porphyrin (**H₂TF₅PP**) was prepared by condensation of 2,3,4,5,6-pentafluorobenzaldehyde with pyrrole as previously described in the Chapter 2 (see section 2.3 for the experimental details), according to the procedure described elsewhere.⁶⁹

For the immobilization, a mixture of **H₂TF₅PP** (20 mg; 20.5 μmol) and 3-aminopropyl-functionalized silica (1 g) in 10 mL of diglyme was heated at 140 °C under nitrogen in a Schlenk flask and was maintained under stirring protected from light for 24

h.⁶⁸ The yellowish-brown solid obtained was filtered under vacuum, using a Hirsch funnel with filter paper, washed several times with dichloromethane previously passed through alumina, and dried in the oven (55 °C) overnight. The unreacted porphyrin, recovered from the filtration, was transferred to a 25 mL volumetric flask after evaporation of the solvent and dissolved in THF. This solution was diluted (50 μ L to 25 mL with THF) and analysed by UV-Vis spectroscopy in order to quantify the amount of porphyrin immobilized on the silica support. For the conversion of absorbance into concentration, a calibration curve was prepared using **H₂TF₃PP** standard solutions prepared in THF in the concentration range of 6.64×10^{-7} M to 1.99×10^{-6} M. The UV-Vis spectra were acquired on a dual beam spectrophotometer Shimadzu UV-2501-PC in 1 cm glass cells. The obtained solid materials were analysed by diffuse reflectance spectroscopy on a Jasco V-560 spectrophotometer, using MgO as reference, which was also used to dilute the samples, when needed. Attenuated total reflectance (ATR) FT-IR spectra were measured on a Bruker optics Tensor 27 equipped with a Specac Golden Gate Mk II ATR accessory having a diamond top plate and KRS-5 focusing lenses (resolution 4 cm^{-1} , 256 scans). Routine Powder X-ray Diffraction (PXRD) data for all the prepared materials were collected at ambient temperature on a Empyrean PANalytical diffractometer (Cu $K_{\alpha 1,2}$ X-radiation, $\lambda_1 = 1.540598 \text{ \AA}$; $\lambda_2 = 1.544426 \text{ \AA}$), equipped with an PIXcel 1D detector and a flat-plate sample holder in a Bragg-Brentano para-focusing optics configuration (45 kV, 40 mA). Intensity data were collected by the step-counting method (step 0.03°), in continuous mode, in the ca. $5^\circ \leq 2\theta \leq 60^\circ$ range.

5.3.3. Irradiation apparatus

The irradiations studies of metoprolol solutions were performed under simulated solar radiation, using a Solarbox 1500 (Co.fo.me.gra, Italy) equipped with a 1500 W arc xenon lamp and outdoor filters that restrict the transmission of light with wavelengths $< 290 \text{ nm}$. The irradiance was kept constant at 55 W m^{-2} in the wavelength range 295-400 nm, corresponding to 550 W m^{-2} in the whole spectrum. A multimeter (Co.fo.me.gra, Italy), equipped with temperature and UV 290-400 nm large band sensors, was used to control the temperature and the irradiance, respectively. The samples (20 mL) were placed in 19.5 cm quartz or glass tubes with an internal diameter of 1.8 cm and the tubes were disposed inside the chamber using a home-made metallic support which keeps the tubes

leaning positioned under the lamp. In the heterogeneous experiments, the irradiations were also performed under stirring and, for this purpose a stirring plate was positioned below the Solarbox.

5.3.4. Photodegradation experiments in aqueous solutions

For the homogeneous photodegradation experiments, the solutions were prepared in order to obtain a final metoprolol concentration of 50 mg L⁻¹ and 1.0 × 10⁻⁵ mol L⁻¹ of the porphyrin by dilution with Milli-Q water. In the case of HPLC-UV-ESI-MSⁿ analysis the solutions were prepared with a metoprolol concentration of 250 mg L⁻¹ for a better detection of the degradation products. Solutions of metoprolol with the porphyrin were irradiated under the same conditions in the presence of selective scavengers. For the quenching of the hydroxyl radical ([•]OH), propan-2-ol was added to the solution to obtain a final concentration of 20 mM, and for the quenching of both hydroxyl radical ([•]OH) and singlet oxygen (¹O₂), sodium azide was added to attain a final concentration of 2 mM. Samples of 20 mL were placed in the tubes and irradiated during different time periods.

For the heterogeneous photodegradation experiments, 20 mL of the 50 mg L⁻¹ metoprolol solution were added to the tubes containing 1.23 × 10⁻⁵ M of the photosensitizer (2.5 g L⁻¹ of **H₂TF₅PP-silica** with a porphyrin content of 4.9 μmol g⁻¹). Aliquots of 500 μL were removed from the tubes and filtered through a Millex-GV syringe filter from Millipore (0.22 μm pore size, PVDF membrane) into a 2 mL glass vial for further analysis. Experiments with and without stirring were performed. To evaluate the pH effect, experiments were also made with 20 mL of metoprolol solution buffered at pH 7.5 with 0.01 M phosphate buffer under stirring.

Replicates of the experiments were non-simultaneous in order to better evaluate reproducibility. For both homogeneous and heterogeneous photocatalysis experiments, metoprolol solutions (50 mg L⁻¹) without the photosensitizer, and photosensitizer in water without metoprolol were also irradiated. Dark controls with the same amount of metoprolol and photosensitizer in tubes covered with aluminum foil were also prepared and submitted to the same irradiation conditions inside the Solarbox.

5.3.5. Solar irradiation experiments

Experiments under real sunlight were carried out at the roof of the Department of Chemistry of the University of Aveiro, using the heterogeneous photosensitizer in buffered metoprolol solutions at pH 7.5 under stirring. For these experiments, the tubes and the volumes of solution were the same as those used in the experiments made in the Solarbox. They were also kept in a leaning position relatively to sunlight, in order to assure that the exposition area was the same as in the Solarbox. In parallel, a dark control in the same place was also performed involving the tube in an aluminum foil. The solar irradiation was performed during 6 h in a typical day of summer between 11 a.m. and 5 p.m. (higher solar irradiation period).

Solar irradiance (W m^{-2}) was measured with a Campbell-Stokes recorder and the data obtained every 10 min were supplied by the Meteorological Tower of the University of Aveiro. Solar energy (J m^{-2}) received by the samples was calculated as $\sum_{i=1}^n \bar{I}_i \times 600$, where n is the number of 10 min intervals corresponding to the total time of samples exposition under sunlight and \bar{I}_i is the medium solar irradiance in each 10 min interval.

5.3.6. Photodegradation experiments in wastewater

Photodegradation experiments were also performed in a sample of the secondary effluent of the municipal wastewater treatment plant (WWTP) located at Gafanha da Encarnação (ETAR de Ílhavo), which treats urban effluents from the municipalities of Ílhavo and Mira and from part of the municipalities of Aveiro, Cantanhede and Vagos, in Portugal. It treats an average of 25600 m^3 per day. Data on the characterization of the effluent were provided by the WWTP Direction and are presented in **Table 5.3**. The effluent was filtered immediately after arrival at our laboratories (0.2 μm filter after pre-filtration through larger pore filter) and kept in the refrigerator at 4 °C. Aliquots of the filtered effluent were spiked with metoprolol (50 mg L^{-1}) and 20 mL of the spiked effluent were added to 0.05 g of **H₂TF₅PP-silica** (2.5 g L^{-1}) and irradiated in the Solarbox as described previously in section 5.3.4. For these experiments, a new batch of immobilized porphyrin was prepared, following the same immobilization procedure described in section 5.3.2. Additional assays of the photodegradation of metoprolol in buffered aqueous solution were also performed with the second batch of immobilized porphyrin for comparison.

Table 5.3. Characterization of the secondary effluent from the WWTP of Gafanha da Encarnação, Aveiro Portugal

Sampling day	pH	TSS (mg L ⁻¹)	COD (mg O ₂ L ⁻¹)	BOD (mg O ₂ L ⁻¹)	N _{total} (mg L ⁻¹)	P _{total} (mg L ⁻¹)
2018/09/04	8.3	25	90	18	60	8.1
2018/09/06	8.2	55	81.8	24		
2018/09/10	8.3	43	67.7			
2018/09/13	7.1	50	73.2			

TSS – Total Suspended Solids; COD – Chemical Oxygen Demand; BOD –Biochemical Oxygen Demand

5.3.7. HPLC-UV analysis

The metoprolol samples were analysed by HPLC in a Shimadzu apparatus equipped with a DGU-20A5 degasser, a LC-20AD pump, a UV-Vis SPD-20A detector, a CTO-10ASVP column oven (with constant temperature at 25 °C), a PFP ACE[®] C18 column (150 × 4.60 mm, 5 µm), and a 20 µL loop. The mobile phase was acetonitrile:water (acidified with HCO₂H 0.1%) 20:80 (v/v) for kinetic studies of the metoprolol degradation and acetonitrile:water (acidified with HCO₂H 0.1%) 10:90 (v/v) for the detection and identification of the photodegradation products and was previously filtered by a membrane filter 0.2 µm NL16 (Schleicher & Schuell). The flow rate was 0.7 mL min⁻¹ and the detection wavelength was 222 nm.

The calibration of the HPLC apparatus was made using metoprolol standards prepared in Milli-Q water with concentrations in the range of 10 mg L⁻¹ to 50 mg L⁻¹. The validation of the calibration curve was made daily, analysing two standards. The calibration was considered valid whenever the difference between the calculated and the real concentration of the standard did not differ more than 5%.

5.3.8. HPLC-UV-ESI-MSⁿ analysis

The HPLC system consists of a variable loop Accela autosampler (set at a temperature of 16 °C), an Accela 600 LC pump and an Accela 80 Hz PDA detector (Thermo Fisher Scientific, San Jose, Ca, USA). The analyses were carried out using a PFP ACE[®] C18 column (150 mm x 4.6 mm, 5 µm). The separation of the compounds was carried out with a mobile phase of acetonitrile: water (with 0.1% HCO₂H) 10:90 (v/v), at a flow rate of 0.7 mL min⁻¹, at 25 °C. The injection volume in the HPLC system was 20 µL. Single online detection was carried out in the PDA detector, at 222 nm, and UV spectra in a range of 200-600 nm were also recorded.

The HPLC system was coupled to a LCQ Fleet ion trap mass spectrometer (ThermoFinnigan, San Jose, CA, USA), equipped with an ESI source and operating in positive mode. The nitrogen sheath and auxiliary gas were 40 and 10 (arbitrary units), respectively. The spray voltage was 5 kV and the capillary temperature was 350 °C. The capillary and tune lens voltages were set at 32 V and 110 V, respectively. CID-MSⁿ experiments were performed on mass-selected precursor ions in the range of m/z 50-1000. The isolation width of precursor ions was 1.0 mass units. The scan time was equal to 100 ms and the collision energy was optimized between 15-40 (arbitrary units), using helium as collision gas. The data acquisition was carried out by using Xcalibur[®] data system (ThermoFinnigan, San Jose, CA, USA).

5.4. References

- 1 R. P. Schwarzenbach, B. I. Escher, K. Fenner, T. B. Hofstetter, C. A. Johnson, U. von Gunten and B. Wehrli, *Science*, 2006, **313**, 1072–1077.
- 2 I. Oller, S. Malato and J. A. Sánchez-Pérez, *Sci. Total Environ.*, 2011, **409**, 4141–4166.
- 3 M. C. DeRosa and R. J. Crutchley, *Coord. Chem. Rev.*, 2002, **233–234**, 351–371.
- 4 R. Bonnett, *Chem. Soc. Rev.*, 1995, **24**, 19.
- 5 M. R. Detty, S. L. Gibson and S. J. Wagner, *J. Med. Chem.*, 2004, **47**, 3897–3915.
- 6 E. S. Nyman and P. H. Hynninen, *J. Photochem. Photobiol. B Biol.*, 2004, **73**, 1–28.
- 7 L. M. Moreira, F. V. Dos Santos, J. P. Lyon, M. Maftoum-Costa, C. Pacheco-Soares and N. S. Da Silva, *Aust. J. Chem.*, 2008, **61**, 741–754.
- 8 A. E. O'Connor, W. M. Gallagher and A. T. Byrne, *Photochem. Photobiol.*, 2009, **85**, 1053–1074.
- 9 M. Ethirajan, Y. Chen, P. Joshi and R. K. Pandey, *Chem. Soc. Rev.*, 2011, **40**, 340–362.
- 10 L. B. Josefsen and R. W. Boyle, *Theranostics*, 2012, **2**, 916–966.
- 11 H. Abrahamse and M. R. Hamblin, *Biochem. J.*, 2016, **473**, 347–364.
- 12 L. Costa, M. A. F. Faustino, M. G. P. M. S. Neves, Â. Cunha and A. Almeida, *Viruses*, 2012, **4**, 1034–1074.
- 13 E. Alves, M. A. F. Faustino, M. G. P. M. S. Neves, Â. Cunha, H. Nadais and A. Almeida, *J. Photochem. Photobiol. C Photochem. Rev.*, 2015, **22**, 34–57.
- 14 G. Jori and S. B. Brown, *Photochem. Photobiol. Sci.*, 2004, **3**, 403–405.
- 15 Ž. Lukšienė, *Food Technol. Biotechnol.*, 2005, **43**, 411–418.
- 16 G. Jori, C. Fabris, M. Soncin, S. Ferro, O. Coppellotti, D. Dei, L. Fantetti, G. Chiti and G. Roncucci, *Lasers Surg. Med.*, 2006, **38**, 468–481.
- 17 A. Maldotti, L. Andreotti, A. Molinari, G. Varani, G. Cerichelli and M. Chiarini, *Green Chem.*, 2001, **3**, 42–46.
- 18 M. Hajimohammadi and H. Ghasemi, *J. Porphyr. Phthalocyanines*, 2016, **20**, 670–676.
- 19 M. Hajimohammadi, N. Safari, H. Mofakham and F. Deyhimi, *Green Chem.*, 2011, **13**, 991–997.

- 20 J. C. Barona-Castaño, C. C. Carmona-Vargas, T. J. Brocksom and K. T. De Oliveira, *Molecules*, 2016, **21**, 310.
- 21 M. Thandu, C. Comuzzi and D. Goi, *Int. J. Photoenergy*, 2015, **2015**, 1–22.
- 22 L. Fernández, V. I. Esteves, Â. Cunha, R. J. Schneider and J. P. C. Tomé, *J. Porphyr. Phthalocyanines*, 2016, **20**, 150–166.
- 23 M.-Y. Chang, C.-Y. Chang, Y.-H. Hsieh, K.-S. Yao, T.-C. Cheng and C.-T. Ho, *Adv. Mater. Res.*, 2008, **47–50**, 471–474.
- 24 D. Li, W. Dong, S. Sun, Z. Shi and S. Feng, *J. Phys. Chem. C*, 2008, **112**, 14878–14882.
- 25 L. Shao, H. Xie, J. Mo, Z. Yang, Z. Fan and C. Qi, *Environ. Eng. Sci.*, 2012, **29**, 807–813.
- 26 S. Afzal, W. A. Daoud and S. J. Langford, *J. Mater. Chem.*, 2012, **22**, 4083–4088.
- 27 X.-T. Zhou, H.-B. Ji and X.-J. Huang, *Molecules*, 2012, **17**, 1149–1158.
- 28 L. Shao, G. Xing, W. Lv, H. Yu, M. Qiu, X.-M. Zhang and C. Qi, *Polym. Int.*, 2013, **62**, 289–294.
- 29 M.-Y. Chang, Y.-H. Hsieh, T.-C. Cheng, K.-S. Yao, M.-C. Wei and C.-Y. Chang, *Thin Solid Films*, 2009, **517**, 3888–3891.
- 30 E. Silva, M. M. Pereira, H. D. Burrows, M. E. Azenha, M. Sarakha and M. Bolte, *Photochem. Photobiol. Sci.*, 2004, **3**, 200–204.
- 31 K.-H. Choi, K.-K. Wang, E. P. Shin, S.-L. Oh, J.-S. Jung, H.-K. Kim and Y.-R. Kim, *J. Phys. Chem. C*, 2011, **115**, 3212–3219.
- 32 T. Shiragami, Y. Shimizu, K. Hinoue, Y. Fueta, K. Nobuhara, I. Akazaki and M. Yasuda, *J. Photochem. Photobiol. A Chem.*, 2003, **156**, 115–119.
- 33 S.-G. Chung, Y.-S. Chang, J.-W. Choi, K.-Y. Baek, S.-W. Hong, S.-T. Yun and S.-H. Lee, *Chem. Eng. J.*, 2013, **215–216**, 921–928.
- 34 W. Kim, J. Park, H. J. Jo, H.-J. Kim and W. Choi, *J. Phys. Chem. C*, 2008, **112**, 491–499.
- 35 R. Gerdes, D. Wöhrle, W. Spiller, G. Schneider, G. Schnurpfeil and G. Schulz-Ekloff, *J. Photochem. Photobiol. A Chem.*, 1997, **111**, 65–74.
- 36 V. Héquet, P. Le Cloirec, C. Gonzalez and B. Meunier, *Chemosphere*, 2000, **41**, 379–386.
- 37 S. L. H. Rebelo, A. Melo, R. Coimbra, M. E. Azenha, M. M. Pereira, H. D. Burrows

- and M. Sarakha, *Environ. Chem. Lett.*, 2007, **5**, 29–33.
- 38 M. Silva, M. E. Azenha, M. M. Pereira, H. D. Burrows, M. Sarakha, M. F. Ribeiro, A. Fernandes, P. Monsanto and F. Castanheira, *Pure Appl. Chem.*, 2009, **81**, 2025–2033.
- 39 G. Granados-Oliveros, E. A. Páez-Mozo, F. M. Ortega, C. Ferronato and J.-M. Chovelon, *Appl. Catal. B Environ.*, 2009, **89**, 448–454.
- 40 M. Silva, M. E. Azenha, M. M. Pereira, H. D. Burrows, M. Sarakha, C. Forano, M. F. Ribeiro and A. Fernandes, *Appl. Catal. B Environ.*, 2010, **100**, 1–9.
- 41 S. Murphy, C. Saurel, A. Morrissey, J. Tobin, M. Oelgemöller and K. Nolan, *Appl. Catal. B Environ.*, 2012, **119–120**, 156–165.
- 42 H. Kim, W. Kim, Y. MacKeyev, G.-S. Lee, H.-J. Kim, T. Tachikawa, S. Hong, S. Lee, J. Kim, L. J. Wilson, T. Majima, P. J. J. Alvarez, W. Choi and J. Lee, *Environ. Sci. Technol.*, 2012, **46**, 9606–9613.
- 43 B. Mathon, J.-M. Choubert, C. Miege and M. Coquery, *Sci. Total Environ.*, 2016, **551–552**, 712–724.
- 44 J. Peuravuori and K. Pihlaja, *Anal. Bioanal. Chem.*, 2009, **394**, 1621–1636.
- 45 A. Piram, A. Salvador, C. Verne, B. Herbreteau and R. Faure, *Chemosphere*, 2008, **73**, 1265–1271.
- 46 Q.-T. Liu, R. I. Cumming and A. D. Sharpe, *Photochem. Photobiol. Sci.*, 2009, **8**, 768–777.
- 47 F. J. Rivas, O. Gimeno, T. Borralho and M. Carbajo, *J. Hazard. Mater.*, 2010, **179**, 357–362.
- 48 H. Yang, T. An, G. Li, W. Song, W. J. Cooper, H. Luo and X. Guo, *J. Hazard. Mater.*, 2010, **179**, 834–839.
- 49 V. Romero, N. De La Cruz, R. F. Dantas, P. Marco, J. Giménez and S. Esplugas, *Catal. Today*, 2011, **161**, 115–120.
- 50 B. Abramović, S. Kler, D. Šojić, M. Laušević, T. Radović and D. Vione, *J. Hazard. Mater.*, 2011, **198**, 123–132.
- 51 V. Romero, P. Marco, J. Giménez and S. Esplugas, *Int. J. Photoenergy*, 2013, **2013**, 1–10.
- 52 D. D. Četojević-Simin, S. J. Armačić, D. V. Šojić and B. F. Abramović, *Sci. Total Environ.*, 2013, **463–464**, 968–974.

- 53 B. Czech and K. Rubinowska, *Adsorption*, 2013, **19**, 619–630.
- 54 D. H. Quiñones, A. Rey, P. M. Álvarez, F. J. Beltrán and P. K. Plucinski, *Appl. Catal. B Environ.*, 2014, **144**, 96–106.
- 55 P. M. Álvarez, J. Jaramillo, F. López-Piñero and P. K. Plucinski, *Appl. Catal. B Environ.*, 2010, **100**, 338–345.
- 56 M. Šćepanović, B. Abramović, A. Golubović, S. Kler, M. Grujić-Brojčin, Z. Dohčević-Mitrović, B. Babić, B. Matović and Z. V. Popović, *J. Sol-Gel Sci. Technol.*, 2012, **61**, 390–402.
- 57 A. Rey, D. H. Quiñones, P. M. Álvarez, F. J. Beltrán and P. K. Plucinski, *Appl. Catal. B Environ.*, 2012, **111–112**, 246–253.
- 58 A. Rey, P. García-Muñoz, M. D. Hernández-Alonso, E. Mena, S. García-Rodríguez and F. J. Beltrán, *Appl. Catal. B Environ.*, 2014, **154–155**, 274–284.
- 59 V. Romero, F. Méndez-Arriaga, P. Marco, J. Giménez and S. Esplugas, *Chem. Eng. J.*, 2014, **254**, 17–29.
- 60 R. P. Cavalcante, R. F. Dantas, B. Bayarri, O. González, J. Giménez, S. Esplugas and A. Machulek, *Catal. Today*, 2015, **252**, 27–34.
- 61 R. P. Cavalcante, R. F. Dantas, H. Wender, B. Bayarri, O. González, J. Giménez, S. Esplugas and A. Machulek, *Appl. Catal. B Environ.*, 2015, **176–177**, 173–182.
- 62 R. P. Cavalcante, R. F. Dantas, B. Bayarri, O. González, J. Giménez, S. Esplugas and A. Machulek, *Appl. Catal. B Environ.*, 2016, **194**, 111–122.
- 63 D. Pei and J. Luan, *Int. J. Photoenergy*, 2012, **2012**, 1–13.
- 64 O. Carp, C. L. Huisman and A. Reller, *Prog. Solid State Chem.*, 2004, **32**, 33–177.
- 65 J. I. T. Costa, A. C. Tomé, M. G. P. M. S. Neves and J. A. S. Cavaleiro, *J. Porphyr. Phthalocyanines*, 2011, **15**, 1116–1133.
- 66 A. M. S. Silva, M. G. P. M. S. Neves, R. R. L. Martins, J. A. S. Cavaleiro, T. Boschi and P. Tagliatesta, *J. Porphyrins Phthalocyanines*, 1998, **02**, 45–51.
- 67 J. A. S. Cavaleiro, H. Görner, P. S. S. Lacerda, J. G. MacDonald, G. Mark, M. G. P. M. S. Neves, R. S. Nohr, H.-P. Schuchmann, C. von Sonntag and A. C. Tomé, *J. Photochem. Photobiol. A Chem.*, 2001, **144**, 131–140.
- 68 P. Battioni, J. F. Bartoli, D. Mansuy, Y. S. Byun and T. G. Traylor, *J. Chem. Soc. Chem. Commun.*, 1992, **5**, 1051–1053.
- 69 A. M. d'A. R. Gonsalves, J. M. T. B. Varejão and M. M. Pereira, *J. Heterocycl.*

- Chem.*, 1991, **28**, 635–640.
- 70 A. W. van der Made, E. J. H. Hoppenbrouwer, R. J. M. Nolte and W. Drenth, *Recl. des Trav. Chim. des Pays-Bas*, 1988, **107**, 15–16.
- 71 K. M. Kadish, B. C. Han, M. M. Franzen and C. Araullo-McAdams, *J. Am. Chem. Soc.*, 1990, **112**, 8364–8368.
- 72 F. R. Longo, M. G. Finarelli and J. B. Kim, *J. Heterocycl. Chem.*, 1969, **6**, 927–931.
- 73 M. A. C. de Medeiros, S. Cosnier, A. Deronzier and J.-C. Moutet, *Inorg. Chem.*, 1996, **35**, 2659–2664.
- 74 J. P. C. Tomé, M. G. P. M. S. Neves, A. C. Tomé, J. A. S. Cavaleiro, A. F. Mendonça, I. N. Pegado, R. Duarte and M. L. Valdeira, *Bioorg. Med. Chem.*, 2005, **13**, 3878–3888.
- 75 R. Scaffaro, L. Botta, G. Lo Re, R. Bertani, R. Milani and A. Sassi, *J. Mater. Chem.*, 2011, **21**, 3849.
- 76 P. S. Parker, in *Applications of Infrared, Raman, and Resonance Raman Spectroscopy in Biochemistry*, ed. Frank S. Parker, Plenum Press, New York, 1983, pp. 233–236.
- 77 J. R. Harbour and S. L. Issler, *J. Am. Chem. Soc.*, 1982, **104**, 903–905.
- 78 O. M. S. Filipe, N. Mota, S. A. O. Santos, M. R. M. Domingues, A. J. D. Silvestre, M. G. P. M. S. Neves, M. M. Q. Simões and E. B. H. Santos, *J. Hazard. Mater.*, 2017, **323**, 250–263.
- 79 S. J. Armaković, S. Armaković, N. L. Finčur, F. Šibul, D. Vione, J. P. Šetrajčić and B. F. Abramović, *RSC Adv.*, 2015, **5**, 54589–54604.
- 80 J. Radjenović, C. Sirtori, M. Petrović, D. Barceló and S. Malato, *Appl. Catal. B Environ.*, 2009, **89**, 255–264.
- 81 P. Neta, Y. Simón-Manso, Y. Liang and S. E. Stein, *Rapid Commun. Mass Spectrom.*, 2014, **28**, 1871–1882.

Final Remarks

Metalloporphyrins as biomimetic catalysts of CYP450 have been the subject of intense studies under the context of oxidative catalysis. Environmental concerns have encouraged the design of sustainable and cleaner oxidation processes by using heterogeneous catalysts, benign oxidants and alternative solvents to the common volatile organic solvents, ideally water. A substantial part of the work described in this thesis consists in the development of catalytic systems based on manganese(III) porphyrins that intend to contribute to a greater sustainability of oxidation processes.

Two robust second-generation manganese(III) porphyrins bearing 3,5-dichloropyridyl substituent(s) at the *meso* position(s) were synthesized for the first time: the tetra-substituted **Mn(TDCPyP)Cl** and the mono-substituted **Mn(mono-DCPyP)Cl**. The synthesis of these ligands was considered taking into account that the presence of the pyridine unit(s) with bulky substituents at the *ortho* positions would allow their posterior immobilization on adequate solid supports.

The manganese(III) complexes were first tested as catalysts in the oxidation of cyclooctene under homogeneous conditions using aqueous hydrogen peroxide as an environmentally benign oxidant, acetonitrile as solvent and ammonium acetate as co-catalyst. Both catalysts were highly efficient in the oxidation of cyclooctene giving the corresponding epoxide as the sole product. The catalytic activity of the mono-substituted **Mn(mono-DCPyP)Cl** was very similar to that obtained with the well-known, second-generation robust catalyst **Mn(TDCPP)Cl**. The tetra-substituted catalyst, which evidences some solubility in water, was also tested in the oxidation of cyclooctene, using a mixture of acetonitrile/water, in the presence of different co-catalysts. The best results were obtained for ammonium benzoate as co-catalyst with total conversion of cyclooctene to the corresponding epoxide in 120 min. The good results obtained herein under an aqueous medium and the possibility of improving the **Mn(TDCPyP)Cl** solubility by cationization of the pyridyl groups, will offer the possibility to use this catalyst in water or in aqueous biphasic system, highly desirable in a green chemistry context. **Mn(TDCPyP)Cl** also presents structural characteristics that could lead to the synthesis of other materials with interesting catalytic properties, namely MOFs (Metal–Organic Frameworks) or CPs (Coordination Polymers). Although the results obtained in homogeneous oxidative catalysis mediated by the new manganese(III) porphyrins have been quite satisfactory,

there are still some issues that should be improved, namely the low yields obtained in the ligand synthesis, especially in the case of **H₂TDCPyP**.

The higher catalytic activity exhibited by **Mn(mono-DCPyP)Cl** under homogeneous conditions and the better yield obtained in its synthesis were the main reasons that led us to choose this metalloporphyrin to be immobilized onto the two solid supports (Merrifield resin – **MR**, and functionalized silica – **Si**). **Mn(mono-DCPyP)Cl** was immobilized onto **MR** with classic heating and with MW irradiation. The later allowed us to reduce the reaction time from 96 h to 30 min; moreover, the loading of catalyst increased when the single-mode MW equipment was used. The solids obtained (**CAT-MR** and **CAT-Si**) showed to be efficient catalysts in the epoxidation of cyclooctene. The best results were obtained with the Merrifield-supported catalyst, using TBHP as oxidant, thus allowing five catalytic cycles.

Mn(TDCPyP)Cl and **Mn(mono-DCPyP)Cl** were also highly efficient in the oxidation of styrene under homogeneous conditions, using H₂O₂ as oxidant. For both catalysts, the main product obtained was styrene epoxide together with phenylacetaldehyde and traces of benzaldehyde. The oxidation of styrene under heterogeneous conditions was carried out with **CAT-MR** and TBHP as oxidant, allowing an even higher selectivity to the styrene epoxide, along with the formation of benzaldehyde. The absence of phenylacetaldehyde as product in these heterogeneous reactions was justified considering the steric hindrance caused by the solid support, which unable the formation of the intermediate responsible for phenylacetaldehyde formation.

A sustainable process to obtain thymoquinone by catalytic oxidation of carvacrol and thymol, both highly available natural compounds, was also developed in this work. The water solubility exhibited by **H₂TPP(PEG)₄** led us to study the possible application of its manganese(III) complex as catalyst using an aqueous biphasic medium. In a water/hexane (1:1) biphasic medium, using TBHP as oxidant and ammonium acetate as co-catalyst, **MnTPP(PEG)₄OAc** was able to efficiently catalyse the above mentioned oxidative process. The methodology was also applied directly to an oregano essential oil, rich in carvacrol and thymol, thus resulting in a high amount of thymoquinone. At the end of the reaction, the catalyst was isolated and recovered by simple phase separation allowing its reutilization. Therefore, this liquid-liquid biphasic methodology is attractive for a potential industrial application, since enables a straightforward separation of the products from the

catalyst and could be adapted to continuous operation. In addition, the use of water as an alternative to the common chlorinated organic solvents fits well with environmental issues. The catalytic biphasic system was less efficient in the oxidation of other organic compounds such as cyclooctene, *o*-cresol or *m*-cresol. Better results will be expected if more robust second- or third-generation porphyrins are used in a future work.

Another objective of the work was the use of porphyrins as photosensitizers in the degradation of pollutants usually existing in aqueous environments. Metoprolol, which is slow-photodegradable by direct photolysis, undergone a photodegradation of about 90%, after 12 h, in the presence of **H₂TF₅PP**, under homogeneous conditions, in a MilliQ water matrix and using simulated solar light. The main photoproducts formed were identified by HPLC-UV-ESI-MSⁿ. For greater environmental applicability, **H₂TF₅PP** was immobilized onto a solid support, silica. In the presence of the heterogeneous photosensitizer, **H₂TF₅PP-silica**, and under stirring, the photodegradation of metoprolol was about 62% after 12 h in buffered conditions. The photodegradation of metoprolol under real solar exposition led to identical results. The photodegradation was also carried out in a secondary effluent matrix from a wastewater treatment plant fortified with metoprolol. The studies revealed that, contrarily to what happens with other photocatalysts typically used, such as TiO₂, the efficiency of **H₂TF₅PP-silica** was not decreased, showing a promising applicability of **H₂TF₅PP-silica** as photocatalyst in a context of water remediation. In addition, the photodegradation of organic pollutants in the presence of solar light and O₂ (air), without the addition of other oxidants, is economically and environmentally attractive.